José Carlos Marinello Filho

Energy and Spectral Efficiency Optimization in Multiuser Massive MIMO Communication Systems

Doctoral Thesis presented to the Escola Politécnica da Universidade de São Paulo for obtaining the degree of Doctor of Science.

São Paulo
2018

José Carlos Marinello Filho

Energy and Spectral Efficiency Optimization in Multiuser Massive MIMO Communication Systems

Doctoral Thesis presented to the Escola Politécnica da Universidade de São Paulo for obtaining the degree of Doctor of Science.

Concentration Area:
3142 – Electronic Systems

Advisor:
Prof. Dr. Taufik Abrão

Co-Advisor:
Prof. Dr. Cristiano Panazio

São Paulo
2018

Este exemplar foi revisado e corrigido em relação à versão original, sob responsabilidade única do autor e com a anuência de seu orientador.

São Paulo, _____ de _____ de _____

Assinatura do autor: _____

Assinatura do orientador: _____

Catalogação-na-publicação

Marinello, José Carlos
Energy and Spectral Efficiency Optimization in Multiuser Massive MIMO Communication Systems / J. C. Marinello -- versão corr. -- São Paulo, 2018.
163 p.

Tese (Doutorado) - Escola Politécnica da Universidade de São Paulo. Departamento de Engenharia de Telecomunicações e Controle.

1.Telecomunicações 2.Wireless 3.Energia (Eficiência) 4.Espectro (Eficiência) 5.MIMO massivo I.Universidade de São Paulo. Escola Politécnica. Departamento de Engenharia de Telecomunicações e Controle II.t.

A Nossa Senhora Aparecida.

Acknowledgements

Firstly, I would like to thank God for giving me the knowledge, ability, and opportunity to complete this work. I would like to express my sincere gratitude to my advisor Prof. Taufik Abrão, and co-advisor Prof. Cristiano Panazio for the continuous support of my study and related research. I would like to thank my family for their constant love, encouragement, and limitless support throughout my life: my wife Luciana, my parents José Carlos and Jane, my brother Diego and sister Poliana, and all other relatives which are very important for me. Finally, I would like to thank my friends and colleagues from State University of Londrina for their special support throughout this work.

Resumo

Sistemas de comunicação de múltiplas antenas (*multiple-input multiple-output* - MIMO) têm se destacado como a principal tecnologia para a camada física dos padrões de comunicação da próxima geração, como o 5G. Enquanto a comunicação convencional entre a estação base (*base station* - BS) e seus usuários atendidos é realizada em recursos ortogonais de tempo-frequência, a grande capacidade de redução da interferência inter-usuários possibilitada pelo grande número de antenas da BS habilita a BS a se comunicar com diversos usuários no mesmo recurso tempo-frequência. Este melhor uso do escasso espectro disponível eleva a eficiência espectral a níveis muito apreciáveis, e tem um efeito similar na eficiência energética, pois a potência de transmissão não é aumentada. Por outro lado, se o objetivo é fornecer um desempenho desejado para os usuários, a potência de transmissão necessária em ambos os enlaces direto e reverso pode ser feita inversamente proporcional ao número de antenas na BS.

Nesta Tese de Doutorado, diversos aspectos importantes de sistemas MIMO massivo são sistematicamente investigados com o objetivo de melhorar suas eficiências energética e espectral. Pode-se enumerar as principais contribuições alcançadas como se segue. Considerando uma rede celular MIMO massivo, propõe-se uma política de atribuição de sequências de treinamento aos usuários otimizada, a qual é depois combinada com apropriados algoritmos de controle de potência. Também investiga-se a adoção neste cenário de formas de onda alternativas, tal como a transmissão de portadora única, visando superar as deficiências da convencional multiplexagem por divisão de portadoras ortogonais (*orthogonal frequency-division multiplexing* - OFDM). As principais contribuições obtidas neste tema são derivar expressões de desempenho analíticas para um equalizador de portadora única no domínio do tempo que aproveita o grande número de antenas na BS, e avaliar e comparar a eficiência energética total de sistemas MIMO massivo OFDM *versus* portadora única. Finalmente, considerando redes MIMO massivo sobrecarregadas, compostas por usuários humanos bem como dispositivos de comunicação do tipo máquina, propõe-se um protocolo de acesso aleatório melhorado visando diminuir o número médio de tentativas de acesso para os usuários e diminuir a probabilidade de falhas de tentativa de acesso.

Palavras-Chaves: MIMO massivo; eficiência energética; eficiência espectral; atribuição de pilotos; portadora única; controle de potência; acesso aleatório.

Abstract

Massive MIMO communication systems have been highlighted as the main technology for physical layer of next generation communication standards, like 5G. While conventional communication between BS and its covered users is performed in orthogonal time-frequency resources, the improved interuser interference mitigation capability provided by the large number of BS antennas enables the BS to communicate with several users in the same time-frequency resource. This better usage of available but scarce spectrum elevates the spectral efficiency to very appreciable levels, and has a similar effect on energy efficiency, since the transmit power is not increased. On the other hand, if the objective is to provide a target performance for the users, the required transmit power in both direct and reverse links can be made inversely proportional to the number of BS antennas employed.

In this Doctoral Thesis, several important aspects of massive MIMO systems are systematically investigated aiming to improve their energy and spectral efficiencies. We can enumerate our main contributions as follows. Considering a cellular massive MIMO network, we proposed an optimized assignment policy of training sequences to the users, which is then combined with suitable power control algorithms. We have also investigated the adoption of alternative waveforms in this scenario, such as single-carrier transmission, in order to overcome the issues of conventional OFDM. Our contributions in this topic are to derive analytical performance expressions for a time-domain single-carrier equalizer taking advantage of the large number of BS antennas, and to evaluate and compare the total energy efficiency of OFDM *versus* single-carrier massive MIMO systems. Finally, considering crowded massive MIMO networks, composed by both human users as well as machine-type communication devices, we proposed an improved random access protocol aiming to decrease the average number of access attempts for the users and decreasing the probability of failed access attempts.

Keywords: Massive MIMO; energy efficiency; spectral efficiency; pilot assignment; single-carrier; power control; random access.

List of Figures

List of Tables

List of Acronyms

ACB	Access Class Barring
AWGN	Additive White Gaussian Noise
BER	Bit Error Rate
bpcu	Bits per channel use
BS	Base-Station
CDMA	Code Division Multiple Access
CIR	Channel Impulse Response
CP	Cyclic Prefix
CSI	Channel State Information
DL	Downlink
FC	Fast Convolution
FC-TRMRC	Fast Convolution Time-Reversal Maximum-Ratio Combining
FD	Frequency-Domain
FDD	Frequency-Division Duplexing
FDCSI	Frequency-Domain Channel State Information
FDMRC	Frequency-Domain Maximum-Ratio Combining
FFT	Fast Fourier Transform
IFFT	Inverse Fast Fourier Transform
i.i.d.	Independent and identically distributed
IoT	Internet of Things
ISI	Inter-Symbol Interference
LoS	Line-of-Sight
LTE	Long Term Evolution
MF	Matched Filter

MIMO	Multiple-Input Multiple-Output
ML	Maximum Likelihood
MMSE	Minimum Mean Square Error
MRC	Maximum-Ratio Combining
MRT	Maximum-Ratio Transmission
MSE	Mean Square Error
MT	Mobile Terminal
MU-MIMO	Multiuser MIMO
M2M	Machine-to-machine
RF	Radio Frequency
OFDM	Orthogonal Frequency Division Multiplexing
PA	Pilot Assignment
PAPR	Peak-to-Average Power Ratio
PC	Power Control
PDP	Power Delay Profile
QAM	Quadrature Amplitude Modulation
QoS	Quality of Service
QPSK	Quadrature Phase Shift Keying
RA	Random Access
RF	Radio-Frequency
RRC	Radio Resource Control
SC	Single-Carrier
SIC	Successive Interference Cancellation
SISO	Single-Input Single-Output
SINR	Signal-to-Interference-plus-Noise Ratio
SIR	Signal-to-Interference Ratio
SM	Spatial Modulation
SNR	Signal-to-Noise Ratio

SUCRe	Strongest User Collision Resolution
SUCR-IPA	SUCRe combined Idle Pilots Access
SUCR-GBPA	SUCRe combined Graph-Based Pilots Access
TC	Total Capacity
TDD	Time-Division Duplexing
TRMRC	Time-Reversal Maximum-Ratio Combining
UE	User Equipment
UL	Uplink
ZF	Zero Forcing

Notations

Variables definitions

k, γ, M	Scalar, italic character
$\mathbf{a}$	Vector, lower case bold character
$\mathbf{A}$	Matrix, upper case bold character
$\mathcal{A}$	Set, upper case calligraphic character

Operators

$\max(\cdot)$	Returns the maximum element of the argument
$\min(\cdot)$	Returns the minimum element of the argument
$\arg\max_{a \in A}[\cdot]$	Element of the set A that maximizes the argument
$\arg\min_{a \in A}[\cdot]$	Element of the set A that minimizes the argument
$\overline{[\cdot]}$	Mean value of the argument
$\mathbb{E}\{\cdot\}$	Statistical Expectation Operator
$\mathrm{Var}\{\cdot\}$	Statistical Variance Operator
$\lvert a \rvert$	Magnitude Operator (absolute value)
$\lvert \mathbf{a} \rvert$	Cardinality of vector $\mathbf{a}$
$f(a)$	Probability density function of a
$\log_b a$	Logarithm of a in base b
$\ln a$	Natural logarithm of a
$\sum_{a=1}^{N}(\cdot)$	Summation considering $a = 1$ to $a = N$, with unitary increment
$p(a)$	Probability of a
$p(a\|b)$	Conditional Probability of a given b
$p(a, b)$	Joint Probability of a and b
$\Re\{\cdot\}$	Real part of a complex number
$\Im\{\cdot\}$	Imaginary part of a complex number
$\exp(a)$	Exponential of a, i.e., e^a
$\mathrm{Tr}(\cdot)$	Trace operator
$\det(\cdot)$	Determinant operator
$\mathrm{sign}(\cdot)$	Signal operator
$\mathcal{CN}(\mathbf{0}_M, \mathbf{I}_M)$	Complex normal distribution with mean $\mathbf{0}_M$ and covariance $\mathbf{I}_M$
$\mathfrak{B}(K_0, \frac{P_a}{\tau})$	Binomial distribution with number of trials K_0 and success probability $\frac{P_a}{\tau}$

Superscript indexes

$\mathbf{A}^*$	Conjugate of matrix $\mathbf{A}$

$\mathbf{A}^T$	Transpose of matrix $\mathbf{A}$
$\mathbf{A}^H$	Conjugate transpose, or Hermitian transpose, of matrix $\mathbf{A}$
$\mathbf{A}^{-1}$	Inverse of matrix $\mathbf{A}$

Subscript indexes

$\mathbf{a}_i$	i-th element of vector $\mathbf{a}$
$\mathbf{A}_{i,j}$	Element of i-th row and j-th column of matrix $\mathbf{A}$
$\mathbf{A}_k$	Vector represented by the k-th column of matrix $\mathbf{A}$

List of Symbols

N	Number of OFDM subcarriers
N_{CP}	Number of samples in the cyclic prefix
γ	Factor representing the inefficiency of CP transmission
L	Number of CIR taps
N_{sm}	Number of subcarriers per frequency smoothness interval
$\mathcal{T}$	Number of OFDM symbols per channel coherence time
$\mathcal{S}$	Number of symbols per channel coherence block
T_c	Channel coherence time
T_n	Nyquist sampling period
T_d	Largest possible delay spread
T_s	OFDM symbol period
W_c	Channel coherence bandwidth
τ	Length of UL pilot sequences
K	Number of users
K_{max}	Maximum number of users
M	Number of BS antennas
ρ^{u}	UL transmit power
ρ^{d}	DL transmit power
ρ^{p}	UL pilot transmit power
σ_n^2	AWGN variance
$\mathcal{C}$	Channel capacity
C	Number of cells
ν_k	k-th singular value resultant from a singular value decomposition
$\mathcal{I}_k$	Set of subcarriers in which the k-th user sends its pilots
β_{ikj}	Long-term fading power coefficient between the i-th BS and the k-th user at the j-th cell
$\boldsymbol{\Psi}$	Set of orthogonal pilot sequences
$\boldsymbol{\psi}_k$	k-th orthogonal pilot sequence

x^{u}_{kin}	UL data symbol of k-th user of i-th cell in n-th subcarrier
$\widehat{x}^{\mathrm{u}}_{kin}$	Estimated UL data symbol of k-th user of i-th cell in n-th subcarrier
x^{d}_{ik}	DL data symbol transmitted from i-th BS to its k-th user
$y^{\mathrm{d}}_{k'j}$	DL signal received at k'-th MT of j-th cell
$\varsigma^{\mathrm{u}}_{k'i}$	UL SINR of k'-th MT of i-th cell
$\varsigma^{\mathrm{d}}_{k'j}$	DL SINR of k'-th MT of j-th cell
$\varsigma^{\mathrm{u}\infty}_{k'i}$	Asymptotic UL SINR of k'-th MT of i-th cell
$\varsigma^{\mathrm{d}\infty}_{k'j}$	Asymptotic DL SINR of k'-th MT of j-th cell
$s^{\mathrm{u}}_{kj}[t]$	Time-domain UL symbol transmitted by the k-th user of j-th cell at time t
$\widehat{s}^{\mathrm{u}}_{ki}[t]$	Estimated time-domain UL symbol of the k-th user of i-th cell at time t
ξ^{u}	Fraction of the data transmit interval dedicated to uplink transmissions
ξ^{d}	Fraction of the data transmit interval dedicated to downlink transmissions
α	Precoding normalization factor
B	System bandwidth
$\hat{\varsigma}^{\mathrm{d}}_{k'\ell}$	Target DL SINR for the k'-th user of the ℓ-th cell
$\hat{\varsigma}^{\mathrm{u}}_{k'\ell}$	Target UL SINR for the k'-th user of the ℓ-th cell
$\mathcal{R}^{\mathrm{F}}_{k'i}$	Achievable rate of the k'-th user at the ith cell employing FDMRC
$\mathcal{R}^{\mathrm{T}}_{k'i}$	Achievable rate of the k'-th user at the ith cell employing TRMRC
ζ^{f}	Frequency reuse factor
ζ^{p}	Pilot reuse factor
EE	Energy efficiency
P_{TX}	Power consumed by the transmitter power amplifier
η	Power amplifier efficiency
P_{CP}	Circuit power consumption
P_{FIX}	Fixed power consumption
P_{TC}	Power consumption of the transceiver chains
P_{SYN}	Power consumed by the local oscillator
P_{BS}	Power necessary to the circuit components of each BS antenna operate
P_{MT}	Power required by the circuit components of each MT operate
P_{CE}	Power consumption of channel estimation
$P_{\mathrm{C/D}}$	Power consumption of the channel coding and decoding units
$\mathcal{P}_{\mathrm{COD}}$	Coding power density

$\mathcal{P}_{\mathrm{DEC}}$	Decoding power density
$\mathcal{L}_{\mathrm{BS}}$	Computational efficiency at BS
$\mathcal{L}_{\mathrm{MT}}$	Computational efficiency at MTs
$\mathcal{P}_{\mathrm{BT}}$	Backhaul traffic power density
λ	Smoothness parameter of the sigmoid curve
κ	Path-loss exponent
d_{max}	Cell radius
d_{min}	Minimum distance between UEs and BS
$\overline{d}$	Constant regulating the channel attenuation at distance d_{min}
$\mathcal{U}_i$	Set of UEs in cell i
$\mathcal{A}_i$	Set of active UEs in cell i
$\mathcal{K}_0$	Set of inactive UEs in cell 0
K_0	Number of inactive UEs in cell 0
P_a	Probability of each UE becoming active
$c(k)$	Index of the pilot selected by the k-th UE
$\mathcal{Q}_t$	Set of UEs which selected pilot t
$\mathbf{x}$	UL transmit signal vector
$\mathbf{n}$	AWGN sample vector in BS
$\mathbf{y}^{\mathrm{u}}$	UL received signal vector at BS
$\mathbf{g}_{ikjn}$	FDCSI vector between the i-th BS and the k-th user at the j-th cell in the n-th subcarrier
$\underline{\mathbf{g}}_{ikjn}$	Short-term fading vector between the i-th BS and the k-th user at the j-th cell in the n-th subcarrier
$\widehat{\mathbf{g}}_{ikn}$	Estimated FDCSI vector available at i-th BS of its k-th user in the n-th subcarrier
$\mathbf{v}_{ikn}$	Noise vector in FDCSI estimates
$\mathbf{p}_{ik}$	Precoding vector that i-th BS employs for its k-th user
$\mathbf{h}_{ikjt}$	t-th CIR vector tap between the i-th BS and the k-th user of the j-th cell
$\widehat{\mathbf{h}}_{ikt}$	Estimated CIR vector tap available at i-th BS of its k-th user at time t
$\mathbf{r}_i^{\mathrm{u}}[t]$	UL time-domain received signal at the i-th BS in time t
$\mathbf{w}_l$	Channel vector of the l-th interferer to the BS in cell 0
$\mathbf{d}_l$	Random data the l-th interferer transmits

$\mathbf{H}$	Complex matrix containing the Rayleigh distributed flat fading channel coefficients
$\mathbf{\Phi}$	Unitary matrix resultant from a singular value decomposition
$\mathbf{D}_{\nu}$	Diagonal matrix containing singular values resultant from a singular value decomposition
$\mathbf{\Psi}$	Unitary matrix resultant from a singular value decomposition
$\mathbf{Y}_{in}^{\mathrm{p}}$	Received signal matrix during training stage at i-th BS in n-th subcarrier
$\mathbf{N}_{in}^{\mathrm{p}}$	AWGN matrix at BS when receiving pilot signals
$\mathbf{W}$	Interference matrix at BS from adjacent cells
$\mathbf{I}_K$	Identity matrix of size $K \times K$
$\mathbf{0}_M$	Null vector of size M
j	Imaginary number ($\mathrm{j} = \sqrt{-1}$)

Contents

1 Introduction

This chapter aims to introduce the basic concepts regarding some specific massive multiple-input multiple-output (MIMO) problems: pilot assignment (PA), massive MIMO waveforms, power allocation, total energy efficiency evaluation, and random access (RA) in crowded networks. Besides, the major contributions achieved during this Doctoral work are listed. Finally, it is briefly described the structure and organization of this Thesis.

1.1 Concepts and Motivation

Over the past century, the wireless data traffic has grown at an exponential rate [1], as predicted by the Cooper's law. This rapid growth is motivated by new applications that demand increased data transfers, such as video callings and augmented reality, as well as due to the increasing number of connected devices, formulating the concept of Internet of Things (IoT). The fifth generation (5G) wireless networks are expected to provide peak data rates up to 20 Gb/s, average data rates greater than 100Mb/s and connectivity for a dozens thousand devices in a same geographical area [2]. As the communication community makes progress towards such goals following a sustainable evolution, the energy efficiency becomes one of the most important design criterions. In this regard, the massive MIMO technology appears as one of the key enablers for achieving 5G requirements, while being able to handle orders of magnitude more data traffic, and facilitating the network access for a huge number of devices as in the crowded networks.

By coherently processing the signals over the antenna array, transmit precoding can be used in the downlink (DL) to beamform each signal at its desired terminal. Similarly, receive combining can be employed in the uplink (UL) to discriminate between signals sent from different mobile terminals (MTs). As long as the base station (BS) employs many antennas, the spatial focusing can be very accurate. In this regard, while in conventional communications systems either time or frequency resources should be splitted and allocated for different users in order to mitigate multiuser interference, the massive MIMO concept allows several users to communicate simultaneously over the entire available bandwidth. This fundamental difference results in quite appreciable spectral efficiency gains. Besides, as transmit power can be reduced significantly by increasing the number of antennas at BS, and lower levels of circuit power are required due to simple linear processing techniques, the energy efficiency can also be significantly improved [2].

A propagation scenario can be achieved by deploying a large number of antennas at the BS, which is known as favorable propagation. In this scenario, the wireless channel becomes near-deterministic since the different radio links between BS and MTs result asymptotically orthogonal to each other. Such a phenomenon is justified due to the effects of short-term fading, uncorrelated noise, and intra-cell interference gradually disappear with the increasing number of BS antennas, while large multiplexing and array gains can be achieved under favorable

propagation by serving more users and employing more BS antennas, respectively. It was shown in [3] that using an excessive number of BS antennas and under favorable propagation, the simplest linear processing techniques, *e.g.* maximum-ratio combining (MRC) in the UL and maximum-ratio transmission (MRT) in the DL, become nearly optimal. Assuming *independent and identically distributed* (i.i.d.) Gaussian transmit signals and perfect channel state information (CSI) estimates available at the receiver, the instantaneous achievable rate can be expressed as [4]

$$\mathcal{C} = \log_2 \det \left(\mathbf{I}_K + \frac{\rho}{M} \mathbf{H}\mathbf{H}^H \right), \tag{1.1}$$

where K is the number of MTs, $\mathbf{I}_K$ is an identity matrix of order K, ρ is the signal-to-noise ratio (SNR), M is the number of antennas at the BS, $\mathbf{H} \in \mathbb{C}^{K \times M}$ is the channel matrix, and $\{\cdot\}^H$ is the Hermitian operator. The real implications of (1.1) are most easily seen by expressing the achievable rate in terms of the singular values of the propagation matrix, $\mathbf{H} = \mathbf{\Phi}\mathbf{D}_\nu\mathbf{\Psi}^H$, in which $\mathbf{\Phi}$ and $\mathbf{\Psi}$ are unitary matrices of dimension $K \times K$ and $M \times M$, respectively, and $\mathbf{D}_\nu$ is a diagonal matrix whose diagonal elements are the singular values, $\{\nu_1, \nu_2, \ldots \nu_K\}$. Thus, the achievable rate in (1.1) can be alternatively expressed as

$$\mathcal{C} = \sum_{k=1}^{K} \log_2 \left(1 + \frac{\rho \nu_k^2}{M} \right), \tag{1.2}$$

which can be seen as the combined achievable rates of K parallel links of SNR $\rho\nu_k^2/M$. In order to analyze the worst and the best possible results for the achievable rates in (1.2), we first obtain the following constraint

$$\mathrm{Tr}\left(\mathbf{H}\mathbf{H}^H\right) = \mathrm{Tr}\left(\mathbf{\Phi}\mathbf{D}_\nu\mathbf{\Psi}^H\mathbf{\Psi}\mathbf{D}_\nu\mathbf{\Phi}^H\right) = \mathrm{Tr}\left(\mathbf{\Phi}^H\mathbf{\Phi}\mathbf{D}_\nu\mathbf{\Psi}^H\mathbf{\Psi}\mathbf{D}_\nu\right) = \mathrm{Tr}\left(\mathbf{D}_\nu\mathbf{D}_\nu\right) = \sum_{k=1}^{K} \nu_k^2.$$

Assuming normalized magnitudes for the propagation coefficients in the channel matrix such that $\mathrm{Tr}\left(\mathbf{H}\mathbf{H}^H\right) = K\,M$, we have that

$$\mathrm{Tr}\left(\mathbf{H}\mathbf{H}^H\right) = \sum_{k=1}^{K} \nu_k^2 = K\,M,$$

which fixes the sum of the squared singular values. As a simple consequence of the concavity of the logarithmic function, among all channel matrices satisfying this constraint, the worst case occurs with that having only one non-zero singular value, while the best achievable rate are achieved by the ones with all equal singular values. One can associate the worst case result to a scenario with line-of-sight (LoS) propagation, while the best case can be approached in the limit by a scenario where all of the channel coefficients are i.i.d.. Thus, the achievable rate in (1.1) are confined to the following interval

$$\log_2 \left(1 + \frac{\rho \mathrm{Tr}\left(\mathbf{H}\mathbf{H}^H\right)}{M} \right) \leq \mathcal{C} \leq K \log_2 \left(1 + \frac{\rho \mathrm{Tr}\left(\mathbf{H}\mathbf{H}^H\right)}{KM} \right), \tag{1.3}$$

$$\log_2 \left(1 + \rho K \right) \leq \mathcal{C} \leq K \log_2 \left(1 + \rho \right). \tag{1.4}$$

By letting the number of BS antennas grows largely while keeping fixed the number of MTs, the following asymptotic condition is assured by the law of the large numbers: $\frac{1}{M}\mathbf{H}\mathbf{H}^H \approx \mathbf{I}_K$. Thus, the achievable rate in (1.1) becomes

$$\mathcal{C} = \log_2 \det \left(\mathbf{I}_K + \rho \mathbf{I}_K \right) = K \log_2 \left(1 + \rho \right), \tag{1.5}$$

which matches the upper bound in (1.4), demonstrating that the asymptotic orthogonality of massive MIMO leads to the best achievable rates of a MIMO communication system. It can also be shown that simple MRC processing at BS can achieve the capacity in (1.5). Expressing the UL received symbol at BS as

$$\mathbf{y}^{\mathrm{u}} = \sqrt{\rho^{\mathrm{u}}}\mathbf{H}^{T}\mathbf{x} + \mathbf{n}, \tag{1.6}$$

in which ρ^{u} is the UL SNR, $\{\cdot\}^{T}$ is the transpose operator, $\mathbf{x} \in \mathbb{C}^{K\times 1}$ is the transmit symbol vector, and $\mathbf{n} \in \mathbb{C}^{M\times 1}$ is the additive white Gaussian noise (AWGN) vector. The BS using MRC rule multiplies the received signal by the conjugate of the channel matrix:

$$\begin{aligned} \mathbf{H}^{*}\mathbf{y}^{\mathrm{u}} &= \sqrt{\rho^{\mathrm{u}}}\mathbf{H}^{*}\mathbf{H}^{T}\mathbf{x} + \mathbf{H}^{*}\mathbf{n}, \\ &\approx M\sqrt{\rho^{\mathrm{u}}}\mathbf{x} + \mathbf{H}^{*}\mathbf{n}. \end{aligned} \tag{1.7}$$

It is important to note that the filtered noise term $\mathbf{H}^{*}\mathbf{n}$ in (1.7) remains white, since the columns of matrix $\mathbf{H}$ are asymptotically orthogonal. Thus, the MRC processing separates the signals from different MTs into different streams, asymptotically eliminating the inter-user interference; hence, the signals transmissions from different users can be treated as if they came from a single-input-single-output (SISO) channel with equivalent SNR ρ^{u}. Therefore, the rate achieved by the MRC receiver in this case is

$$\mathcal{C}_{\mathrm{MRC}} = K\log_2\left(1+\rho^{\mathrm{u}}\right), \tag{1.8}$$

which matches the upper bound (1.4), and thus the simple MRC receiver is asymptotically optimal with infinite number of BS antennas, *i.e.*, when $M \to \infty$. Similar derivation for DL shows the optimality of the simple MRT scheme.

Another notorious benefit attained by favorable propagation in massive MIMO channels can be observed as the channel becomes nearly deterministic, and hence different resource allocation schemes such as power control and user scheduling can be performed based on long-term fading coefficients, instead of short-term fading ones. Thus, the obtained solutions can be found at a lower computational complexity while remaining valid for a larger time period.

1.1.1 Pilot Contamination

The main phenomenon that limits the performance of massive MIMO systems is pilot contamination [3]. The BS requires CSI estimates to enable suitable communication in both UL and DL. Thus, in time-division duplex (TDD) systems, the MTs send UL pilot sequences to enable the BS estimating the UL channel, while the DL channel is obtained by reciprocity. The coherence time of the channel (T_c) is limited due to the users' mobility, and thus also the time available for pilot transmissions. This fact in conjunction with the limited system bandwidth makes the number of available pilot sequences restricted, in such a way that some users in different cells have to reuse the same sequence. Therefore, while the BS tries to estimate the CSI of its covered users, it inadvertently estimates the channel of the users reusing such pilots. As a result, in the DL the transmitted signals from this BS will be partially beamformed to the users reusing such pilots, while in UL the receiver processing will separate the signals of users reusing pilots in the same way as it does for the

intended users. This pilot contamination interference, also referred as coherent interference in [5], is harmful, since it does not vanish with the increasing number of BS antennas.

The performance of the massive MIMO system can be improved by suitably assigning the pilot sequences to the users in a given cell if the adopted PA strategy is able to mitigate the pilot contamination effect. This occurs since the pilot contamination interference is proper of each pilot sequence: it reflects the directed UL interference from users in adjacent cells reusing this sequence, or the directed DL interference from adjacent BS's to a given user in the considered cell. Thus, one can for example assign in a given cell the sequences with higher pilot contamination interferences to the users with better channel conditions, when adopting a fairness metric. The PA problem was solved in [6] from the UL perspective, and a low-complexity near-optimal solution was proposed. Such simple and very efficient solution was possible due to the simple dependence between performance and pilot assignment seen in UL, as discussed in Chapter 3. Pilot contamination interference in UL is due to the signals transmitted from users in adjacent cells sharing a given pilot sequence that reaches certain BS. The user that will experience such interference is the one to which this pilot sequence is assigned in the cell. Under a max-min optimization perspective, the solution proposed in [6] simply assigns the worst pilot sequences in a given instant, in terms of pilot contamination arising from adjacent cells, to the best located users, *i.e.*, those with the higher long-term fading coefficients.

The pilot assignment should be unique within a coherence interval, since it would not be practical to reassign the pilots during the frame transmission. Besides, in the TDD architecture, there exist UL and DL data transmissions in a given coherence interval. Therefore, if a pilot assignment strategy like the scheme of [6] is designed only for optimizing the UL performance, the DL performance will not be improved. Similarly, several other pilot assignment schemes, for instance, those proposed in [7] and [8] are designed for only optimizing DL performance, while not improving the UL one. In this Doctoral work, we have demonstrated that a pilot assignment strategy able to jointly optimize UL and DL performance can be much more suitable in order to improve the overall massive MIMO system performance.

1.1.2 Power Allocation Strategies

Several power allocation schemes have been proposed for massive MIMO systems. These schemes can be conceived based on different problem formulations. One can for example attempt to maximize the sum rate of the cell [9]. However, the solution of such problem may lead to very unfair situations, with few users transmitting at very high rates and the rest transmitting at low rates. There exist another fairer formulations, like max-min approaches [5], which try to maximize the lowest rate of the system, and the proportional fairness [10], which attempts to maximize the logarithmic sum of the rates within the cell. By the concavity of the logarithmic function, incrementing the rate of a user in bad channel conditions may have a higher impact on objective function than improving the rate of a user already in good conditions, automatically achieving fairness.

Another classical power control algorithm allocates for each user the exact power required for achieving a desired signal-to-interference ratio (SIR), which is known as target-SIR-tracking algorithm [11]. However, some users in high multiuser interference conditions would require a very increased power to achieve the target

SIR, which exceeds the maximum transmit power constraint for this user. In this case, the algorithm of [11] allocates for this user his maximum transmit power. In [12], it is shown that this is not the most suitable strategy, since this class of users will consume a significant amount of power, irradiating increased interference levels for other users, while still achieving a poor performance. So, in the opportunistic power allocation algorithm proposed in [12], the users who cannot achieve the target-SIR in a given iteration are allocated a decreasing power level. This procedure after some iterations results in lower levels of interference for all users, and thus can increase the number of users achieving their target performance. In this Doctoral work, we have adapted the opportunistic power control algorithm of [12] to the massive MIMO scenarios; moreover, we have investigated its performance when combined with suitable pilot allocation schemes.

1.1.3 Single-Carrier *vs* Multicarrier Waveforms in Massive MIMO

Most results of massive MIMO literature consider orthogonal frequency-division multiplexing (OFDM) modulation, due to its robustness against inter-symbol interference (ISI), and low complexity fast Fourier transform (FFT) implementation. However, OFDM has several impairments that motivates the investigation of alternative waveforms, like increased peak-to-average power ratio (PAPR) and cyclic-prefix (CP) transmission requirement. Such impairments limit both the spectral and the energy efficiencies of the massive MIMO systems. Another waveform topology that has recently attracted some research attention is single-carrier (SC) waveform. The time-reversal MRC (TRMRC) receiver proposed in [13] is able to deal with the time-dispersive fading channel, while presenting lower PAPR and not requiring CP transmissions. However, the performance of TRMRC receiver had not been investigated yet in realistic massive MIMO scenarios, in the presence of pilot contamination. In this Thesis, we derive an analytical performance expression of TRMRC receiver under pilot contamination, validating the results by extensive numerical simulations. We then compare the performance of this technique with that of conventional MRC receiver under OFDM waveform, in terms of achievable rates. Besides, after our computational complexity study indicating the complexity of TRMRC receiver may be high in some cases, we have proposed a low-complexity implementation with the aid of the overlap-and-add technique.

1.1.4 Energy Efficiency in Massive MIMO

The total energy efficiency metric computes how many bits are transmitted per joule of energy, but taking into account every energy expenditure of the communication system. It can be defined as

$$\mathrm{EE} = \frac{\sum_{k=1}^{K} \left(\mathcal{R}_k^{\mathrm{UL}} + \mathcal{R}_k^{\mathrm{DL}}\right)}{P_{\mathrm{TX}}^{\mathrm{UL}} + P_{\mathrm{TX}}^{\mathrm{DL}} + P_{\mathrm{TX}}^{\mathrm{tr}} + P_{\mathrm{CP}}}, \tag{1.9}$$

in which $\mathcal{R}_k^{\mathrm{UL}}$ and $\mathcal{R}_k^{\mathrm{DL}}$ are the UL and DL rates of the kth user, while $P_{\mathrm{TX}}^{\mathrm{UL}}$, $P_{\mathrm{TX}}^{\mathrm{DL}}$ and $P_{\mathrm{TX}}^{\mathrm{tr}}$ represent the power consumed by the power amplifiers in UL, DL, and UL pilot transmission, respectively. Moreover, P_{CP} accounts for the circuit power consumption, which can be assumed as a fixed parameter in a simplistic model, or as a quantity dependent on several factors in more accurate power consumption models [14].

In [14], the authors have assessed the total energy efficiency of massive MIMO systems operating with OFDM waveform, and have concluded that the optimal energy efficiency is attained with a massive MIMO

setup wherein hundreds of antennas are deployed to serve a relatively large number of users if using zero forcing processing. Accurate power consumption models are presented in [14] for the several stages of a practical communication system, like the power consumed by the transceiver chains, the channel estimation process, the coding and decoding units, the backhaul, the linear processing algorithms, and also by the radiated signal power. In this Doctoral work, we have also evaluated the total energy efficiency of the massive MIMO system employing both the TRMRC receiver and the conventional MRC receiver with OFDM, and compared the results. Since the total energy efficiency metric can weight in a unified way the higher achievable rates of TRMRC and the lower processing energy of the conventional MRC with OFDM, it can provide a more accurate and fair comparison.

1.1.5 Connectivity in Machine-type Massive MIMO Communication

When the number of user equipments (UEs) within the cell is small, no pilot contamination occurs between UEs of the same cell, since it can be allocated an exclusive pilot for each UE in order to obtain CSI estimates. However, in crowded scenarios, like machine-to-machine (M2M) communications, urban environment and hotspots, it is very likely that the number of UEs inside the cell is higher than the number of available pilot resources, and thus a pilot random access protocol should be employed. One classic approach to deal with congestion control in crowded networks is the access class barring (ACB) mechanism [15]. When a machine-type communication device intends to initiate a transmission, it generates a random number between 0 and 1 and compares it with the ACB factor broadcast by the BS. If the number is lower than the ACB factor, the device proceeds to access the network. Otherwise, it needs to back off temporarily and try again later [15]. This ACB factor is dynamically obtained based on the number of available pilots and the number of backlogged users. This congestion control strategy has been reformulated in order to be applied to a M2M MIMO LTE network in [16], in which the authors proposed an adaptive algorithm to iteratively update the ACB factor aiming to reduce the average number of RA attempts without requiring the BS knowing the number of backlogged users in the system.

More recently, it has been shown that the massive MIMO properties of favorable propagation and channel hardening [3], [5] can be very beneficial in order to improve the RA performance of a crowded network. In [17], a distributed queueing random access protocol is proposed for congestion control in M2M networks combined with moderate scale MIMO. However, the proposed protocol detects pilot collisions under a centralized manner at the BS, what may overload the system in very crowded networks. Several works have been disseminated in the last year aiming to improve RA performance in a decentralized fashion by exploiting massive MIMO properties. The strongest-user collision resolution (SUCRe) protocol proposed in [18] is a very efficient solution to improve RA functionality in crowded massive MIMO networks, being able to resolve around 90% of all collisions. Furthermore, the SUCRe protocol exploits the massive MIMO properties of channel hardening and favorable propagation in order to enable distributed collision detection and resolution at the UEs, being thus highly scalable with respect to the number of UEs in the cell.

Some other RA protocols derived from SUCRe are proposed in [19] and [20]. In the SUCRe combined idle pilots access (SUCR-IPA) proposed in [19], the BS detects the idle pilots after the UEs' pilot transmission in the initial stage, and broadcasts the indexes of these pilots as well as an ACB factor to the UEs in the next stage.

Then, the UEs who did not judge themselves as the strongest ones in the third stage reselect a pilot based on the indexes of idle pilots and the ACB factor. As shown in [19], a marginal RA performance improvement can be achieved by this scheme, however at the cost of an increased overhead due to the required information exchange, which decreases the spectral efficiency of the entire system. Similarly, the BS also broadcasts the indexes of idle pilots in the second stage of the SUCRe combined graph-based pilots access (SUCR-GBPA) proposed in [20], but no ACB factor. Then, all failed UEs randomly select a pilot from the set of idle pilots after the initial step. A bipartite graph is established where active UEs and selected pilots are considered variable nodes and factor nodes, respectively. Based on this bipartite graph, a successive interference cancellation (SIC) algorithm is employed to obtain CSI estimates of each UE. One of the main drawbacks of this protocol is also the increased overhead due to the broadcasting of idle pilots indexes. Besides, the CSI estimates present significant errors due to the SIC process, and a slightly more complex processing is required at BS.

Another RA strategy in crowded massive MIMO networks does not focus in avoiding pilot collisions, but in developing robust coding schemes capable of assuring the communication even in the presence of pilot collisions. In the protocol proposed in [21], the transmission is organized into transmission frames consisting of multiple transmission slots. When a given UE has a data codeword to transmit, it divides the codeword into multiple parts and, within a transmission frame, and it transmits the codeword parts in multiple transmission slots. The channels are estimated from UL pilots every time the device transmits. In each time slot, each active UE pseudo-randomly selects a pilot sequence from a predetermined pilot codebook and, during the rest of the slot, it sends a part of the data codeword. Hence, a device performs pilot-hopping over multiple slots and the hopping pattern can be used by the BS to identify the device and appropriately merge and decode the parts of its codeword. This alternative approach of improving coding schemes in conjunction with pilot-hopping seems to be promising, but due to its increased complexity, the former approach of avoiding pilot collisions has attracted much research attention recently; therefore, the former strategy is on the focus of this Doctoral work. It is worth noting that an efficient RA protocol employed in a crowded massive MIMO network also contributes to improve the overall spectral and energy efficiencies, since it alleviates the amount of control information required to be exchanged between BS and UEs, and decreases the number of RA attempts required to establish connection as well as the transmitted energy.

Inspired by the above discussion, in this Doctoral work, we investigate these massive MIMO optimization problems under the perspectives of improving the system spectral and energy efficiencies. In summary, in such scenario, pilot assignment schemes are proposed in conjunction with power control, capacity bounds are derived under practical constraints such as pilot-contaminated CSI estimates, intercell interference, and low-complexity processing. Based on the massive MIMO analysis conducted, resource allocation, random access and system designs are also discussed.

1.2 Justification and Problematics

Arguably, massive MIMO technology can offer several advantages that meet the modern wireless communication systems' requirements. However, some few technical challenges should be surpassed in order to enable the implementation of such systems, among which we can highlight:

- **Deploying large number of antennas and radio-frequency (RF) chains**: the allocation of an increased number of antennas in a practical BS remains a challenging problem. Considering a limited physical space, the densification of antenna elements reduces the distances among them, increasing correlation between channel coefficients and reducing achievable rates. Amongst the most promising strategies to overcome this problem, we can highlight: (**i**) Using high-frequency carriers, which reduces the wavelength and thus the required space to avoid channel correlation; (**ii**) Three dimensional configurations of antenna arrays; (**iii**) Spatial modulation (SM), in which a limited number of the available antennas are activated, and the indexes of the active elements carry information; (**iv**) Investigation of techniques that bring the massive MIMO benefits by requiring a not so large number of antennas. As this issue of large number of RF chains is not the focus of this Doctoral work, only the latter strategy is considered herein, in such a way that a recurrent concern when analyzing our proposed topologies is to verify their performances with finite number of BS antennas.

- **Multicelular operation and pilot contamination**: several challenges appear when considering the massive MIMO in a multicellular environment, and the pilot contamination is arguably one of the most salient. A conventional way of mitigating intercell interference is by means of multicell coordination, in which some information amount is shared between adjacent cells within a cluster via a backhaul link; such strategy enables the BS to adjust its transmit signals in order to reduce interference irradiated to neighbor cells. However, this may not be a feasible solution for massive MIMO systems, since the amount of information to be shared would overload the backhaul link, due to the excessive number of BS antennas. Thus, another strategies to mitigate pilot contamination should be investigated. In this Doctoral work, we address the pilot assignment and power allocation as alternative techniques to mitigate pilot contamination problem.

- **Spectral and energy efficiencies issues**: massive MIMO is a promising candidate technology to reach the spectral efficiency requirements of the upcoming 5G standard, and the environmental concerns of modern society obligate such gains to be achieved at the cost of reduced energy resources. In order to achieve these goals, several topics have to be investigated; for instance, evaluating the performance of the massive MIMO system equipped with cheap, low-power and non-ideal hardware. Besides, most papers in the area assume the adoption of OFDM modulation, which has several drawbacks such as the CP transmission requirement, that harms both spectral and energy efficiencies, and increased PAPR, which either requires a highly-linear energy-inefficient power amplifier, or distorts the transmit signal incurring in intercarrier interference and out-of-band emissions. Thus, the investigation of alternative waveforms is also relevant, and constitutes an important research topic in the context of massive MIMO systems. Traditional single-carrier waveform has been demonstrated to be a promising solution [13]. However, its ability to suitably operate in time-dispersive fading channels and to cope with pilot contamination have not been investigated yet. Therefore, in this Doctoral work we also investigated a time-domain single-carrier equalization scheme, namely TRMRC, which, by taking advantage of the large number of BS antennas, is able to deal with inter-symbol interference and pilot contamination, while not requiring CP transmission and having lower levels of PAPR. Then, we have evaluated its total energy efficiency by adopting realistic models of power consumption for all the components of the communication system, and compared the attainable total energy efficiency with the conventional OFDM massive MIMO systems

aiming at finding out the most efficient scheme.

- **Random access functionality in crowded networks**: the number of wirelessly connected devices and their respective data traffic are growing as we evolve into the next generation telecommunication standard. M2M applications have become the dominant communication paradigm of IoT. Hence, future cellular networks need to handle urban deployment with massive number of connected devices requesting massive data volumes [18]. In these crowded scenarios, it is very likely that the number of devices within the cell is much larger than the number of available pilot sequences, and thus the random access functionality becomes essential to share the limited number of pilots among the UEs. It has been shown recently that massive MIMO technology can significantly improve the RA performance in crowded networks, enabling the UEs to detect and resolve pilot collisions in a decentralized way, as proposed in the SUCRe protocol [18]. Indeed, in this Doctoral work, we revisit the SUCRe protocol, showing that we can improve the RA performance by adopting a soft decision retransmission criterium instead of the hard decision rule of [18].

1.3 Scope and Research Objectives

1.3.1 Scope

Based on the fundamental aspects and on the presented content of Section 1.1, it can be highlighted the main concepts considered in this work:

- **Massive MIMO**: Wireless communication systems deploying a massive number of transmit or receive antennas are the major theme of this work;
- **System Performance**: Main metric of evaluation and optimization considered in this work, usually evaluated here in terms of spectral efficiency and/or energy efficiency, or even bit-error rates (BERs);
- **Pilot Assignment**: Methods of distributing the training sequences among the active users in such a way that the pilot contamination affecting channel estimates is mitigated; such issue, also addressed in this work, remains paramount in the determination of the massive MIMO system performance;
- **Massive MIMO Waveforms**: As discussed above, OFDM presents some important drawbacks that limit the energy efficiency of the system, and may become critical in the massive MIMO scenarios. Thus, investigating the deployment of alternative waveforms like single-carrier in massive MIMO systems also constitutes a goal of this work;
- **Power Allocation**: There are several formulations for the massive MIMO power allocation problem, depending on what performance metric is considered and the desired level of system fairness. Investigating such formulations as well as proposing efficient algorithms to find their solutions also constitutes another concern of this work.
- **Random Access**: The random access functionality becomes essential to share the scarce number of pilot resources among the massive number of UEs in a (over)crowded network, and massive MIMO plays

a key role in this sense. Another objective delineated in this Thesis is to seek contributions aiming at improving the RA performance of crowded massive MIMO networks, by decreasing the average number of access attempts and the probability of failed access attempts; as a consequence, the spectral and energy efficiencies of such systems can be improved.

1.3.2 Objectives

This Doctoral Thesis has the following objectives:

1. **General**: Systematic analysis of promising solutions for the investigated massive MIMO optimization problems: pilot assignment, massive MIMO waveforms, power control, total energy efficiency, and random access in crowded networks. The following metrics are analyzed: a) the performance *versus* implementation complexity trade-off, and b) energy efficiency *versus* spectral efficiency analysis of the proposed schemes, aiming to ellaborate an implementation feasibility study of such schemes for future massive MIMO communication systems.

2. **Specific**:

   (a) Numerical simulation results of multiuser massive MIMO systems under investigation considering: *i*) efficient pilot assignment schemes, *ii*) the use of alternative waveforms like single-carrier, *iii*) employing power control algorithms conceived from different problem formulations, and *iv*) improved RA protocols aiming to reduce the average number of access attempts as well as the probability of failed access attempts;

   (b) Analytical performance results are derived considering the statistical distribution of the related parameters, possibly employing slight simplifications in the problem formulation to improve mathematical tractability, when necessary;

   (c) Computational complexity analysis and spectral/energy efficiency evaluation of the investigated and proposed schemes, in order to portray an implementation feasibility framework of such schemes operating in future massive MIMO communication systems. Aiming to provide a more reliable perspective of the investigated schemes, the total energy efficiency metric is also adopted, incorporating the power expenditures of the system as a whole.

1.4 Organization of the Text

The remainder of this Thesis is organized as: In the Chapter 2, it is defined the adopted system model, as well as some concepts about multiuser massive MIMO systems. It is highlighted the major problems investigated in this work involving massive MIMO systems: pilot assignment, massive MIMO waveforms, power allocation, total energy efficiency evalution regarding different waveforms, and random access in crowded networks.

The Chapter 3 presents the main contributions regarding the problem of pilot assignment and power control in massive MIMO systems, also developed in the Appendices A, C, D. We show that the system performance can be significantly improved by suitably assigning the available pilots among the users within

the cell, and that even higher gains can be achieved by combining this pilot assignment strategy with distinct power control schemes.

In the Chapter 4 we present our main results regarding the investigated problems of massive MIMO waveforms and total energy efficiency evaluation, also shown in the Appendices B and E. We first evaluate the performance of TRMRC in the presence of pilot contamination, deriving lower bounds analytical expressions for its achievable rates. We also propose a low-complexity implementation of this scheme, as well as a method to determine the optimum number of scheduled users in order to maximize the sum rate of the cell. Then, we evaluate the total energy efficiency of the massive MIMO system employing TRMRC and employing conventional OFDM waveform, adopting realistic power consumption models. By comparing the results, and considering the evolution of processing efficiency of computers, we indicate and forecast the most efficient scheme to be employed in the uplink of massive MIMO systems.

Chapter 5 presents our main contributions regarding the problem of random access in (over)crowded massive MIMO networks, with further ellaboration in Appendix F. As shown in [18], deploying a massive MIMO BS in a crowded cellular network allows the UEs to detect and resolve pilot collisions, under a decentralized and uncoordinated manner in the SUCRe protocol. By introducing the concept of probability retransmission, we have improved the RA performance of SUCRe protocol by employing a soft decision retransmission criterium instead of the hard decision rule of the original SUCRe.

The Chapter 6 brings the main conclusions obtained along the development of this Doctoral work, summarizing our main results obtained and highlighting our contributions.

Finally, it is worth noting that Appendices A to F constitute the main results obtained in the form of scientific papers. The first, second, third and fourth papers are already published, while the fifth and the sixth are under review for possible publication in specialized journals.

1.5 Summary of contributions and generated publications

In the following, it is enumerated the main contributions achieved during this Doctoral work. Besides, it is also summarized the scientific production directly and indirectly related to the development of this Thesis, respectively, since the student admission in the Doctorate Program of the EPUSP (February/2016) until the present moment.

1.5.1 Contributions of this Doctoral work

1. **Pilot Assignment**: we first propose a PA method designed to optimize the DL performance under a max-min approach. Then, it was investigated the conflicting behavior between DL and UL PA methods, *i.e.*, if a single link is optimized, the performance in the other link is close to that achieved with random PA. We have thus proposed a PA method able to achieve a significant performance improvement in UL and DL simultaneously, based on the total capacity metric.

2. **Power Control**: we have adapted the opportunistic power control algorithm of [12] to the massive MIMO scenarios with finite number of antennas, as well as investigated its performance when combined

with suitable pilot assignment schemes.

3. **Massive MIMO Waveforms**: we have investigated the employment of SC waveform in the UL of massive MIMO systems. More specifically, we have derived analytical SINR performance expressions for the TRMRC receiver in the presence of pilot contamination, as well as lower bounds for the achievable rates. We also proposed a low-complexity implementation of the TRMRC receiver, as well as an iterative method for obtaining the number of scheduled users able to maximize the system sum-rate.

4. **Total Energy Efficiency Evaluation**: we have evaluated the total energy efficiency of massive MIMO systems employing OFDM and SC waveforms in the UL, aiming to provide a more accurate and fair comparison. Besides, the analysis has pointed out the most efficient waveform to be implemented in the UL of such systems, and how this scenario may change with decreasing cell radius and increasing computational efficiency.

5. **Random Access in Massive MIMO Crowded Networks**: we have proposed the soft retransmission criterion in order to improve the RA performance of the SUCRe protocol, introducing the idea of retransmission probability. Firstly, it was proposed to obtain this probability by mapping the ratio between the long-term fading of a given UE and the estimated sum of the contenders' signal gains with the aid of a sigmoid function. Then, we proposed to relate this probability with the probability of a given UE being the strongest contender, while an approximated expression for computing this probability has been proposed based on the information available at the UE side.

1.5.2 Publications directly associated to the theme

1. J. C. Marinello F., T. Abrão. **Pilot distribution optimization in multi-cellular large scale MIMO systems**. Full paper published in the *International Journal of Electronics and Communications (AEUE)* journal (IF$= 0.786$, B1-Eng. IV in QUALIS-CAPES), in August 2016. Copy of the published article presented in Appendix A.

2. J. C. Marinello F., C. M. Panazio, T. Abrão. **Uplink Performance of Single-Carrier Receiver in Massive MIMO with Pilot Contamination**. Full paper published in the *IEEE Access* journal (IF$= 1.270$, A2-Eng. IV in QUALIS-CAPES), in May 2017. Copy of the published article presented in Appendix B.

3. J. C. Marinello F., C. M. Panazio, T. Abrão. **Joint uplink and downlink optimization of pilot assignment for massive MIMO with power control**. Full paper published in the *Emerging Telecommunications Technologies (ETT-Wiley)* journal (IF$= 1.535$, A2-Eng. IV in QUALIS-CAPES), in December 2017. Copy of the published article presented in Appendix C.

4. J. C. Marinello F., C. M. Panazio, T. Abrão. **Massive MIMO pilot assignment optimization based on total capacity**. Full paper published in the *Telecommunication Systems* journal (IF$= 0.822$, A2-Eng. IV in QUALIS-CAPES), in April 2018. Copy of the published article presented in Appendix D.

5. J. C. Marinello F., C. M. Panazio, T. Abrão, S. Tomasin. **Total Energy Efficiency of TD- and FD-MRC Receivers for Massive MIMO Uplink.**. Full paper submitted to the *IEEE Systems Journal*

(IF$= 3.882$, A1-Eng. IV in QUALIS-CAPES), in February 2018. Copy of the submitted article presented in Appendix E.

6. J. C. Marinello F., T. Abrão, E. de Carvalho, P. Popovsky. **Collision Resolution Protocol via Soft Decision Retransmission Criterium.**. Letter submitted to the *IEEE Transactions on Vehicular Technology* journal (IF$= 4.066$, A1-Eng. IV in QUALIS-CAPES), in June 2018. Copy of the submitted article presented in Appendix F.

1.5.3 Publications indirectly associated to the theme

1. C. H. A. Tavares, J. C. Marinello F., C. M. Panazio, T. Abrão. **Input Back-Off Optimization in OFDM Systems Under Ideal Pre-Distorters**. Full paper published in the *IEEE Wireless Communications Letters* journal (IF$= 1.982$, A1-Eng. IV in QUALIS-CAPES), in June 2016.

2. J. C. Marinello F., F. Ciriaco D. N., T. Abrão. **Bit-error-rate minimisation in multiuser transmission schemes for multiple-input-multiple-output communication with increasing number of base station antennas**. Full paper published in the *IET Communications* journal (IF$= 0.742$, B1-Eng. IV in QUALIS-CAPES), in November 2015.

2 Massive MIMO System Model

This chapter aims to describe the multiuser massive MIMO system model, which is the main scenario adopted in this work. It will be discussed the system model for both reverse and forward links, being presented both the frequency and time descriptions of the investigated scenario. Then, we describe some slight modifications necessary to model a crowded network. Besides the theoretical fundamentals, it is also discussed the main advantages, challenges, and issues regarding the systems in which these concepts are applied.

2.1 System Model

Similarly as [3], we consider a MIMO system composed by C BSs, each equipped with M transmit antennas, and communicating with K single-antenna users. Since TDD is assumed, reciprocity holds, and thus CSI is acquired by means of uplink training signals. We divide the system model description for OFDM and SC waveforms. Besides, the following system model is also valid when employing non-unitary frequency reuse if only users and cells sharing the same subband are considered.

2.1.1 Conventional OFDM waveform

The time-frequency resources are divided into channel coherence blocks of $\mathcal{S} = \lfloor T_c W_c \rfloor$ symbols [22], in which T_c is the channel coherence time in seconds, and W_c is the channel coherence bandwidth in Hz ($W_c = \frac{1}{T_d}$ holds, in which T_d is the largest possible delay spread). Each coherence time interval is divided into $\mathcal{T}$ OFDM symbols ($T_c = \mathcal{T} T_s$, and T_s is the OFDM symbol period), distributed as uplink pilot transmissions, downlink and uplink data transmissions [3]. Using orthogonal pilot sequences, the number of available sequences is equal to its length, τ. CSI is estimated in the frequency domain in the same way as in [3]. If the system employs N subcarriers, and the channel impulse response (CIR) has L i.i.d. taps, the frequency smoothness interval is composed of $N_{\mathsf{sm}} = N/L$ subcarriers. Thus, each user does not need to send pilots in all the N subcarriers, but only in $N/N_{\mathsf{sm}} = L$ equally spaced subcarriers, since the frequency domain CSI (FDCSI) for the intermediate ones can be obtained by interpolation. Up to τ users can send pilots in the same subcarriers in the training stage, and a maximum total number of $K_{\mathsf{max}} = \tau N_{\mathsf{sm}}$ users can be served by each cell. We define the set of subcarriers in which the k-th user sends pilots as $\mathcal{I}_k = \{\mathcal{I}_k(0), \mathcal{I}_k(1), \ldots, \mathcal{I}_k(L-1)\}$, such that $\mathcal{I}_k(0) \in [0, N_{\mathsf{sm}} - 1]$ and $\mathcal{I}_k(i) - \mathcal{I}_k(i-1) = N_{\mathsf{sm}}, \forall i = 0, 1, \ldots, L-1$. Figure 2.1 illustrates how training and data transmission stages are divided in time and frequency domains for a given user, in which T_n is the Nyquist sampling period.

We denote the $M \times 1$ FDCSI vector between the i-th BS and the k-th user at the j-th cell in the n-th

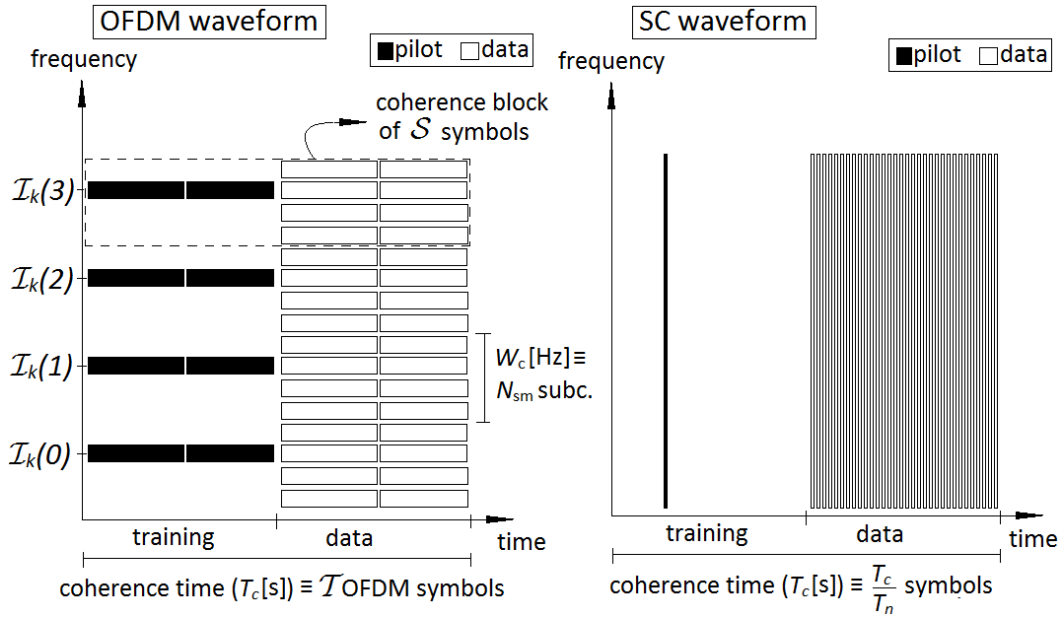

Figure 2.1: Time-frequency diagram illustrating how training and data transmission stages are configured in time-frequency domains, considering OFDM and SC waveforms: $N = 16$, $L = 4$, $N_{\text{sm}} = 4$, $\mathcal{T} = 4$, $\mathcal{S} = 16$ for OFDM; $T_c/T_n = 32$ for SC. Note that $K_{\text{max}} = 8$ for both schemes.

subcarrier by $\mathbf{g}_{ikjn} = \sqrt{\beta_{ikj}}\underline{\mathbf{g}}_{ikjn}$, in which β_{ikj} is the long-term fading power coefficient, that comprises path loss and log-normal shadowing, and $\underline{\mathbf{g}}_{ikjn}$ is the short-term fading channel vector, that follows $\underline{\mathbf{g}}_{ikjn} \sim \mathcal{CN}(\mathbf{0}_M, \mathbf{I}_M)$. The orthogonal pilot sequences' set is $\boldsymbol{\Psi} = [\boldsymbol{\psi}_1\, \boldsymbol{\psi}_2 \ldots \boldsymbol{\psi}_\tau] \in \mathbb{C}^{\tau\times\tau}$, and $\boldsymbol{\Psi}^H\boldsymbol{\Psi} = \mathbf{I}_\tau$ holds. If the sequence $\boldsymbol{\psi}_k = [\psi_{k1}\, \psi_{k2} \ldots \psi_{k\tau}]^T$ is assigned for the k-th user, the received signal for the n-th subcarrier ($n \in \mathcal{I}_k$) at the i-th BS during the training stage is

$$\mathbf{Y}^{\text{p}}_{in} = \sqrt{\rho_{\text{p}}}\sum_{j=1}^{C}\sum_{k=1}^{\tau}\mathbf{g}_{ikjn}\boldsymbol{\psi}_k^H + \mathbf{N}^{\text{p}}_{in}, \tag{2.1}$$

in which ρ_{p} is the UL pilot transmit power, $\mathbf{N}^{\text{p}}_{in} \in \mathbb{C}^{M\times\tau}$ is the AWGN matrix with i.i.d. elements following a complex normal distribution with zero mean and variance σ_n^2. Note that we have assumed synchronism between the signals received from different cells, which is the worst case in terms of pilot contamination [3]. Besides, we have assumed a uniform power allocation policy in the uplink data transmissions, since any effect of pilot power allocation can be alternatively achieved through transmit power allocation and constant pilot transmit power for all users [23]. The i-th BS then estimates the k-th user n-th subcarrier FDCSI by correlating the received signal $\mathbf{Y}^{\text{p}}_{in}$ with $\boldsymbol{\psi}_k$

$$\widehat{\mathbf{g}}_{ikn} = \frac{1}{\sqrt{\rho_{\text{p}}}}\mathbf{Y}^{\text{p}}_{in}\boldsymbol{\psi}_k = \sum_{j=1}^{C}\mathbf{g}_{ikjn} + \mathbf{v}_{ikn}, \tag{2.2}$$

where $\mathbf{v}_{ikn} = \frac{1}{\sqrt{\rho_{\text{p}}}}\mathbf{N}^{\text{p}}_{in}\boldsymbol{\psi}_k \sim \mathcal{CN}(\mathbf{0}_M, \frac{\sigma_n^2}{\rho_{\text{p}}}\mathbf{I}_M)$ is an equivalent noise vector. The pilot contamination effect can be clearly seen in the previous expression. The other $N - L$ subcarriers' FDCSI estimates are obtained by interpolation. By acquiring such FDCSI estimates, the BS is able to perform linear detection in the UL deploying the FDMRC scheme.

During UL data transmission, the i-th BS receives in the n-th subcarrier the signal

$$\mathbf{y}_{in}^{\mathrm{u}} = \sum_{j=1}^{C}\sum_{k=1}^{K}\sqrt{\rho_{kj}^{\mathrm{u}}}\mathbf{g}_{ikjn}x_{kjn}^{\mathrm{u}} + \mathbf{n}_{in}^{\mathrm{u}}, \tag{2.3}$$

in which ρ_{kj}^{u} is the UL data transmit power of the k-th user of the j-th cell, x_{kjn}^{u} is the data symbol from the k-th user of the j-th cell in the n-th subcarrier, and $\mathbf{n}_{in}^{\mathrm{u}} \sim \mathcal{CN}(\mathbf{0}_M, \sigma_n^2\mathbf{I}_M)$ is the $M \times 1$ AWGN sample vector. This BS then estimates the transmitted symbol deploying FDMRC as

$$\widehat{x}_{kin}^{\mathrm{u}} = \frac{1}{M}\widehat{\mathbf{g}}_{ikn}^{H}\mathbf{y}_{in}^{\mathrm{u}}. \tag{2.4}$$

Similarly, during a DL data transmission, the k'-th user of the j-th cell receives the signal

$$y_{k'j}^{\mathrm{d}} = \sum_{i=1}^{C}\sum_{k=1}^{K}\sqrt{\rho_{ik}^{\mathrm{d}}}\mathbf{g}_{ik'j}^{T}\mathbf{p}_{ik}x_{ik}^{\mathrm{d}} + n_{k'j}^{\mathrm{d}}, \tag{2.5}$$

where ρ_{ik}^{d} and x_{ik}^{d} is the DL data transmit power and the DL data transmitted from the i-th BS to his k-th user, and $n_{k'j}^{\mathrm{d}} \sim \mathcal{CN}(0, \sigma_n^2)$ is an AWGN sample. Besides, $\mathbf{p}_{ik}$ is the beamforming vector that the i-th BS computes to precode its k-th user data. Deploying MRT, this vector is defined as [23]:

$$\mathbf{p}_{ik} = \frac{\widehat{\mathbf{g}}_{ik}^{*}}{||\widehat{\mathbf{g}}_{ik}||} = \frac{\widehat{\mathbf{g}}_{ik}^{*}}{\alpha_{ik}\sqrt{M}}, \tag{2.6}$$

in which the scalar $\alpha_{ik} = \frac{||\widehat{\mathbf{g}}_{ik}||}{\sqrt{M}}$ is a normalization factor necessary to guarantee that $||\sqrt{\rho_{ik}^{\mathrm{d}}}\mathbf{p}_{ik}x_{ik}^{\mathrm{d}}||^2 = \rho_{ik}^{\mathrm{d}}$.

Following the analysis in [5], it can be shown from (2.4) and (2.5) that the UL and DL signal-to-interference-plus-noise ratio (SINR) performance of massive MIMO systems with MRC and MRT are given, respectively, by

$$\varsigma_{k'i}^{\mathrm{u}} = \frac{\rho_{k'i}^{\mathrm{u}}\beta_{ik'i}^2}{\sum_{\substack{l=1\\l\neq i}}^{C}\rho_{k'l}^{\mathrm{u}}\beta_{ik'l}^2 + \frac{\alpha_{ik'}^2}{M}\left(\sum_{l=1}^{C}\sum_{k=1}^{K}\rho_{kl}^{\mathrm{u}}\beta_{ikl} + \sigma_n^2\right)}, \tag{2.7}$$

$$\varsigma_{k'j}^{\mathrm{d}} = \frac{\rho_{jk'}^{\mathrm{d}}\beta_{jk'j}^2/\alpha_{jk'}^2}{\sum_{\substack{l=1\\l\neq j}}^{C}\rho_{lk'}^{\mathrm{d}}\beta_{lk'j}^2/\alpha_{lk'}^2 + \frac{1}{M}\left(\sum_{l=1}^{C}\beta_{lk'j}\sum_{k=1}^{K}\rho_{lk}^{\mathrm{d}} + \sigma_n^2\right)}, \tag{2.8}$$

in which $\alpha_{jk}^2 = \sum_{\ell=1}^{C}\beta_{jk\ell} + \frac{\sigma_n^2}{\rho^{\mathrm{p}}}$. It is straightforward to see from (2.7) and (2.8) that the asymptotic UL and DL SINR ($M \to \infty$) converge, respectively, to

$$\varsigma_{k'i}^{\mathrm{u}\infty} = \frac{\rho_{k'i}^{\mathrm{u}}\beta_{ik'i}^2}{\sum_{\substack{l=1\\l\neq i}}^{C}\rho_{k'l}^{\mathrm{u}}\beta_{ik'l}^2}, \tag{2.9}$$

$$\varsigma_{k'j}^{\mathrm{d}\infty} = \frac{\rho_{jk'}^{\mathrm{d}}\beta_{jk'j}^2/\alpha_{jk'}^2}{\sum_{\substack{l=1\\l\neq j}}^{C}\rho_{lk'}^{\mathrm{d}}\beta_{lk'j}^2/\alpha_{lk'}^2}. \tag{2.10}$$

Although UL (2.9) and DL SINR (2.10) are similar-looking expressions, they have different statistical characteristics as discussed in [3]. While interference in UL is irradiated from users in neighboring cells using the same k-th pilot sequence to the i-th BS, interference in DL is irradiated from neighboring BS's to the user

in j-th cell employing the k-th pilot sequence. While in UL the receiver is fixed and the multiple transmitters are moving, in DL multiple fixed transmitters communicate with a mobile receiver.

The performance of the massive MIMO system can be improved both via pilot assignment and by power control. The optimal performance is achieved solving a joint optimization problem of increased complexity due to the mixed variables' types: the pilot assignment is a discrete nature problem, while power control is of continuous nature. In this Doctoral work, we adopt a decoupled approach, in which the pilot assignment is performed assuming uniform power allocation, followed by a power control algorithm evaluated from the optimized pilot distribution obtained in the previous step. This strategy is commonly applied to solve mixed-nature optimization problems, like in [24] and [25].

2.1.2 SC waveform

The t-th CIR vector tap between the i-th BS and the k-th user of the j-th cell and its FDCSI vector are related by

$$\mathbf{h}_{ikjt} = \frac{1}{L}\sum_{l=0}^{L-1} \mathbf{g}_{ikj\mathcal{I}_k(l)} e^{\mathrm{j}2\pi lt/L}. \tag{2.11}$$

With no loss of generality, we assume in this work a normalized uniform power delay profile (PDP) for all users, such that $\mathbf{h}_{ikjt} \sim \mathcal{CN}(\mathbf{0}_M, \frac{1}{L}\mathbf{I}_M)$ for $t = 0, 1, \ldots L-1$. For the systems employing single-carrier waveform, an alternative training scheme to conventional frequency domain training is discussed in [13]. In this alternative scheme for estimating the CIR of the users served by the cell, the users transmit uplink training signals sequentially in time, in such a way that at most one user per cell is transmitting at any given time. The k-th user sends an impulse of amplitude $\sqrt{L\rho_{\mathrm{p}}}$ (in order to spend the same average power as in FD training (2.1)) at the $(k-1)L$-th channel use and is idle for the remaining portion of the training phase. Besides, the next user waits $L-1$ channel uses to send its training signal. It is worth noting that the same maximal number of users K_{max} is supported in both schemes, the OFDM and SC waveform transmissions. This can be proved by noting that the total interval spent with training signals is $K_{\mathsf{max}} L T_n = \tau N_{\mathsf{sm}} L T_n = \tau N T_n \approx \tau T_s$ is nearly the same as in FD training, as illustrated in Figure 2.1. The main advantage of this scheme is because estimating the CSI in the frequency domain would require the users to send FD pilots. This is only possible if the users' terminals were equipped with OFDM circuitry, does not bringing thus all the mentioned benefits of employing SC waveform. Indeed, the time domain training scheme proposed in [13] requires an accurate synchronism between the users of a given cell. It is not in the scope of this work to discuss how stringent are such requirements. However, it is worth to mention that even if conventional frequency domain training is employed, significant gains can be achieved. This occurs because the OFDM circuitry required for only frequency domain training is much more simple and less inefficient, since only L active subcarriers transmit pilots, as opposed to the N data active subcarriers in conventional OFDM data transmission. This reduction for typical OFDM setups is of 16 times (if $L = N/16$), and undoubtedly is very beneficial for the system in terms of energy efficiency and implementation cost. Besides, the performance analysis developed in this work does not suffer any change, since both schemes result in the same pilot contaminated CSI estimates.

This procedure provides to the i-th BS the following CIR estimates for its k-th user

$$\widehat{\mathbf{h}}_{ikt} = \sum_{j=1}^{C} \mathbf{h}_{ikjt} + \mathbf{v}'_{ikt}, \tag{2.12}$$

in which $\mathbf{v}'_{ikt} \sim \mathcal{CN}(\mathbf{0}_M, \frac{\sigma_n^2}{L\rho_{\mathrm{p}}}\mathbf{I}_M)$ is an equivalent AWGN vector. Note that the CIR estimates are also corrupted by the users in adjacent cells that send its impulses at the same channel use, similarly as pilot contamination.

Considering SC waveform, the time-domain received signal at the i-th BS in time t during UL data transmission is

$$\mathbf{r}_i^{\mathrm{u}}[t] = \sum_{j=1}^{C}\sum_{k=1}^{K}\sqrt{\rho_{kj}^{\mathrm{u}}}\sum_{l=0}^{L-1}\mathbf{h}_{ikjl}s_{kj}^{\mathrm{u}}[t-l] + \mathbf{n}'^{\mathrm{u}}_i[t], \tag{2.13}$$

where $s_{kj}^{\mathrm{u}}[t-l]$ is the time-domain UL data transmitted by the k-th user of the j-th cell at time $t-l$, and $\mathbf{n}'^{\mathrm{u}}_i[t] \sim \mathcal{CN}(\mathbf{0}_M, \sigma_n^2\mathbf{I}_M)$ is an AWGN vector. This BS can then estimate the transmitted symbols deploying TRMRC as

$$\widehat{s}_{ki}^{\mathrm{u}}[t] = \frac{1}{M}\sum_{l=0}^{L-1}\widehat{\mathbf{h}}_{ikl}^H\mathbf{r}_i^{\mathrm{u}}[t+l]. \tag{2.14}$$

For causality purpose, it is clear from (2.14) that $L-1$ shift registers are necessary per BS receive antenna for TRMRC, while this number for FDMRC is $N-1$, since the entire frame has to be received to perform FFT operation. This implies not only in hardware simplification, but also in latency reduction. Besides, the fact of TRMRC not requiring CP transmission can be seen from (2.14), since given a sufficiently large M, the BS is able to extract the desired information symbol vector from $\mathbf{r}_i^{\mathrm{u}}[t+l]$, even if the asynchronous interference belongs to another frame of symbols.

Similarly, the TRMRC method can be applied to precode the transmit signal in DL, as in [26], and the data estimates available at the MTs can be obtained in the same way as above. However, as the TRMRC approach in DL is not so advantageous as it is in UL, we omitted such derivations here.

2.1.3 Crowded massive MIMO network

The system model for a crowded massive MIMO network is very similar to the system model already introduced in this Chapter. However, some slight modifications are necessary to represent the very large number of UEs, which become active with a reduced probability. This model can represent a network composed of conventional human users and several machine-type communication devices. In both cases, data packets are the building block of the traffic, and are generated in an intermittent and unpredictable manner in most applications, in such a way that intensive download activities are interwoven with long periods of silence. Many UEs thus switch between being active and inactive at a frequent and irregular basis.

Again, we consider cellular networks where each BS is equipped with M antennas, and the system operates in TDD mode with the time-frequency resources being divided into coherence blocks of $\mathcal{S}$ channel uses. Let $\mathcal{U}_i$ denote the set of UEs in cell i, while $\mathcal{A}_i \subset \mathcal{U}_i$ is the subset of users in this cell that are active at any given time. Tipically, in crowded machine-type network scenarios the UE set is very large, such that $|\mathcal{U}_i| \gg \mathcal{S}$, but the active UEs satisfy $|\mathcal{A}_i| < \mathcal{S}$, and the BS can temporarily assign orthogonal pilots to these UEs and reclaim them when they finish their transmissions. We focus on an arbitrary cell, referred as cell 0 without loss of

generality, and consider how interference from other cells impacts on the considered cell. Let $\mathcal{K}_0 = \mathcal{U}_0 \backslash \mathcal{A}_0$ denote the set of inactive UEs in cell 0, and one can say that there are $K_0 = |\mathcal{K}_0|$ inactive UEs in this cell. These K_0 users are assumed to share τ mutually orthogonal RA pilot sequences $\boldsymbol{\psi}_1 \dots \boldsymbol{\psi}_\tau \in \mathbb{C}^\tau$ which span τ UL channel uses and satisfy $||\boldsymbol{\psi}_t||^2 = \tau$.

The UEs in $\mathcal{K}_0$ randomly select one of the τ pilots in each RA block: UE k selects pilot $c(k) \in \{1, 2, \dots, \tau\}$. Besides, the probability of each UE would like to become active is $P_a \leq 1$. The UE k makes an access attempt by transmitting the pilot $\boldsymbol{\psi}_{c(k)}$ with a non-zero power $\rho_k > 0$. The set $\mathcal{Q}_t = \{k : c(k) = t, \rho_k > 0\}$ contains the indices of the UEs that transmit pilot t. Therefore, $|\mathcal{Q}_t|$ which is the number of UEs transmitting $\boldsymbol{\psi}_t$ presents a binomial distribution [18]:

$$|\mathcal{Q}_t| \sim \mathfrak{B}\left(K_0, \frac{P_a}{\tau}\right). \tag{2.15}$$

The majority of the coherence blocks are used for payload data transmission for active UEs, *i.e.*, which have been allocated dedicated pilots. A few of the blocks are used for RA, where inactive UEs can ask to be admitted to the payload data blocks. Considering the finite number of pilot sequences and the multicell scenario, a strategy for mitigating the pilot contamination interference between adjacent cells proposed in [18] consists in diversifying the locations of resource blocks dedicated for RA between adjacent cells, as illustrated in Figure 2.2, reproduced from [18]. In this way, if the considered cell uses a given resource block for RA, the closest cells use this resource block for payload data transmission.

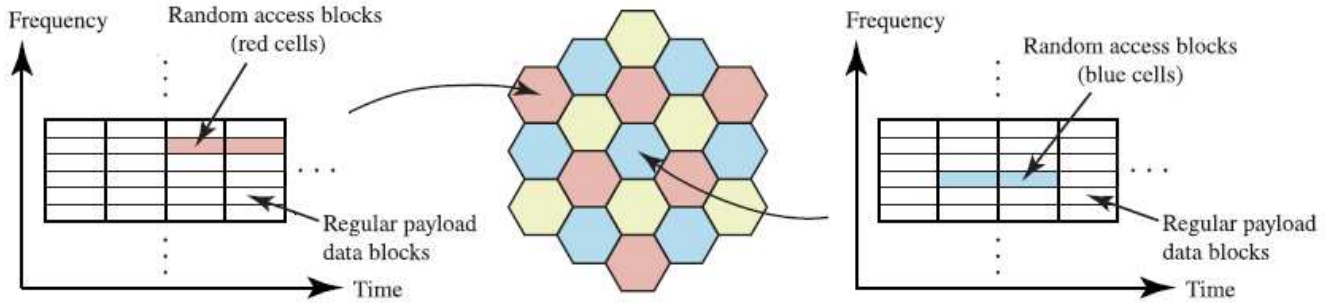

Figure 2.2: Location of resource blocks dedicated for RA between adjacent cells. Source: [18].

We denote the channel vector between UE k and its BS by $\mathbf{g}_k \in \mathbb{C}^M$. Since the number of BS antennas is large, the massive MIMO properties of channel hardening and asymptotic favorable propagation hold [5]. The channel vector also satisfies $\mathbf{g}_k = \sqrt{\beta_k}\underline{\mathbf{g}}_k$, in which β_k is the large-scale fading coefficient between kth user and its cell, comprising path loss and shadowing, and each coefficient of the small-scale fading vector $\underline{\mathbf{g}}_k$ is distributed as $\mathcal{CN}(0,1)$. We assume that β_k is known to UE k, since it can be easily estimated for example if the BS broadcasts a beacon signal periodically.

The BS receives the signal $\mathbf{Y} \in \mathbb{C}^{M \times \tau}$ from the pilot transmission:

$$\mathbf{Y} = \sum_{k \in \mathcal{K}_0} \sqrt{\rho_k}\mathbf{g}_k \boldsymbol{\psi}_{c(k)}^T + \mathbf{W} + \mathbf{N}, \tag{2.16}$$

where $\mathbf{N} \in \mathbb{C}^{M \times \tau}$ is the matrix of noise coefficients at the BS with each element following $\mathcal{CN}(0, \sigma^2)$, and the

matrix $\mathbf{W} \in \mathbb{C}^{M \times \tau}$ represents interference from adjacent cells. The BS then correlates $\mathbf{Y}$ with $\boldsymbol{\psi}_t$ to obtain

$$\begin{aligned} \mathbf{y}_t &= \mathbf{Y}\frac{\boldsymbol{\psi}_t^*}{||\boldsymbol{\psi}_t||} = \sum_{i \in \mathcal{Q}_t} \sqrt{\rho_i}||\boldsymbol{\psi}_t||\mathbf{g}_i + \mathbf{W}\frac{\boldsymbol{\psi}_t^*}{||\boldsymbol{\psi}_t||} + \mathbf{n}_t \\ &= \sum_{i \in \mathcal{Q}_t} \sqrt{\rho_i \tau}\mathbf{g}_i + \mathbf{W}\frac{\boldsymbol{\psi}_t^*}{||\boldsymbol{\psi}_t||} + \mathbf{n}_t, \end{aligned} \tag{2.17}$$

in which $\mathbf{n}_t = \mathbf{N}\frac{\boldsymbol{\psi}_t^*}{||\boldsymbol{\psi}_t||} \sim \mathcal{CN}(\mathbf{0}, \sigma^2\mathbf{I}_M)$ is the effective receiver noise. As in [18], the inter-cell interference $\mathbf{W}$ can be modeled as

$$\mathbf{W} = \sum_l \mathbf{w}_l \mathbf{d}_l^T + \sum_{t=1}^{\tau} \sum_{k \in \mathcal{Q}_t^{\text{interf}}} \sqrt{\rho_{t,k}}\mathbf{g}_{t,k}\boldsymbol{\psi}_t^T. \tag{2.18}$$

The first term in (2.18) refers to the interfering data transmissions from neighboring cells that use a different resource block (in time-frequency domain) as RA block than cell 0, as in Fig. 2.2. $\mathbf{w}_l \in \mathbb{C}^M$ is the channel vector of the lth interferer to the BS in cell 0 and $\mathbf{d}_l \in \mathbb{C}^\tau$ is the random data the interfering user transmits. The second term in (2.18) refers to the interfers in neighboring cells using the same resource block as RA block as cell 0, as in Fig. 2.2, which are also performing RA. Such users are gathered in the set $\mathcal{Q}_t^{\text{interf}}$, and the member $k \in \mathcal{Q}_t^{\text{interf}}$ uses the transmit power $\rho_{t,k}$ and has the channel $\mathbf{g}_{t,k}$ to the BS in cell 0. In [18], it is shown that

$$\frac{\left|\mathbf{W}\frac{\boldsymbol{\psi}_t^*}{||\boldsymbol{\psi}_t||}\right|}{M} \to \underbrace{\sum_l \beta_{w,l}\frac{|\mathbf{d}_l^T\boldsymbol{\psi}_t^*|^2}{||\boldsymbol{\psi}_t||^2} + \sum_{k \in \mathcal{Q}_t^{\text{interf}}} \rho_{t,k}\tau\beta_{t,k}}_{\omega_t} \tag{2.19}$$

as $M \to \infty$, in which $\beta_{w,l}$ is the large-scale fading coefficients related to $\mathbf{w}_l$ ($\frac{||\mathbf{w}_l||^2}{M} \to \beta_{w,l}$), and $\beta_{t,k}$ is the ones related to $\mathbf{g}_{t,k}$ ($\frac{||\mathbf{g}_{t,k}||^2}{M} \to \beta_{t,k}$). It is worth to say that there is interference in ω_t from both data transmission and RA pilots in other cells, but the first is often dominant since the closest neighboring cells transmit data.

2.2 Conclusion of the Chapter

In this Chapter, we have described the massive MIMO system model, which is extensively used in the rest of this Doctoral Thesis. Depending on the subtheme analyzed, we have described the peculiarities the system model assumes, and the main notations adopted.

3 Pilot Assignment and Power Control

This chapter discusses the main contributions regarding pilot assignment and power control achieved by this Doctoral work. We first introduce the investigated problems with respect to the massive MIMO system model introduced in Chapter 2.1. Then, we describe our proposed solutions, and show some performance results in order to verify their effectiveness.

3.1 Pilot Assignment

The massive MIMO system performance is improved by suitably assigning the pilot sequences to the users [6], [27]. We assume a decentralized allocation procedure, in which PA is performed sequentially by each cell, regarding its covered users. The convergence of this procedure is discussed in the following. Besides, in this pilot assignment stage, it is assumed the knowledge of users' power distribution in the cells, and the focus is at the asymptotic performance expressions in (2.9) and (2.10) for simplicity. Then, in Section 3.2, we evaluate the power control algorithm based on the pilot assignment obtained here, and demonstrate the performance improvements of our proposed schemes for finite number of antennas by numerical simulations. SINR expressions in (2.9) and (2.10) were obtained assuming that the k'-th pilot sequence[1] is assigned to the k'-th user, *i.e.*, under a random strategy. However, if we assume that the p-th pilot is assigned to the c_p-th user in the i-th cell, the UL asymptotic SINR can be rewritten as

$$\varsigma_{c_p i}^{\mathrm{u}\infty} = \frac{\rho_{c_p i}^{\mathrm{u}} \beta_{i c_p i}^2}{\sum_{\substack{j=1 \\ j \neq i}}^{C} \rho_{pj}^{\mathrm{u}} \beta_{ipj}^2}, \tag{3.1}$$

that is the UL asymptotic SINR of the user in the i-th cell employing the p-th pilot, namely the c_p-th user. The fixed uplink power distribution ρ_{pj}^{u}, for $p = 1, \dots K$ and $j = 1, \dots C$, is known for the i-th cell. The performance bottleneck in massive MIMO systems is due to users with severe pilot contamination [3]. Thus, a fair objective is to maximize the minimum UL SINR among the users, as the following optimization problem

$$\mathcal{PA}_{\mathrm{u}} : \max_{l} \min_{p} \quad \varsigma_{c_{lp} i}^{\mathrm{u}\infty}, \tag{3.2}$$

in which c_{lp} is the l,p-th element of matrix $\mathbf{C} \in \mathbb{N}^{K! \times K}$, which contains every possible pilot assignment that a given cell can adopt. c_{lp} means that in the l-th PA combination, the p-th pilot is assigned to the c_{lp}-th user. Obviously, the complexity of solving (3.2) via an exhaustive search grows with K in a factorial fashion. A viable and heuristic solution is proposed in [6], where the pilot sequences with the worst interference levels are assigned to the users with the highest long-term fading coefficients. Such *greedy method* achieves a

[1] With "k'-th pilot sequence", we refer to the pilot of index k' in the set of available pilot sequences.

near-optimal solution with reduced complexity.

On the other hand, the DL SINR in (2.10) can also be improved via pilot assignment. Assuming that the p-th pilot is assigned to the c_p-th user in the j-th cell, and that the downlink power distribution is known for the j-th cell, the DL SINR becomes

$$\varsigma_{c_p j}^{\mathrm{d}\infty} = \frac{\rho_{jc_p}^{\mathrm{d}} \beta_{jc_p j}^2}{\beta_{jc_p j} + \vartheta_{jp(j)}} \frac{1}{\sum_{\substack{i=1 \\ i \neq j}}^{C} \frac{\rho_{ic_p}^{\mathrm{d}} \beta_{ic_p j}^2}{\beta_{ic_p j} + \vartheta_{ip(j)}}}, \tag{3.3}$$

where $\vartheta_{ip(j)} = \sum_{\substack{\ell=1 \\ \ell \neq j}}^{C} \beta_{ip\ell} + \frac{\sigma_n^2}{\rho^{\mathrm{p}}}$ does not depend on for what user the p-th pilot will be assigned. Thus, an alternative PA optimization procedure for DL is proposed as:

$$\mathcal{PA}_{\mathrm{d}} \quad : \quad \max_{l} \min_{p} \quad \varsigma_{c_{lp} j}^{\mathrm{d}\infty}, \tag{3.4}$$

One can see that the dependence of the DL SINR with the assignment of pilots to users is not so simple as it is in the UL scenario. However, communication systems are usually asymmetric, and DL data transmission might be predominant in comparison with UL data transmission. Therefore, solving the optimization problem in (3.4) in a low-complexity way is also quite appealing in practice. The main difficulty is that the interference in DL for the p-th pilot (denominator of the second term in (3.3)) is dependent on what user this sequence is assigned, and thus a greedy method cannot be applied as in [6]. If a user changes its pilot sequence, the DL interference due to pilot contamination reaching him is still mainly dominated by his long-term fading coefficients with respect to neighboring BS's, which do not change, as illustrated in Figure 3.1. The exception is due to the DL normalization factors, that retain some dependence with the assigned pilot sequence from the uplink training channel estimation.

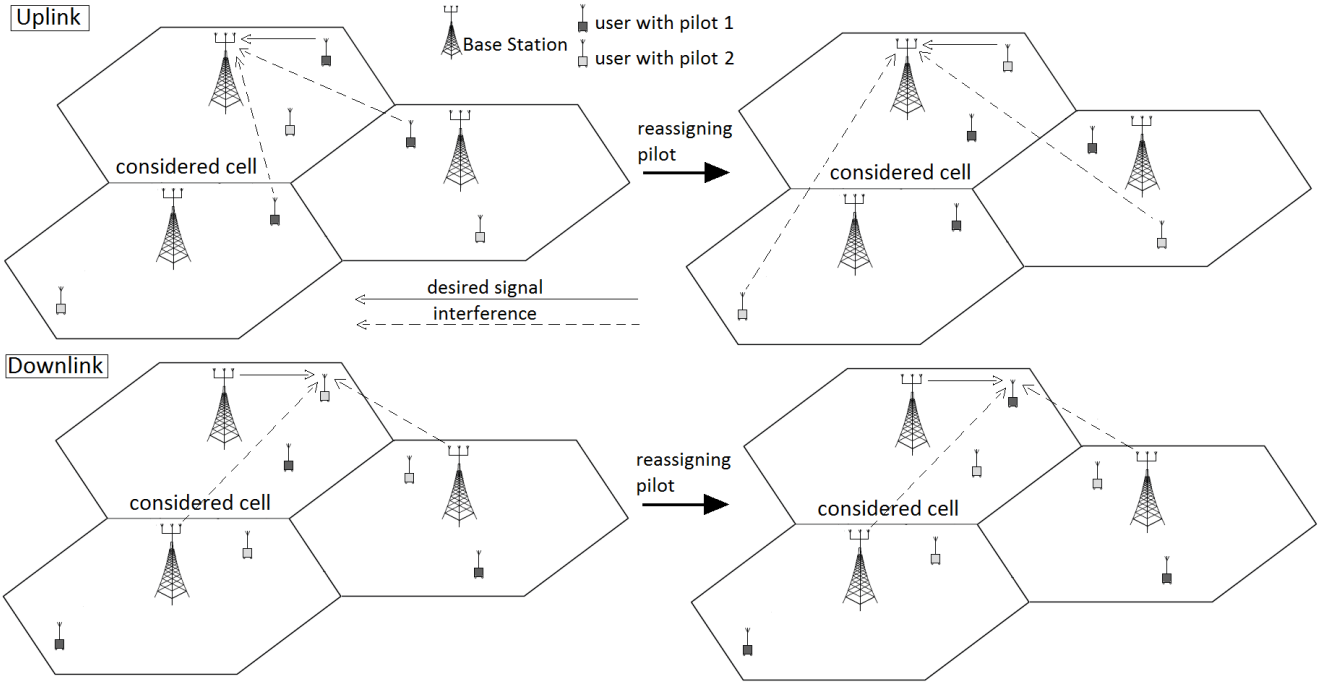

Figure 3.1: Effect of reassigning pilot sequences in the consired cell, in UL (up) and DL (down). Although it appears from the Figure that reassigning pilots has no effect in DL, the previous UL pilot transmission stage results in some variations on the signals' strength.

The convergence of the decentralized pilot allocation procedure is discussed in [27], and shown by numerical results in [6]. The decentralized procedure means that the assignment of pilots can be modified only for users of the ℓth cell when it is carrying out this procedure. Although the strictly optimal solution would test every possible pilot combination among the $K \cdot C$ users, its complexity would be prohibitive. Thus, the solution obtained in the decentralized way is preferable, and it can be shown that it converges to a Nash equilibrium after performing some times by each cell. Note that this problem can be viewed as a *finite potential game*, since: *a*) it exists a global potential function that maps every strategy to some real value according its efficiency; *b*) the set of strategies is of finite dimension [28]. In this case, each cell is a player, the potential function would be the average BER of the whole system in that subcarrier, or the average SINR, and the strategy is the pilot allocation in that cell. Since each player chooses its strategy following a selfish best response dynamics, the convergence of the game to a Nash equilibrium is assured in [28, Theorem 19.12], [29, Proposition 2.2]. Besides, the decentralized solution can achieve appreciable gains in performance, as demonstrated in the next Section.

3.1.1 Joint UL-DL Pilot Assignment

One can note that the optimization problems of (3.2) and (3.4) are conflicting, as numerically demonstrated in the following. If the UL performance metric is optimized, the DL performance will be close to that attained with random assignment policy, and vice-versa. Thus, we elaborate our analysis aiming to jointly achieve the best possible performance in UL and DL, concurrently. One approach could be adopting multiobjective optimization. In this work, we prefer a simpler strategy. We assume in the adopted TDD scheme a channel coherence block of $\mathcal{S}$ symbols, of which K are devoted to UL pilot transmission, $\xi^{\mathrm{u}}\left(\frac{\mathcal{S}-K}{\mathcal{S}}\right)$ and $\xi^{\mathrm{d}}\left(\frac{\mathcal{S}-K}{\mathcal{S}}\right)$ for UL and DL data transmission, respectively, in which the factors ξ^{u} and $\xi^{\mathrm{d}} \in (0,1)$, $\xi^{\mathrm{u}}+\xi^{\mathrm{d}}=1$, and both $\xi^{\mathrm{u}}(\mathcal{S}-K)$ and $\xi^{\mathrm{d}}(\mathcal{S}-K)$ are integers. Then, for a system bandwidth B, the total capacity (TC) of the user in the j-th cell for which the p-th pilot is assigned is defined as

$$\mathcal{C}^{\mathrm{T}}_{c_p j} = B\left(\frac{\mathcal{S}-K}{\mathcal{S}}\right)\left[\xi^{\mathrm{u}}\log_2\left(1+\varsigma^{\mathrm{u}}_{c_p j}\right)+\xi^{\mathrm{d}}\log_2\left(1+\varsigma^{\mathrm{d}}_{c_p j}\right)\right] \tag{3.5}$$

Hence, an alternative optimization problem can be defined as

$$\mathcal{PA}_{\mathrm{TC}} : \max_{l}\min_{p} \quad \mathcal{C}^{\mathrm{T}\infty}_{c_{lp}j}, \tag{3.6}$$

in which $\mathcal{C}^{\mathrm{T}\infty}_{c_{lp}j}$ is obtained evaluating (3.5) from $\varsigma^{\mathrm{u}\infty}_{c_p j}$ and $\varsigma^{\mathrm{d}\infty}_{c_p j}$.

3.1.2 Heuristic Pilot Assignment Solutions

For solving the DL assignment problem avoiding the exhaustive search, we first create a cost matrix $\mathbf{\Gamma}^{(j)} \in \mathbb{R}^{K\times K}$, whose k,p-th element is the DL SINR achieved by the k-th user in the j-th cell when the p-th pilot sequence is assigned to him, *i.e.,* $\gamma^{(j)}_{kp} = \varsigma^{\mathrm{d}}_{c_p j}$ when $c_p = k$. Then, *our proposed low-complexity suboptimal solution* consists of finding the pilot with which each user achieves its maximal DL SINR. The user with the lowest maximal DL SINR will have such pilot sequence assigned to him. This procedure is repeated, excluding the users and the pilots already assigned, until allocating every pilot sequence, as described in Algorithm 3.1.

In order to obtain a low-complexity form for solving the joint UL-DL PA in (3.6) while achieving near-

optimal performance, this same heuristic procedure can be applied. In this case, we initialize the cost matrix $\mathbf{\Gamma}^{(j)}$ (line 1 in Alg. 3.1) in an alternative way, such that $\gamma_{kp}^{(j)} = \mathcal{C}_{c_p j}^{\mathrm{T}}$ when $c_p = k$, since the total capacity as defined in (3.5) is calculated as a weighted log function of both UL and DL SINR's. Then, we apply our proposed heuristic method in a similar way as in Algorithm 3.1.

Algorithm 3.1: Proposed Pilot Assignment Procedure

Input: β_{jkl}, $\forall j,l = 1,2,\ldots C$, $k = 1,2,\ldots K$, σ_n^2, ρ_{p}.

1: Generate cost matrix $\mathbf{\Gamma}^{(i)}$, of size $K \times K$;
2: **for** $j = 1,2,\ldots,K$ **do**
3: **for** $p = 1,2,\ldots,K$ **do**
4: Evaluate $\delta_p = \max_{\ell=1,\ldots,K} \gamma_{p,\ell}^{(i)}$;
5: Evaluate $\eta_p = \arg\max_{\ell=1,\ldots,K} \gamma_{p,\ell}^{(i)}$;
6: **end for**
7: Evaluate $\phi = \arg\min_{p=1,\ldots,K} \delta_p$;
8: Evaluate $c_{\eta_\phi}^{(i)} = \phi$;
9: Invalidate the ϕ-th line and η_ϕ-th column of $\mathbf{\Gamma}^{(i)}$;
10: **end for**

Output: $\mathbf{c}^{(i)}$.

3.1.3 Numerical Results

Several results of our proposed pilot assignment techniques are shown in Appendices A, C, and D. In the paper presented in Appendix A, only DL pilot assignments were considered, the solutions were found by exhaustive search, and results were presented only for infinite number of BS antennas and uniform power allocation. Then, in the papers of Appendices C and D, we have investigated pilot assignment methods based on UL, DL, and joint UL-DL metrics, as well as proposing a near-optimal low-complexity method for finding the solutions in each case. The performance with finite number of antennas was also investigated, with and without efficient power allocation algorithms. Besides, in the paper of Appendix D, we have compared in detail the performance improvements achieved by the max-min approach in comparison with conventional average approaches.

We first compare in this Section the performance of max-min approach and the average approach, *i.e.*, a PA strategy that finds the highest average SINR performance via exhaustive search. Besides, Table 3.1 describes the notation adopted when referring to the different techniques investigated in this Chapter. The main advantage of adopting the max-min approach instead of the average approach when solving the PA problem can be shown in Figure 3.2, which compares the 95%-likely rate achieved by each PA technique with the increasing number of antennas. The 95%-likely rate corresponds to the rate assured to the users with probability of 95%, and thus can be used to compare how fair is the performance of a given technique. As one can note from Figure 3.2, a significant gain can be seen when comparing a max-min based PA technique with its average based counterpart in terms of its respective performance metric. For example with 128 BS antennas, there is a 0.12Mbps improvement in the 95%-likely DL rate of MaxminSINR DL in comparison with MaxSINR DL. Similarly, there is 0.05Mbps improvement in the 95%-likely UL rate of MaxminSINR UL in comparison with MaxSINR UL, and a 1.01Mbps improvement in the 95%-likely total capacity of MaxminTC in comparison with MaxTC.

Figure 3.3 depicts the fraction of users above a given rate for a BS with 128 antennas, in terms of DL, UL,

Table 3.1: Acronyms for the investigated schemes.

Acronym	Technique
MaxSINR DL	The PA method that obtains the highest mean DL SINR via exhaustive search
MaxMinSINR DL	The PA method that solves (3.4) via exhaustive search
H-MaxMinSINR DL	Our proposed PA method that solves (3.4) applying Algorithm 3.1
H-MaxMinSINR DL PA+PC	H-MaxMinSINR DL combined with the power control of Algorithm 3.2
MaxSINR UL	The PA method that obtains the highest mean UL SINR via exhaustive search
MaxMinSINR UL	The PA method that solves (3.2) via exhaustive search
H-MaxMinSINR UL	The PA method that solves (3.2) proposed in [6]
H-MaxMinSINR UL PA+PC	H-MaxMinSINR UL combined with the power control of Algorithm 3.2
MaxTC	The PA method that obtains the highest mean Total Capacity via exhaustive search
MaxMinTC	The PA method that solves (3.6) via exhaustive search
H-MaxMinTC	Our proposed PA method that solves (3.6) applying Algorithm 3.1
H-MaxMinTC PA+PC	H-MaxMinTC combined with the power control of Algorithm 3.2

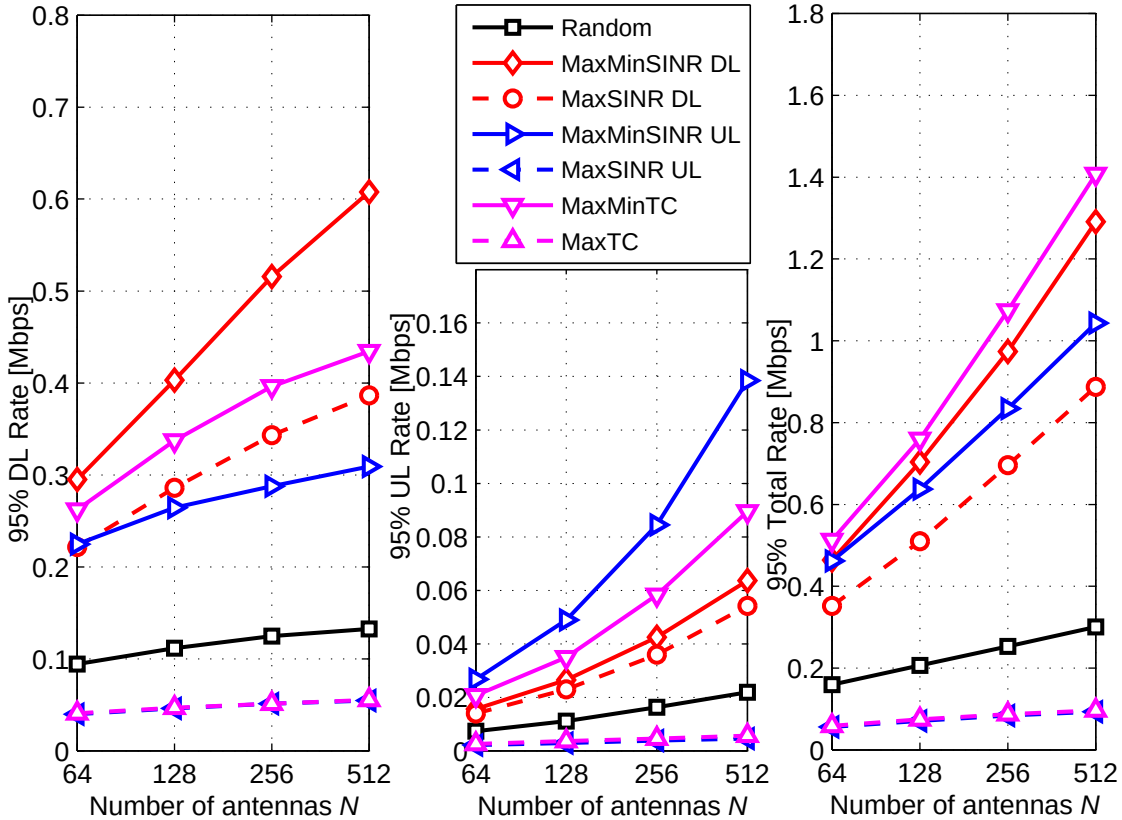

Figure 3.2: 95%-likely Rate for $K = 4$: a) DL; b) UL; c) Total.

and total rate, and Figure 3.4 shows the 95%-likely rate achieved by each technique with increasing number of antennas. In both cases, an uniform power allocation policy was assumed for simplicity, and $K = 4$ users in order to allow the evaluation of exhaustive search in a feasible time. It is noteworthy from Figure 3.3 the very unfair behavior of primitive massive MIMO systems (with no pilot and power allocation policies), which provides very high data rates for some portion of the users, while providing low quality of service for others. One can note also that appreciable improvements can be achieved with PA techniques. The conflicting behavior of UL and DL optimization metrics is represented in the Figure, since while MaxminSINR DL achieves the best performance in DL, its UL performance is close to that attained by random PA. The opposite occurs with MaxminSINR UL. On the other hand, MaxminTC achieves good performance in both directions, at the same time that achieves the best performance in terms of total rates. Besides, no significant performance loss can be seen for any heuristic PA when compared with its respective exhaustive search solution. Similar findings can be taken from Figure 3.4, that also reveals that it is always beneficial improving the number of antennas in BS.

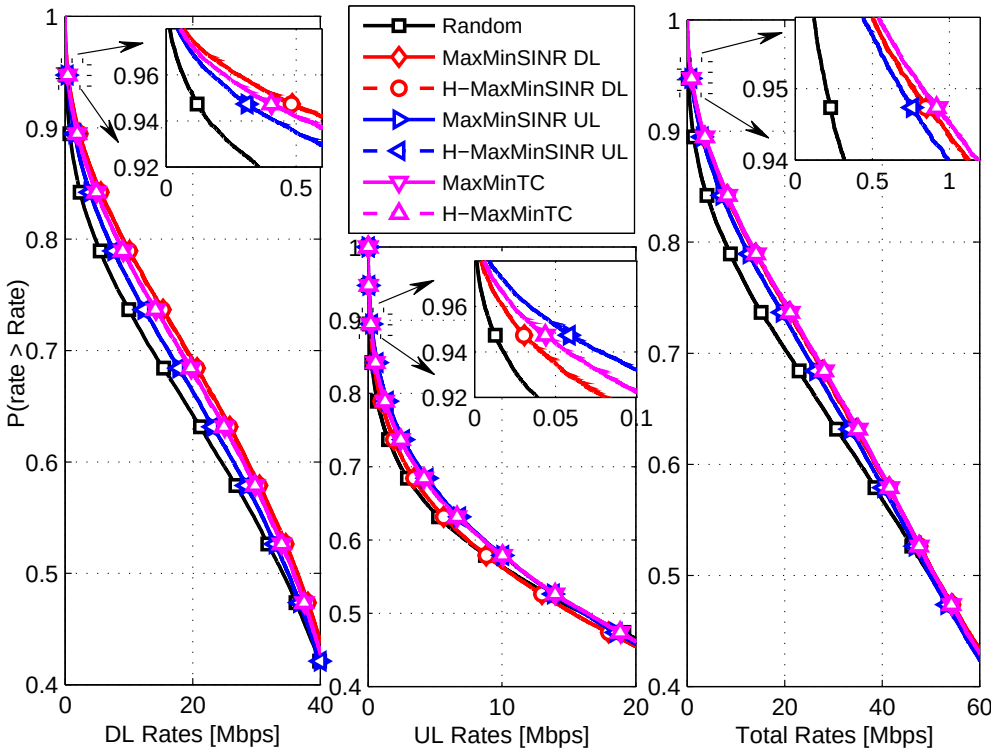

Figure 3.3: Fraction of users above a given Rate for $N = 128$ and $K = 4$: a) DL; b) UL; c) Total.

3.2 Power Allocation

We assume a decentralized power allocation procedure, similarly to pilot assignment. With the purpose of serving the users with a target SINR, the target-SIR-tracking algorithm [11] measures the interference seen by each user, and assigns to each one the exact power to reach the target SINR, unless if this power exceeds the maximum power available. In this case, the maximum power is allocated for this user. It is shown in [12] that this power allocation procedure is not the most suitable, since assigning the maximum power for the users with poor channel conditions causes an excessive interference for the other users, and waste energy because this user may remain with a low SINR. Being $\hat{\varsigma}^{\mathrm{d}}_{k'\ell}$ the target downlink SINR for the k'-th user of the ℓ-th cell, and $\overline{\rho}^{\mathrm{d}}_{\ell k'}$ the maximum DL transmit power that can be assigned to this user, the target-SIR-tracking algorithm

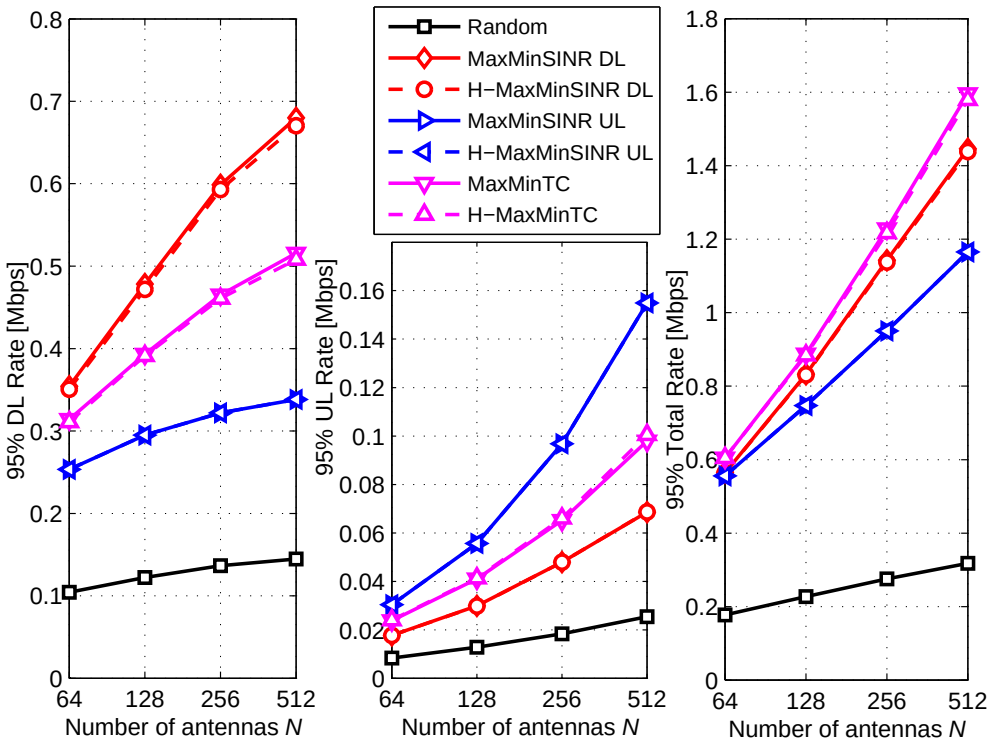

Figure 3.4: 95%-likely Rate for $K = 4$: a) DL; b) UL; c) Total.

updates power at the i-th iteration according to

$$\rho^{\mathrm{d}}_{\ell k'}(i) = \min\left[\hat{\varsigma}^{\mathrm{d}}_{k'\ell}\mathfrak{I}^{\mathrm{d}}_{k'\ell}(i), \overline{\rho}^{\mathrm{d}}_{\ell k'}\right], \tag{3.7}$$

in which $\mathfrak{I}^{\mathrm{d}}_{k'\ell}(i) = \rho^{\mathrm{d}}_{\ell k'}(i-1)/\varsigma^{\mathrm{d}}_{k'\ell}(i-1)$ is the interference plus noise seen by this user (denominator of (2.8)) divided by $\beta^2_{\ell k'\ell}/\alpha^2_{\ell k'}$. By contrast, the power control algorithm proposed in [12] updates users' powers as

$$\rho^{\mathrm{d}}_{\ell k'}(i) = \begin{cases} \hat{\varsigma}^{\mathrm{d}}_{k'\ell}\mathfrak{I}^{\mathrm{d}}_{k'\ell}(i) & \text{if} \quad \mathfrak{I}^{\mathrm{d}}_{k'\ell}(i) \leq \frac{\overline{\rho}^{\mathrm{d}}_{\ell k'}}{\hat{\varsigma}^{\mathrm{d}}_{k'\ell}}, \\ \frac{\left(\overline{\rho}^{\mathrm{d}}_{\ell k'}\right)^2}{\hat{\varsigma}^{\mathrm{d}}_{k'\ell}\mathfrak{I}^{\mathrm{d}}_{k'\ell}(i)} & \text{otherwise.} \end{cases} \tag{3.8}$$

One can see that the method of [12] assigns power to the users in the same way as the target-SIR-tracking algorithm if the target SINR can be achieved for the user at that iteration. Otherwise, instead of allocating the maximum power, *it allocates to each user a transmit power inversely proportional to that required to achieve the target*. Thus, besides of saving energy relative to users that cannot reach the target SINR, the interference irradiated to other users also decreases. This procedure is repeated for a predefined number of iterations N_{it}, and the power coefficients for each user can be initialized with half of the maximum transmit power for the considered user, as described in Algorithm 3.2. The convergence of such algorithm is proved in [12], and in our simulations we have noted that 10 iterations were sufficient for achieving convergence. Equivalently, this same procedure can be applied in UL user power allocation as

$$\rho^{\mathrm{u}}_{k'\ell}(i) = \begin{cases} \hat{\varsigma}^{\mathrm{u}}_{k'\ell}\mathfrak{I}^{\mathrm{u}}_{k'\ell}(i) & \text{if} \quad \mathfrak{I}^{\mathrm{u}}_{k'\ell}(i) \leq \frac{\overline{\rho}^{\mathrm{u}}_{k'\ell}}{\hat{\varsigma}^{\mathrm{u}}_{k'\ell}}, \\ \frac{\left(\overline{\rho}^{\mathrm{u}}_{k'\ell}\right)^2}{\hat{\varsigma}^{\mathrm{u}}_{k'\ell}\mathfrak{I}^{\mathrm{u}}_{k'\ell}(i)} & \text{otherwise,} \end{cases} \tag{3.9}$$

in which $\hat{\varsigma}^{\mathrm{u}}_{k\ell}$ is the target UL SINR of the user, $\overline{\rho}^{\mathrm{u}}_{k\ell}$ its maximum UL transmit power, and

$$\mathfrak{I}^{\mathrm{u}}_{k'\ell}(i) = \frac{\sum_{\substack{l=1\\ l\neq\ell}}^{C} \rho^{\mathrm{u}}_{k'l}(i-1)\beta^2_{\ell k'l} + \frac{\alpha^2_{\ell k'}}{M}\left(\sum_l \sum_k \rho^{\mathrm{u}}_{kl}(i-1)\beta_{\ell kl} + \sigma^2_n\right)}{\beta^2_{\ell k'\ell}}.$$

When deploying these power control algorithms, the target SINR parameter should be carefully chosen. If a somewhat lower value is adopted, the algorithm saves energy by delivering just the target SINR to the users, taking low advantage of the resources and providing poor performance for the system. If an excessive target SINR is considered, many poor located users will have their powers gradually turned off in order to provide the desired performance for the other users. Hence, in this work, the target SINR was chosen in each scenario by finding the value that achieves the higher throughput for 95% of the users, by means of numerical simulations, as indicated in Table 3.2.

Algorithm 3.2: Power Control Algorithm

Input: β_{jkl} and $\overline{\rho}^{\mathrm{d}}_{lk}$, $\forall j,l = 1,2,\ldots C$, $k = 1,2,\ldots K$, σ^2_n, ρ_{p}.

```
Initialize ρ^d_{jk'}(0) = 0.5 ρ̄^d_{jk'};
for i = 1, 2, ..., N_it do
    for k' = 1, 2, ..., K do
        Evaluate I^d_{k'j}(i) = ρ^d_{jk'}(i−1)/ς^d_{k'j}(i−1);
        if I^d_{k'j}(i) ≤ ρ̄^d_{jk'} / ς̂^d_{k'j} then
            Evaluate ρ^d_{jk'}(i) = ς̂^d_{k'j} I^d_{k'j}(i);
        else
            Evaluate ρ^d_{jk'}(i) = (ρ̄^d_{jk'})^2 / (ς̂^d_{k'j} I^d_{k'j}(i));
        end if
    end for
end for
```

Output: $\rho^{\mathrm{d}}_{jk'}$.

Table 3.2: Target SINR's of power control algorithm adopted for each PA technique.

Number of users	PA Scheme	DL	UL
$K = 10$	Random	-9 dB	-10 dB
	H-MaxminSINR DL	-2 dB	-9 dB
	H-MaxminSINR UL	-6 dB	-4 dB
	H-MaxminTC	-3 dB	-5 dB
$K = 32$	Random	-11 dB	-14 dB
	H-MaxminSINR DL	-7 dB	-11 dB
	H-MaxminSINR UL	-9 dB	-7 dB
	H-MaxminTC	-7 dB	-8 dB

3.2.1 Numerical Results

The paper of Appendix D brings several numerical results of the investigated power control algorithm applied to massive MIMO systems with finite number of antennas. For $K = 32$ users and employing power control, Figure 3.5 shows the fraction of users above a given rate for $M = 128$, while Figure 3.6 shows the 95%-likely rate achieved with increasing number of antennas. The target SINR's performances of power control algorithm for each scheme were empiricaly chosen in order to provide the higher throughput for 95% of the users, as

indicated in Table 3.2. It can be seen that much more uniform user performances are achieved with the power control scheme of Algorithm 3.2, and that the assured performance can be considerably improved with a proper choice of the PA employed. For example, as can be seen in Figure 3.6, with random assignment the 95%-likely DL rate increases from 41.3 kbps to 746.2 Mbps with $M = 128$ antennas when employing power control, while this DL rate increase is from 191.6 kbps to 1.782 Mbps when the H-MaxminTC is the PA adopted. Similarly, in the UL, the 95%-likely UL rate with random assignment increases from 0.5 kbps to 382.5 Mbps when employing power control, and from 2.0 kbps to 1.442 Mbps with H-MaxminTC as PA policy and $M = 128$. It can also be seen that H-MaxminTC with power control has the ability of jointly assuring an appreciable quality of service in both DL and UL, contrary to H-MaxminSINR DL and H-MaxminSINR UL that assure good rates only on its preferential direction. The assured rates are decreased with this higher number of users not only due to the increased multiuser interference, but also due to the increased pilot overhead, necessary to obtain CSI estimates of this increased number of users. On the other hand, it allows the PA schemes to achieve improved gains in comparison with random assignment because of the greater multiuser diversity.

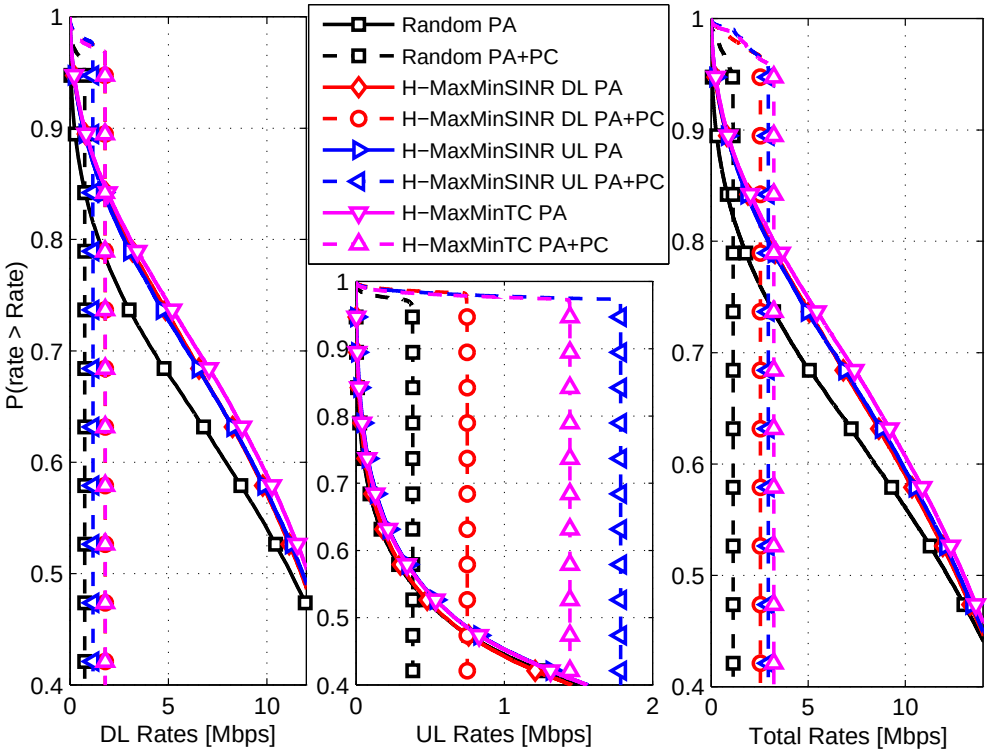

Figure 3.5: Fraction of users above a given Rate for $M = 128$ BS antennas and $K = 32$ users: a) DL; b) UL; c) Total. Power control evaluated with target SINR's of Table 3.2.

Performance results with power control as depicted in Figures 3.5 and 3.6 were obtained after a careful but non-exhaustive process of finding suitable target SINR performances for each scheme under the considered scenarios, as summarized in Table 3.2. However, this values of target performances are dependent of the instantaneous conditions of the communications systems, like the number of users served and pilot and data SNR's, which are dynamically changing. Thus, a more practical scenario consists in fixing a DL and UL target rates, from which the target SINR's input parameters of the power control algorithm are obtained. Under this strategy, Figure 3.7 shows the 95%-likely rates obtained when fixing a target per user rate of 1.4 Mbps for both DL and UL when serving $K = 32$ users. It can be seen from Figure 3.7 that H-MaxminTC PA with power control is able to assure the target rates in both DL and UL even with just $M = 64$ antennas,

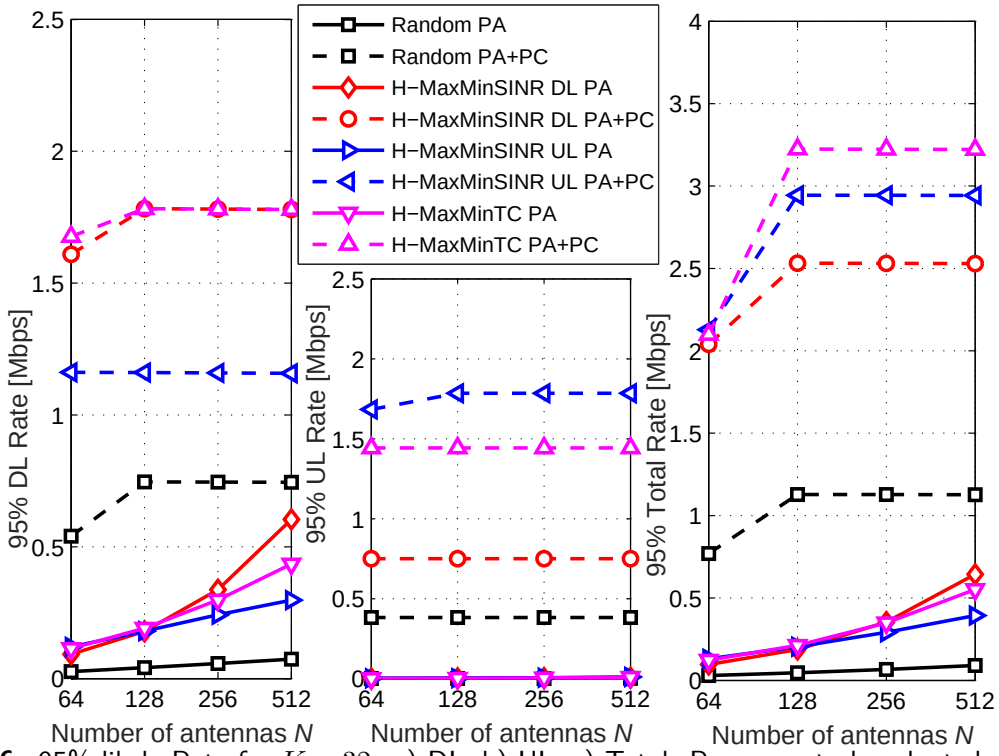

Figure 3.6: 95%-likely Rate for $K = 32$: a) DL; b) UL; c) Total. Power control evaluated with target SINR's of Table 3.2.

while the H-MaxminSINR DL PA with power control fails in this objective for UL, and the opposite holds for H-MaxminSINR UL. It is important to note that even with the 95%-likely DL and UL rate of 1.4 Mbps assured by H-MaxminTC PA with power control, it is not assured a 95%-likely total rate of 2.8 Mbps, since the set of users that do not achieve the target DL rate is not necessarily the same that do not achieve the target UL rate. This result shows that H-MaxminTC PA with power control is able to assure an appreciable 95%-likely DL and UL per user rates of 1.4 Mbps for $K = 32$ users with only $M = 64$ BS antennas.

3.3 Conclusion of the Chapter

We have shown in this Chapter that massive MIMO system performance can be greatly improved via suitable pilot assignment schemes, since the pilot contamination interference seen by each UE is dependent on the pilot sequence it is employing. Therefore, in order to improve fairness, we can seek to assign the pilots with the lowest interference levels to the users with poor channel conditions. We have discussed the influence of PA in DL performance, and showed that it is not so simple as in UL. Also, we have shown that UL and DL PA metrics are conflicting, in such a way that if a scheme seeks to optimize the performance in a single link, it will achieve just a standard performance in the other link. Therefore, we have proposed a joint UL-DL PA metric based on Total Capacity, which is able to achieve promising performance results in both links. Besides, in order to avoid the exhaustive search of prohibitive complexity when solving a PA problem, we have proposed low-complexity near-optimal solutions for the investigated PA strategies. Finally, the PA algorithms have been combined with suitable power control algorithms aiming to prove its effectiveness and take full advantage of the available resources.

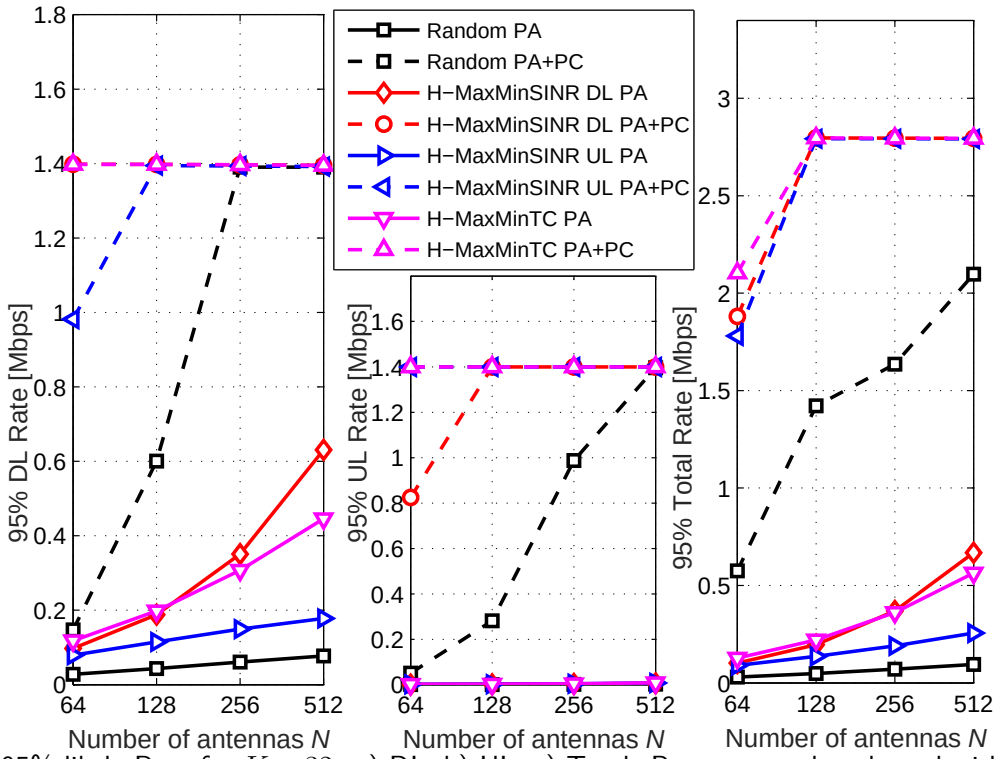

Figure 3.7: 95%-likely Rate for $K = 32$: a) DL; b) UL; c) Total. Power control evaluated with a target rate of 1.4 Mbps per user, for both UL and DL.

4 Massive MIMO Waveforms and Total Energy Efficiency

This chapter discusses about the main contributions achieved by this Doctoral work regarding to massive MIMO waveforms and total energy efficiency. It is firstly described our derived expressions for the UL massive MIMO system performance, both in terms of SINR as well as achievable rates. Then, aiming to validate the proposed expressions, we compare them with numerical results obtained via Monte-Carlo simulation. Finally, we evaluate the total energy efficiency of the massive MIMO system employing different UL waveforms aiming to provide a more accurate comparison about the theme.

4.1 Massive MIMO Waveforms

We have derived in this work approximated UL performance expressions for the massive MIMO systems employing either OFDM or SC waveforms. The detailed derivations can be seen in Appendix B, while the obtained approximated SINR expressions for OFDM and SC, respectively, are

$$\varsigma^{\mathrm{F}}_{k'i} = \frac{M\beta^2_{ik'i}}{M\sum\limits_{\substack{c=1\\c\neq i}}^{C}\beta^2_{ik'c} + \left[\sum_{j=1}^{C}\sum_{k=1}^{K}\beta_{ikj} + \frac{\sigma_n^2}{\gamma\rho_{\mathrm{u}}}\right]\left[\sum_{c=1}^{C}\beta_{ik'c} + \frac{\sigma_n^2}{\rho_{\mathrm{p}}}\right]}, \tag{4.1}$$

$$\varsigma^{\mathrm{T}}_{k'i} = \frac{M\beta^2_{ik'i}}{M\sum\limits_{\substack{c=1\\c\neq i}}^{C}\beta^2_{ik'c} + \left[\sum_{j=1}^{C}\sum_{k=1}^{K}\beta_{ikj} + \frac{\sigma_n^2}{\rho_{\mathrm{u}}}\right]\left[\sum_{c=1}^{C}\beta_{ik'c} + \frac{\sigma_n^2}{\rho_{\mathrm{p}}}\right]}. \tag{4.2}$$

Both expressions are very similar, except by the factor $\gamma = N/(N+N_{CP})$ in (4.1), which reflects the transmit power reduction in OFDM systems due to the CP transmission. Besides, reminding that $\sum_{c=1}^{C}\beta_{ik'c} + \frac{\sigma_n^2}{\rho_{\mathrm{p}}} = \alpha^2_{ik'}$, the performance expression in (4.1) is identical to that of (2.7), which was derived in [5] assuming a minimum mean square error (MMSE) CSI estimator. Our most novel result is that a MRC receiver operating under SC waveform, namely the TRMRC receiver, is able to reach the same performance of FDMRC, with a slight transmit power gain by not transmitting CP. Based on such expressions, on the convexity of $\log_2(1+\frac{1}{x})$, and using Jensen's inequality as in [30], we obtain the following lower bound on the achievable rate of the k'th user at the ith cell

$$\mathcal{R}^{\mathrm{F}}_{k'i} \geq \widetilde{\mathcal{R}}^{\mathrm{F}}_{k'i} = \xi^{\mathrm{u}}\gamma\left(1-\frac{K}{\mathcal{S}}\right)\log_2\left(1+\left(\frac{1}{\varsigma^{\mathrm{F}}_{k'i}}\right)^{-1}\right), \tag{4.3}$$

$$\mathcal{R}^{\mathrm{T}}_{k'i} \geq \widetilde{\mathcal{R}}^{\mathrm{T}}_{k'i} = \xi^{\mathrm{u}} \left(1 - \frac{K}{\mathcal{S}}\right) \log_2 \left(1 + \left(\frac{1}{\varsigma^{\mathrm{T}}_{k'i}}\right)^{-1}\right), \tag{4.4}$$

in which the term $\left(1 - \frac{K}{\mathcal{S}}\right)$ accounts for the pilot transmission overhead, and ξ^{u} is the fraction of the data transmit interval spent with uplink.

4.1.1 Numerical Results

In the paper presented in Appendix B, the above expressions were validated by comparison with Monte-Carlo simulation results, with respect to the variation of several parameters, like number of antennas, number of users, transmit power, and number of CIR taps. As an example, Figure 4.1 shows the variation of the SINR and of the achievable rates, both simulated and analytic, with the increasing SNR, while Figure 4.2 does the same with increasing number of users. We have assumed in the simulations $M = 100$ BS antennas, $K = 4$ users, $N = 256$ subcarriers when OFDM is employed, a time-dispersive channel with $L = 16$, $\xi^{\mathrm{u}} = 0.5$, and an SNR of 0dB for both pilots and UL data transmission.

From Figure 4.1, one can see that the massive MIMO system is able to operate with low UL SNR's, due to the large number of BS antennas, in such a way that the system performance saturates near 0dB. Besides, both schemes result in very similar SINR performance, but the achievable rates of TRMRC are higher than that of FDMRC due to the inefficiency of the CP transmission, required by the latter. It is also shown that the approximate expressions for SINR and the proposed lower bounds for achievable rates are tight. While the error for SINR was about 0.06dB, the error between the simulated rates and the proposed lower bound was about 0.075 bits per channel use (bpcu).

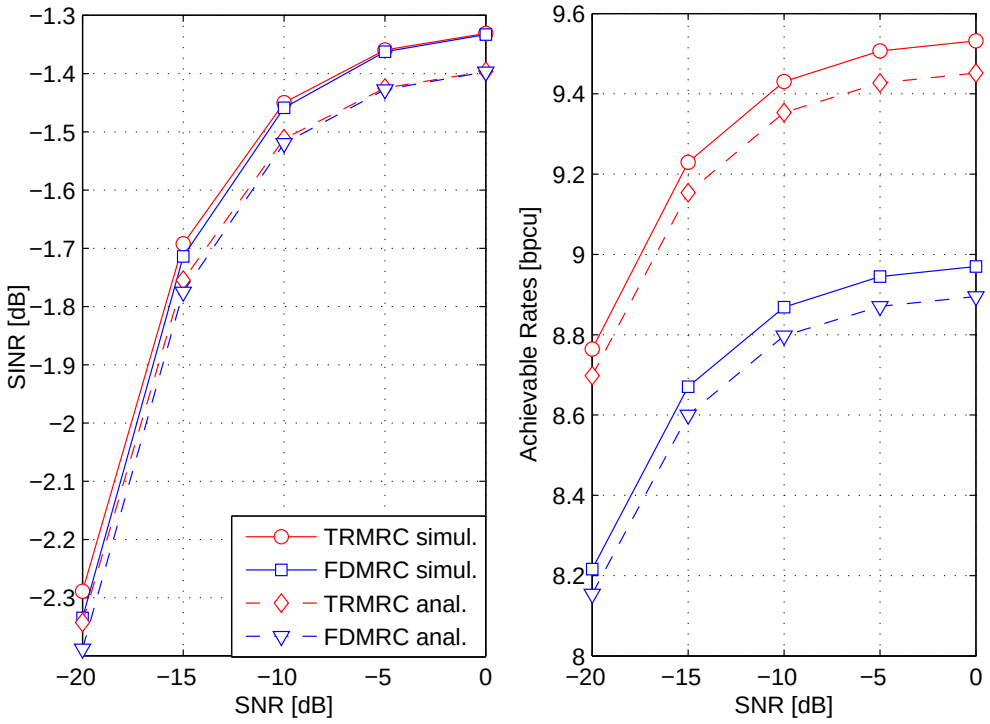

Figure 4.1: Performance of the investigated schemes with increasing $\frac{\rho_{\mathrm{u}}}{\sigma_n^2}$, with $M = 100$ BS antennas.

Figure 4.2 shows how the massive MIMO system performance evolves with the increasing number of users

per cell, K. As expected, the average SINR per user decreases, due to the increasing multiuser interference. However, the achievable rates grow with more users, since the sum rate increase of each additional user in the investigated interval compensates the decrease of the individual SINR. Besides, the errors between simulated performances and analytical expressions in terms of individual SINR have decreased for higher values of K, being 0.01dB for $K = 32$. However, the achievable rate errors have increased to 0.09 bpcu for $K = 32$, because the higher number of users makes the accumulated error large.

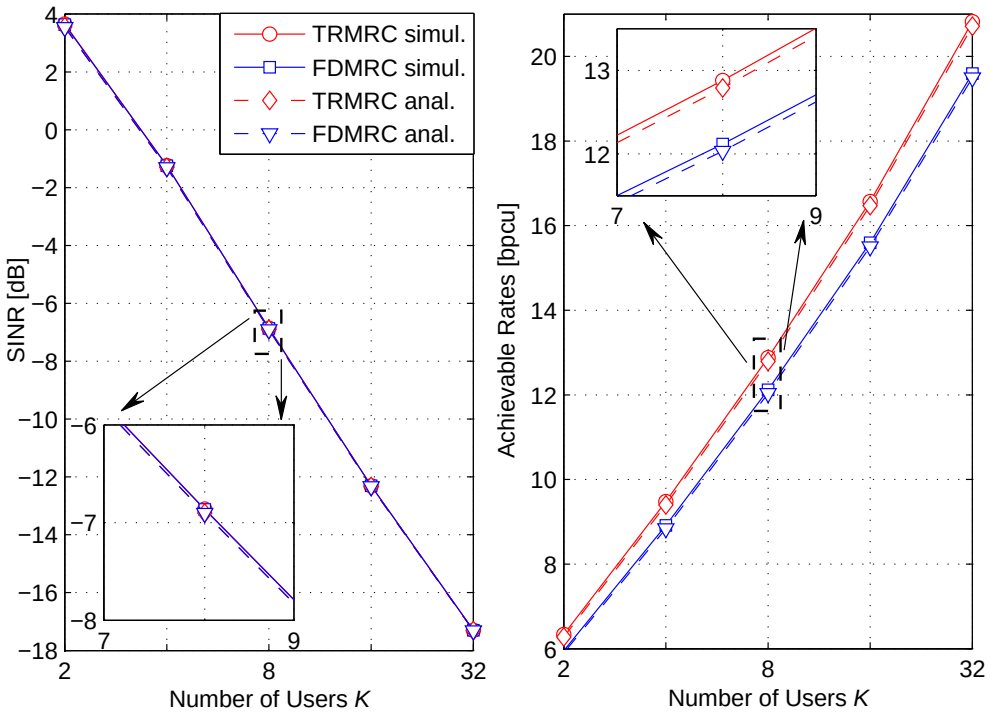

Figure 4.2: Performance of the investigated schemes with increasing K.

Complexity Analysis

In order to establish a performance-complexity trade-off, the paper presented in Appendix B evaluate the computational complexity of TRMRC and FDMRC massive MIMO receivers in terms of *floating-point operations (flops)* [31]. The main assumptions made are: *i*) A real sum operation has the same complexity than a real multiplication, which are defined as 1 *flop*; *ii*) A complex sum has the complexity of 2 *flops*, while a complex multiplication has the complexity of 6 *flops*; *iii*) An inner product between 2 complex vectors of size M has the complexity of M complex multiplications and $M-1$ complex additions, resulting in a total complexity of $8M-2$ *flops*; *iv*) A FFT or IFFT operation of a complex sequence of N samples has the complexity (supposing N power of two and adopting the Cooley Tukey algorithm [31]) of $(N/2)\log_2(N)$ complex multiplications and $N\log_2(N)$ complex additions, and an overall complexity of $5N\log_2(N)$ *flops*; *v*) The complexity related with the CSI estimation is neglected for all the investigated schemes, since these estimates remain valid for several frame periods, and account in the same way for all the schemes. Aiming to reduce the computational complexity of the TRMRC receiver, the paper in Appendix B also proposes a low-complexity implementation of this receiver, by employing the fast-convolution (FC) with overlap-and-add method [32], namely the FC-TRMRC receiver.

The complexities are found in Table 4.1. For the FDMRC under OFDM, the complexity to detect the

N symbols of the OFDM frame is mainly due to: *i*) the N-points IFFT operations of each user transmission ($K[5N\log_2(N)]$ *flops*), *ii*) the N-points FFT operations of each BS receive antenna ($M[5N\log_2(N)]$ *flops*), and due to *iii*) the N FDMRC data symbols' estimation, as in (2.4), for each user ($NK[8M-2]$ *flops*). On the other hand, the complexity of the TRMRC with overlap-and-add method is mainly given by: *i*) $\mu=(N+L)/L$ FFT's of size $2L$ for the received signals of each receive antenna, resulting in a complexity of $M\mu[10L\log_2(2L)]$ *flops*; *ii*) For each user and each receive antenna: μ element-wise multiplication of size $2L$ vectors, followed by an IFFT operation of size $2L$, and the addition of the overlaping segments (of size L) ($KM\mu[10L\log_2(2L)+12L+2L]$ *flops*); *iii*) For each user, the results of the M fast convolutions are added (only the N elements of interest), with a complexity of $K(2N(M-1))$ *flops*.

The overall complexity of the TRMRC receiver employing the fast convolution with overlap-and-add method is also given in Table 4.1 and plotted in Figure 4.3. It can be seen that the complexity of the FC-TRMRC receiver results $\mathcal{O}(\log_2(2L)MK)$ per detected symbol vector, which is a significant complexity reduction in comparison with TRMRC ($\mathcal{O}(LMK)$). However, it is still significantly higher than that of FDMRC ($\mathcal{O}(MK)$). We found thus that employing TRMRC at the massive MIMO UL presents several advantages in comparison to FDMRC, like lower PAPR, cheaper and more energy efficient mobile terminals, lower sensitivity to phase noise and carrier frequency offset, CP transmission not required, improving energy and spectral efficiency of the system, and compatibility with previous standards. However, at the cost of an increased computational complexity.

Table 4.1: Number of operations (flops) for each scheme.

Scheme	Number of Operations
FDMRC	$K[5N\log_2(N)]+M[5N\log_2(N)]$ $+NK[8M-2]$
TRMRC	$NK[L(8M-2)+2(L-1)]$
FC-TRMRC	$K[M(N+L)(10\log_2(2L)+14)+2N(M-1)]$ $+M(N+L)10\log_2(2L)$

Optimizing the Number of Scheduled Users

Based on the derived performance expressions, the paper in Appendix B also proposes an iterative method for obtaining the number of scheduled users that maximizes the system sum rate. Figure 4.4 depicts the system sum rate variation with increasing number of users, and also indicates the solution of our proposed method. It can be clearly seen that the result obtained by the proposed method is able to find the optimal number of scheduled users, with different pilot and frequency reuse schemes. Further details about the proposed method can be seen in Appendix B.

The dependence of the optimal number of users and the optimal sum rate with the increasing number of antennas is shown in Figure 4.5. One can note that the optimal number of scheduled users converges with $M\to\infty$ to $\mathcal{S}/(2\zeta^{\mathrm{p}})$, as discussed in [22]. On the other hand, an interesting conclusion that has not been drawn is that both resources' reuse schemes have the same asymptotic performance, as demonstrated in Appendix B. However this equivalence holds only for unpractical values of M, while pilot reuse presents an improved performance in comparison with frequency reuse for a not so large number of antennas.

Figure 4.6 shows how the increasing SNR affects the optimal number of scheduled users and sum rate

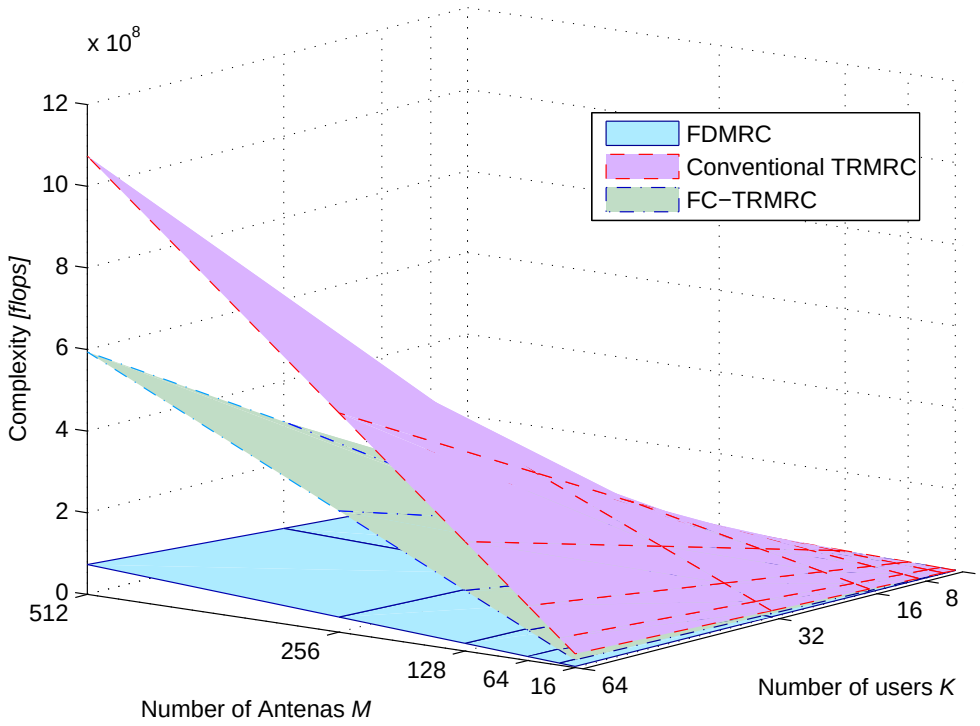

Figure 4.3: Computational complexities of the investigated schemes.

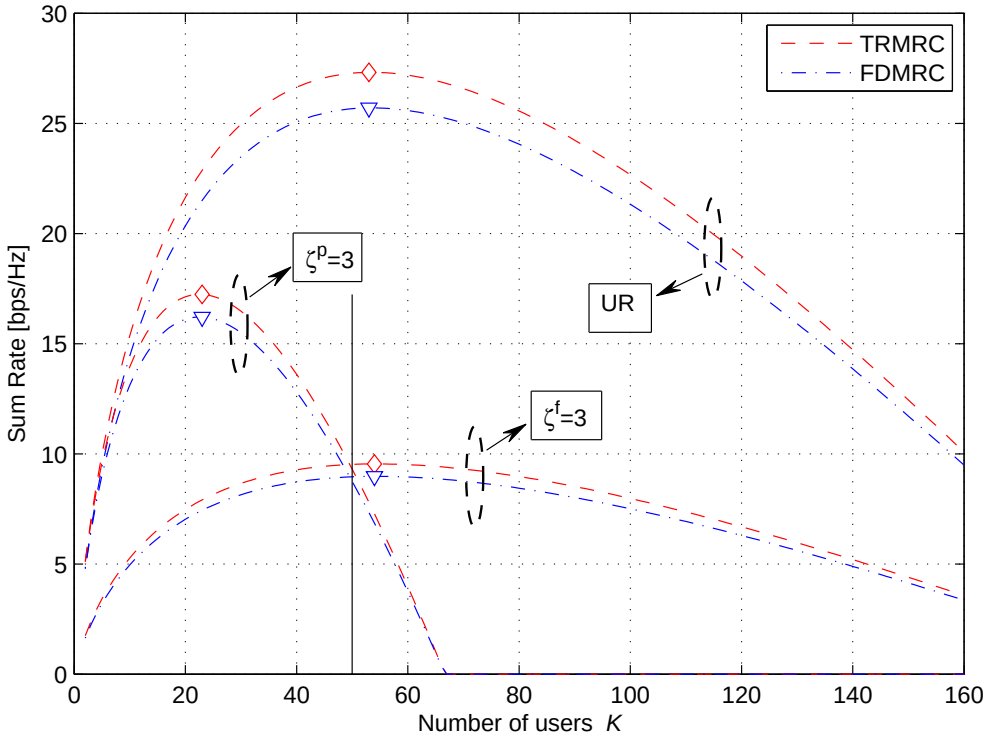

Figure 4.4: Sum Rate with increasing K for $M = 100$ and $\mathcal{S} = 200$ symbols. ζ^{p} and ζ^{f} are the pilot and frequency reuse factor, respectively, while UR refers to universal reuse factor.

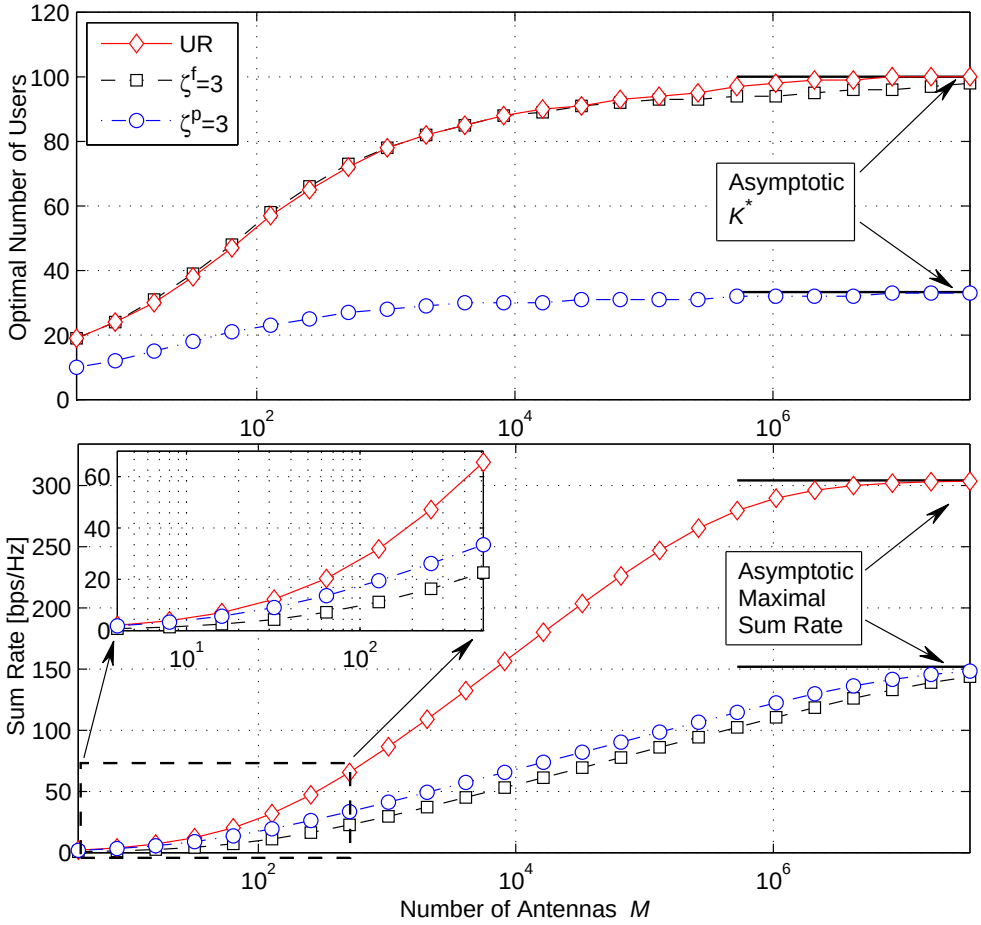

Figure 4.5: K^* and sum rate with increasing M for $\mathcal{S} = 200$.

performance. In the left hand side, it is investigated the increasing data SNR with the training SNR fixed as 0dB, while in the right hand side the increasing training SNR is considered with data SNR fixed as 0 dB. Although any SNR increase has the effect of improving the system sum rate performance, the optimal number of users in each case have opposite behaviors, as discussed in Appendix B. While it decreases with increasing $\frac{\rho_u}{\sigma_n^2}$, it increases with increasing $\frac{\rho_p}{\sigma_n^2}$. Besides, the variation of the optimal number of users and of the sum rate with increasing training SNR is more notorious. This occurs since the increase of $\frac{\rho_p}{\sigma_n^2}$ leads to better CSI estimates, which in turn improves the interference mitigation capacity of the MRC receiver, allowing the scheduling of a higher number of users in order to obtain the optimal sum rate performance. On the other hand, the increasing $\frac{\rho_u}{\sigma_n^2}$ results in a higher level of multiuser interference, both intra-cell and inter-cell, in such a way that the best sum rate performance is found with a slightly reduced number of users.

4.2 Total Energy Efficiency Evaluation

We found in the previous Section that TRMRC under SC presents several advantages over FDMRC with OFDM, however at the cost of increased computational complexity. In order to further ellaborate the comparison between these topologies, we evaluate in this Section the *total energy efficiency* of a massive MIMO system employing either FDMRC or TRMRC in the UL. Our main objective with this analysis is to identify the best scheme to be implemented in the upcoming massive MIMO systems based on a comprehensive analysis. The choice of the total energy efficiency metric is due to its ability of incorporating different aspects of

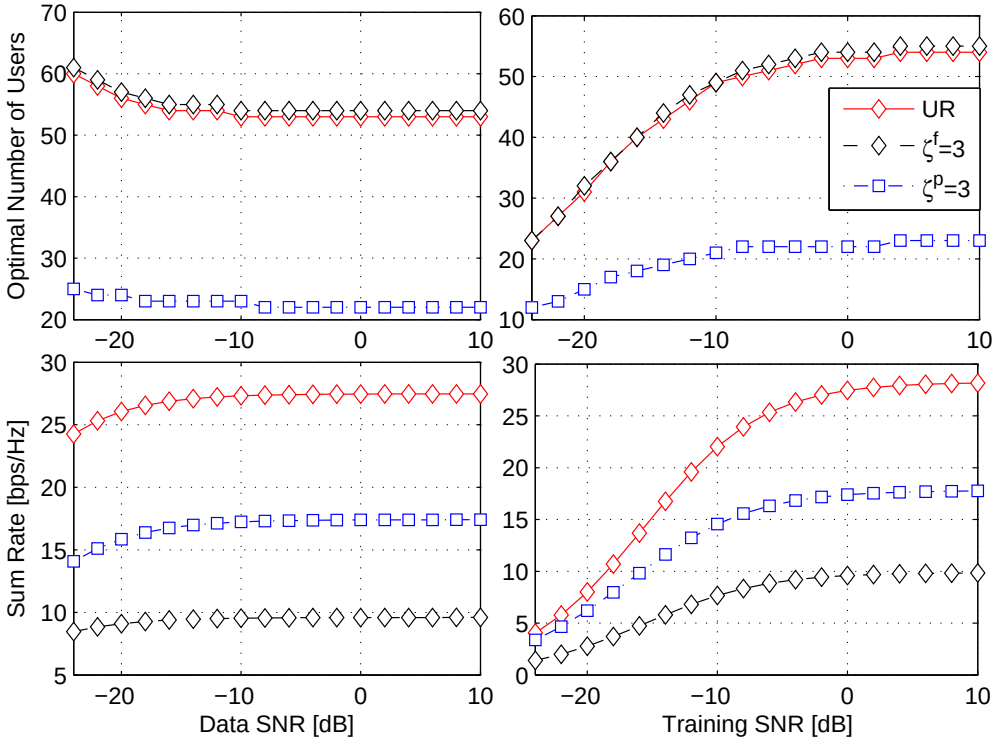

Figure 4.6: Optimal number of users and sum rate with increasing data and training SNR for $\mathcal{S} = 200$.

each investigated topology, making the analysis more comprehensive and fair. The higher achievable rates of TRMRC, the reduced complexity of FDMRC, and also the consequent better power efficiency of the power amplifier in a SC scheme due to the lower PAPR levels are examples of different features that are incorporated on this analysis. The analysis and the results of this Section can also be found in the paper of Appendix E.

The total energy efficiency metric is defined as

$$\mathrm{EE} = \frac{\sum_{k=1}^{K} \left(\mathcal{R}_{ki}^{\mathrm{UL}\star} + \mathcal{R}_{ki}^{\mathrm{DL}}\right)}{P_{\mathrm{TX}}^{\mathrm{UL}\star} + P_{\mathrm{TX}}^{\mathrm{DL}} + P_{\mathrm{TX}}^{\mathrm{tr}\star} + P_{\mathrm{CP}}^{\star}}. \tag{4.5}$$

The superscript $\{\cdot\}^{\star}$ is used in order to indicate that a given parameter depends on which waveform/detector has been employed in UL. In (4.5), $\mathcal{R}_{ki}^{\mathrm{UL}\star}$ constitutes the UL rate of the kth user of the ith cell, and can be found by (4.3) or (4.4), *i.e.*, $\mathcal{R}_{ki}^{\mathrm{UL}\star} = \mathcal{R}_{ki}^{\mathrm{F}}$ or $\mathcal{R}_{ki}^{\mathrm{UL}\star} = \mathcal{R}_{ki}^{\mathrm{T}}$. Besides, $\mathcal{R}_{ki}^{\mathrm{DL}}$ is the DL rate of this user. We assume that a MRT precoding has been employed in downlink under OFDM waveform, since the practical appeal for SC usage in DL is not so strong as it is in UL, and thus $\mathcal{R}_{ki}^{\mathrm{DL}}$ can be found similarly to (4.3) as:

$$\mathcal{R}_{k'i}^{\mathrm{DL}} \geq \widetilde{\mathcal{R}}_{k'i}^{\mathrm{DL}} = \xi^{\mathrm{d}} \gamma \left(1 - \frac{K}{\mathcal{S}}\right) \log_2 \left(1 + \left(\frac{1}{\varsigma_{k'i}^{\mathrm{DL}}}\right)^{-1}\right), \tag{4.6}$$

in which ξ^{d} is the fraction of the data transmit interval spent with downlink, and

$$\varsigma_{k'i}^{\mathrm{DL}} = \frac{\beta_{ik'i}^2 / \alpha_{ik'}^2}{\sum_{\substack{l=1 \\ l \neq i}}^{C} \beta_{lk'i}^2 / \alpha_{lk'}^2 + \frac{1}{M}\left(K \sum_{l=1}^{C} \beta_{lk'i} + \frac{\sigma_n^2}{\rho^{\mathrm{d}}}\right)} \tag{4.7}$$

is the DL SINR of the k'th user of the ith cell, while ρ^{d} is the uniform DL transmit power.

Furthermore, $P_{\mathrm{TX}}^{\mathrm{UL}\star}$, $P_{\mathrm{TX}}^{\mathrm{DL}}$, and $P_{\mathrm{TX}}^{\mathrm{tr}\star}$ in (4.5) represent the power consumed by the power amplifiers in UL,

DL, and UL pilot transmission, respectively. In our scenario of uniform power allocation we have

$$P_{\mathrm{TX}}^{\mathrm{UL}\star} = \frac{K\xi^{\mathrm{u}}\left(1-\frac{K}{\mathcal{S}}\right)\rho^{\mathrm{u}}}{\eta^{\mathrm{u}\star}}, \tag{4.8}$$

$$P_{\mathrm{TX}}^{\mathrm{DL}} = \frac{K\xi^{\mathrm{d}}\left(1-\frac{K}{\mathcal{S}}\right)\rho^{\mathrm{d}}}{\eta^{\mathrm{d}}}, \tag{4.9}$$

$$P_{\mathrm{TX}}^{\mathsf{tr}\star} = \frac{K\left(\frac{K}{\mathcal{S}}\right)\rho^{\mathrm{p}}}{\eta^{\mathrm{u}\star}}, \tag{4.10}$$

in which $\eta^{\mathrm{u}\star}$ and η^{d} represent the power amplifier efficiency at the MT's and at the BS's, respectively. The parameter $\eta^{\mathrm{u}\star}$ is specific for each topology chosen as waveform/detector, since a power amplifier with better eficiency can be employed in the MT's if SC is adopted instead of OFDM.

Finally, $P_{\mathrm{CP}}^{\star}$ accounts for the circuit power consumption, which is discussed in detail in the following.

4.2.1 Realistic Circuit Power Consumption Model

The paper of Appendix E brings a detailed discussion about realistic models for the circuit power consumption of the different stages in a practical MIMO communication system. The adopted approach is similar to that of [14]. Adopting a realistic circuit power consumption model, the parameter $P_{\mathrm{CP}}^{\star}$ is not fixed, but dependent on several factors, like number of antennas, number of users, waveform employed, adopted precoding and detector schemes, data throughput, among others. Following [14], a refined circuit power consumption model for multiuser MIMO systems can be stated as

$$P_{\mathrm{CP}}^{\star} = P_{\mathrm{FIX}} + P_{\mathrm{TC}} + P_{\mathrm{CE}} + P_{\mathrm{C/D}}^{\star} + P_{\mathrm{BH}}^{\star} + P_{\mathrm{LP}}^{\star}, \tag{4.11}$$

in which P_{FIX} is a constant quantity accounting for the fixed power consumption required for site-cooling, control signaling, and load-independent power of backhaul infrastructure and baseband processors [14]. The other terms in (4.11) are defined in the following subsections.

Transceiver Chains

In (4.11), P_{TC} accounts for the power consumption of the transceiver chains. As described in [14], [33], one can quantify the power consumption of a set of transmitters and receivers as

$$P_{\mathrm{TC}} = P_{\mathrm{SYN}} + MP_{\mathrm{BS}} + KP_{\mathrm{MT}}, \tag{4.12}$$

in which P_{SYN} is the power consumed by the local oscillator, P_{BS} is the power necessary to the circuit components of each BS antenna operate, like converters, mixers, and filters, while P_{MT} accounts for the power required by the circuit components of each single-antenna MT operate, including amplifiers, mixer, oscillator and filters.

Channel Estimation

P_{CE} accounts for the power consumption of channel estimation in (4.11). We assume only UL training by UL pilot transmissions. Thus, all processing is carried out at the BS, which has a *computational efficiency* of $\mathcal{L}_{\mathrm{BS}}\left[\frac{\mathrm{flops}}{\mathrm{watt}}\right]$. The pilot-based CSI estimation is performed once per coherence block, and there are $B/\mathcal{S}$ coherence blocks per second, being $B=1/T_n$ the total bandwidth. The CSI estimation procedure as described in (2.2) consists of simply multiplying the $M\times\tau$ matrix $\mathbf{Y}_{in}^{\mathrm{p}}$ with the $\tau\times 1$ pilot sequence $\boldsymbol{\psi}_k$ of each user, demanding thus $MK(8\tau-2)$ *flops*. Therefore, the power consumption spent with the channel estimation procedure is

$$P_{\mathrm{CE}}=\frac{B}{\mathcal{S}}\frac{MK(8\tau-2)}{\mathcal{L}_{\mathrm{BS}}}. \tag{4.13}$$

Coding and Decoding

In (4.11), $P_{\mathrm{C/D}}^{\star}$ accounts for the power consumption of the channel coding and decoding units. The BS performs channel coding and modulation to K sequences of information symbols in the DL, while each MT performs some suboptimal fixed-complexity algorithm for decoding its own sequence [14]. The opposite is performed in the UL. The consumed power on these procedures will thus depend on the actual rates, being expressed as

$$P_{\mathrm{C/D}}^{\star}=\sum_{k=1}^{K}\left(\mathcal{R}_{ki}^{\mathrm{UL}\star}+\mathcal{R}_{ki}^{\mathrm{DL}}\right)\left(\mathcal{P}_{\mathrm{COD}}+\mathcal{P}_{\mathrm{DEC}}\right). \tag{4.14}$$

where $\mathcal{P}_{\mathrm{COD}}$ and $\mathcal{P}_{\mathrm{DEC}}$ are the coding and decoding *power densities*, respectively, in $\left[\frac{\mathrm{watt}}{\mathrm{bit/s}}\right]$. In the same way as [14], it was assumed for simplicity that the power densities $\mathcal{P}_{\mathrm{COD}}$ and $\mathcal{P}_{\mathrm{DEC}}$ are the same in UL and DL.

Backhaul

$P_{\mathrm{BH}}^{\star}$ accounts for the power consumption of the load-dependent backhaul in (4.11), which is necessary to transfer UL/DL data between the BS and the core network. The backhaul consumption power is usually modeled with two components [14], one load-independent and one load-dependent. For convenience, the first one can be included in P_{FIX}, while the second one is proportional to the average sum rate. Therefore, the load-dependent backhaul consumption power can be computed as

$$P_{\mathrm{BH}}^{\star}=\sum_{k=1}^{K}\left(\mathcal{R}_{ki}^{\mathrm{UL}\star}+\mathcal{R}_{ki}^{\mathrm{DL}}\right)\mathcal{P}_{\mathrm{BT}}, \tag{4.15}$$

in which $\mathcal{P}_{\mathrm{BT}}$ is the *backhaul traffic power density* in $\left[\frac{\mathrm{watt}}{\mathrm{bit/s}}\right]$.

Linear Processing

In (4.11), $P_{\mathrm{LP}}^{\star}$ accounts for the power consumption of the linear processing at the BS. This power component can be divided for UL and DL. The power spent with the DL linear processing, which is a common factor for both investigated schemes, is represented as the sum of two terms: the first one is that required by making one matrix-vector multiplication per DL data symbol, and the second one is that required to obtain

the precoding matrix. Each multiplication between a $M \times K$ precoding matrix and a $K \times 1$ symbol vector demands the complexity of $M(8K-2)$ *flops*. Besides, in order to obtain the MRT precoders, it is just necessary to normalize the CSI estimate vectors aiming to obtain the precoding vector of each user, demanding thus $K(14M-2)$ *flops*. Therefore, the power consumption of the DL linear processing at the BS can be quantified as

$$P_{\mathrm{LP}}^{\mathrm{DL}} = B\left(1-\frac{\tau}{\mathcal{S}}\right)\xi^{\mathrm{d}}\frac{M(8K-2)}{\mathcal{L}_{\mathrm{BS}}} + \frac{B}{\mathcal{S}}\frac{K(14M-2)}{\mathcal{L}_{\mathrm{BS}}}. \tag{4.16}$$

The computational complexity of UL linear processing when employing FDMRC scheme under OFDM waveform is presented in Table 4.1. As the first term refers to a processing evaluated at the MT's, while the others refer to BS processing, this power can be quantified as

$$P_{\mathrm{LP}}^{\text{UL-F}} = B\left(1-\frac{\tau}{\mathcal{S}}\right)\xi^{\mathrm{u}}\left[K\frac{5N\log_2(N)}{\mathcal{L}_{\mathrm{MT}}} + M\frac{5N\log_2(N)}{\mathcal{L}_{\mathrm{BS}}} + N\frac{K(8M-2)}{\mathcal{L}_{\mathrm{BS}}}\right], \tag{4.17}$$

in which $\mathcal{L}_{\mathrm{MT}}$ is the computational efficiency of MT's in $\left[\frac{\text{flops}}{\text{watt}}\right]$. Note that, different than [14], we included the power required to the MT's perform OFDM modulation, and the power required to the BS's perform OFDM demodulation. The computational complexity of UL linear processing when employing TRMRC scheme under SC waveform is also presented in Table 4.1. As this processing is entirely evaluated at the BS, the power can be quantified as

$$P_{\mathrm{LP}}^{\text{UL-T}} = B\left(1-\frac{\tau}{\mathcal{S}}\right)\frac{\xi^{\mathrm{u}}}{\mathcal{L}_{\mathrm{BS}}}\{K[M(N+L)(10\log_2(2L)+14)+2N(M-1)]+M(N+L)10\log_2(2L)\} \tag{4.18}$$

Finally, the total power required by linear processing is given by

$$P_{\mathrm{LP}}^{\star} = P_{\mathrm{LP}}^{\mathrm{DL}} + P_{\mathrm{LP}}^{\mathrm{UL}\star}, \tag{4.19}$$

in which $P_{\mathrm{LP}}^{\mathrm{UL}\star} = P_{\mathrm{LP}}^{\text{UL-F}}$ or $P_{\mathrm{LP}}^{\mathrm{UL}\star} = P_{\mathrm{LP}}^{\text{UL-T}}$.

The main parameters adopted in our power consumption model are summarized in Table 4.2, which are adapted from [2], [14] and [34].

4.2.2 Numerical Results

We present in this subsection simulation results for the total energy efficiencies of massive MIMO systems employing either OFDM/FDMRC or SC/TRMRC as waveform/detector in the UL. The main parameters adopted in our simulations are summarized in Table 4.2. Fig. 4.7 depicts the total energy efficiencies of the investigated systems, with the variation of both number of BS antennas M and number of users K. As can be seen, the massive MIMO system employing FDMRC detector under OFDM waveform has a higher total energy efficiency than TRMRC under SC. The only exception occurs with low number of BS antennas ($M < 35$), in which TRMRC/SC outperforms FDMRC/OFDM. However, in the massive MIMO scenario (typically with $M > 80$), the total energy efficiency of FDMRC/OFDM is higher. Fig. 4.8 corroborates this result, showing the total energy efficiency percentage gain of FDMRC/OFDM in comparison with TRMRC/SC. As one can note from the figure, the total energy efficiency gain can achieve almost 20% in the range of our investigation, and can be even higher for increased values of M and K.

Table 4.2: Simulation parameters, adapted from [2], [14] and [34].

Parameter	**Value**
Cell radius: $d_{\max}$	500 m
Minimum distance: $d_{\min}$	50 m
Transmission bandwidth: B	20 MHz
Channel coherence bandwidth: W_c	100 kHz
Channel coherence time: T_c	2 ms
Total noise power: σ_n^2	-96 dBm
UL transmit power: ρ_{u}	200 mW
UL pilot transmit power: ρ_{p}	200 mW
DL radiated transmit power: $P_{\mathrm{TX}}^{\mathrm{DL}} \cdot \eta^{\mathrm{d}}$	2 W
Coherence block: $\mathcal{S}$	200 symbols
Computational efficiency at BSs: $\mathcal{L}_{\mathrm{BS}}$	$12.8 \left[\frac{\mathrm{Gflops}}{\mathrm{W}}\right]$
Computational efficiency at MTs: $\mathcal{L}_{\mathrm{MT}}$	$5.0 \left[\frac{\mathrm{Gflops}}{\mathrm{W}}\right]$
Fraction of DL transmission: ξ^{d}	0.60
Fraction of UL transmission: ξ^{u}	0.40
Power amplifier efficiency at the BSs: η^{d}	0.39
Power amplifier efficiency at the MTs under OFDM: η^{uF}	0.30
Power amplifier efficiency at the MTs under SC: η^{uT}	0.5
Fixed power consumption: P_{FIX}	18 W
Power consumed by local oscillators at BSs: P_{SYN}	2 W
Power required to run the circuit components at BSs: P_{BS}	1 W
Power required to run the circuit components at MTs: P_{MT}	0.10 W
Power density required for coding of data signals: $\mathcal{P}_{\mathrm{COD}}$	$0.10 \left[\frac{\mathrm{W}}{\mathrm{Gbits}}\right]$
Power density required for decoding of data signals: $\mathcal{P}_{\mathrm{DEC}}$	$0.80 \left[\frac{\mathrm{W}}{\mathrm{Gbits}}\right]$
Power density required for backhaul traffic: $\mathcal{P}_{\mathrm{BT}}$	$0.25 \left[\frac{\mathrm{W}}{\mathrm{Gbits}}\right]$

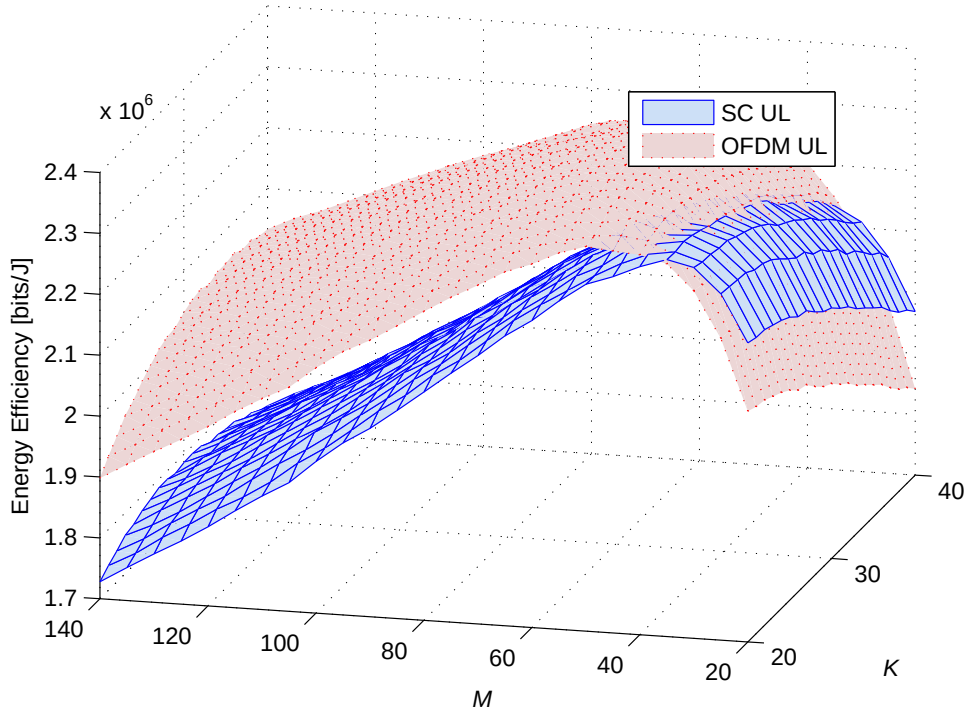

Figure 4.7: Total energy efficiency *vs* M and K for both investigated schemes.

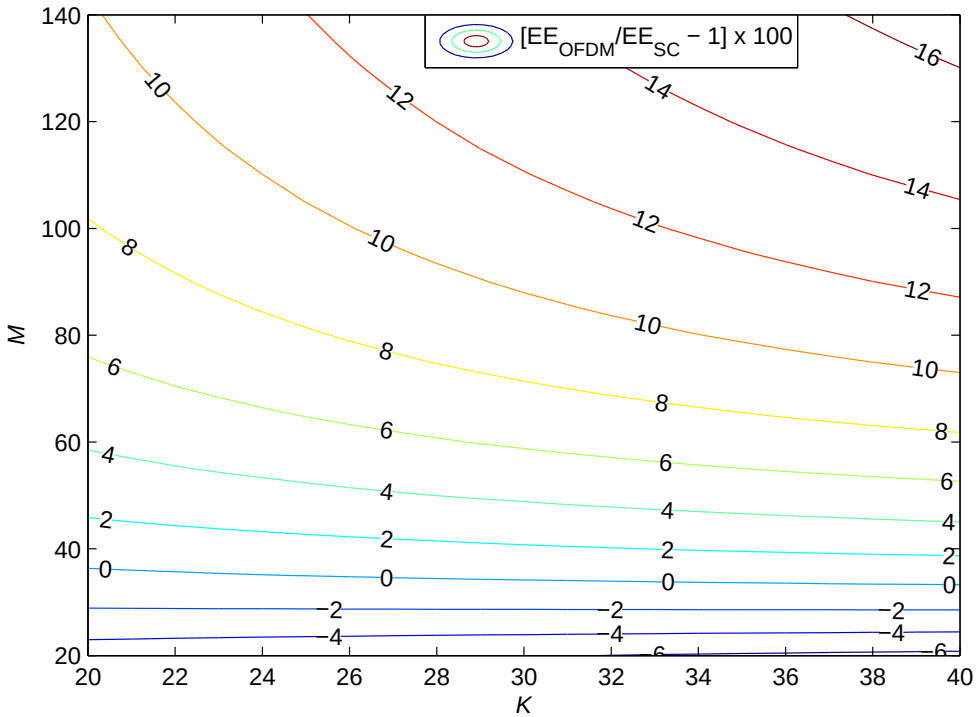

Figure 4.8: Contour plot showing the total energy efficiency gain (%) of OFDM/FDMRC in comparison with SC/TRMRC.

Then, aiming to compare the best total energy efficiencies achieved by each scheme, we restrict the range of K and M in a shorter interval centered on their maxima. Fig. 4.9 shows that the optimal total energy efficiency achieved by TRMRC/SC is of 2.315 Mbits/J, which is attained with $M = 35$ antennas serving $K = 22$ users. On the other hand, the optimal operation point for FDMRC/OFDM is attained with $M = 50$ antennas serving $K = 22$ users, in which a total energy efficiency of 2.359 Mbits/J can be achieved. Therefore, FDMRC/OFDM is able to provide a total energy efficiency improvement of 0.044 Mbits/J with respect to TRMRC/SC, considering both schemes in their respective optimal total energy efficiency operation points.

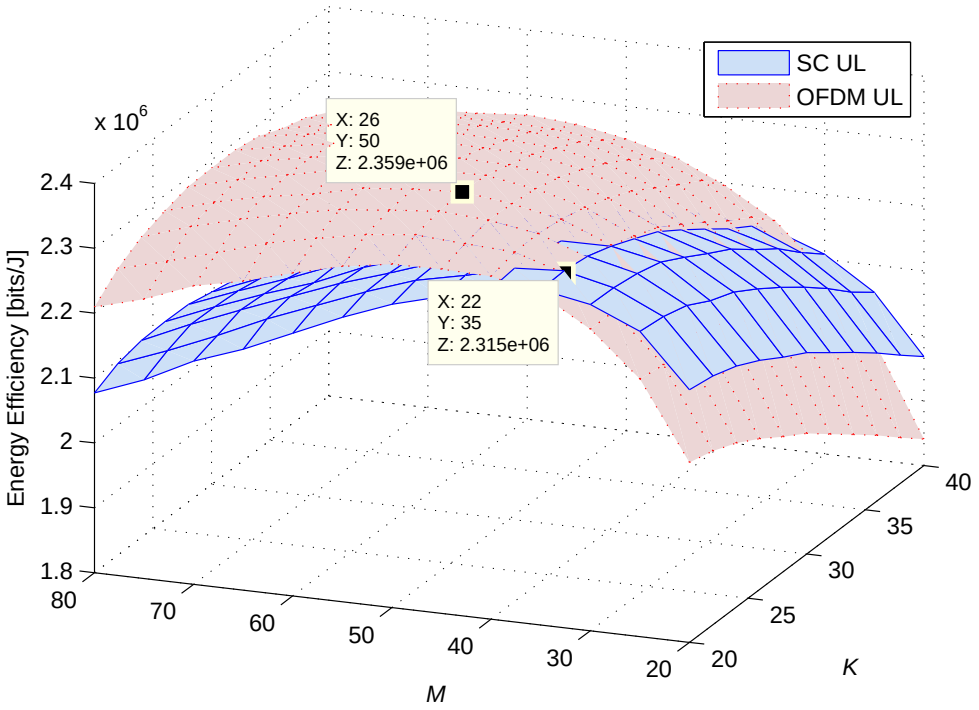

Figure 4.9: Total energy efficiency as a function of M and K (zoom of Fig. 4.7).

Finally, Fig. 4.10 shows the total energy efficiency and spectral efficiency trade-off for both investigated schemes. Each curve shows the total energy efficiency against spectral efficiency achieved for each scheme with the increasing number of BS antennas. For each number of BS antennas, the number of active users is set as the one leading to the maximum total energy efficiency for a given detector/waveform, as can be seen in Figure 4.7. As one can infer, TRMRC/SC is a good alternative only for low number of BS antennas ($M < 35$). Indeed, for higher values of M, FDMRC/OFDM provides a higher total energy efficiency under the same spectral efficiency, or alternatively a higher spectral efficiency under a target total energy efficiency.

4.2.3 Analysis with Increasing Computational Efficiency

Our previous results demonstrated that TRMRC/SC achieves a higher sum rate than FDMRC/OFDM, while spending less power with the irradiated signal and power amplifier. However, the higher computational complexity of TRMRC processing makes its total energy efficiency lower than that of FDMRC/OFDM. In this subsection we conjecture that such situation may change in a few years, since the evolution of computers and processors tends to improve the computational efficiency parameters, $\mathcal{L}_{\mathrm{BS}}$ and $\mathcal{L}_{\mathrm{MT}}$. Therefore, the power required to run the TRMRC processing would decrease, increasing its total energy efficiency. Fig. 4.11 shows

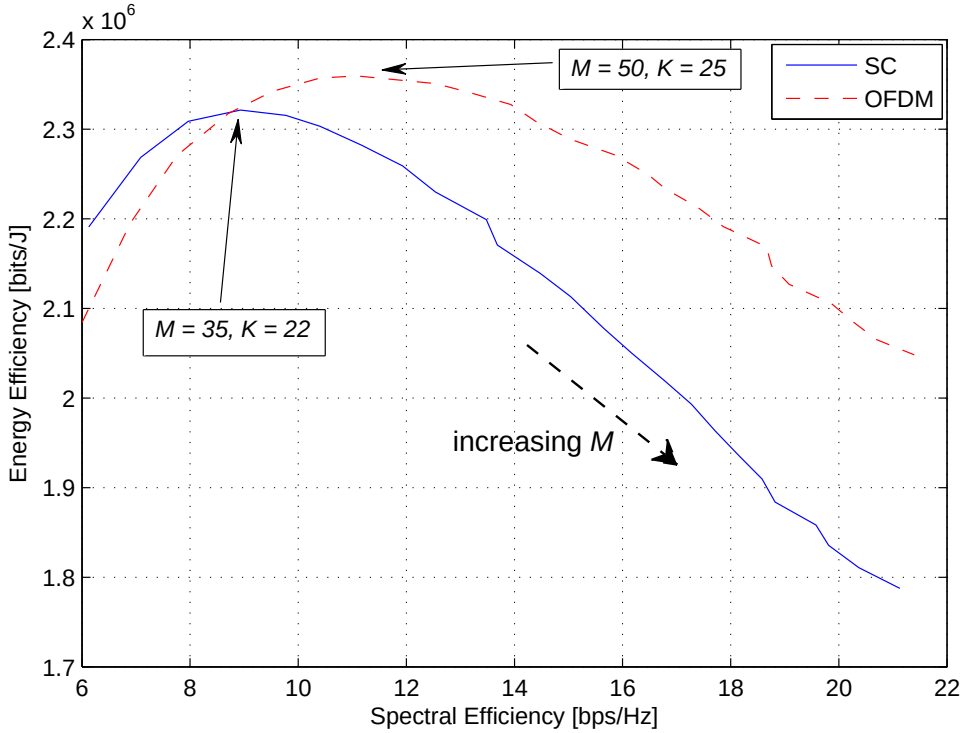

Figure 4.10: Total energy efficiency and sum spectral efficiency trade-off with increasing M.

the maximum total energy efficiency achieved by both schemes with increasing computational efficiencies, *i.e.*, the $\mathcal{L}_{\mathrm{BS}}$ and $\mathcal{L}_{\mathrm{MT}}$ in Table 4.2 were scaled by the factor represented in the horizontal axis. As depicted in the Figure, a 30% improvement in computational efficiencies is sufficient to make the total energy efficiency of TRMRC/SC higher than that of FDMRC/OFDM. This computational efficiency improvement is in accordance with the evolution of manufacturing process of transistors (14 nm to 10 nm) [35], or even with the improvement of current manufacturing process [36]. Therefore, employing TRMRC under SC waveform in the UL of massive MIMO systems may become a promising alternative in a near future aiming to implement very energy efficient communication systems.

4.3 Conclusion of the Chapter

In this Chapter, we have investigated the employment of SC and OFDM waveforms in the massive MIMO UL. We first derived performance expressions for TRMRC and FDMRC receivers, and validated them through numerical simulations. Then, we have analyzed the computational complexity of these schemes, in terms of *flops*, and proposed a low-complexity implementation of TRMRC. We also proposed an iterative method for obtaining the number of scheduled users able to maximize the system sum-rate, and investigated how this number varies with respect to different system parameters. Then, aiming to provide a more accurate comparison between TRMRC/SC and FDMRC/OFDM, we evaluated the total energy efficiency of the massive MIMO system employing such receivers/waveforms in the UL. Our main conclusion is that FDMRC/OFDM achieves better total energy efficiency than TRMRC/SC, since the higher sum-rates and higher power-amplifier efficiency due to lower PAPR of the latter do not compensate its higher processing power consumed. However, we predict that this scenario may change in a near future, with the evolution of processors technology and the consequent improvement on their computational efficiency.

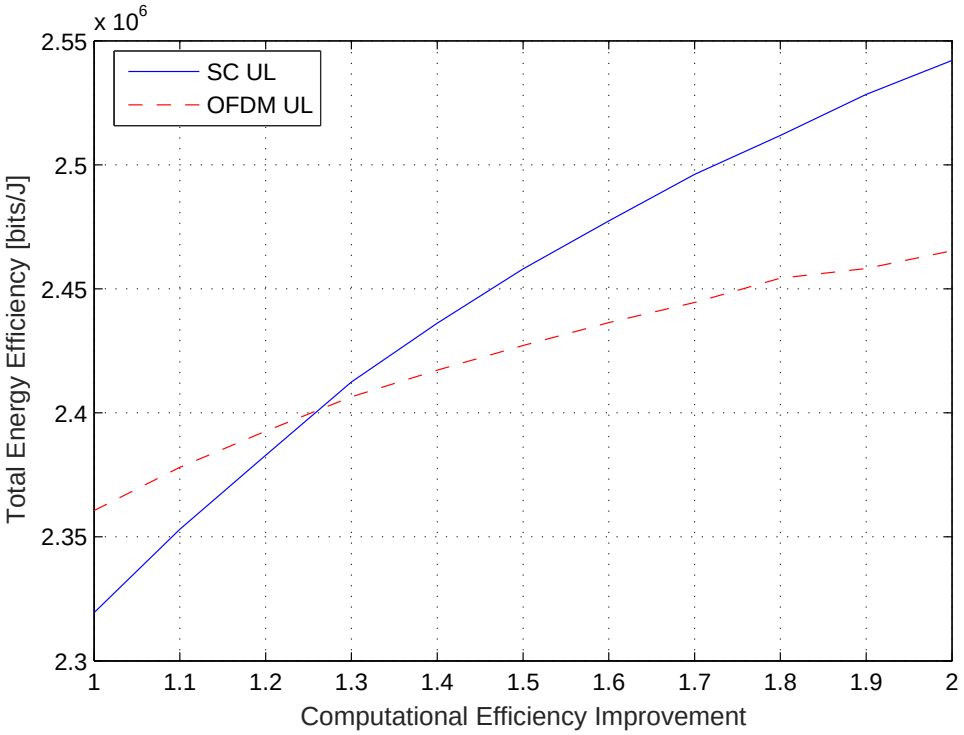

Figure 4.11: Total energy efficiency with increasing computational efficiency (both $\mathcal{L}_{\mathrm{BS}}$ and $\mathcal{L}_{\mathrm{MT}}$), for L=16 and $d_{\max} = 500$.

5 Random Access in Crowded Networks

We present in this chapter the main contributions achieved by this Doctoral work on the theme of random access in crowded massive MIMO networks. We first describe in detail the SUCRe protocol, and next show how can it be improved by employing a soft decision retransmission criterium. We then propose two approaches for computing the retransmission probability of each UE, and compare the results achieved by each one by means of numerical simulations.

5.1 RA in Crowded Networks

In crowded networks, it is a common interest to employ RA protocols able to detect and resolve pilot collisions under a distributed and uncoordinated manner. Since the number of UEs inside a given cell may be very large, conventional RA protocols in which the the task of detect and resolve pilot collisions is solely performed by the BS become impractical. Besides, if the protocol requires the periodical exchange of certain amount of control information, this may result in a severe overhead in performance as long as the number of UEs becomes very large. Massive MIMO is a key technology for obtaining decentralized and uncoordinated RA protocols due to its properties of channel hardening and favorable propagation. In this sense, the SUCRe protocol [18] appears as one of the most promising solutions. In the paper of Appendix F, the performance of this protocol is improved by implementing some modifications on its retransmission criterium, as described in the sequel.

In the SUCRe protocol, an accessing UE asks for a dedicated pilot by sending an uncoordinated random access pilot, with a risk that other UEs send the same pilot, hence, the collision probability increases when the number of UEs increases, *e.g.* in crowded and over-crowded machine-type scenarios. The favorable propagation of massive MIMO channels is utilized to enable distributed collision detection at each UE, thereby determining the strength of the contenders' signals and deciding to repeat the pilot if the UE judges that its signal at the receiver is the strongest.

Four Steps of the SUCRe Protocol

The four steps of the SUCRe protocol can be summarized as follows:

S.0. BS broadcasts a control signal. Each UE uses this signal to estimate its average channel gain and to synchronize itself towards the BS.

S.1 A subset of the inactive UEs in cell i wants to become active. Each UE selects a pilot sequence at random

from a predefined pool of RA pilots. The ith BS estimates the channel that each pilot has propagated over. If multiple UEs selected the same RA pilot, a *collision* has occurred and the BS obtains an estimate of the superposition of the UE channels. The BS cannot detect if collisions occurred at this point.

S.2 BS responds by sending DL pilots that are precoded using the channel estimates, which results in spatially directed signals toward the UEs that sent the particular RA pilot. The DL signal features an array gain of M that is divided between the UEs that sent the RA pilot. Due to channel reciprocity, the share of the array gain is proportional to their respective UL signal gains, particularly when M is large, which enables each UE to estimate the sum of the signal gains and compare it with its own signal gain (using information obtained in Step 0). Each UE can thereby detect RA collisions in a distributed way. This departs from the conventional approach in which collisions are detected in a centralized way at the BS and broadcasted to the UEs.

S.3 The UEs can resolve RA contentions in this step based on the detection in step S.2 and the favorable propagation of massive MIMO channels, by applying a local decision rule: *only the UE with the strongest UL signal gain should repeat the RA pilot*. The probability of non-colliding pilot transmission in step S.3 is vastly increased in the SUCRe protocol, which enables the network to admit UEs also in crowded scenarios. The transmission in Step 3 also contains the identity of the UE and a request for payload transmission, resembling the Radio Resource Control (RRC) Connection Request in LTE.

S.4 In this step, the connection is granted by assigning a pilot sequence that can be used in the payload blocks or starts further contention resolution (*e.g.*, in an LTE fashion or by repeating the SUCRe protocol) in the few cases when RA collisions remain. Hence, the SUCRe protocol both stands on its own and can complement conventional contention resolution methods.

5.1.1 Detailed description of SUCRe protocol

Adopting the system model described in Sec. 2.1.3, the BS receives the signal $\mathbf{Y} \in \mathbb{C}^{M \times \tau}$ as in (2.16) after the pilot transmissions in step 1. The BS then generates channel estimates $\mathbf{y}_t$ as in (2.17) for the UEs transmitting pilot $\boldsymbol{\psi}_t$.

In the second step of SUCRe protocol, the BS responds to the RA pilots by sending orthogonal precoded DL pilot signal with respect to each pilot sequence. The precoded DL pilot signal $\mathbf{V} \in \mathbb{C}^{M \times \tau}$ is

$$\mathbf{V} = \sqrt{q} \sum_{t=1}^{\tau} \frac{\mathbf{y}_t^*}{||\mathbf{y}_t||} \boldsymbol{\psi}_t^T, \tag{5.1}$$

where q is the DL transmit power. The received signal $\mathbf{z}_k \in \mathbb{C}^{\tau}$ at UE $k \in \mathcal{Q}_t$ is

$$\mathbf{z}_k^T = \mathbf{g}_k^T \mathbf{V} + \boldsymbol{\nu}_k^T + \boldsymbol{\eta}_k^T, \tag{5.2}$$

in which $\boldsymbol{\nu}_k \in \mathbb{C}^{\tau}$ is inter-cell interference, and $\boldsymbol{\eta}_k \sim \mathcal{CN}(\mathbf{0}, \sigma^2 \mathbf{I}_\tau)$ is receiver noise. Then, by correlating $\mathbf{z}_k$ with its respective pilot sequence $\boldsymbol{\psi}_t$, the UE obtains

$$z_k = \mathbf{z}_k^T \frac{\boldsymbol{\psi}_t^*}{||\boldsymbol{\psi}_t||} = \sqrt{q\tau} \mathbf{g}_k^T \frac{\mathbf{y}_t^*}{||\mathbf{y}_t||} + \boldsymbol{\nu}_k^T \frac{\boldsymbol{\psi}_t^*}{||\boldsymbol{\psi}_t||} + \eta_k, \tag{5.3}$$

in which $\eta_k \sim \mathcal{CN}(0, \sigma^2)$ is the effective receiver noise.

Defining the sum of the signal and interference gains received at the BS during the UL transmission of pilot $\boldsymbol{\psi}_t$ as

$$\alpha_t = \sum_{i \in \mathcal{Q}_t} \rho_i \beta_i \tau + \omega_t, \tag{5.4}$$

it was proposed in [18] an asymptotically error free estimator for α_t as

$$\hat{\alpha}_{t,k} = \max\left(\left[\frac{\Gamma(M + \frac{1}{2})}{\Gamma(M)} \right]^2 \frac{q \rho_k \beta_k^2 \tau^2}{[\Re(z_k)]^2} - \sigma^2,\ \rho_k \beta_k \tau \right), \tag{5.5}$$

in which $\Re(\cdot)$ gives the real part of its argument, and $\Gamma(\cdot)$ is the Gamma function.

The main goal of the SUCRe protocol is to resolve pilot collisions in a decentralized and uncoordinated manner in the third step, so that each pilot is retransmitted by only one UE (collision resolved). Each UE $k \in \mathcal{Q}_t$ knows its own average signal gain $\rho_k \beta_k \tau$ and has an estimate $\hat{\alpha}_{t,k}$ of the sum of the signal gains of the contender UEs and inter-cell interference. Therefore, they apply the following distributed *decision rule*:

$$\mathcal{R}_k: \quad \text{if} \quad \rho_k \beta_k \tau > \frac{\hat{\alpha}_{t,k}}{2} + \epsilon_k \qquad \text{(repeat)} \tag{5.6}$$

$$\mathcal{I}_k: \quad \text{if} \quad \rho_k \beta_k \tau \leq \frac{\hat{\alpha}_{t,k}}{2} + \epsilon_k \qquad \text{(inactive)}. \tag{5.7}$$

The UE $k \in \mathcal{Q}_t$ concludes that it has the strongest signal gain if $\mathcal{R}_k$ is true, repeating thus the transmission of pilot $\boldsymbol{\psi}_t$ in Step 3. Otherwise, if $\mathcal{I}_k$ is true, it remains inactive in step 3 and try again later. Besides, the bias parameter $\epsilon_k \in \mathbb{R}$ can be used to tune the system behavior to the final performance criterion, and is empirically adjusted in [18] to $\epsilon_k = \frac{-\beta_k}{\sqrt{M}} - \frac{\overline{\omega}}{2}$, where the *average UL interference* is given by

$$\overline{\omega} = \frac{1}{M} \cdot \mathbb{E}\left\{ \left\| \mathbf{W} \frac{\boldsymbol{\psi}_t^*}{||\boldsymbol{\psi}_t||} \right\|^2 \right\},$$

in which the expectation is taken over user locations and shadow fading realizations; moreover, shadow fading parameter values are assumed to be known at the UEs, since it is the same for all UEs.

5.2 Improving the Performance of SUCRe Protocol

The SUCRe protocol is able to resolve great part of the pilot collisions in crowded machine-type massive-MIMO scenarios while continues to admit UEs efficiently in overloaded networks [18]. Besides, it is able to achieve this under a decentralized fashion, since it is the UEs who performs the contention resolution, and uncoordinated manner, without the need of excessive exchange of control information. Both properties allow this protocol to be highly scalable with respect to the number of UEs within the cell.

However, one of the main limitations of the SUCRe protocol is because it requires a noticeable disparity between the large-scale fading coefficients of the contending UEs, so that the decision rule of (5.6) is true for only one contending UE. With a not so large number of UEs, this condition is usually satisfied in the few cases when a collision occurs. On the other hand, as long as the number of UEs within the cell increases, the collisions occur more often and sometimes with more than two contenders, so that the probability of the

strongest user signal gain be higher than half of the sum of contending's signal gains decreases, with no UE retransmitting the pilot in the third step.

This fact has motivated we propose in this Doctoral work a different decision rule for the UEs retransmit their pilots. As one can note from (5.6), the SUCRe protocol as proposed in [18] implements a hard decision rule, since if the condition is true the UE retransmit its pilot, but if it is false the UE remains inactive. We show in the sequel that the protocol performance can be improved by making the decision rule soft, in such a way that the UE retransmit its pilot with a probability as high as its signal gain compared with the estimated sum of signal gains. Our first approach is to obtain this probability with the aid of a sigmoid function (Sec. 5.2.1). Then, we propose to determine the probability of retransmission for a given UE according to the probability of this UE be the strongest contender (Sec. 5.2.2), taking advantage of knowing $\rho_k\beta_k\tau$ and $\hat{\alpha}_{t,k}$ quantities.

5.2.1 First Approach: Soft Sigmoid Function

As discussed before, in the SUCRe protocol [18], a given kth user decides to retransmit its chosen pilot sequence in step 3 if the following distributed decision rule is satisfied

$$\rho_k\beta_k\tau > \widehat{\alpha}_{t,k}/2 + \epsilon_k = 0.5\,(\widehat{\alpha}_{t,k} + 2\epsilon_k) \tag{5.8}$$

By defining $\gamma_{t,k} = \widehat{\alpha}_{t,k} + 2\epsilon_k$, (5.8) can be rewritten if $\gamma_{t,k}$ is positive as

$$\frac{\rho_k\beta_k\tau}{\gamma_{t,k}} > 0.5, \tag{5.9}$$

and if $\gamma_{t,k}$ is negative as

$$\frac{\rho_k\beta_k\tau}{-\gamma_{t,k}} > -0.5. \tag{5.10}$$

In a unified way, (5.8) can thus be rewritten as

$$\frac{\rho_k\beta_k\tau}{|\gamma_{t,k}|} > \mathrm{sign}(\gamma_{t,k})\,0.5, \tag{5.11}$$

in which $\mathrm{sign}(\cdot)$ is the signal operator.

It is noteworthy in (5.11) that the SUCRe decentralized decision rule is characterized by a hard decision: if $\frac{\rho_k\beta_k\tau}{|\gamma_{t,k}|}$ is higher than $\mathrm{sign}(\gamma_{t,k})\,0.5$, the user retransmits its sequence. This hard decision criterium may lead to contradictory situations in which if $\frac{\rho_k\beta_k\tau}{|\gamma_{t,k}|}$ for a given user is approaching $\mathrm{sign}(\gamma_{t,k})\,0.5$ by the left, this user remains inactive in step 3, but if it is approaching it by the right, this user decides to retransmit its pilot. Besides, in situations in which there are a higher number of users contending for the same pilot resource, and the difference in their large-scale coefficients is not so apparent, it becomes quite difficult to the decision rule in (5.11) be satisfied for any contending user, in such a way that there are no chance of retransmission for these users. Aiming to circumvent these shortcomings of the conventional SUCRe decision rule, we investigate a soft decision rule for the SUCRe protocol, in which the value of $\frac{\rho_k\beta_k\tau}{|\gamma_{t,k}|}$ can be mapped into a probability of retransmission for each user, without losing the decentralized and uncoordinated features of SUCRe.

Our first approach in this Doctoral work consists in smoothing the hard decision in (5.11) with the aid of a sigmoid function[1], as depicted in Figure 5.1. It was assumed in the Figure the case of positive $\gamma_{t,k}$. If $\gamma_{t,k}$ is negative, the curve is horizontally shifted in order to be centered in -0.5. Besides, the λ parameter sets the smoothness of the sigmoid curve: the curve becomes sharper with the increase in λ.

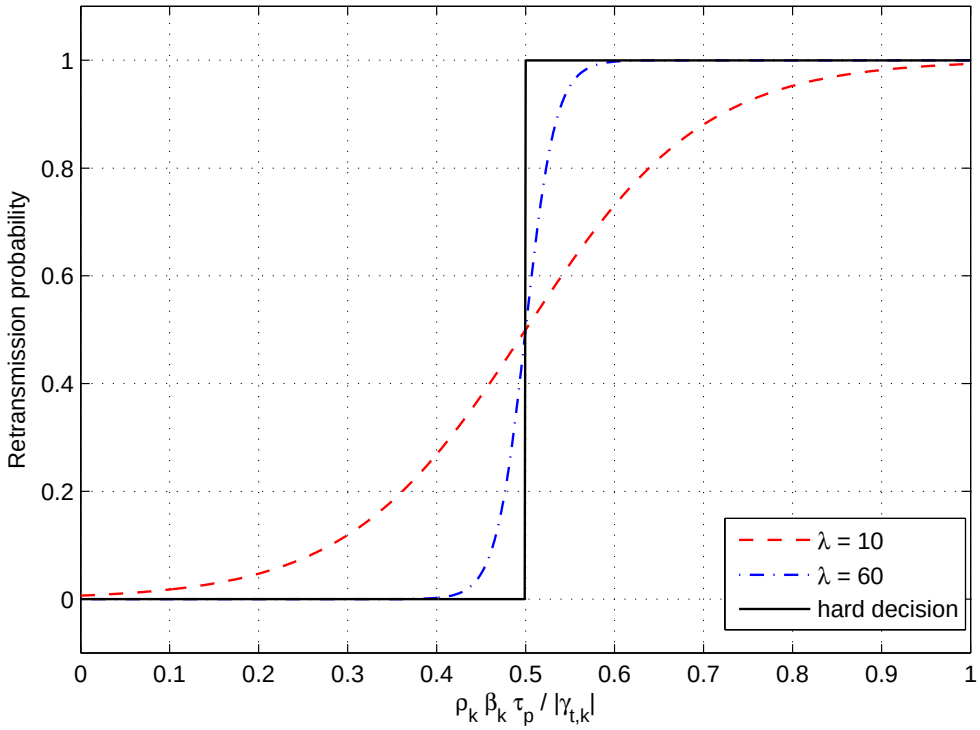

Figure 5.1: Probability of retransmission according $\frac{\rho_k \beta_k \tau}{|\gamma_{t,k}|}$, for the conventional SUCRe decision rule (hard decision) and the proposed soft decision rule with different λ parameters.

5.2.2 Second Approach: Probability of being the Strongest Contender

Our second approach is to associate the retransmission probability for a given user with the probability of this user being the strongest contender. For this sake, we obtain in this subsection an approximated expression for this probability. We denote by $\mathbf{x}_k \in \mathbb{R}^2$ the physical location of UE k with respect to the BS (assumed to be located in the origin), and assume a uniform distribution for the UEs' positions in a circular cell with radius d_{max} and minimum distance d_{min} (in order to consider only non-line-of-sight propagation) [14]. This user distribution is described by the density function

$$f(\mathbf{x}_k) = \begin{cases} \frac{1}{\pi(d_{\text{max}}^2 - d_{\text{min}}^2)} & , \quad d_{\text{min}} \leq ||\mathbf{x}_k|| \leq d_{\text{max}}, \\ 0 & , \quad \text{otherwise.} \end{cases} \tag{5.12}$$

Let the large-scale fading be dominated by path-loss [14]. This is often modeled as

$$\beta_k = \frac{\overline{d}}{||\mathbf{x}_k||^{\kappa}} \qquad \text{for} \quad ||\mathbf{x}_k|| \geq d_{\text{min}}, \tag{5.13}$$

where $\kappa \geq 2$ is the path-loss exponent and the constant $\overline{d} > 0$ regulates the channel attenuation at distance

[1] A sigmoid function refers to the special case of the logistic function, and defined by $f(x) = \frac{1}{1+e^{-\lambda x}}$, $\forall x \in \mathbb{R}$.

$$P(\beta_{k'} > \beta_k) = \begin{cases} 0 & , \quad \text{if} \quad \beta_k \geq \overline{\beta}_{t,k}, \\ \int_{\beta_k}^{\overline{\beta}_{t,k}} f(\beta) d\beta = \frac{\overline{d}^{\frac{2}{\kappa}}}{\kappa(d_{\max}^2 - d_{\min}^2)} \left(\beta_k^{-\frac{2}{\kappa}} - (\overline{\beta}_{t,k})^{-\frac{2}{\kappa}} \right) & , \quad \text{if} \quad \beta_k < \overline{\beta}_{t,k} < \beta_{\max}, \\ \int_{\beta_k}^{\beta_{\max}} f(\beta) d\beta = \frac{\overline{d}^{\frac{2}{\kappa}}}{\kappa(d_{\max}^2 - d_{\min}^2)} \left(\beta_k^{-\frac{2}{\kappa}} - (\beta_{\max})^{-\frac{2}{\kappa}} \right) & , \quad \text{if} \quad \beta_k < \beta_{\max} < \overline{\beta}_{t,k}. \end{cases} \tag{5.16}$$

$d_{\min}$ [37]. The uniform user location distribution in (5.12) results in the following distribution for $||\mathbf{x}_k||$

$$f(||\mathbf{x}_k||) = \begin{cases} \frac{2||\mathbf{x}_k||}{(d_{\max}^2 - d_{\min}^2)} & , \quad d_{\min} \leq ||\mathbf{x}_k|| \leq d_{\max}, \\ 0 & , \quad \text{otherwise.} \end{cases} \tag{5.14}$$

This distribution can be directly mapped with the aid of (5.13) to obtain the distribution of the large-scale fading coefficients as

$$f(\beta_k) = \begin{cases} \frac{2\overline{d}^{\frac{2}{\kappa}}}{\kappa(d_{\max}^2 - d_{\min}^2)} \beta_k^{-\frac{\kappa+2}{\kappa}} & , \quad \beta_{\min} \leq \beta_k \leq \beta_{\max}, \\ 0 & , \quad \text{otherwise,} \end{cases} \tag{5.15}$$

in which $\beta_{\min} = \frac{\overline{d}}{(d_{\max})^{\kappa}}$ and $\beta_{\max} = \frac{\overline{d}}{(d_{\min})^{\kappa}}$.

The kth UE has knowledge of β_k and $\hat{\alpha}_{t,k}$, which is an estimate of $\sum_{i \in \mathcal{Q}_t} \rho_i \beta_i \tau + \omega_t$. Therefore, if another contender $k' \in \mathcal{Q}_t$ is the strongest, its large scale fading coefficient is within the interval $\beta_k < \beta_{k'} \leq \overline{\beta}_{t,k}$, in which $\overline{\beta}_{t,k} = \frac{\hat{\alpha}_{t,k} - \overline{\omega}}{\rho \tau}$ is an estimated upper bound for the large scale fading coefficient of any contending of pilot $\boldsymbol{\psi}_t$ that UE k can adopt. The probability of this event can be readily obtained from (5.15), resulting in (5.16).

The kth UE will not be the strongest contender if another contender (any of them) has a higher large-scale fading coefficient. Since the average number of contenders is $K_0 P_a$, we can approximate the probability of the UE k be the strongest $P_{\text{strong}}(k) = P(\beta_k > \beta_{k'}, \forall k' \in \mathcal{Q}_t, k' \neq k)$, for $K_0 > 1/P_a$, as

$$P_{\text{strong}}(k) = 1 - \min\left[(K_0 P_a - 1) P(\beta_{k'} > \beta_k), 1 \right]. \tag{5.17}$$

Therefore, in our second proposed approach, each UE compute $P_{\text{strong}}(k)$ in (5.17), and then use this value as its probability of retransmission in step 3, under a decentralized and uncoordinated manner.

5.3 Numerical Results and Discussion

We have modified the Matlab codes available at `https://github.com/emilbjornson/sucre-protocol` [18] to generate the average number of access attempts and the probability of failed access attempts (when the number of attempts exceeds 10), but using the soft decision rule approaches for the retransmission probability. The probability of activation for each device is $P_a = 0.1\%$, the length of training sequences is $\tau = 10$, and the number of inactive devices K_0 is varied. The adopted parameters are summarized in Table 5.1.

For illustration purpose, Figure 5.2 depicts the performance results with $\lambda = 60$. As one can see, there is no significant change in performance between the SUCRe techniques, what was already expected since the sigmoid curve with $\lambda = 60$ is close to the hard decision curve.

On the other hand, Figure 5.3 depicts the performance of the proposed SUCRe with the soft decision

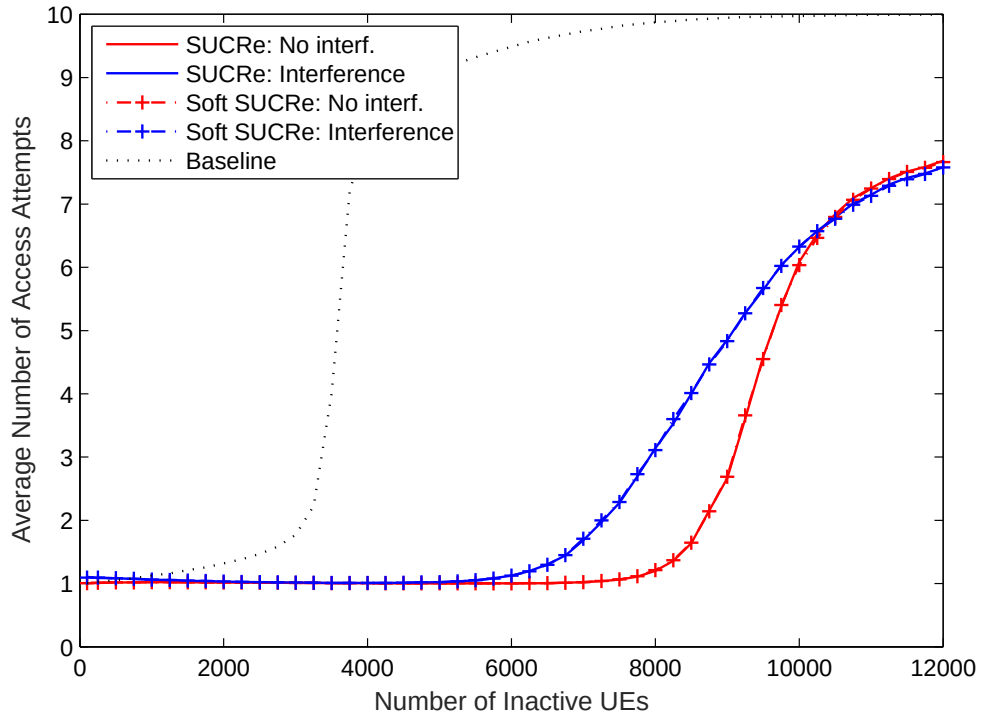

a) Average number of RA attempts

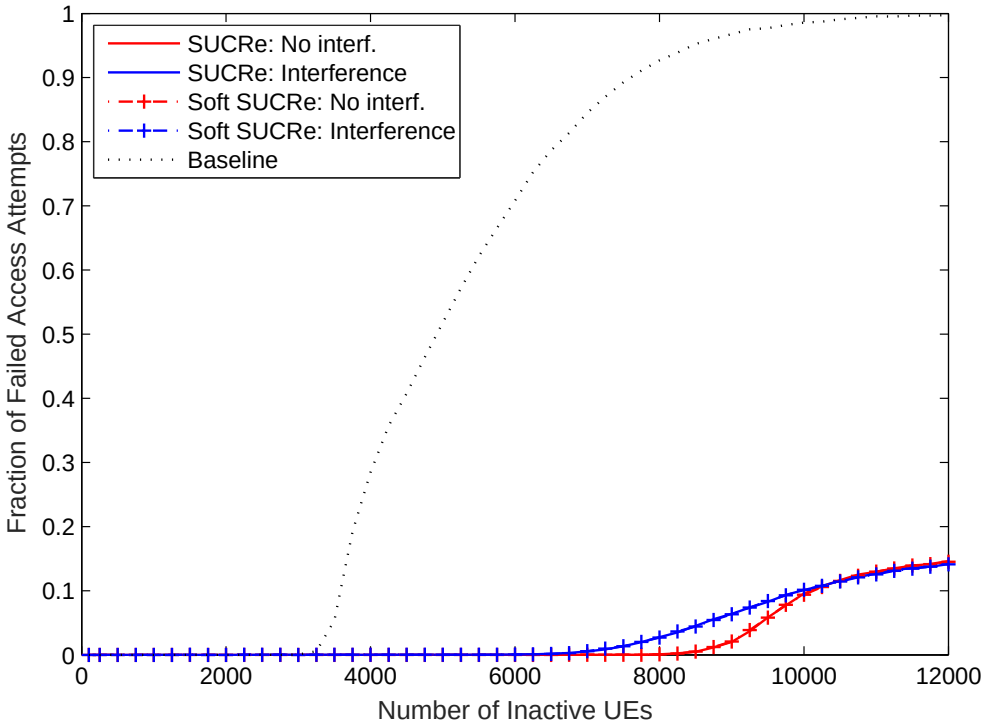

b) Probability of failed RA attempt

Figure 5.2: RA performance in a crowded machine-type network as a function of the number of devices in a cell. Sigmoid with smoothness $\lambda = 60$ for the soft SUCRe.

Table 5.1: System parameters

Parameter	Value
Soft decision rule	Sigmoid function (Sec. 5.2.1)
	$P_{\text{strong}}(k)$ (Sec. 5.2.2)
Sigmoid smoothness	$\lambda \in [5; 90]$
Device activation probability	$P_a = 0.1\%$
Length of training sequences	$\tau = 10$
# Inactive devices	$K_0 \in [1; 16000]$
d_{max}	250m
d_{min}	25m
$\overline{d}$	$10^{-3.53}$
κ	3.8
Shadowing standard deviation	8 dB
Other parameters	same as in [18]

rule with $\lambda = 10$ for the sigmoid function. As one can see, a worse performance is achieved when the number of users is lower than $\tau/P_a = 10000$, but a better performance is obtained above this threshold. This can be justified since the motivation of employing a soft decision rule in SUCRe is to resolve collisions with high number of contentions and/or a low disparity between their large-scale fading coefficients, which occurs more often when $K_0 > \tau/P_a$. Under this threshold the soft decision rule is not so efficient, since it introduces a probability of the strongest user remain inactive and a probability of weaker users retransmit pilots.

5.3.1 Tuning λ with increasing Inactive Devices K_0

Aiming to investigate the best value for the λ parameter with increasing inactive machine-type devices K_0, we let the sigmoid smoothness parameter vary in the range $\lambda \in [5, 90]$, and find for each value of K_0 the best performance obtained by the SUCRe with soft sigmoid decision rule. Figure 5.4 shows the best performance achieved following this methodology. As one can see from the Figure, an appreciable performance improvement can be obtained when adopting the soft decision rule in the SUCRe protocol in the very crowded scenario ($K_0 > \tau/P_a$). Table 5.2 shows the reduction in the average number of access attempts of the proposed SUCRe protocol with soft decision rule via sigmoid function (denoted as sSUCRe1 in the Table) in comparison with conventional SUCRe, with and without intercell interference. One can see for example that 0.497 less RA attempts are required on average for 11000 UEs without interference, while 0.336 less RA attempts for 12000 UEs with interference. Besides, one can see from the Figure that the probability of failed access attempts can reduce from 16.39% to 15.12% for 16000 UEs with interference. It means that adopting the soft decision rule can provide successful access to $0.0127 \times 16000 \times P_a = 0.2032$ additional devices on average if compared to the conventional SUCRe, *i.e.*, in about one out of 5 frame periods, the SUCRe protocol with soft decision rule will have one additional active UE in comparison with the conventional SUCRe. Table 5.3 shows the average number of additional active devices of our proposed RA protocol in comparison with SUCRe.

Analyzing the best values of the λ parameter, we have noted that it have oscillated near values around 60 in the range of $K_0 < \frac{0.9\tau}{P_a}$, indicating that any high λ value, which is able to approach the hard decision, will be suitable in this moderately crowded scenario, but it have converged to 10 for $K_0 \approx \tau/P_a = 10000$ and slightly decreased to 9 for $K_0 \approx 1.4\tau/P_a = 14000$, as depicted in Figure 5.5. This can be justified since

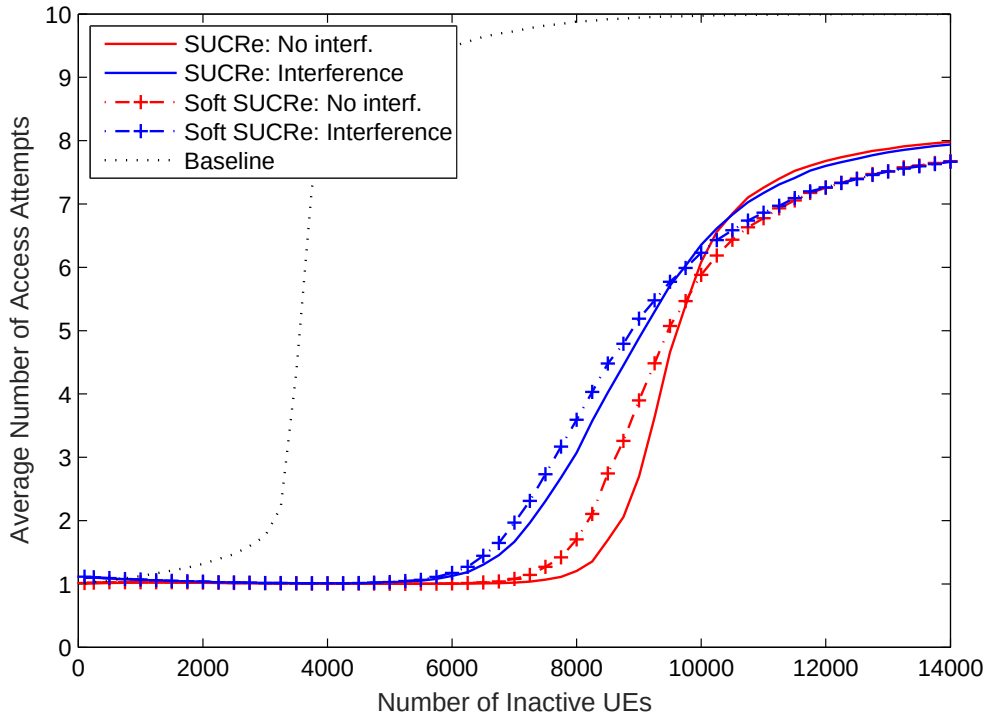

a) Average number of RA attempts

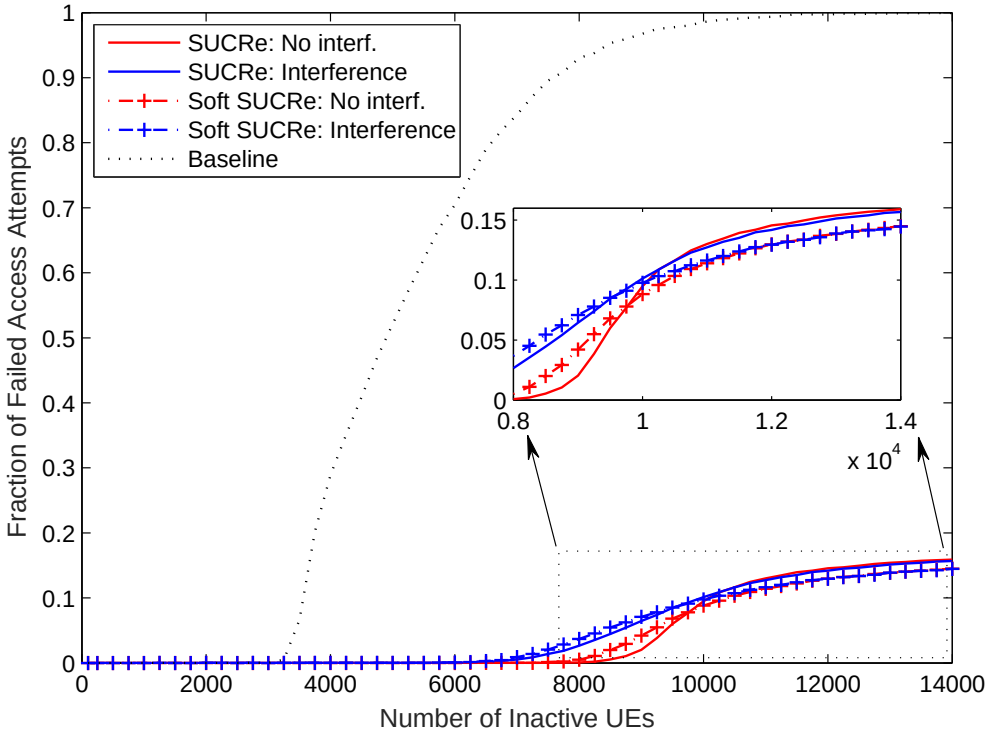

b) Probability of failed RA attempt

Figure 5.3: RA performance in a crowded machine-type network as a function of the number of devices in a cell. $\lambda = 10$ for the soft SUCRe.

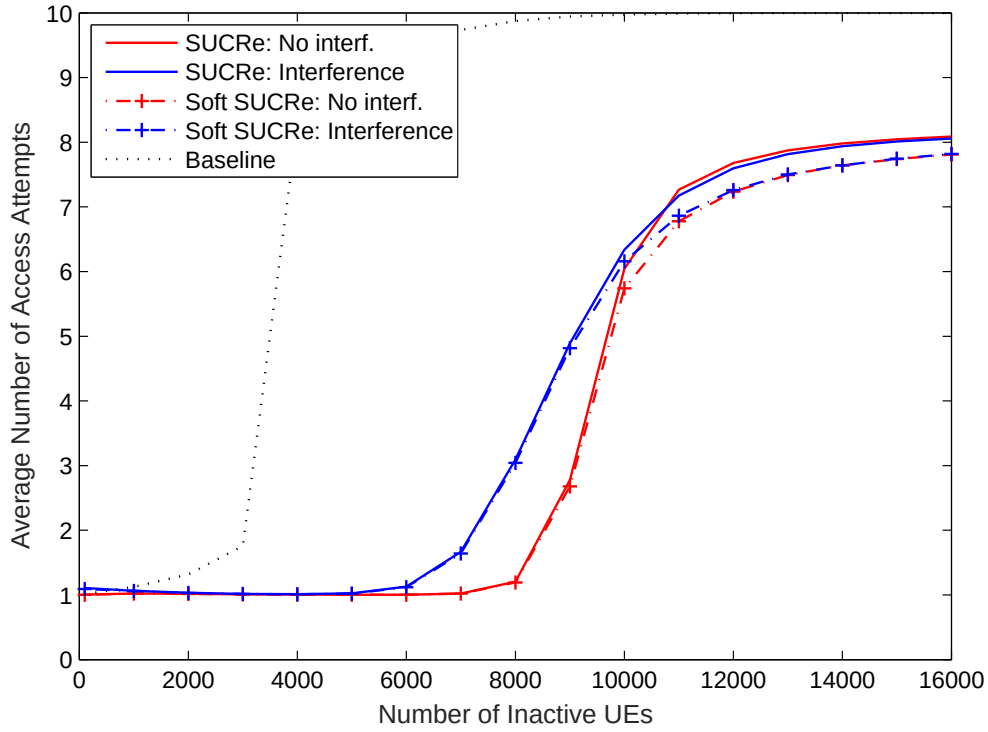

a) Average number of RA attempts

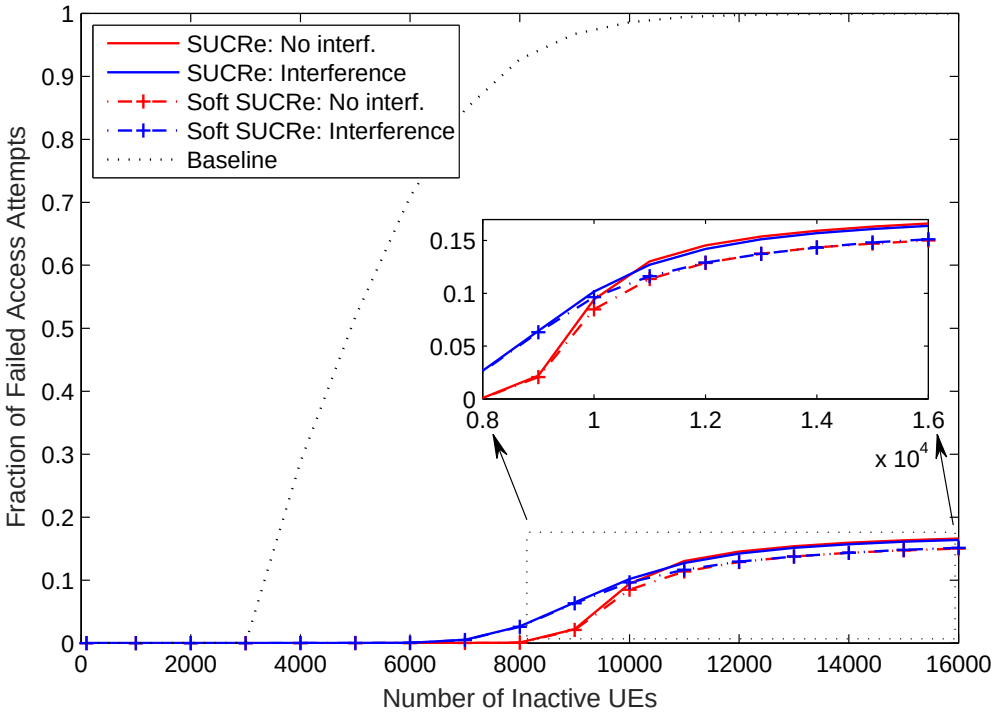

b) Probability of failed RA attempt

Figure 5.4: RA performance in a crowded machine-type network as a function of the number of devices in a cell. Best $\lambda \in [5, 90]$ for the soft SUCRe.

for $K_0 > \tau/P_a = 10000$, it will have on average more than one active UE per pilot sequence, and thus, the collisions will occur more often. In this scenario, employing the SUCRe protocol with soft decision rule is more appealing. Therefore, a suitable solution in practice is to switch between the conventional SUCRe in the scenario with $K_0 < \tau/P_a$ to the SUCRe with soft decision rule with $\lambda = 10$ when $K_0 > \tau/P_a$ (over-crowded scenarios).

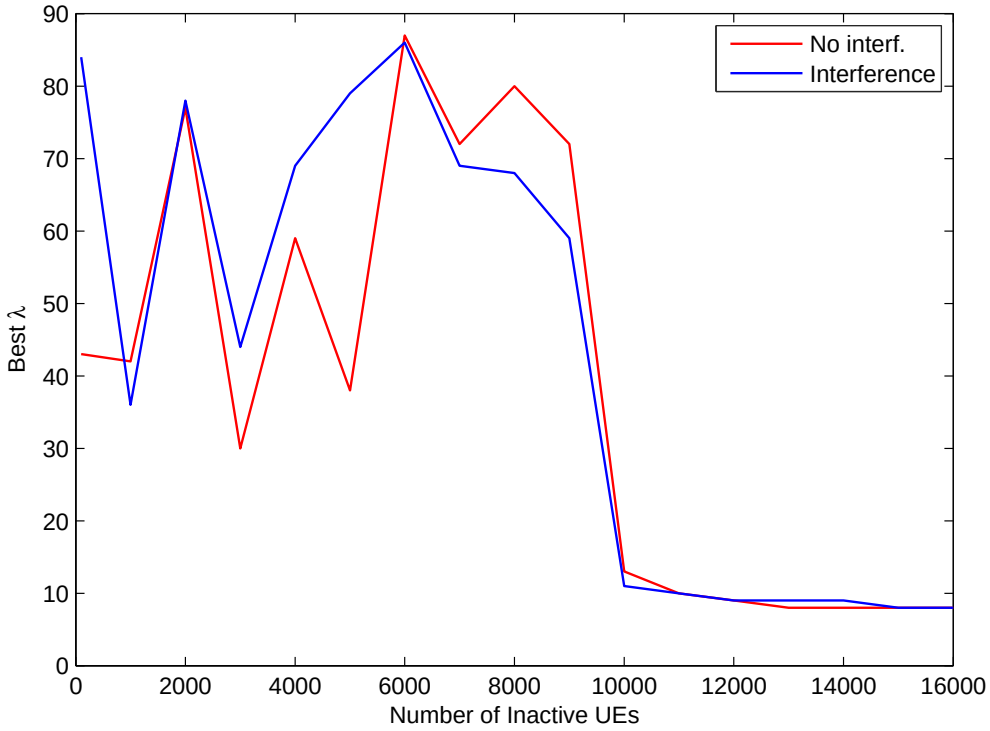

Figure 5.5: Values of λ parameter which leaded to the best RA performance.

5.3.2 Computing the Probability of being the Strongest User

We present in this subsection the numerical results adopting a soft decision rule, in which the probability of retransmission for each user is computed as in eq. (5.17) and (5.16). Figure 5.6 depicts the average number of access attempts and the probability of failed RA attempts, while Tables 5.2 and 5.3 shows the reduction on the average number of access attempts and the average number of active UEs increase in comparison with conventional SUCRe, respectively. The SUCRe with soft decision rule discussed in this subsection is denoted as sSUCRe2 in both Tables. In terms of the average number of access attempts, the soft decision can achieve a reduction on this number of 2.336 in the scenario without intercell interference with $K_0 = \tau_p/P_a = 10000$ UEs, and of 1.392 in the presence of intercell interference for the same number of UEs. Moreover, in terms of the probability of failed access attempts, the soft decision approach is able to reduce this number from 11.61% to 5.59% in the scenario without interference with $K_0 = \tau/P_a = 10000$ UEs, providing access to 0.6327 additional UEs in comparison with conventional SUCRe. In the scenario with intercell interference, 0.4446 additional active UEs can be supported for 11000 UEs. This shows that computing the retransmission probability of SUCRe employing our proposed expression for the probability of the UE being the strongest contender can be a promising solution for RA in crowded massive MIMO networks, while still benefiting of the decentralized and uncoordinated features of SUCRe protocol.

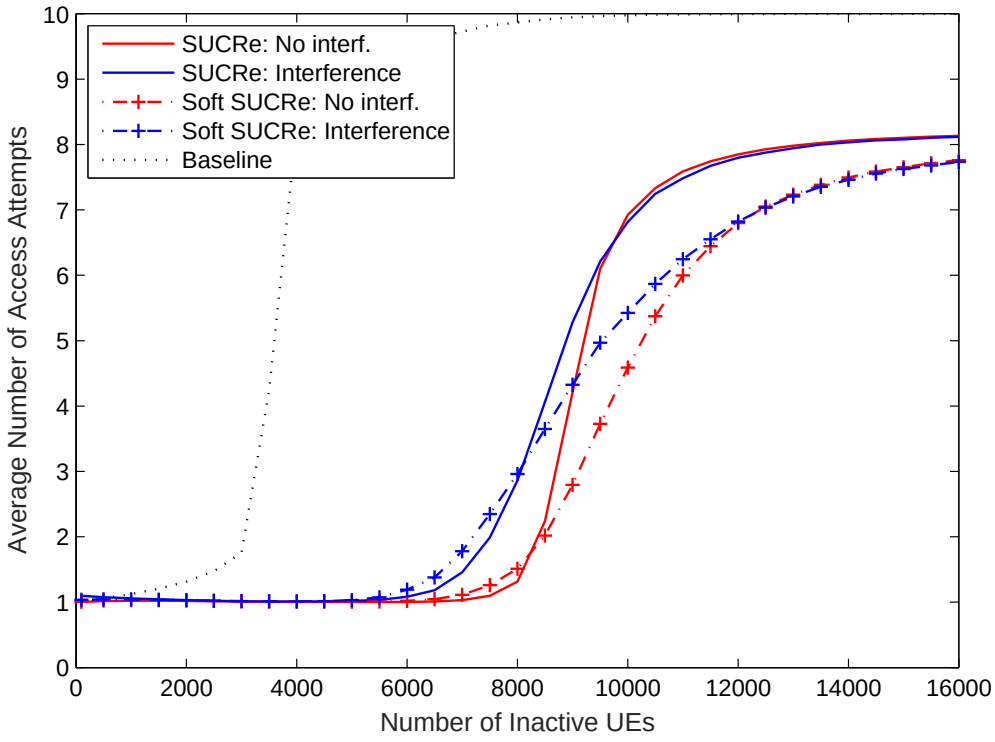

a) Average number of RA attempts

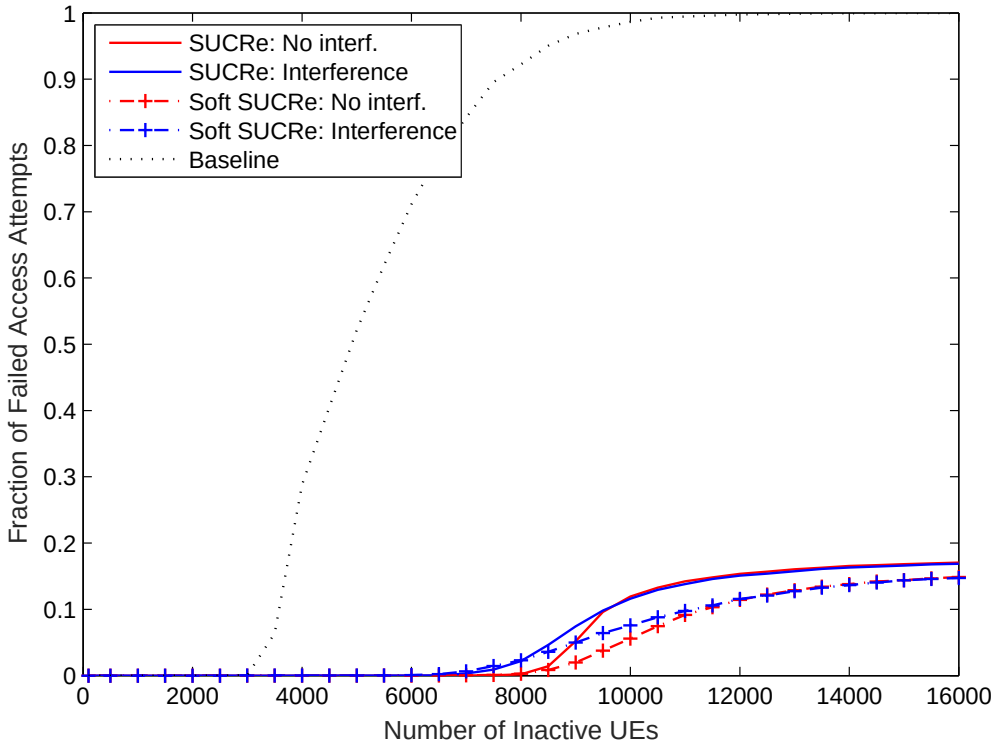

b) Probability of failed RA attempt

Figure 5.6: RA performance in a crowded machine-type network as a function of the number of devices in a cell. Soft SUCRe approach computing the probability of being the strongest user.

Table 5.2: Average Number of Access Attempts Reduction in Comparison with Conventional SUCRe.

Interf.	Scheme	K_0					
		8000	9000	10000	11000	12000	16000
without	sSUCRe1	0.014	0.098	0.306	**0.497**	0.441	0.276
	sSUCRe2	-0.196	1.414	**2.336**	1.592	1.049	0.372
with	sSUCRe1	0.053	0.078	0.181	0.313	**0.336**	0.240
	sSUCRe2	-0.100	0.955	**1.392**	1.239	0.973	0.384

Table 5.3: Average Number of Active UEs Increase in Comparison with Conventional SUCRe.

Interf.	Scheme	K_0					
		8000	9000	10000	11000	12000	16000
without	sSUCRe1	0.0015	0.0120	0.0936	0.1837	0.2004	**0.2560**
	sSUCRe2	-0.0073	0.2892	**0.6327**	0.5569	0.4728	0.3504
with	sSUCRe1	0.0054	0.0121	0.0518	0.1188	0.1548	**0.2032**
	sSUCRe2	-0.0104	0.2198	0.4033	**0.4446**	0.4224	0.3408

5.4 Conclusion of the Chapter

In this Chapter, we have addressed the problem of RA in crowded massive MIMO networks. When seeking to obtain a distributed and uncoordinated protocol to detect and resolve pilot collisions, the SUCRe protocol shows itself as a very promising solution. However, one of its main weaknesses is in requiring a noticeable disparity between large scale fading coefficients of contending users, what may limit its RA performance in very crowded scenarios. In order to overcome this issue, we have proposed to employ a soft decision retransmission criterium in the SUCRe protocol, by introducing the concept of retransmission probability. The first proposed approach consists in obtaining the retransmission probability by simply mapping the ratio between the signal gain of a given user and the sum of signal gains of the contenders with the aid of a sigmoid function. The second proposed approach consists in associating the retransmission probability with the probability of a given user being the strongest contending. Based on the information available at the UE side, we have proposed also an approximate expression to evaluate this probability. Despite of the simplicity of the first approach, the second one presented better results. Therefore, employing a soft decision retransmission criterium can be seen as a very effective strategy for improving random access in very crowded massive MIMO networks.

6 Conclusions

This Thesis presented the main research results achieved during this Doctorate Program, which has as central theme analyzing and improving the spectral and energy efficiencies of massive MIMO systems. In the course of this process, we have investigated several specific issues, with finding and achievements summarized as follows.

The first investigated problem is the pilot assignment in massive MIMO systems. In this scenario, we have conceived a problem formulation in which the DL and UL performance metrics were jointly optimized. Besides, as the exhaustive search for the optimal pilot distribution would require an excessive computational burden, of factorial order with the number of users, we have proposed a near-optimal low-complexity algorithm for solving the formulated problems. Our heuristic scheme can be applied both for optimizing the DL performance, as well as for optimizing our joint DL-UL problem formulation. The proposed approaches have presented appreciable gains in spectral efficiency. Then, we have applied the target-SIR-tracking algorithm of [12], that gradually reduces the transmit power of users that cannot reach the target performance, to our scenario of massive MIMO with finite number of BS antennas. The obtained results have presented significant improvements in comparison with uniform power allocation, and demonstrated to perform very well when combined with pilot assignment schemes.

In the second investigated problem, we have made a systematic performance comparison on the MRC receiver operating with both transmission techniques, the OFDM and single-carrier waveforms. It was derived approximated performance expressions for the SINR of both schemes, as well as lower bounds for the achievable rates of such transmission topologies. The proposed expressions have been validated by comparison with Monte-Carlo simulation results. The complexity of the TRMRC receiver was shown to be higher than that of FDMRC, and thus a low-complexity implementation of the TRMRC scheme was proposed based on the fast convolution with overlap-and-add method. Then, slight simplifications were made in the analytical expressions for improving mathematical tractability, and an iterative procedure for obtaining the optimal number of scheduled users were proposed, in the sense of maximizing the system sum rate. Based on this procedure, several insights were given with respect to the impact of different system parameters on the optimal number of scheduled users, such as the number of antennas, data and pilot transmit power, as well as different frequency and pilot reuse schemes.

Furthemore, we have evaluated the total energy efficiency of massive MIMO systems employing these schemes in UL aiming to further elaborate and refine the comparison between FDMRC and TRMRC. We have found that TRMRC outperforms FDMRC in terms of spectral efficiency, but at the cost of a higher computational complexity. The total energy efficiency metric as in [14] was able to incorporate all the energy

expenditures of the massive MIMO system, being, thus, able to answer if the spectral efficiency improvement of TRMRC compensates its higher computational complexity. Our results have demonstrated that FDMRC/OFDM presents a better total energy efficiency than TRMRC/SC, due to the increased complexity of the latter which results in high energy levels required for processing. Besides, we predicted that this scenario may change in a near future, since with the technology evolution of the computers, the computational efficiency in *flops*/W is expected to increase. Our numerical results have portrayed that a 30% improvement in computational efficiency of the processors is sufficient for TRMRC outperforming FDMRC in terms of total energy efficiency.

In the third investigated problem, we proposed to employ a soft decision retransmission criterium in the SUCRe protocol aiming to improve the random access in (over)crowded massive MIMO networks. Our proposed approach is that each user decides to retransmit or not its selected pilot with a probability retransmission as high as its signal gain in comparison with the sum of signal gains of the contenders. Two strategies have been proposed to obtain this retransmission probability: the first by simply mapping the relative signal gain of a given UE with the aid of a sigmoid function, and the second by associating this probability with the probability of this UE being the strongest contending. Based on the information available at the UE side, we have also proposed an approximated expression for computing this probability. Our numerical results have shown that the SUCRe protocol employing the soft decision retransmission criterium achieves appreciable improvements in terms of reducing the average number of access attempts as well as the probability of failed access attempts in the very (over)crowded scenario. Remarkably, such improvements are achieved maintaining the distributed and uncoordinated desired features of the SUCRe protocol.

6.1 Future Research Directions

A number of issues and challenges regarding massive MIMO remain to be investigated. Some open research directions can be highlighted as follows:

- **Pilot assignment**: we have shown in Chapter 3 and in Appendices C, D the conflicting behavior of pilot assignment techniques designed to optimize only uplink or downlink, proposing thus the total capacity pilot allocation metric. However, an alternative approach could be formulating a pilot assignment optimization problem aiming to optimize a single link but imposing a constraint about the other link performance. In this way, a good performance may be achieved concomitantly in both links if a suitable performance constraint can be chosen.

- **Distributed massive MIMO**: we have considered in this work massive MIMO with collocated antenna arrays at BS. However, one can distribute the massive BS antenna arrays in a large area. A spectral efficiency comparison between centralized and distributed massive MIMO systems has been made in [38], and it was shown a larger multiplexing gain achieved by the latter scheme. Besides, the cell free massive MIMO [7], in which a very large number of distributed single-antenna access points serve a smaller number of users with no cells or cell boundaries, has been shown to present a considerably improved performance with respect to conventional schemes.

- **Second antenna at the user side**: while single-antenna users are usually assumed in most massive MIMO works, an experimental study of the benefits of a second antenna at the user side has been carried out in [39]. It was shown a sum-rate improvement provided by the implementation of the second antenna, and that the achieved benefits become more significant with the increasing number of BS antennas.

- **Exploiting channel covariance matrix for improving performance**: pilot contamination is usually seen as the performance bottleneck of massive MIMO systems. However, it was recently shown in [40] that this is not the case when exploiting channel covariance matrices for channel estimation and multicell precoding/combining schemes in the presence of a tiny amount of channel correlation and/or large-scale fading variations over the antenna arrray. More precisely, the authors have shown that when the channel covariance matrices of the contaminating users are asymptotically linearly independent, an unlimited asymptotic capacity can be achieved. However, efficient methods for estimating these channel covariance matrices still have to be conceived.

- **Including the shadowing effect in the SUCRe RA protocol with soft retransmission criterion**: although the shadowing effect has been considered in the numerical simulations channel realizations of Chapter 5 and Appendix F, it has been neglected in the computation of the probability of being the strongest contender of the proposed SUCRe with soft retransmission criterion. Including the shadowing effect in the computation of this probability may improve even more the RA performance of the protocol, but probably with some complexity increase in the obtained expressions.

Bibliography

[1] CISCO. *Cisco Visual Networking Index: Global Mobile Data Traffic Forecast Update, 2015-2020*. [S.l.], February 2016. Disponível em: <http://www.cisco.com/c/en/us/solutions/collateral/service-provider/visual-networking-index-vni/mobile-white-paper-c11-520862.html>.

[2] PRASAD, K. N. R. S. V.; HOSSAIN, E.; BHARGAVA, V. K. Energy efficiency in massive MIMO-based 5g networks: Opportunities and challenges. *IEEE Wireless Communications*, PP, n. 99, p. 2–10, 2017. ISSN 1536-1284.

[3] MARZETTA, T. Noncooperative cellular wireless with unlimited numbers of base station antennas. *IEEE Transactions on Wireless Communications*, v. 9, n. 11, p. 3590–3600, 2010. ISSN 1536-1276.

[4] TELATAR, E. Capacity of multi-antenna gaussian channels. *European Transactions on Telecommunications*, v. 10, n. 6, p. 585–595, 1999.

[5] MARZETTA, T.; LARSSON, E.; YANG, H.; NGO, H. *Fundamentals of Massive MIMO*. 1. ed. New York, NY, USA: Cambridge University Press, 2016. ISBN 9781316799895.

[6] ZHU, X.; WANG, Z.; DAI, L.; QIAN, C. Smart pilot assignment for massive MIMO. *IEEE Commun. Lett.*, v. 19, n. 9, p. 1644–1647, Sept 2015. ISSN 1089-7798.

[7] NGO, H. Q.; ASHIKHMIN, A.; YANG, H.; LARSSON, E. G.; MARZETTA, T. L. Cell-Free Massive MIMO Versus Small Cells. *IEEE Transactions on Wireless Communications*, v. 16, n. 3, p. 1834–1850, March 2017. ISSN 1536-1276.

[8] CHEN, Z.; YANG, C. Pilot decontamination in wideband massive MIMO systems by exploiting channel sparsity. *IEEE Transactions on Wireless Communications*, v. 15, n. 7, p. 5087–5100, July 2016. ISSN 1536-1276.

[9] ZHANG, Q.; JIN, S.; MCKAY, M.; MORALES-JIMENEZ, D.; ZHU, H. Power allocation schemes for multicell massive MIMO systems. *IEEE Transactions on Wireless Communications*, v. 14, n. 11, p. 5941–5955, Nov 2015. ISSN 1536-1276.

[10] LIN, Y.; WANG, Y.; LI, C.; HUANG, Y.; YANG, L. Joint design of user association and power allocation with proportional fairness in massive MIMO hetnets. *IEEE Access*, v. 5, p. 6560–6569, 2017. ISSN 2169-3536.

[11] FOSCHINI, G. J.; MILJANIC, Z. A simple distributed autonomous power control algorithm and its convergence. *IEEE Transactions on Vehicular Technology*, v. 42, n. 4, p. 641–646, Nov 1993. ISSN 0018-9545.

[12] RASTI, M.; SHARAFAT, A.-R. Distributed uplink power control with soft removal for wireless networks. *IEEE Transactions on Communications*, v. 59, n. 3, p. 833–843, March 2011. ISSN 0090-6778.

[13] PITAROKOILIS, A.; MOHAMMED, S. K.; LARSSON, E. G. Uplink performance of time-reversal MRC in massive MIMO systems subject to phase noise. *IEEE Transactions on Wireless Communications*, v. 14, n. 2, p. 711–723, Feb 2015. ISSN 1536-1276.

[14] BJöRNSON, E.; SANGUINETTI, L.; HOYDIS, J.; DEBBAH, M. Optimal design of energy-efficient multi-user MIMO systems: Is massive MIMO the answer? *IEEE Transactions on Wireless Communications*, v. 14, n. 6, p. 3059–3075, June 2015. ISSN 1536-1276.

[15] LIEN, S. Y.; LIAU, T. H.; KAO, C. Y.; CHEN, K. C. Cooperative Access Class Barring for Machine-to-Machine Communications. *IEEE Transactions on Wireless Communications*, v. 11, n. 1, p. 27–32, January 2012. ISSN 1536-1276.

[16] DUAN, S.; SHAH-MANSOURI, V.; WANG, Z.; WONG, V. W. S. D-ACB: Adaptive Congestion Control Algorithm for Bursty M2M Traffic in LTE Networks. *IEEE Transactions on Vehicular Technology*, v. 65, n. 12, p. 9847–9861, Dec 2016. ISSN 0018-9545.

[17] YUAN, J.; SHAN, H.; HUANG, A.; QUEK, T. Q. S.; YAO, Y. D. Massive Machine-to-Machine Communications in Cellular Network: Distributed Queueing Random Access Meets MIMO. *IEEE Access*, v. 5, p. 2981–2993, 2017.

[18] BJöRNSON, E.; CARVALHO, E. de; SøRENSEN, J. H.; LARSSON, E. G.; POPOVSKI, P. A Random Access Protocol for Pilot Allocation in Crowded Massive MIMO Systems. *IEEE Transactions on Wireless Communications*, v. 16, n. 4, p. 2220–2234, April 2017. ISSN 1536-1276.

[19] HAN, H.; GUO, X.; LI, Y. A High Throughput Pilot Allocation for M2M Communication in Crowded Massive MIMO Systems. *IEEE Transactions on Vehicular Technology*, v. 66, n. 10, p. 9572–9576, Oct 2017. ISSN 0018-9545.

[20] HAN, H.; LI, Y.; GUO, X. A Graph-Based Random Access Protocol for Crowded Massive MIMO Systems. *IEEE Transactions on Wireless Communications*, v. 16, n. 11, p. 7348–7361, Nov 2017. ISSN 1536-1276.

[21] CARVALHO, E. de; BJöRNSON, E.; SøRENSEN, J. H.; LARSSON, E. G.; POPOVSKI, P. Random Pilot and Data Access in Massive MIMO for Machine-Type Communications. *IEEE Transactions on Wireless Communications*, v. 16, n. 12, p. 7703–7717, Dec 2017. ISSN 1536-1276.

[22] BJöRNSON, E.; LARSSON, E. G.; DEBBAH, M. Massive MIMO for maximal spectral efficiency: How many users and pilots should be allocated? *IEEE Transactions on Wireless Communications*, v. 15, n. 2, p. 1293–1308, Feb 2016. ISSN 1536-1276.

[23] FERNANDES, F.; ASHIKHMIN, A.; MARZETTA, T. Inter-cell interference in noncooperative TDD large scale antenna systems. *IEEE Journal on Selected Areas in Communications*, v. 31, n. 2, p. 192–201, February 2013. ISSN 0733-8716.

[24] NGUYEN, T. M.; HA, V. N.; LE, L. B. Resource Allocation Optimization in Multi-User Multi-Cell Massive MIMO Networks Considering Pilot Contamination. *IEEE Access*, v. 3, p. 1272–1287, 2015.

[25] XU, H.; HUANG, N.; YANG, Z.; SHI, J.; WU, B.; CHEN, M. Pilot Allocation and Power Control in D2D Underlay Massive MIMO Systems. *IEEE Communications Letters*, v. 21, n. 1, p. 112–115, Jan 2017. ISSN 1089-7798.

[26] PITAROKOILIS, A.; MOHAMMED, S. K.; LARSSON, E. G. On the optimality of single-carrier transmission in large-scale antenna systems. *IEEE Wireless Communications Letters*, v. 1, n. 4, p. 276–279, August 2012. ISSN 2162-2337.

[27] MARINELLO, J. C.; ABRãO, T. Pilot distribution optimization in multi-cellular large scale MIMO systems. *AEU - International Journal of Electronics and Communications*, v. 70, n. 8, p. 1094 – 1103, 2016. ISSN 1434-8411.

[28] NISAN, N.; ROUGHGARDEN, T.; TARDOS, E.; VAZIRANI, V. V. *Algorithmic Game Theory*. New York, NY, USA: Cambridge University Press, 2007. ISBN 0521872820.

[29] VOORNEVELD, M. Best-response potential games. *Economics Letters*, v. 66, n. 3, p. 289–295, March 2000.

[30] NGO, H. Q.; LARSSON, E.; MARZETTA, T. Energy and spectral efficiency of very large multiuser MIMO systems. *IEEE Transactions on Communications*, v. 61, n. 4, p. 1436–1449, April 2013. ISSN 0090-6778.

[31] GOLUB, G. H.; LOAN, C. F. V. *Matrix Computations*. Maryland, USA: Johns Hopkins University Press, 1996.

[32] DINIZ, P.; SILVA, E. da; NETTO, S. *Digital Signal Processing: System Analysis and Design*. 2. ed. New York, NY, USA: Cambridge University Press, 2010. ISBN 9780511781667.

[33] CUI, S.; GOLDSMITH, A. J.; BAHAI, A. Energy-efficiency of MIMO and cooperative MIMO techniques in sensor networks. *IEEE Journal on Selected Areas in Communications*, v. 22, n. 6, p. 1089–1098, Aug 2004. ISSN 0733-8716.

[34] YANG, H.; MARZETTA, T. L. Total energy efficiency of cellular large scale antenna system multiple access mobile networks. In: *2013 IEEE Online Conference on Green Communications (OnlineGreenComm)*. [S.l.: s.n.], 2013. p. 27–32.

[35] INTEL'S New 10 nm Process: The Wind in our Sails. Disponível em: <http://fpga.org/2017/03/29/intel-10nm-the-wind-in-our-sails/>.

[36] LEADING at the Edge: Intel Technology and Manufacturing. Disponível em: <https://newsroom.intel.com/press-kits/leading-edge-intel-technology-manufacturing/>.

[37] FURTHER Advancements for E-UTRA Physical Layer Aspects (Release 9). [S.l.]: 3GPP TS 36.814, 2010.

[38] KAMGA, G. N.; XIA, M.; AïSSA, S. Spectral-Efficiency Analysis of Massive MIMO Systems in Centralized and Distributed Schemes. *IEEE Transactions on Communications*, v. 64, n. 5, p. 1930–1941, May 2016. ISSN 0090-6778.

[39] MARTíNEZ, . O.; POPOVSKI, P.; NIELSEN, J. .; CARVALHO, E. D. Experimental Study of the Benefits of a Second Antenna at the User Side in a Massive MIMO System. *IEEE Access*, v. 6, p. 2899–2907, 2018. ISSN 2169-3536.

[40] BJöRNSON, E.; HOYDIS, J.; SANGUINETTI, L. Massive MIMO Has Unlimited Capacity. *IEEE Transactions on Wireless Communications*, v. 17, n. 1, p. 574–590, Jan 2018. ISSN 1536-1276.

APPENDIX A – Full paper published in the journal "*International Journal of Electronics and Communications (AEUE)*"

Title: Pilot distribution optimization in multi-cellular large scale MIMO systems.

Authors: José Carlos Marinello Filho and Taufik Abrão.

Journal: International Journal of Electronics and Communications (AEUE) (ISSN 1434-8411). Volume 70, Issue 9, Pages 1094-1103.

Classification (Qualis-CAPES): B1 / IF$= 0.786$ (Engenharias IV).

Publication Date: August 2016.

Int. J. Electron. Commun. (AEÜ) 70 (2016) 1094–1103

Contents lists available at ScienceDirect

International Journal of Electronics and Communications (AEÜ)

journal homepage: www.elsevier.com/locate/aeue

Regular Paper

Pilot distribution optimization in multi-cellular large scale MIMO systems

José Carlos Marinello, Taufik Abrão *

State University of Londrina, Electrical Engineering Department (DEEL-UEL), Rod. Celso Garcia Cid – PR445, s/n, Campus Universitário, Po. Box 10.011, 86057-970 Londrina, Parana, Brazil

ARTICLE INFO

Article history:
Received 11 February 2016
Accepted 11 May 2016

Keywords:
Massive MIMO systems
BER
Multiuser MIMO
Precoding
Pilot sequences

ABSTRACT

Salient characteristics of a wireless communication system deploying a great number of antennas at the base station (BS), namely a massive MIMO system, are investigated in this work. The asymptotic performance of the linear zero-forcing precoding scheme is found, both in terms of signal-to-interference-plus-noise ratio (SINR) and bit-error rate (BER), and shown to be equivalent to the matched-filter beamforming performance. Furthermore, analysis of the massive MIMO system downlink is carried out from the viewpoint of uncoded BER performance, including some realistic adverse effects, such as interference from neighbouring cells, channel estimation errors due to background thermal noise, and pilot contamination. The latter has been shown to be the only impairment that remains in the MIMO multicell system with infinite number of BS antennas. For such scenario, we derive expressions for the asymptotic BER, *i.e.* in the limit of infinite number of antennas at BS. A quite simple and efficient method for optimizing the massive MIMO system performance under different optimization metrics is proposed, which consists of simply distributing the pilot sequences among the users of the cell in an efficient manner. As a result, a user rate gain of six times regarding the random strategy has been achieved for the downlink with unitary reuse factor, while the user rate increases twice for reuse factor of three. These benefits are achieved by only knowing the powers and the long-term fading coefficients of users in adjacent cells, for each pilot sequence.

1. Introduction

Multiple-input–multiple-output (MIMO) techniques constitute one of the key features in most of recent telecommunications standards, such as WiFi, WiMAX, LTE [6]. In order to fully exploit the benefits of MIMO systems, a new concept has been proposed by increasing the number of base station (BS) antennas N to infinity [9]. This massive MIMO systems are viewed as a potential technology for physical layer in next telecommunications standards, such as 5G [2]. A review of most important results recently disseminated in this theme can be found in [17].

It was shown in [9] that in a time division duplex (TDD) noncooperative multi-cell MIMO system, employing training pilots for channel state information (CSI) acquisition in the uplink and an infinite number of BS antennas, the effects of uncorrelated thermal noise and fast fading are averaged out. Hence, the only factor that remains limiting performance in the large MIMO scenario is inter-cell interference, that when associated with the finite time available to send pilot sequences makes the estimated CSI at one BS "contaminated" by the CSI of users in adjacent cells, in the so-called pilot contamination effect. This phenomenon results from unavoidable reuse of reverse-link pilot sequences by terminals in different cells. As a consequence of increasing the number of BS antennas to infinity, the transmit power can be designed arbitrarily small, since interference decreases in the same rate of the desired signal power, *i.e.*, signal-to-interference-plus-noise ratio (SINR) is independent of transmit power [9].

Alternative strategies to achieve better CSI estimates exist, such as (a) frequency division duplex (FDD) [3], in which pilots for CSI acquisition are transmitted in downlink, and estimates are fed back to BS in a feedback channel; and (b) network MIMO [7], where CSI and information data of different coordinated cells are shared among them in a backhaul link, creating a distributed antenna array that serves the users altogether. However, both schemes become unfeasible when $N \to \infty$ [9], since lengths of forward pilot sequences and capacity of backhaul links increase substantially with N. Therefore, TDD has been assumed in this work without CSI sharing among different cells.

* Corresponding author. Tel.: +55 43 3371 4790.
E-mail addresses: zecarlos.ee@gmail.com (J.C. Marinello), taufik@uel.br (T. Abrão).

http://dx.doi.org/10.1016/j.aeue.2016.05.007
1434-8411/

Operating with a large excess of BS antennas compared with the number of terminals K is a challenging but desirable condition, since some results from random matrix theory become applicable [4]. It is known, for instance, that very tall/wide matrices tend to be very well conditioned, since their singular values distribution appears to be deterministic, showing a stable behavior (low variances) and a relatively narrow spread [14]. Besides, in the large scale MIMO, the most simple reception/transmission techniques, *i.e.*, maximum ratio combining (MRC) deployed in the uplink and the matched-filtering (MF) precoding used in the downlink, become optimal [14].

An interesting investigation about precoding techniques of single-cell multiuser MIMO systems downlink is carried out in [16]. Specifically, authors compared MF precoding, also known as conjugate beamforming, and zero-forcing (ZF) beamforming, with respect to net spectral-efficiency and radiated energy-efficiency in a simplified single-cell scenario. It is found that, for high spectral-efficiency and low energy-efficiency, ZF outperforms MF, while at low spectral-efficiency and high energy-efficiency the opposite holds. A similar result is found for the uplink in [11], where for low signal-to-noise ratio (SNR), the simple MRC receiver outperforms the ZF receiver. On the other hand, when considering the multi-cell environment, it is found in [14] that the asymptotic SINR of MF outperforms ZF, although MF requires much more antennas to approach the asymptotic condition.

A more rigorous expression for the achievable SINR of MF precoding in massive MIMO systems, in comparison with that derived in [9] and adopted in [14], has been obtained in [5]. Authors of latter showed that, for downlink, the effect of the transmit power constraint at BS still accounts in the massive MIMO regime, as opposed to what was assumed in [9]. Besides, authors of [5] discuss an efficient technique for temporally distribute the uplink transmissions of pilot sequences, avoiding simultaneous transmissions from adjacent cells and reducing interference as well, in conjunction with power allocation strategy. On the other hand, a precoding technique that eliminates pilot contamination and leads to unlimited gains with $N \to \infty$ has been proposed in [1]. However, these gains come at the expense of sharing the information data between BSs, what can overload the backhaul signaling channel for high rate systems, or high number of users per cell.

An analysis of *non-linear precoding* techniques applied to the downlink of a massive MIMO system is conducted in [10]. Authors investigated the time domain vector perturbation (TDVP) scheme, which has been shown previously to almost achieve the downlink capacity of conventional MIMO channels. However, in the large-system analysis, it was shown that linear precoding schemes outperforms TDVP, in terms of increased sum rates, regardless of the user scheduling method adopted. Thus, linear precoding techniques has been investigated in our contribution. In [18], the pilot contamination is tackled by dividing the users within each cell in two groups, which are: the center users, and the edge users. As the edge users would suffer from severe pilot contamination if the same set of pilot sequences were reused by every cell, it is assigned for each edge user an exclusive training sequence in a cluster of L cells, while the center users reuse the same pilot's set. Although this so-called soft pilot reuse scheme effectively reduces the pilot contamination, the cost of devoting orthogonal pilots for every edge user may limit its practical appeal in TDD systems. Hence, we aim to reduce the pilot contamination in this paper adopting the challenging but realistic scenario of full pilot reuse among cells.

In this paper, we focus on the pilot distribution optimization and its impact on the performance of multi-cellular massive MIMO systems. The novelty and contributions of this paper are as follows:

(i) We derive an analytical expression for the downlink SINR system under ZF precoding, considering the effect of power constraint at BS. It is shown that the achieved SINR corresponds to the same value achieved by MF, as opposed to what is found in [14] neglecting the effects of the transmit power constraint.
(ii) Different from previous works that have analysed the SINR and the capacity of the massive MIMO system [9,5,14], we investigate also its downlink uncoded bit-error rate (BER) performance, which is another important figure of merit in communication systems. An exact expression for the BER of each user is derived, depending on the transmit power of users and on the long-term fading coefficients.
(iii) We propose a novel and expedite method of optimizing the massive MIMO downlink transmission under different metrics, based on our derived BER expression, and on the asymptotic SINR expression of [5]. This method consists of simply assigning the available training sequences among the users within a cell in an efficient manner, by knowing only the power and the long-term fading coefficients of users in adjacent cells that reuse such pilot sequences. Different pilot allocation metrics enable us to minimize the average BER, or maximize the average SINR, minimize the maximal BER or even maximize the minimum SINR. The proposed algorithms can lead to appreciable performance gains, both in terms of data rate, as well as in terms of BER of a massive MIMO system.

The paper is organized as follows. Beyond this introductory Section, the system model is described in Section 2. Some asymptotic limits of the massive MIMO system are revisited and extended in Section 3. Our proposed methods of assigning the pilots among the users within the cell in an efficient manner, namely the Pilot Allocation (PA) schemes, are presented in Section 4. Representative numerical results are discussed in Section 5, while Section 6 concludes the paper.

1.1. Notations

Boldface lower and upper case symbols represent vectors and matrices, respectively. $\mathbf{I}_N$ denotes the identity matrix of size N, while $\mathbf{1}_K$ and $\mathbf{0}_K$ are the unitary vector and null vector of length K, respectively. The transpose and the Hermitian transpose operator are denoted by $\{\cdot\}^T$ and $\{\cdot\}^H$, respectively, while $\mathrm{diag}(\cdot)$ is the diagonal matrix operator. $||\cdot||$ is the Euclidean norm of a vector. We use $\mathcal{CN}(\mathbf{m},\mathbf{V})$ to refer to a circular symmetric complex Gaussian distribution with mean vector $\mathbf{m}$ and covariance matrix $\mathbf{V}$. Also, $\mathbb{E}[\cdot]$ denotes the expectation operator, $\mathrm{u}[x]$ is the Heaviside step function ($\mathrm{u}[x] = 1$ if $x \geqslant 0, \mathrm{u}[x] = 0$ otherwise), while δ_{ij} is the Kronecker delta function ($\delta_{ij} = 1$ if $i = j$ and 0 otherwise).

2. System model

The adopted MIMO system is composed by L BSs, each equipped with N transmit antennas, reusing the same spectrum and the same set of K pilot signals. Since TDD is assumed, reciprocity holds, and thus CSI is acquired by means of uplink training sequences. During a channel coherence time interval, the symbol periods are divided in uplink pilot transmissions, processing, downlink and uplink data transmissions [5,18]. Using orthogonal pilot sequences, the number of available sequences is equal to its length, K. Thus, K is limited due to mobility of the users, which reduces the coherence time of the channel. Orthogonal frequency-division

multiplexing (OFDM) is assumed in the same way as in [9]. The channel coherence band is divided into N_{smooth} subcarriers, and each subcarrier is shared by K users. As discussed in [9], dividing the channel coherence band by the subcarrier spacing,

$$N_{\text{smooth}} = \frac{1-\Delta t_{CP}}{\Delta t_{CP}}, \tag{1}$$

where Δt_{CP} is the fraction of the OFDM symbol duration devoted to the cyclic prefix, typically about 7% in current standards. Note that only one out of N_{smooth} subcarriers is assigned to a certain user for each coherence band; therefore, a total number of $K \cdot N_{\text{smooth}}$ users is allowed for each cell. We assume perfect orthogonality in the frequency domain, such that interference is only due to the K users sharing the same subcarrier. Hence, we define our model for a generic subcarrier, assuming flat fading environment in which the BS communicates with K users equipped with single-antenna mobile terminals (MTs). We denote the $1 \times N$ channel vector between the ℓth BS and the kth user of jth cell by $\mathbf{g}_{\ell kj} = \sqrt{\beta_{\ell kj}}\mathbf{h}_{\ell kj}$, in which $\beta_{\ell kj}$ is the long-term fading power coefficient, that comprises path loss and log-normal shadowing, and $\mathbf{h}_{\ell kj}$ is the short-term fading channel vector, that follows $\mathbf{h}_{\ell kj} \sim \mathcal{CN}(\mathbf{0}_N, \mathbf{I}_N)$. The channel matrix $\mathbf{H}$ is admitted constant over the entire frame and changes independently from frame to frame (block fading channel assumption). Note that $\beta_{\ell kj}$ is assumed constant for all N BS antennas. For the kth user of each cell in a given subcarrier, it is assigned the sequence $\boldsymbol{\psi}_k = [\psi_{1k}\ \psi_{2k} \dots \psi_{Kk}]^T$, $\boldsymbol{\psi}_k \in \mathbb{C}^{K\times 1}$. It holds that $|\psi_{ik}| = 1$ and $|\boldsymbol{\psi}_k^H \boldsymbol{\psi}_{k'}| = K\delta_{kk'}$ since the set of sequences is orthogonal.

In the training transmission phase, we have assumed synchronization in the uplink pilot transmissions, since this situation characterizes the worst case for inter-cellular interference [9]. Hence, the $N \times K$ received signal at the ℓth BS is:

$$\mathbf{Y}_\ell = \sum_{j=1}^{L} \mathbf{G}_{\ell j}^T \sqrt{\boldsymbol{\Gamma}_j}\boldsymbol{\Psi} + \mathbf{N}, \tag{2}$$

where $\boldsymbol{\Gamma}_j = \text{diag}(\gamma_{1j}\ \gamma_{2j} \dots \gamma_{Kj})$, being γ_{kj} the uplink transmit power of the kth user of jth cell, $\mathbf{G}_{\ell j} = [\mathbf{g}_{\ell 1j}^T\ \mathbf{g}_{\ell 2j}^T \dots \mathbf{g}_{\ell Kj}^T]^T$, such that the $K \times N$ matrix $\mathbf{G}_{\ell j} = \sqrt{\mathcal{B}_{\ell j}}\mathbf{H}_{\ell j}, \mathcal{B}_{\ell j} = \text{diag}(\beta_{\ell 1j}\ \beta_{\ell 2j} \dots \beta_{\ell Kj}), \mathbf{H}_{\ell j} = [\mathbf{h}_{\ell 1j}^T\ \mathbf{h}_{\ell 2j}^T \dots \mathbf{h}_{\ell Kj}^T]^T$ is of dimension $K \times N$, $\boldsymbol{\Psi} = [\boldsymbol{\psi}_1\ \boldsymbol{\psi}_2 \dots \boldsymbol{\psi}_K]$, and $\mathbf{N}$ is a $N \times K$ additive white Gaussian noise (AWGN) matrix whose entries have zero mean and unitary variance.

In order to generate the estimated CSI matrix $\widehat{\mathbf{G}}_\ell$ of their served users, the ℓth BS correlates its received signal matrix with the known pilot sequences:

$$\widehat{\mathbf{G}}_\ell^T = \frac{1}{K}\mathbf{Y}_\ell \boldsymbol{\Psi}^H = \sum_{j=1}^{L} \mathbf{G}_{\ell j}^T \sqrt{\boldsymbol{\Gamma}_j} + \mathbf{N}', \tag{3}$$

where $\mathbf{N}' \in \mathbb{C}^{N\times K}$ is an equivalent AWGN matrix with zero mean and variance $\frac{1}{K}$. Hence, the channel estimated by the ℓth BS is contaminated by the channel of users that use the same pilot sequence in all other cells.

Information transmit symbols of the ℓth cell is denoted by the $K \times 1$ vector $\mathbf{x}_\ell = [x_{1\ell}\ x_{2\ell} \dots x_{K\ell}]^T$, where $x_{k\ell}$ is the transmit symbol to the kth user of the ℓth cell, and takes a value from the squared quadrature amplitude modulation (M-QAM) alphabet, normalized in order to preserve unitary average power. For analysis simplicity, using matrix notation, the $K \times 1$ complex-valued signal received by users of the ℓth cell is written as:

$$\mathbf{r}_\ell = \sum_{j=1}^{L} \mathbf{G}_{j\ell}\mathbf{P}_j \sqrt{\boldsymbol{\Phi}_j}\mathbf{x}_j + \mathbf{n}_\ell, \tag{4}$$

where $\boldsymbol{\Phi}_j = \text{diag}(\phi_{1j}\ \phi_{2j} \dots \phi_{Kj})$, being ϕ_{kj} the downlink transmit power devoted by the jth BS to its kth user, $\mathbf{P}_j$ denotes the complex valued $N \times K$ precoding matrix of the jth BS, being each column $\mathbf{p}_{kj}$ the $N \times 1$ precoding vector of the kth user. Finally, $\mathbf{n}_\ell \sim \mathcal{CN}(\mathbf{0}_K, \mathbf{I}_K)$ represents the AWGN vector observed at the K MTs of the ℓth cell.

Under the matched-filter beamforming technique, the vector $\mathbf{p}_{kj}$ is computed as [5]:

$$\mathbf{p}_{kj}^{mf} = \frac{\widehat{\mathbf{g}}_{jk}^H}{||\widehat{\mathbf{g}}_{jk}^H||} = \frac{\widehat{\mathbf{g}}_{jk}^H}{\alpha_{kj}\sqrt{N}}, \tag{5}$$

in which $\alpha_{kj} = \frac{||\widehat{\mathbf{g}}_{jk}^H||}{\sqrt{N}}$, and $\widehat{\mathbf{g}}_{jk}$ is the kth row of the matrix $\widehat{\mathbf{G}}_j$. Note that the normalization in (5) is necessary to satisfy the maximum transmit power available at the BS.

In the same way, in the zero-forcing beamforming technique, the vector $\mathbf{p}_{kj}$ is computed as:

$$\mathbf{p}_{kj}^{zf} = \frac{\mathbf{w}_{jk}}{||\mathbf{w}_{jk}||}, \tag{6}$$

in which the vector $\mathbf{w}_{jk} = \widehat{\mathbf{G}}_j^H \mathbf{a}_{jk}$, and $\mathbf{a}_{jk}$ is the kth column of $\mathbf{A}_j = \left[\widehat{\mathbf{G}}_j \widehat{\mathbf{G}}_j^H\right]^{-1}$.

3. Asymptotic limits of massive MIMO

Most of the asymptotic limits for massive MIMO systems can be build upon the following well known lemma:

Lemma 1. *Let $\mathbf{s}_1, \mathbf{s}_2 \in \mathbb{C}^{N\times 1}$ be two independent complex-valued vectors following a normal distribution, with zero mean and variance σ^2. Then*

$$\lim_{N\to\infty} \frac{\mathbf{s}_1^H \mathbf{s}_2}{N} \overset{a.s.}{=} 0 \quad \text{and} \quad \lim_{N\to\infty} \frac{\mathbf{s}_1^H \mathbf{s}_1}{N} \overset{a.s.}{=} \sigma^2. \tag{7}$$

Since the channel vectors of different users can be seen as independent random vectors, the above lemma is widely used for deriving limits in the massive MIMO scenarios. It can be justified since as the vector's length grows, the inner products between independent vectors grow at lesser rates than the inner products of vectors with themselves.

3.1. Asymptotic limits of MF beamforming

From (3), it is proved in [5] that $\alpha_{kj}^2 \overset{a.s.}{=} \sum_{l=1}^{L} \gamma_{kl}\beta_{jkl} + \frac{1}{K}$. Then authors show that $r_{k\ell}$, *i.e.*, the received signal at the kth user of ℓth cell, can be written as [5, Eq. (5)]:

$$r_{k\ell} = \sum_{l=1}^{L}\sum_{j=1}^{K} \sqrt{\phi_{jl}\beta_{lk\ell}}\mathbf{h}_{lk\ell}^H \mathbf{p}_{jl}^{\text{mf}} x_{jl} + n_{k\ell}. \tag{8}$$

Based on (5) and Lemma 1, (8) can be simplified when $N \to \infty$ as:

$$\begin{aligned} r_{k\ell} &= \sum_{l=1}^{L} \sqrt{\phi_{kl}\beta_{lk\ell}}\mathbf{h}_{lk\ell}^H \mathbf{p}_{kl}^{\text{mf}} x_{kl} + n_{k\ell}, \\ &= \sum_{l=1}^{L} \frac{1}{\alpha_{kl}} \sqrt{N\phi_{kl}\gamma_{k\ell}}\beta_{lk\ell} x_{kl} + n_{k\ell}, \\ &= \sqrt{N\gamma_{k\ell}} \sum_{l=1}^{L} \frac{\sqrt{\phi_{kl}}\beta_{lk\ell} x_{kl}}{\alpha_{kl}} + n_{k\ell}. \end{aligned} \tag{9}$$

Note that the AWGN of the estimated CSI in (3) vanishes in (9). This occurs since it is independent of $\mathbf{h}_{lk\ell}^H$, and thus its product as $N \to \infty$ is averaged out according to Lemma 1.

From (9), it is straightforward to see the asymptotic downlink SINR of the system as:

$$\mathrm{SINR}_{k\ell}^{dl} = \lim_{N\to\infty} \frac{N\gamma_{k\ell}\,\phi_{k\ell}\beta_{\ell k\ell}^2/\alpha_{k\ell}^2}{N\gamma_{k\ell}\left(\sum_{\substack{j=1\\ j\neq\ell}}^{L}\phi_{kj}\beta_{jk\ell}^2/\alpha_{kj}^2\right)+1} = \frac{\phi_{k\ell}\beta_{\ell k\ell}^2/\alpha_{k\ell}^2}{\sum_{\substack{j=1\\ j\neq\ell}}^{L}\phi_{kj}\beta_{jk\ell}^2/\alpha_{kj}^2}. \tag{10}$$

Note that this limit depends mainly on the long-term fading coefficients β_{jki}, which are related to the spatial distribution of the users in the different cells.

3.2. Asymptotic limits of ZF beamforming

For the ZF beamforming, Eq. (8) becomes

$$r_{k\ell} = \sum_{l=1}^{L}\sum_{j=1}^{K}\sqrt{\phi_{jl}\beta_{lk\ell}}\,\mathbf{h}_{lk\ell}^H\mathbf{p}_{jl}^{zf}x_{jl} + n_{k\ell}. \tag{11}$$

In order to find the asymptotic limits when employing the ZF scheme, we begin analysing the matrix $\mathbf{A}_\ell = \left[\widehat{\mathbf{G}}_\ell\widehat{\mathbf{G}}_\ell^H\right]^{-1}$. From (3), we have that

$$\mathbf{A}_\ell = \left[\left(\sum_{j=1}^{L}\sqrt{\boldsymbol{\Gamma}_j\mathcal{B}_{\ell j}}\mathbf{H}_{\ell j} + \mathbf{N}'\right)\left(\sum_{l=1}^{L}\mathbf{H}_{\ell l}^H\sqrt{\boldsymbol{\Gamma}_l\mathcal{B}_{\ell l}} + \mathbf{N}'^H\right)\right]^{-1} \tag{12}$$

Note that from Lemma 1, we can neglect all the terms corresponding to products of independent matrices, since in the limit of $N\to\infty$, they will not account. So, (12) simplifies to:

$$\begin{aligned}\mathbf{A}_\ell &= \left[\sum_{j=1}^{L}\sqrt{\boldsymbol{\Gamma}_j\mathcal{B}_{\ell j}}\mathbf{H}_{\ell j}\sum_{l=1}^{L}\mathbf{H}_{\ell l}^H\sqrt{\boldsymbol{\Gamma}_l\mathcal{B}_{\ell l}} + \mathbf{N}'\mathbf{N}'^H\right]^{-1}\\ &= \left[\sum_{j=1}^{L}\sqrt{\boldsymbol{\Gamma}_j\mathcal{B}_{\ell j}}\mathbf{H}_{\ell j}\mathbf{H}_{\ell j}^H\sqrt{\boldsymbol{\Gamma}_j\mathcal{B}_{\ell j}} + \mathbf{N}'\mathbf{N}'^H\right]^{-1}\\ &= \left[N\left(\sum_{j=1}^{L}\boldsymbol{\Gamma}_j\mathcal{B}_{\ell j} + \frac{1}{K}\mathbf{I}_K\right)\right]^{-1}\\ &= [\mathbf{D}_\ell]^{-1}.\end{aligned} \tag{13}$$

It can be seen that the matrix $\mathbf{D}_\ell$ is a diagonal matrix, in which the kth term can be written as $[\mathbf{D}_\ell]_{kk} = N\left(\sum_{j=1}^{L}\gamma_{kj}\beta_{\ell kj} + \frac{1}{K}\right)$. Thus, the matrix $\mathbf{A}_\ell$ will also be a diagonal matrix, and the kth term can be written as $[\mathbf{A}_\ell]_{kk} = 1/[\mathbf{D}_\ell]_{kk}$. Hence, the vector $\mathbf{w}_{jk} = \widehat{\mathbf{G}}_j^H\mathbf{a}_{jk}$ is simplified to $\mathbf{w}_{jk} = \widehat{\mathbf{g}}_{jk}^H\frac{1}{N\left(\sum_{j=1}^{L}\gamma_{kj}\beta_{\ell kj}+\frac{1}{K}\right)}$, and Eq. (6) can be rewritten as

$$\mathbf{p}_{kj}^{zf} = \frac{\widehat{\mathbf{g}}_{jk}^H\frac{1}{N\left(\sum_{j=1}^{L}\gamma_{kj}\beta_{\ell kj}+\frac{1}{K}\right)}}{\left\|\widehat{\mathbf{g}}_{jk}^H\frac{1}{N\left(\sum_{j=1}^{L}\gamma_{kj}\beta_{\ell kj}+\frac{1}{K}\right)}\right\|} = \frac{\widehat{\mathbf{g}}_{jk}^H}{\left\|\widehat{\mathbf{g}}_{jk}^H\right\|} = \mathbf{p}_{kj}^{mf}. \tag{14}$$

It is important to note that the convergence of the MF precoding to the ZF scheme in the limit of $N\to\infty$ is just achieved when considering the constraint of maximum transmit power available at BS, *i.e.*, normalizing the precoding vector. Otherwise, the asymptotic performances of such techniques will differ, as shown in [14, Fig. 11]. Furthermore, this equality holds only for N very large. For intermediate values, it is seen that the ZF scheme approaches the asymptotic limit faster than the MF beamforming, as numerically demonstrated in Section 5.1. However, the MF technique is quite less complex, and can be implemented in a decentralized way since the precoding vector of each user is not dependent on the estimated channels of other users, as opposed to ZF.

3.3. Asymptotic BER in downlink

We demonstrated that the MF and ZF schemes converge to the same precoding vector when the number of BS antennas grows to infinity. So, the results obtained in [5] for MF are also valid for ZF, specially Eqs. (9) and (10). Analysing the received signal of the kth user of the ℓth cell (9), we can also obtain some information about the bit-error probability:

$$r_{k\ell} = \sqrt{N\gamma_{k\ell}}\left(\frac{\sqrt{\phi_{k\ell}}\beta_{\ell k\ell}x_{k\ell}}{\alpha_{k\ell}} + \sum_{\substack{l=1\\ l\neq\ell}}^{L}\frac{\sqrt{\phi_{kl}}\beta_{lk\ell}x_{kl}}{\alpha_{kl}}\right) + n_{k\ell}. \tag{15}$$

Indeed, the effect of AWGN is averaged out when $N\to\infty$. For notation simplicity, but with no loss of generality, we consider 4-QAM modulation. Thus, the probability of error for this user can be written as (16a) in the next page, where $\Pr(\cdot)$ is the probability of an event. Hence, (16a) can be simplified as (16b), since both terms in the sum have the same statistical behaviour. The errors will occur whenever the interfering signal that reaches the user is greater than its intended signal.

$$\begin{aligned}\mathrm{Pe}_{k\ell} &= \frac{1}{2}\Pr\left(\Re\left\{\frac{\sqrt{\phi_{k\ell}}\beta_{\ell k\ell}x_{k\ell}}{\alpha_{k\ell}}\right\} < \Re\left\{\sum_{\substack{l=1\\ l\neq\ell}}^{L}\frac{\sqrt{\phi_{kl}}\beta_{lk\ell}x_{kl}}{\alpha_{kl}}\right\}\right)\\ &\quad+\frac{1}{2}\Pr\left(\Im\left\{\frac{\sqrt{\phi_{k\ell}}\beta_{\ell k\ell}x_{k\ell}}{\alpha_{k\ell}}\right\} < \Im\left\{\sum_{\substack{l=1\\ l\neq\ell}}^{L}\frac{\sqrt{\phi_{kl}}\beta_{lk\ell}x_{kl}}{\alpha_{kl}}\right\}\right),\end{aligned} \tag{16a}$$

$$\begin{aligned}&= \frac{1}{2}\Pr\left(\frac{\sqrt{\phi_{k\ell}}\beta_{\ell k\ell}\Re\{x_{k\ell}\}}{\alpha_{k\ell}} < \sum_{\substack{l=1\\ l\neq\ell}}^{L}\frac{\sqrt{\phi_{kl}}\beta_{lk\ell}\Re\{x_{kl}\}}{\alpha_{kl}}\right)\\ &\quad+\frac{1}{2}\Pr\left(\frac{\sqrt{\phi_{k\ell}}\beta_{\ell k\ell}\Im\{x_{k\ell}\}}{\alpha_{k\ell}} < \sum_{\substack{l=1\\ l\neq\ell}}^{L}\frac{\sqrt{\phi_{kl}}\beta_{lk\ell}\Im\{x_{kl}\}}{\alpha_{kl}}\right),\\ &= \Pr\left(\frac{\sqrt{\phi_{k\ell}}\beta_{\ell k\ell}\Re\{x_{k\ell}\}}{\alpha_{k\ell}} < \sum_{\substack{l=1\\ l\neq\ell}}^{L}\frac{\sqrt{\phi_{kl}}\beta_{lk\ell}\Re\{x_{kl}\}}{\alpha_{kl}}\right).\end{aligned} \tag{16b}$$

In order to determine the exact value of the probability in (16b), we must analyse every possible combination of interfering signals. Thus, the result can be written as

$$\mathrm{Pe}_{k\ell} = \frac{1}{2^{L-1}}\sum_{j=1}^{2^{L-1}}\mathrm{u}\left[\left(\sum_{\substack{l=1\\ l\neq\ell}}^{L}\frac{\sqrt{\phi_{kl}}\beta_{lk\ell}b_{jl}}{\alpha_{kl}}\right) - \frac{\sqrt{\phi_{k\ell}}\beta_{\ell k\ell}}{\alpha_{k\ell}}\right] \tag{17}$$

where b_{jl} is the j,lth element of the $2^{L-1}\times L$ matrix $\mathbf{B} = [\mathbf{B}'_{1:\ell-1}, \mathbf{1}_{2^{L-1}}, \mathbf{B}'_{\ell:L-1}]$, in which $\mathbf{B}'$ contains every possible combination of $\{\pm1\}^{L-1}$. Although we restricted our investigation for 4-QAM modulation, similar analysis can be conducted for $M>4$ by appropriately defining the decision bounds for $r_{k\ell}$ in (15).

The expression in (17) gives the exact BER of the kth user of the ℓth cell, as a function of the powers and the long-term fading coefficients of users in adjacent cells sharing the same training sequence. Thus it can be adopted as a performance optimization metric, in the same way as defined in Eq. (10). One possible approach is invoking a power allocation algorithm, as done in [5] with respect to (10). In this paper, we prefer a more simple strategy, that consists of simply *optimizing the assignment of pilot sequences to users*, by knowing the interference experienced by each sequence. We call this procedure of pilot allocation scheme.

4. Pilot allocation schemes

Eq. (15) shows that the received signal for a given user in the downlink of a massive MIMO system presents interference from another users in adjacent cells that share the same pilot sequence.

Besides, from this received signal in the limit of $N \to \infty$, the asymptotic expressions for SINR, Eq. (10), and for BER, Eq. (17), have been derived. At first glance, it may appear that the interference term in (15) does not depend on which user in ℓth cell is assigned the kth pilot sequence. However, reminding that $\alpha_{kl}^2 \overset{a.s.}{=} \sum_{j=1}^{L}\gamma_{kj}\beta_{lkj} + \frac{1}{K}$, one can see it is not true.

Thus, varying to which user is assigned the kth pilot sequence according its long-term fading coefficient can enhance the SINR, Eq. (10), and/or[1] decrease the probability of error, Eq. (17). This fact allows us the formulation of alternative optimization criteria, as described in the sequel.

Initially, we define the matrix $\mathbf{C}$, of size $K! \times K$, containing every possible combination of pilot sequences to the users, *i.e.*, c_{ij} says that, in the ith combination, the jth pilot sequence is allocated to the c_{ij}th user. Then we define four pilot allocation criterion aiming to optimise BER or SINR figure of metric. The four criteria are described in the following.

4.1. MinBER-based pilot allocation metric

In the first pilot allocation scheme, we search the best pilot distribution in the sense of minimizing the mean BER among users of the ℓth cell, leading to the MinBER pilot allocation scheme:

$$i_{mb} = \arg\ \min_{i} \frac{1}{K}\sum_{k=1}^{K} \mathrm{Pe}_{c_{ik}\ell}, \tag{18}$$

in which

$$\mathrm{Pe}_{c_{ik}\ell} = \frac{1}{2^{L-1}} \times \sum_{j=1}^{2^{L-1}} \mathrm{u}\left[\left(\sum_{\substack{l=1\\ l\neq\ell}}^{L} \frac{\sqrt{\phi_{kl}}\beta_{lk\ell}b_{jl}}{\alpha_{kl}^{(i)}}\right) - \frac{\sqrt{\phi_{c_{ik}\ell}}\beta_{\ell c_{ik}\ell}}{\alpha_{c_{ik}\ell}^{(i)}}\right]$$

corresponds to the BER of the c_{ik}th user of ℓth cell when the kth pilot sequence is assigned to him. Note that the superscript in $\alpha_{kl}^{(i)}$ and $\alpha_{c_{ik}\ell}^{(i)}$ evidences that these terms depend on the ith pilot distribution, since $\left(\alpha_{kl}^{(i)}\right)^2 = \gamma_{c_{ik}\ell}\beta_{lc_{ik}\ell} + \sum_{\substack{j=1\\ j\neq\ell}}^{L}\gamma_{kj}\beta_{lkj} + \frac{1}{K}$, and $\left(\alpha_{c_{ik}\ell}^{(i)}\right)^2 = \gamma_{c_{ik}\ell}\beta_{\ell c_{ik}\ell} + \sum_{\substack{j=1\\ j\neq\ell}}^{L}\gamma_{kj}\beta_{\ell kj} + \frac{1}{K}$, where we have put in evidence the terms related to the c_{ik}th user of the ℓth cell. The pilot allocation procedure is evaluated in a decentralized way; therefore, the assignment of pilots can be modified only for users of the ℓth cell when it is carrying out this procedure. Although the strictly optimal solution would test every possible pilot combination among the $K \cdot L$ users, its complexity would be prohibitive. Thus, the solution obtained in the decentralized way is preferable, and it can be shown that it converges to a Nash equilibrium after performing some times by each cell. Note that this problem can be viewed as a *finite potential game*, since: (a) it exists a global potential function that maps every strategy to some real value according its efficiency; (b) the set of strategies is of finite dimension [12]. In this case, each cell is a player, the potential function would be the average BER of the whole system in that subcarrier, *i.e.*, the average of (17) evaluated for the $K \cdot L$ users, and the strategy is the pilot allocation in that cell. Since each player chooses its strategy following a selfish best response dynamics, the convergence of the game to a Nash equilibrium is assured in [12, Theorem 19.12], [15, Proposition 2.2]. Besides, the decentralized solution can achieve appreciable gains in performance, as demonstrated in the next Section.

[1] Maximizing the SINR not necessarily minimizes the BER in the limit of $N \to \infty$, as can be seen from expressions (10) and (17), and discussed in Section 5.2.

4.2. MaxSINR-based pilot allocation metric

In the same way, in the second pilot allocation scheme, we define the pilot distribution that maximizes the mean SINR in the downlink of the ℓth cell, namely MaxSINR pilot allocation scheme:

$$i_{\mathrm{ms}} = \arg\ \max_{i} \frac{1}{K}\sum_{k=1}^{K} \mathrm{SINR}_{c_{ik}\ell}^{\mathrm{dl}}, \tag{19}$$

in which

$$\mathrm{SINR}_{c_{ik}\ell}^{\mathrm{dl}} = \frac{\phi_{c_{ik}\ell}\beta_{\ell c_{ik}\ell}^2/\left(\alpha_{c_{ik}\ell}^{(i)}\right)^2}{\sum_{\substack{j=1\\ j\neq\ell}}^{L}\phi_{kj}\beta_{jk\ell}^2/\left(\alpha_{kj}^{(i)}\right)^2} \tag{20}$$

is the downlink SINR of the c_{ik}th user of ℓth cell when the kth pilot sequence is assigned to him.

4.3. MiniMaxBER-based pilot allocation metric

Both optimization schemes, *e.g.* (18) and (20), find the pilot distribution by optimizing the mean value of some performance criterion. However, the "average" approach may be not completely adequate in modern communications systems, since it may lead to a great improvement in performance for a few users, while providing low quality of service (QoS) to those users poorly located, typically in the edge of the cell. Hence, we also look for pilot allocation schemes that ensure improvement in QoS for every user within the ℓth cell. The MinimaxBER pilot allocation scheme is defined as:

$$i_{mmb} = \arg\ \min_{i}\ \max_{k} \mathrm{Pe}_{c_{ik}\ell}, \tag{21}$$

which minimizes the worst BER within the cell.

4.4. MaxMinSINR-based pilot allocation metric

On the other hand, the MaxminSINR pilot allocation criterion constitutes an alternative way to optimally allocate pilots in multi-celular massive MIMO systems. The MaxminSINR pilot allocation scheme can be defined from the following optimization problem:

$$i_{mms} = \arg\ \max_{i}\ \min_{k} \mathrm{SINR}_{c_{ik}\ell}^{dl}, \tag{22}$$

which finds the pilots' set that maximizes the lowest SINR among the users of the cell.

4.5. Pilot allocation algorithm and its complexity

In the analysis of the pilot allocation strategies for multi-cellular massive MIMO we have assumed the asymptotic condition, i.e, when $N \to \infty$. Hence, the complexity of implementation of these pilot allocation algorithms will be independent of the number of antennas N. Algorithm 1 describes the general pilot allocation procedure, defining its inputs, outputs, and main steps. After its computation, the ℓth cell assigns the kth pilot sequence to the $c_{i_{opt}k}$th user. Note that each cell should be able to find the optimal pilot combination set among its covered users following one of these four criteria given respectively by Eq. (18), (19), (21), (22), in a decentralized way, reducing the overall computational complexity of the massive MIMO system.

Indeed, the computational complexity for the SINR-based pilot allocation procedures results $\mathcal{O}(K! \cdot K \cdot L^2)$, since operation of lines 4 and 6 demands $2L+1$ *flops* (floating point operations) each one, and will be evaluated $K! \cdot K \cdot L$ times. On the other hand, the

BER-based pilot allocation schemes result in a computational complexity of $\mathcal{O}(K! \cdot K \cdot L \cdot 2^{L-1})$, since evaluation of Eq. (18) or (21) in line 10 becomes prevalent, *i.e.* of $\mathcal{O}(K \cdot L \cdot 2^{L-1})$, and should be evaluated for the $K!$ pilot combinations. Such complexities may appear excessive. However, bearing in mind that K must assume low values in practical scenarios,[2] as well as the number L of cells within a cluster, one can conclude that the complexity of pilot allocation procedures is not prohibitive. As described in [9], there is no appeal to consider higher values of K in practical mobile TDD massive MIMO scenarios, since great part of the coherence time interval would be spent acquiring CSI from the moving terminals. Besides, once the optimization is complete, it remains valid for a relatively large time-interval, since the scheme depends only on the transmit powers and long-term fading coefficients of the users. Even for specific scenarios in which K may assume higher values, *i.e.*, with reduced mobility such as pedestrian scenarios, the exhaustive search approach can be replaced by some low-complexity heuristic method, and the optimization remains valid.

Algorithm 1 Pilot allocation procedure

Input: $\mathcal{B}_{jl}, \mathbf{\Phi}_j, \mathbf{\Gamma}_j, \forall j, l = 1, 2, \ldots L$.

1: Generate matrix $\mathbf{C}$, of size $K! \times K$;
2: **for** each combination $i = 1, 2, \ldots, K!$ **do**
3: **for** each pilot sequence $k = 1, 2, \ldots, K$ **do**
4: Evaluate $\alpha_{c_{ik}\ell}^{(i)} = \sqrt{\gamma_{c_{ik}\ell}\beta_{\ell c_{ik}\ell} + \sum_{\substack{j=1 \\ j\neq\ell}}^{L}\gamma_{kj}\beta_{\ell kj} + \frac{1}{K}}$;
5: **for** each cell $l = 1, 2, \ldots, L, l \neq \ell$ **do**
6: Evaluate $\alpha_{kl}^{(i)} = \sqrt{\gamma_{c_{ik}\ell}\beta_{lc_{ik}\ell} + \sum_{\substack{j=1 \\ j\neq\ell}}^{L}\gamma_{kj}\beta_{lkj} + \frac{1}{K}}$;
7: **end for**
8: **end for**
9: **end for**
10: Find $i_{opt} \in i = 1, 2, \ldots, K!$, corresponding to the optimal combination in $\mathbf{C}$ according some metric: (18), (19), (21), (22);

Output: i_{opt}.

5. Numerical results

Aiming to demonstrate the effectiveness of the proposed pilot allocation methods for multi-cellular massive MIMO systems, we provide in this Section performance results for both BER and SINR downlink metrics. The asymptotic condition ($N \to \infty$) for the number of BS antennas has been assumed, except for the convergence analysis for increasing N depicted in Fig. 2. We have adopted a multi-cell scenario with hexagonal cells of radius 1600 m, where $K = 4$ users are uniformly distributed in its interior, except in a circle of 100m radius around the cell centered BS. Besides, only the first ring of interfering cells has been considered, both for frequency reuse factors (RF) of one and three. We have assumed a similar TDD protocol of that in [5], in which the coherence interval is composed of 11 symbol periods: 4 for sending uplink training sequences, 1 for processing, 4 and 2 for downlink and uplink data transmission, respectively. As discussed in [8], in order to maximize the net throughput for a TDD protocol, it is beneficial to dedicate the same time with pilots and data transmissions. If more time is spent with pilots, more users can be served, but its rates decrease substantially due to the excessive overhead, and vice-versa. The system uses a carrier frequency of 1.9 GHz and a frequency band of 20 MHz.

Furthermore, the coherence time of 500 microseconds has been adopted, which could accommodate any terminal moving slower than 80 meters/second (associating the coherence time with the interval required by a terminal to move no more than 1/4 wavelength [9, Sec.VII-D]). The log-normal shadowing has been modelled with a standard deviation of 8dB, and the path loss term $d_{\ell kj}^{-\lambda}$ with decay exponent equal to $\lambda = 3.8$, and $d_{\ell kj}$ denoting the distance between the ℓth BS to kth mobile user of jth cell. Besides, we have considered 4-QAM modulation, a SNR target of 10 dB and an equal power allocation policy for all users, valid both for downlink[3] and uplink. The constraint of maximum transmit power available at BS is satisfied by the precoding schemes in our formulation, as represented in expressions (5) and (6), in which the precoding vectors are normalized. It is important to note that the numerical results in this Section (except part of Fig. 2) were obtained from the analytical expressions derived in Section 3, averaged from the evaluation of at least 10^5 independent trials for the user's location.

Fig. 1 depicts a single realization of the multi-cell scenario adopted in our numerical simulations, for frequency reuse factors of one and three. Notice that for clarity purpose, only users sharing the same frequency band, *i.e.*, interfering with each other, have been represented. Indeed, one can see that interfering users are much closer with smaller reuse factors. In our numerical results presented in the sequel, only the performance metrics of users positioned inside the central cell were computed, since these users experience a more realistic condition of interference.

5.1. Performance convergence of precoding techniques

Considering both MF and ZF precoding techniques, Fig. 2 depicts the asymptotic convergence[4] (as the number of BS antennas increases) for both BER and SINR performance metrics to the bounds defined in (17) and (10), respectively. The curves present mean values of each performance metric, taken among the users of the cell. One can note that the SINR of the ZF precoding scheme indeed converges to the same bound of Eq. (10), which was derived in [5] as the asymptotic SINR of MF beamforming. This occurs since we have considered the constraint of maximum transmit power available at BS, as opposed to [14]. These numerical results also show that MF needs at least one order of magnitude more BS antennas than ZF to reach that bound. Furthermore, the performance of both schemes are also analysed from the perspective of BER, validating Eq. (17) as the asymptotic BER that such techniques are able to achieve when $N \to \infty$. Indeed, in terms of BER, the performances of both techniques rapidly approach the asymptotic limit, being necessary $\approx 10^4$ BS antennas for both precoding techniques reaching the bound.

5.2. Performance of pilot allocation schemes

In this subsection, we investigate the performance of the four pilot allocation schemes proposed in Section 4, in terms of mean values, as well as in terms of distribution among users. The simu-

[2] K represents the length of the training sequences, which is equal to the number of users sharing one of N_{smooth} subcarriers in each coherence band. N_{smooth}, as given in (1), is desired to be high for an efficient OFDM communication; for example, $N_{\text{smooth}} = 14$ for $\Delta t_{CP} = 7\%$. On the other hand, K is limited by the coherence time, due to the user's mobility, by the efficiency of the TDD scheme, which cannot spend much time with pilots, and by the subcarrier spacing. For example, in [9], for a cell serving 42 users, $K = 3$ and $N_{\text{smooth}} = 14$.

[3] Despite of the average equal power allocation policy, the instantaneous power for users in downlink may differ due to the precoding scheme.

[4] Notice that in Fig. 2 simulation and analysis results have been compared, since performances of the techniques for increasing N are computed with independent realizations of small-scale fading, AWGN, and long-term fading, and they converge to the analytical bounds dependent only on the long-term fading.

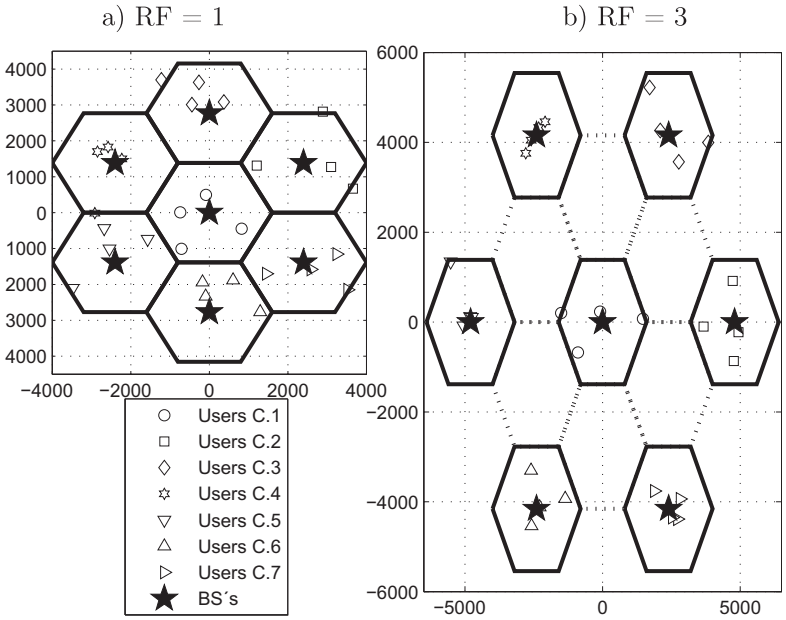

Fig. 1. Single spatial realization for both investigated multi-cell scenarios, with $K = 4$ mobile terminals.

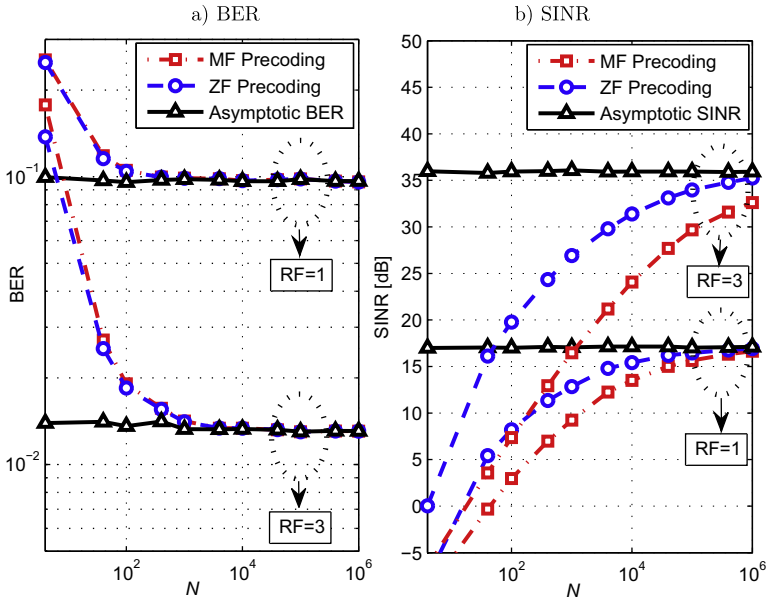

Fig. 2. Asymptotic convergences of MF and ZF precoding techniques to the performance bounds, under reuse factors of one and three, with increasing N.

lation results presented here were averaged over 100,000 spatial realizations.

Fig. 3 shows the cumulative distribution function (CDF) as a function of the BER of the users, regarding different pilot allocation techniques. For reference of comparison, it is also depicted the very large MIMO performance with no optimization in the distribution of pilot sequences, *i.e.*, with random allocation strategy. An interesting behavior on the BER distribution among users in the massive MIMO system can be observed from these numerical results. One can note that a significant portion of users communicates to BS with no errors, *i.e.*, BER = 0. This occurs because, for these users, even the strongest interference that can reach them is lower than their intended signal, and thus the probability of error is null. On the other hand, the other small portion of users, that are not free of errors, presents excessive values of BER. This disparity becomes more noticeable for unitary frequency reuse factor, in which the portion of users that presents excessive error rates is $\approx 10\%$, while for reuse factor of three it is about 1% for a BER $\geqslant 0.2$.

Furthermore, it shows that the pilot allocation schemes are able to significantly decrease the fraction of users with excessive BER's. As shown in Tables 1 and 2, the fraction of users with BER $\geqslant 0.1$ reduces from 23.63% to 14.92%, for frequency reuse factor of one, and from 3.47% to 1.06%, for frequency reuse factor of three, when deploying the MinBER approach.

Fig. 4 shows the fraction of users above a given SINR, for frequency reuse factors of one and three. It can be seen that increasing the frequency reuse factor has the effect of significantly improving the SINR of the users, as if the curve was shifted right

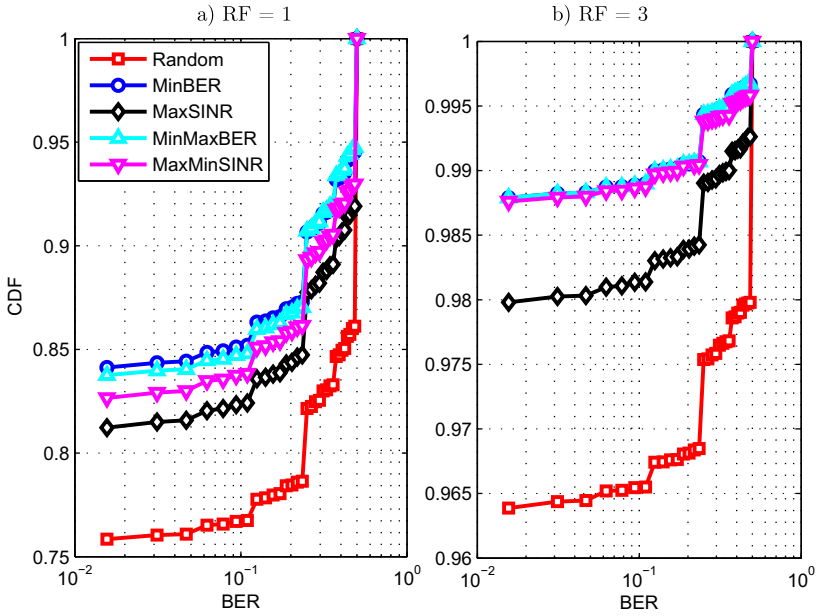

Fig. 3. Cumulative distribution function for the BER of the users, for different pilot allocation schemes.

Table 1
Performance of pilot allocation schemes for frequency-reuse factor of one.

PA scheme	Mean BER (%)	Users BER = 0 (%)	Users BER ⩾ 0.1 (%)	Mean user rate (Mbps)	95%-likely user rate (Mbps)
Random	9.84	75.41	23.63	48.50	0.1344
MinBER	5.48	83.98	14.92	55.54	0.4471
MaxSINR	6.85	80.85	17.78	56.59	0.4611
MinimaxBER	5.52	83.68	15.21	55.48	0.4609
MaxminSINR	6.17	82.45	16.28	52.62	0.7937

Table 2
Performance of pilot allocation Schemes for frequency-reuse factor of three.

PA scheme	Mean BER (%)	Users BER = 0 (%)	Users BER ⩾ 0.1 (%)	Mean user rate (Mbps)	95%-likely user rate (Mbps)
Random	1.41	96.33	3.47	29.07	4.79
MinBER	0.36	98.83	1.06	32.84	8.82
MaxSINR	0.66	98.01	1.86	32.91	8.81
MinimaxBER	0.37	98.82	1.06	32.84	8.82
MaxminSINR	0.39	98.78	1.09	31.68	11.15

≈ 18 dB, without noticeable changes on its format and slope. One can see that the MaxSINR technique has the ability of improving the SINR of the best located users, increasing ≈ 4 dB of SINR for the best 20% of the users. On the other hand, the MaxminSINR scheme increases ≈ 10 dB of SINR for the 95% level, *i.e.*, it benefits the less favorably located users.

Finally, Fig. 5 depicts the fraction of users above a given data rate, for frequency reuse factors of one and three, regarding the different proposed pilot allocation schemes. Notice that the downlink data rate $\mathcal{R}_{k\ell}$ of the kth user in the ℓth cell can be defined as:

$$\mathcal{R}_{k\ell} = \left(\frac{bw}{rf}\right)\left(\frac{\mathcal{D}}{\mathcal{T}}\right)\log_2\left(1+\text{SINR}_{k\ell}^{dl}\right), \tag{23}$$

where bw is the system total bandwidth, rf is the reuse factor, $\mathcal{D}$ is the number of symbol periods spent sending downlink data, and $\mathcal{T}$ is the total number of symbol periods within a channel coherence time.

Examining the curves, one can conclude that the slope of curves for reuse factor three is greater than the slope of unitary reuse factor curves. This fact means that the distribution for unitary reuse factor is much more irregular, unequal, in the sense that some users have very high rates while others have low QoS. On the other hand, for reuse factor of three, this distribution is much more uniform, guaranteeing simultaneously an improved QoS for much more users.

As shown in Table 1, 95% of users communicates with rates greater than 0.1344 Mbps with random pilot distribution, while when employing the MaxminSINR PA scheme the 95%-likely rate per user increases to 0.7937 Mbps. This means that a gain of 6 times can be achieved for unitary frequency reuse factor, while providing a mean rate of 52.62 Mbps per user. Furthermore, if the minimum assured performance per terminal is a more important concern, then the MaxminSINR scheme can be employed in conjunction with a frequency reuse factor of three. As described in Table 2, the 95%-likely rate passes from 4.79 Mbps to 11.15 Mbps, a gain greater than 6 Mbps. Note that the mean rate, however, decreases, since the gain in SINR for the best located users does not offset the loss due to reduction in bandwidth, given the logarithmic increase of rate according SINR gains. Larger reuse

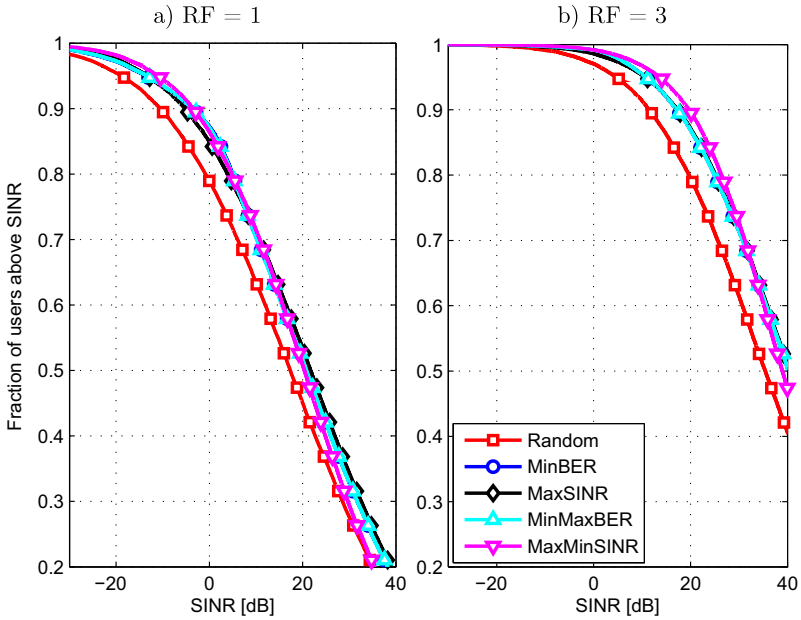

Fig. 4. Fraction of users above a given SINR, for different pilot allocation schemes.

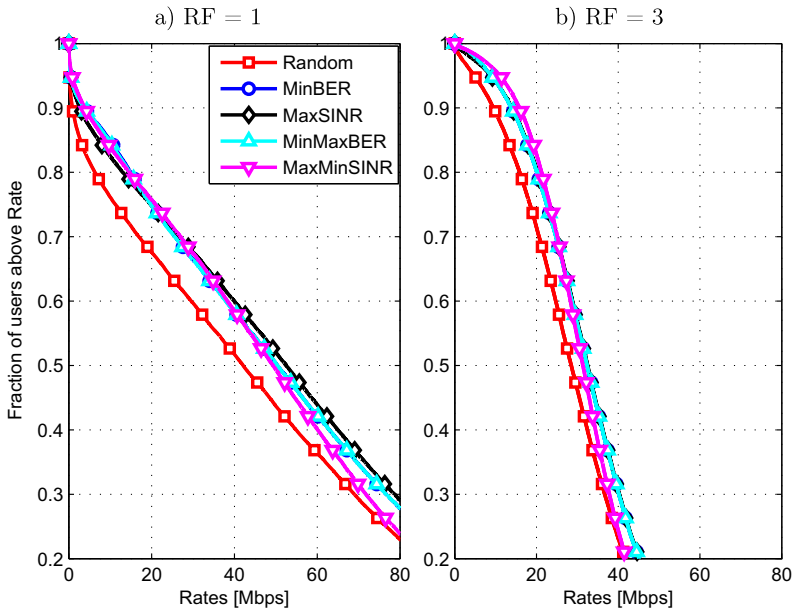

Fig. 5. Fraction of users above a given Rate, for different pilot allocation schemes.

factors are more beneficial for poor located users, since the logarithm is in its linear region, as discussed in [9].

Comparing both Tables, we note that the assured QoS, in terms of 95%-likely rate, can pass from 0.1344 Mbps, with unitary reuse factor and random pilot allocation, to 11.15 Mbps, for the Maxmin-SINR scheme and reuse factor of three. Thus, gains of ≈85 times can be achieved combining both RF and PA techniques, with appropriate conditions. Besides, the mean BER reduces from 9.84% to 0.39%, and the portion of users communicating in the absence of errors increases from 75.41% to 98.78%. These benefits are achieved by simply assigning the pilot sequences to the users within the cell in a more efficient way, in conjunction with a large frequency reuse factor, and remain valid whenever the long-term fading coefficients stay unchanged.

6. Conclusion

In this work we have characterized the asymptotic performance of the massive MIMO system downlink under the point of view of the BER performance. We have demonstrated that both MF and ZF precoding schemes result in the same signal as $N \to \infty$, and thus the results of [5] are also valid for the ZF beamforming. Then, we derived the exact asymptotic expression of the BER of a given user, based on the long-term fading coefficients and the power levels of other users. In the same way as the asymptotic SINR expression found in [5], the BER expression derived also depends only on the users in neighboring cells that reuse the same pilot sequence.

Furthermore, we have proposed efficient forms of assigning these pilots to the users within the cell, by optimizing several per-

formance metrics, including the asymptotic BER or alternatively the maximization of SINR found herein. The significant gains achieved by these pilot allocation techniques were demonstrated numerically. For instance, we have showed that a gain of 6 times regarding the random strategy can be achieved for the downlink rate with unitary reuse factor, while the data rate is increased from 4.79 Mbps to 11.15 Mbps for reuse factor of three. When combining the MaxminSINR technique with an appropriated reuse factor, we showed that the massive MIMO system are able to operate with a 95%-likely downlink rate of 11.15 Mbps, providing a communication free of errors for 98.78% of the users, guaranteeing the reliability of the system.

All of these benefits are achieved in a quite simple and expeditious way, by just knowing the powers and the long-term fading coefficients of users in adjacent cells, for each pilot sequence. Since these informations do not scale with the number of BS antennas, and remains constant within a long time and frequency interval, the implementation of the proposed pilot training sequence assignment method in massive MIMO system is surely feasible. Besides, even greater gains might be achieved by combining the proposed schemes with power allocation and time-shifting techniques [5,13], which is the continuity of this work.

Acknowledgement

This work was supported in part by the National Council for Scientific and Technological Development (CNPq) of Brazil under Grant 304066/2015-0, and in part by Londrina State University – Paraná State Government (UEL).

References

[1] Ashikhmin A, Marzetta T. Pilot contamination precoding in multi-cell large scale antenna systems. In: IEEE international symposium on information theory proceedings (ISIT), 2012. p. 1137–41.
[2] Boccardi F, Heath R, Lozano A, Marzetta T, Popovski P. Five disruptive technology directions for 5G. IEEE Commun Mag 2014;52(2):74–80.
[3] Choi J, Chance Z, Love D, Madhow U. Noncoherent trellis coded quantization: a practical limited feedback technique for massive MIMO systems. IEEE Trans Commun 2013;61(12):5016–29.
[4] Couillet R, Debbah M. Signal processing in large systems: a new paradigm. IEEE Signal Process Mag 2013;30(1):24–39.
[5] Fernandes F, Ashikhmin A, Marzetta T. Inter-cell interference in noncooperative TDD large scale antenna systems. IEEE J Sel Areas Commun 2013;31(2):192–201.
[6] Hanzo L, Akhtman Y, Wang L, Jiang M. MIMO-OFDM for LTE, WiFi and WiMAX: coherent versus non-coherent and cooperative turbo transceivers. IEEE Press and John Wiley & Sons; 2010.
[7] Karakayali M, Foschini G, Valenzuela R. Network coordination for spectrally efficient communications in cellular systems. IEEE Wirel Commun 2006;13(4):56–61.
[8] Marzetta T. How much training is required for multiuser MIMO? In: Fortieth asilomar conference on signals, systems and computers, ACSSC '06, 2006. p. 359–63.
[9] Marzetta T. Noncooperative cellular wireless with unlimited numbers of base station antennas. IEEE Trans Wireless Commun 2010;9(11):3590–600.
[10] Mazrouei-Sebdani M, Krzymien W, Melzer J. Massive MIMO with non-linear precoding: large-system analysis. IEEE Trans Veh Technol 2015;PP(99). 1–1.
[11] Ngo HQ, Larsson E, Marzetta T. Energy and spectral efficiency of very large multiuser MIMO systems. IEEE Trans Commun 2013;61(4):1436–49.
[12] Nisan N, Roughgarden T, Tardos E, Vazirani VV. Algorithmic game theory. Cambridge University Press; 2007.
[13] Rasti M, Sharafat A-R. Distributed uplink power control with soft removal for wireless networks. IEEE Trans Commun 2011;59(3):833–43.
[14] Rusek F, Persson D, Lau BK, Larsson E, Marzetta T, Edfors O, Tufvesson F. Scaling up MIMO: opportunities and challenges with very large arrays. IEEE Signal Process Mag 2013;30(1):40–60.
[15] Voorneveld M. Best-response potential games. Econ Lett 2000;66(3):289–95.
[16] Yang H, Marzetta T. Performance of conjugate and zero-forcing beamforming in large-scale antenna systems. IEEE J Sel Areas Commun 2013;31(2):172–9.
[17] Zheng K, Zhao L, Mei J, Shao B, Xiang W, Hanzo L. Survey of large-scale MIMO systems. IEEE Commun Surv Tutorials 2015;17(3):1738–60.
[18] Zhu X, Wang Z, Qian C, Dai L, Chen J, Chen S, Hanzo L. Soft pilot reuse and multi-cell block diagonalization precoding for massive MIMO systems. IEEE Trans Veh Technol 2015;PP(99). 1–1.

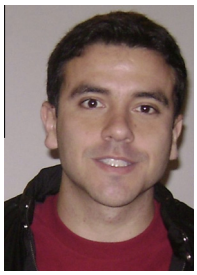

José Carlos Marinello received his B.S. and M.S. degree in Electrical Engineering (the first with Summa Cum Laude) from Londrina State University, PR, Brazil, in December 2012 and Sept 2014, respectively. He is currently working towards his Ph.D. at Polytechnic School of Sao Paulo University, São Paulo, Brazil. His research interests include physical layer aspects, such as heuristic and convex optimization of 4G and 5G MIMO systems.

Taufik Abrão (SM'12) received the B.S., M.Sc., and Ph.D. degrees in electrical engineering from the Polytechnic School of the University of São Paulo, São Paulo, Brazil, in 1992, 1996, and 2001, respectively. Since March 1997, he has been with the Communications Group, Department of Electrical Engineering, Londrina State University, Londrina, Brazil, where he is currently an Associate Professor of Communications engineering. In 2012, he was an Academic Visitor with the Communications, Signal Processing and Control Research Group, University of Southampton, Southampton, U.K. From 2007 to 2008, he was a Post-doctoral Researcher with the Department of Signal Theory and Communications, Polytechnic University of Catalonia (TSC/UPC), Barcelona, Spain. He has participated in several projects funded by government agencies and industrial companies. He is involved in editorial board activities of six journals in the communication area and he has served as TPC member in several symposium and conferences. He has been served as an Editor for the IEEE COMMUNICATIONS SURVEYS & TUTORIALS since 2013. He is a member of SBrT and a senior member of IEEE. His current research interests include communications and signal processing, specially the multi-user detection and estimation, MC-CDMA and MIMO systems, cooperative communication and relaying, resource allocation, as well as heuristic and convex optimization aspects of 3G and 4G wireless systems. He has co-authored of more than 170 research papers published in specialized/international journals and conferences.

APPENDIX B – Full paper published in the journal "*IEEE Access*"

Title: Uplink Performance of Single-Carrier Receiver in Massive MIMO with Pilot Contamination.

Authors: José Carlos Marinello Filho, Cristiano Panazio and Taufik Abrão.

Journal: IEEE Access (ISSN 2169-3536). Volume 5.

Classification (Qualis-CAPES): A2 / IF$= 1.270$ (Engenharias IV).

Publication Date: May 2017.

IEEE Access
Multidisciplinary ⋮ Rapid Review ⋮ Open Access Journal

Received April 13, 2017, accepted May 2, 2017. Date of publication xxxx 00, 0000, date of current version xxxx 00, 0000.

Digital Object Identifier 10.1109/ACCESS.2017.2703632

Uplink Performance of Single-Carrier Receiver in Massive MIMO With Pilot Contamination

JOSÉ CARLOS MARINELLO FILHO[1], CRISTIANO PANAZIO[1], AND TAUFIK ABRÃO[2], (Senior Member, IEEE)

[1]Electrical Engineering, Polytechnic School, University of São Paulo, São Paulo 05508-010, Brazil
[2]Electrical Engineering Department, State University of Londrina, Londrina 86057-970, Brazil

Corresponding author: Taufik Abrão (taufik@uel.br)

This work was supported by the National Council for Scientific and Technological Development of Brazil under Grant 304066/2015-0.

ABSTRACT We investigate the uplink (UL) performance of multicell massive MIMO (maMIMO) communication systems in frequency-selective fading channels, when the channel estimates are corrupted by pilot contamination, and the receiver employs maximum-ratio combining (MRC). Specifically, two fundamental schemes (receivers/waveforms) are considered: the time-reversal MRC (TRMRC) under single-carrier, and the conventional frequency-domain MRC (FDMRC) for orthogonal frequency-division multiplexing. We first derive approximate analytical expressions for the UL signal-to-interference-plus-noise ratio (SINR) performance of maMIMO systems, deploying both TRMRC and FDMRC. Then, lower bounds for the achievable rates of both systems are presented, and the derived expressions are validated by means of Monte–Carlo simulations. The performance of the investigated systems are compared regarding the variation of several parameters, such as the number of base station (BS) antennas M, number of users for each cell K, UL transmit power ρ_u, and the number of taps of the time-dispersive channel L. Our results demonstrate that the attained SINR performance of both schemes are very similar, but, in terms of achievable rates, TRMRC in general outperforms FDMRC by not requiring cyclic prefix transmission. On the other hand, our computational complexity analysis demonstrates that the TRMRC scheme demands somewhat higher processing resources ($\mathcal{O}(LMK)$) than FDMRC ($\mathcal{O}(MK)$). Thus, we propose a reduced complexity implementation for the TRMRC receiver, by employing the fast convolution with overlap-and-add technique, which is able to achieve the same result of TRMRC with a complexity of $\mathcal{O}(\log_2(2L)MK)$. For a practical maMIMO setup, the complexity reduction is about 50%. Finally, based on the derived expressions, we propose an iterative way to obtain the number of users that is able to maximize the sum rate of the cell, and investigate its behavior with the variation of different parameters, such as number of antennas, data, and pilot transmit power, as well as different frequency and pilot reuse schemes.

INDEX TERMS Large MIMO systems, pilot contamination, time-reversal MRC, frequency-domain MRC, single-carrier, OFDM.

I. INTRODUCTION

Massive multiple-input-multiple-output (maMIMO) communication systems are able to achieve high spectral and energy efficiencies with increased reliability [1], and have attracted huge research attention in wireless communication fields [2]. It is well-known from [3] that in a time-division duplex (TDD) noncooperative multicell MIMO system employing training pilots for channel state information (CSI) acquisition in the uplink and an infinite number of base station (BS) antennas M, the only effect that hinders performance is pilot contamination. This phenomenon results from unavoidable reuse of reverse-link pilot sequences by terminals in different cells. As a consequence of increasing the number of BS antennas to infinity, the transmit power can be designed arbitrarily small, since interference decreases at the same rate of the desired signal power, *i.e.*, signal-to-interference-plus-noise ratio (SINR) is independent of transmit power [3]. Besides, in this scenario, the most simple reception/transmission techniques, *i.e.*, maximum ratio combining (MRC) deployed in the uplink and the matched-filtering (MF) precoding used in the downlink, are able to achieve optimal capacity [4].

Most papers in the area consider maMIMO in conjunction with orthogonal frequency-division multiplexing (OFDM), in such a way that flat fading can be assumed for each subcarrier. On the other hand, single-carrier (SC) waveform has

been widely used in the uplink (UL) of current standards, such as LTE, while OFDM is adopted in downlink (DL). Among the advantages of employing SC in UL instead of OFDM [5], we can highlight: (**i**) the lower peak-to-average power ratio (PAPR) of the transmit signal, which enables the mobile terminal (MT) to be cheaper and more energy efficient. Besides, this implies in a lower distortion level imposed by the transmit amplifier, and as a consequence in a lower out-of-band radiation, which simplifies spectrum shaping and improves spectral efficiency by reducing the guard band. (**ii**) Lower sensitivity to phase noise and carrier frequency offset. (**iii**) The complexity of the MT is also simplified since the inverse fast fourier transform (IFFT) operation is not required. (**iv**) For the maMIMO scenario, we show in this paper that cyclic prefix (CP) transmission can be not required employing SC, which improves spectral and energy efficiencies. Due to these several benefits, and the fact of SC be already implemented in current standards, such waveform shows itself as a promising candidate for implementation in the next standards, *e.g.* 5G [2]. For this sake, much research has to be carried out to investigate SC application in the physical layer of that systems, in conjunction with maMIMO, for example.

Conventionally, SC receivers require complex equalization techniques in either time or frequency domain, such as decision-feedback equalizer (DFE) [6]. Frequency domain equalization is usually less complex than its time-domain version, but often requiring CP transmission and one FFT module per receive antenna similarly as OFDM. Alternatively, time-domain equalization can achieve a reasonable performance at the expense of increased complexity, but in some cases not requiring CP and FFT operations. However, when employed in conjunction with maMIMO, a different time-domain receiver can be adopted, which, taking advantage of the large excess of BS antennas, is able to alleviate the equalization complexity, namely the time-reversal MRC (TRMRC) receiver [7].

SC was first investigated in conjunction with maMIMO in [8], where it was proposed a precoding scheme that was able to deal with the time dispersive channel. Then, an UL version of this scheme was proposed in [9]. The TRMRC receiver, as described in [7], coherently combines the received symbols arising from different paths with the appropriate channel impulse response (CIR) vector. The robustness of this scheme was investigated in [7] against the phase noise effect, that results from imperfections in the circuitry of the local oscillators. However, it was assumed a single-cell scenario, and CSI estimates were corrupted only by additive white Gaussian noise (AWGN), but not by pilot contamination. Recently, both waveforms have been compared in maMIMO DL in [10], and low PAPR precoding schemes were proposed for both systems, but again in a single-cell scenario with no pilot contamination.

In order to provide a more uniform performance experience for the covered users, different schemes of reusing the available resources can be employed. Frequency reuse schemes, as discussed in [1] and [3], divide the available bandwidth into a predefined number of subbands, and assign different subbands for the cells aiming to maximize the distance between cells sharing the same subband, *i.e.*, under the maximum relative distance criterion. On the other hand, pilot reuse schemes, as in [11], divide the set of orthogonal pilot sequences into a predefined number of subgroups, assigning them to the cells according to the maximum relative distance criterion. A fundamental difference between both strategies is that frequency reuse reduces inter-cell interference not only in the training stage like pilot reuse, but also in the data transmission stage. Thus, while both schemes have the same ability to mitigate pilot contamination, which results from inter-cell interference during the training stage, frequency reuse scheme usually results in an improved SINR performance due to the lower inter-cell interference during data transmission stage. However, depending on the number of scheduled users per cell, the capacity loss due to the bandwidth division in frequency reuse may be higher than that resultant from the transmission of longer pilot sequences as in pilot reuse. Hence, a systematic study is necessary to indicate which scheme is able to improve system fairness with better capacity.

In this paper, we focus on the UL performance of multicell maMIMO systems under frequency-selective fading channels and subject to pilot contamination. Our main contributions are: (**i**) We provide a systematic comparison between two fundamental topologies: the conventional MRC receiver in conjunction with OFDM, and the TRMRC scheme operating under SC waveform, in order to indicate the merits and shortcomings of each scheme, and to investigate the feasibility of employing SC waveform in the next generation maMIMO systems. Such study has not been made yet to the best of our knowledge. (**ii**) We derive approximate expressions for the SINR performance of the investigated schemes, and propose lower bounds for their achievable capacities. The proposed expressions are validated by means of Monte-Carlo simulations. In the case of FDMRC, our derived expressions are very similar to that obtained in [4]. However in the case of TRMRC, such analysis was conducted only in [7], but in a single-cell scenario, with the CSI estimates corrupted only by AWGN. It is worth noting that our scenario is much more realistic, taking into account inter-cell interference as well as the procedure of obtaining CSI estimates from uplink pilot transmissions, which results in pilot contamination. Our performance expressions are derived based on this pilot contaminated CSI estimates, which is the most salient limiting factor for the maMIMO performance. (**iii**) We investigate also the computational complexity of both schemes, aiming to establish a performance-complexity trade-off. Due to the increased complexity of TRMRC found, we propose a low complexity implementation of this receiver by employing the fast convolution with overlap-and-add technique [12], which is able to reduce about one half the receiver complexity for a typical maMIMO setup without any performance loss. Such complexity study has not been conducted yet in the context

of maMIMO. Besides, although fast convolution techniques are widely known [12], they have not been adopted yet for reducing TRMRC complexity. (**iv**) After some slight simplifications on our derived expressions in order to improve mathematical tractability, we propose an iterative method to determine the number of users served by each cell which is able to obtain maximal sum rate, for any maMIMO system configuration. The dependence of this optimal number of users K^* is investigated with the variation of several system parameters, and a number of interesting insights are given.

A similar investigation was conducted in [11] for FDMRC and in [13] for a joint minimum mean square error (MMSE) receiver in flat fading channels. In [11], the optimal number of users is given in closed-form with $M \to \infty$, while for finite number of antennas K^* is analysed only via Monte-Carlo simulations for certain maMIMO configurations. Differently, our proposed method are valid both for FDMRC and TRMRC, and for any maMIMO parameters configuration, like number of antennas, pilot and data transmit power, and different pilot and frequency reuse schemes. In [13], authors find the number of scheduled users that maximizes an averaged area spectral efficiency expression, which is derived after some approximations for finding the expectation of the long-term fading coefficients with respect to the users' spatial distribution. Besides of such approximations being valid in restricted conditions, like large number of users and BS antennas, large number of cells, and low reference signal-to-noise ratio, the final result is found in a somewhat untractable form, based on incomplete elliptic integrals of the first and second kind in the Legendre normal form [13, Appendix B]. Our approximations for fixing the long-term fading coefficients of intra-cell and inter-cell users is much simpler, without restrictions, and shown to achieve appreciable results by simulations as demonstated in this paper. Besides, the analysis in [13] assumes a joint MMSE receiver, which requires matrix inversions that might impose a computational burden to the massive MIMO system. On the other hand, our analysis is based on MRC receiver, that is much less complex and highly parallelizable. Also, we compare the performance of frequency and pilot reuse schemes, indicating for which conditions each topology is preferable. Such interesting comparison has not been conducted yet to the best of our knowledge.

Besides this introductory Section, the system model is described in Section II. Our analytical expressions are developed in Section III. Representative numerical results are presented in Section IV, as well as our computational complexity analysis. In Section V, we propose a method to obtain the optimal number of users to be served by each cell, while Section VI concludes the paper.

Notations: Boldface lower and upper case symbols represent vectors and matrices, respectively. $\mathbf{I}_N$ denotes the identity matrix of size N, while $\mathbf{1}_K$ and $\mathbf{0}_K$ are the unitary vector and null vector of length K, respectively. The transpose and the Hermitian transpose operator are denoted by $\{\cdot\}^T$ and $\{\cdot\}^H$, respectively. $||\cdot||$ is the Euclidean norm of a vector. We use $\mathcal{CN}(\mathbf{m}, \mathbf{V})$ to refer to a circular symmetric complex Gaussian distribution with mean vector $\mathbf{m}$ and covariance matrix $\mathbf{V}$. Finally, $\mathbb{E}[\cdot]$ is the expectation statistical operator.

II. SYSTEM MODEL

Similarly as [3], we consider a MIMO system composed by C BSs, each equipped with M transmit antennas, and communicating with K single-antenna users. Since TDD is assumed, reciprocity holds, and thus CSI is acquired by means of uplink training signals. We divide the system model description for OFDM and SC waveforms. Besides, the following system model is also valid when employing non-unitary frequency reuse if only users and cells sharing the same subband are considered.

A. OFDM WAVEFORM

The time-frequency resources are divided into channel coherence blocks of $\mathcal{S} = T_c W_c$ symbols [11], in which T_c is the channel coherence time in seconds, and W_c is the channel coherence bandwidth in Hz ($W_c = \frac{1}{T_d}$ holds, in which T_d is the largest possible delay spread). Each coherence time interval are divided into $\mathcal{T}$ OFDM symbols ($T_c = \mathcal{T} T_s$, and T_s is the OFDM symbol period), distributed as uplink pilot transmissions, downlink and uplink data transmissions [3]. Using orthogonal pilot sequences, the number of available sequences is equal to its length, τ. CSI is estimated in the frequency domain in the same way as in [3]. If the system employs N subcarriers, and the CIR has L independent and identically distributed (i.i.d.) taps, the frequency smoothness interval is composed of $N_{\text{sm}} = N/L$ subcarriers. Thus, each user does not need to send pilots in all the N subcarriers, but only in $N/N_{\text{sm}} = L$ equally spaced subcarriers, since the frequency domain CSI (FDCSI) for the intermediate ones can be obtained by interpolation. Up to τ users can send pilots in the same subcarriers in the training stage, and a maximum total number of $K_{\max} = \tau N_{\text{sm}}$ users can be served by each cell. We define the set of subcarriers in which the kth user sends pilots as $\boldsymbol{\mathcal{I}}_k = \{\mathcal{I}_k(0), \mathcal{I}_k(1), \ldots, \mathcal{I}_k(L-1)\}$, such that $\mathcal{I}_k(0) \in [0, N_{\text{sm}} - 1]$ and $\mathcal{I}_k(i) - \mathcal{I}_k(i-1) = N_{\text{sm}}, \forall i = 0, 1, \ldots, L-1$. Figure 1 illustrates how training and data transmission stages are divided in time and frequency domains for a given user, in which T_n is the Nyquist sampling period.

We denote the $M \times 1$ FDCSI vector between the ith BS and the kth user at the jth cell in the nth subcarrier by $\mathbf{g}_{ikjn} = \sqrt{\beta_{ikj}}\underline{\mathbf{g}}_{ikjn}$, in which β_{ikj} is the long-term fading power coefficient, that comprises path loss and log-normal shadowing, and $\underline{\mathbf{g}}_{ikjn}$ is the short-term fading channel vector, that follows $\underline{\mathbf{g}}_{ikjn} \sim \mathcal{CN}(\mathbf{0}_M, \mathbf{I}_M)$. The orthogonal pilot sequences' set is $\boldsymbol{\Psi} = [\boldsymbol{\psi}_1\ \boldsymbol{\psi}_2 \ldots \boldsymbol{\psi}_\tau] \in \mathbb{C}^{\tau \times \tau}$, and $\boldsymbol{\Psi}^H\boldsymbol{\Psi} = \mathbf{I}_\tau$ holds. If the sequence $\boldsymbol{\psi}_k = [\psi_{k1}\ \psi_{k2} \ldots \psi_{k\tau}]^T$ is assigned for the kth user, the received signal for the nth subcarrier ($n \in \boldsymbol{\mathcal{I}}_k$) at the ith BS during the training stage is

$$\mathbf{Y}^{\text{p}}_{in} = \sqrt{\rho_{\text{p}}} \sum_{j=1}^{C} \sum_{k=1}^{\tau} \mathbf{g}_{ikjn} \boldsymbol{\psi}_k^H + \mathbf{N}^{\text{p}}_{in}, \tag{1}$$

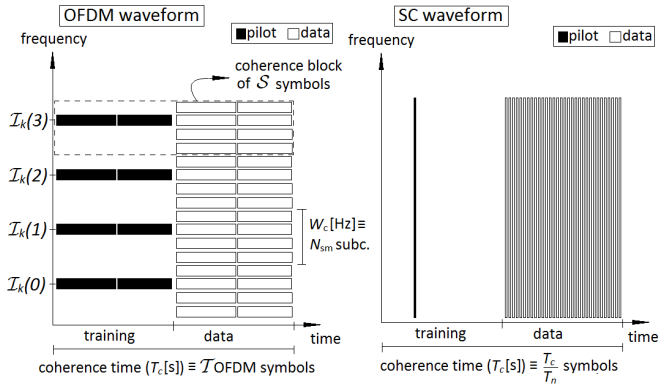

FIGURE 1. Time-frequency diagram illustrating how training and data transmission stages are divided for the kth user, for OFDM and SC waveforms: $N = 16$, $L = 4$, $N_{sm} = 4$, $\mathcal{T} = 4$, $\mathcal{S} = 16$ for OFDM; $T_c/T_n = 32$ for SC. Note that $K_{max} = 8$ for both schemes.

in which ρ_p is the UL pilot transmit power, $\mathbf{N}_{in}^{p} \in \mathbb{C}^{M\times\tau}$ is the AWGN matrix with i.i.d. elements following a complex normal distribution with zero mean and variance σ_n^2. Note that we have assumed synchronism between the signals received from different cells, which is the worst case in terms of pilot contamination [3]. The ith BS then estimates the kth user nth subcarrier FDCSI by correlating the received signal $\mathbf{Y}_{in}^{p}$ with $\boldsymbol{\psi}_k$

$$\widehat{\mathbf{g}}_{ikn} = \frac{1}{\sqrt{\rho_p}}\mathbf{Y}_{in}^{p}\boldsymbol{\psi}_k = \sum_{j=1}^{C}\mathbf{g}_{ikjn} + \mathbf{v}_{ikn}, \tag{2}$$

where $\mathbf{v}_{ikn} = \frac{1}{\sqrt{\rho_p}}\mathbf{N}_{in}^{p}\boldsymbol{\psi}_k \sim \mathcal{CN}(\mathbf{0}_M, \frac{\sigma_n^2}{\rho_p}\mathbf{I}_M)$ is an equivalent noise vector. The pilot contamination effect can be clearly seen in the previous expression. The other $N-L$ subcarriers' FDCSI estimates are obtained by interpolation. By acquiring such FDCSI estimates, the BS is able to perform linear detection in the UL deploying the FDMRC scheme. During UL data transmission, the ith BS receives in the nth subcarrier the signal

$$\mathbf{y}_{in}^{u} = \sqrt{\rho_u}\sum_{j=1}^{C}\sum_{k=1}^{K}\mathbf{g}_{ikjn}x_{kjn}^{u} + \mathbf{n}_{in}^{u}, \tag{3}$$

in which ρ_u is the UL data transmit power, x_{kjn}^{u} is the data symbol from the kth user of the jth cell in the nth subcarrier, and $\mathbf{n}_{in}^{u} \sim \mathcal{CN}(\mathbf{0}_M, \sigma_n^2\mathbf{I}_M)$ is the $M\times 1$ AWGN sample vector. This BS then estimates the transmitted symbol deploying FDMRC as

$$\widehat{x}_{kin}^{u} = \frac{1}{M}\widehat{\mathbf{g}}_{ikn}^{H}\mathbf{y}_{in}^{u}. \tag{4}$$

B. SC WAVEFORM

The tth CIR vector tap between the ith BS and the kth user of the jth cell and its FDCSI vector are related by

$$\mathbf{h}_{ikjt} = \frac{1}{L}\sum_{l=0}^{L-1}\mathbf{g}_{ikj\mathcal{I}_k(l)}e^{\jmath 2\pi lt/L}. \tag{5}$$

With no loss of generality, we assume in this paper a normalized uniform power delay profile (PDP) for all users, such that $\mathbf{h}_{ikjt} \sim \mathcal{CN}(\mathbf{0}_M, \frac{1}{L}\mathbf{I}_M)$ for $t = 0, 1, \ldots L-1$. For the systems employing single-carrier waveform, an alternative training scheme to conventional frequency domain training is discussed in [7]. In this alternative scheme for estimating the CIR of the users served by the cell, the users transmit uplink training signals sequentially in time, in such a way that at most one user per cell is transmitting at any given time. The kth user sends an impulse of amplitude $\sqrt{L\rho_p}$ (in order to spend the same average power as in FD training (1)) at the $(k-1)L$th channel use and is idle for the remaining portion of the training phase. Besides, the next user waits $L-1$ channel uses to send its training signal. It is worth noting that the same maximal number of users K_{max} is supported in this scheme. This can be proved by noting that the total interval spent with training signals is $K_{max}L\,T_n = \tau N_{sm}L\,T_n = \tau N\,T_n \approx \tau T_s$ is nearly the same as in FD training, as illustrated in Figure 1. The main advantage of this scheme is because estimating the CSI in the frequency domain would require the users to send FD pilots. This is only possible if the users' terminals were equipped with OFDM circuitry, does not bringing thus all the mentioned benefits of employing SC waveform.[1]

This procedure provides to the ith BS the following CIR estimates for its k-th user

$$\widehat{\mathbf{h}}_{ikt} = \sum_{j=1}^{C}\mathbf{h}_{ikjt} + \mathbf{v}'_{ikt}, \tag{6}$$

in which $\mathbf{v}'_{ikt} \sim \mathcal{CN}(\mathbf{0}_M, \frac{\sigma_n^2}{L\rho_p}\mathbf{I}_M)$ is an equivalent AWGN vector. Note that the CIR estimates are also corrupted by the users in adjacent cells that send its impulses at the same channel use, similarly as pilot contamination.

Considering SC waveform, the time-domain received signal at the ith BS in time t during UL data transmission is

$$\mathbf{r}_i^{u}[t] = \sqrt{\rho_u}\sum_{j=1}^{C}\sum_{k=1}^{K}\sum_{l=0}^{L-1}\mathbf{h}_{ikjl}s_{kj}^{u}[t-l] + \mathbf{n}'^{u}_{i}[t], \tag{7}$$

where $s_{kj}^{u}[t-l]$ is the time-domain UL data transmitted by the kth user of the jth cell at time $t-l$, and $\mathbf{n}'^{u}_{i}[t] \sim \mathcal{CN}(\mathbf{0}_M, \sigma_n^2\mathbf{I}_M)$ is an AWGN vector. This BS can then estimate the transmitted symbols deploying TRMRC as

$$\widehat{s}_{ki}^{u}[t] = \frac{1}{M}\sum_{l=0}^{L-1}\widehat{\mathbf{h}}_{ikl}^{H}\mathbf{r}_i^{u}[t+l]. \tag{8}$$

[1] Discussing whether the scheme proposed in [7] is practical or not due to the synchronization requirements is outside the scope of our paper. Furthermore, even if employing conventional frequency domain training, significant gains can be achieved, since the OFDM circuitry required for only frequency domain training is much more simple and less inefficient, since only L active subcarriers transmit pilots, as opposed to the N data active subcarriers in conventional OFDM data transmission. This reduction for typical OFDM setups is of 16 times, and undoubtedly is very beneficial for the system in terms of energy efficiency and implementation cost. It is worth to mention that the performance analysis developed in the following Sections does not suffer any change, since both schemes result in the same pilot contaminated CSI estimates.

For causality purpose, it is clear from (8) that $L-1$ shift registers are necessary per BS receive antenna for TRMRC, while this number for FDMRC is $N-1$, since the entire frame has to be received to perform FFT operation. This implies not only in hardware simplification, but also in latency reduction. Besides, the fact of TRMRC not requiring CP transmission can be seen from (8), since given a sufficiently large M, the BS is able to extract the desired information symbol vector from $\mathbf{r}_i^{\mathrm{u}}[t+l]$, even if the asynchronous interference belongs to another frame of symbols.

III. PERFORMANCE ANALYSIS

In this Section we analyse the performance of both investigated schemes. As the exact distribution of the interference terms would be very difficult to compute, we adopt a similar analysis of [7], [8], in which the estimated signal for each scheme is decomposed as a sum of uncorrelated terms: the desired signal, interference and noise terms. Then, the approximate SINR is computed as the ratio of the desired signal power and the power of the interference plus noise terms.

A. FDMRC UNDER OFDM TRANSMISSION SCHEME

Given the FDCSI estimates available at the ith BS (2), and the UL received signal at the UL data transmission stage (3), the nth subcarrier estimated data symbol of the k'th user deploying FDMRC in (4) can be written as

$$\widehat{x}^{\mathrm{u}}_{k'in} = A^{\mathrm{f}}_{k'in}x^{\mathrm{u}}_{k'in} + \mathtt{IF}^{\mathrm{f}}_{k'in} + \mathtt{PCI}^{\mathrm{f}}_{k'in} + \mathtt{AI}^{\mathrm{f}}_{k'in} + \mathtt{AN}^{\mathrm{f}}_{k'in}, \tag{9}$$

where the desired signal term $A^{\mathrm{f}}_{k'in} = \frac{\sqrt{\rho_{\mathrm{u}}}}{M}\mathbb{E}[||\mathbf{g}_{ik'in}||^2]$, with the expectation taken over the channel gains. Note that this term is a constant, which is known at the BS since the BS has knowledge of the channel statistics. Besides, we relegate the variation of $||\mathbf{g}_{ikin}||^2$ around its mean as another form of interference [7], [8], such that

$$\mathtt{IF}^{\mathrm{f}}_{k'in} = \frac{\sqrt{\rho_{\mathrm{u}}}x^{\mathrm{u}}_{k'in}}{M}\left[||\mathbf{g}_{ik'in}||^2 - \mathbb{E}[||\mathbf{g}_{ik'in}||^2]\right]. \tag{10}$$

The pilot contamination interference term is

$$\mathtt{PCI}^{\mathrm{f}}_{k'in} = \frac{\sqrt{\rho_{\mathrm{u}}}}{M}\sum_{\substack{j=1\\ j\neq i}}^{C}||\mathbf{g}_{ik'jn}||^2 x^{\mathrm{u}}_{k'jn}, \tag{11}$$

while the additional interference term is

$$\mathtt{AI}^{\mathrm{f}}_{k'in} = \frac{\sqrt{\rho_{\mathrm{u}}}}{M}\sum_{c=1}^{C}\mathbf{g}^{H}_{ik'cn}\left[\sum_{j=1}^{C}\sum_{k=1}^{K}\mathbf{g}_{ikjn}x^{\mathrm{u}}_{kjn} - \mathbf{g}_{ik'cn}x^{\mathrm{u}}_{k'cn}\right]. \tag{12}$$

TABLE 1. Expected power of the terms in (9) and (16).

Term	Expected Power
$A^{\mathrm{F}}_{k'in}$	$\rho_{\mathrm{u}}\beta^2_{ik'i}$
$\mathtt{IF}^{\mathrm{F}}_{k'in}$	$\frac{\rho_{\mathrm{u}}}{M}\beta^2_{ik'i}$
$\mathtt{PCI}^{\mathrm{F}}_{k'in}$	$\frac{\rho_{\mathrm{u}}(M+1)}{M}\sum_{\substack{c=1\\c\neq i}}^{C}\beta^2_{ik'c}$
$\mathtt{AI}^{\mathrm{F}}_{k'in}$	$\frac{\rho_{\mathrm{u}}}{M}\sum_{c=1}^{C}\beta_{ik'c}\left[\sum_{j=1}^{C}\sum_{k=1}^{K}\beta_{ikj}-\beta_{ik'c}\right]$
$\mathtt{AN}^{\mathrm{F}}_{k'in}$	$\frac{\rho_{\mathrm{u}}}{M}\frac{\sigma_n^2}{\rho_{\mathrm{p}}}\sum_{j=1}^{C}\sum_{k=1}^{K}\beta_{ikj}+\frac{\sigma_n^2}{\gamma M}\left[\sum_{c=1}^{C}\beta_{ik'c}+\frac{\sigma_n^2}{\rho_{\mathrm{p}}}\right]$
$A^{\mathrm{T}}_{k'i}$	$\rho_{\mathrm{u}}\beta^2_{ik'i}$
$\mathtt{IF}^{\mathrm{T}}_{k'i}[t]$	$\frac{\rho_{\mathrm{u}}}{ML}\beta^2_{ik'i}$
$\mathtt{PCI}^{\mathrm{T}}_{k'i}[t]$	$\frac{\rho_{\mathrm{u}}(M+\frac{1}{L})}{M}\sum_{\substack{c=1\\c\neq i}}^{C}\beta^2_{ik'c}$
$\mathtt{AI}^{\mathrm{T}}_{k'i}[t]$	$\frac{\rho_{\mathrm{u}}}{M}\sum_{c=1}^{C}\beta_{ik'c}\left[\sum_{j=1}^{C}\sum_{k=1}^{K}\beta_{ikj}-\frac{1}{L}\beta_{ik'c}\right]$
$\mathtt{AN}^{\mathrm{T}}_{k'i}[t]$	$\frac{\rho_{\mathrm{u}}}{M}\frac{\sigma_n^2}{\rho_{\mathrm{p}}}\sum_{j=1}^{C}\sum_{k=1}^{K}\beta_{ikj}+\frac{\sigma_n^2}{M}\left[\sum_{c=1}^{C}\beta_{ik'c}+\frac{\sigma_n^2}{\rho_{\mathrm{p}}}\right]$

It is important to note the differences between $\mathtt{PCI}^{\mathrm{f}}_{k'in}$ and $\mathtt{AI}^{\mathrm{f}}_{k'in}$: the FDCSI dot products in (12) are taken over independent vectors, while such products in (11) are taken over coincident vectors. This implies that $\mathtt{PCI}^{\mathrm{f}}_{k'in}$ grows at much higher rates when M increases than $\mathtt{AI}^{\mathrm{f}}_{k'in}$, becoming the most salient interference term in the maMIMO scenario. Finally, the additive noise term is

$$\mathtt{AN}^{\mathrm{f}}_{k'in} = \frac{\sqrt{\rho_{\mathrm{u}}}}{M}\mathbf{v}^{H}_{ik'n}\sum_{j=1}^{C}\sum_{k=1}^{K}\mathbf{g}_{ikjn}x^{\mathrm{u}}_{kjn} + \frac{1}{M}\sum_{j=1}^{C}\mathbf{g}^{H}_{ik'jn}\mathbf{n}^{\mathrm{u}}_{in} + \frac{1}{M}\mathbf{v}^{H}_{ik'n}\mathbf{n}^{\mathrm{u}}_{in}. \tag{13}$$

Evaluating the power of the terms presented in (9) (see Table 1), one can approximate the average SINR of the k'th user at the ith cell as $\varsigma^{\mathrm{f}}_{k'i}$ in (14), as shown at the bottom of this page. The parameter $\gamma = \frac{N}{N+N_{CP}}$ accounts for the transmit power loss due to CP, since we have assumed for a fair comparison that both schemes spend the same energy with data transmission, and $N_{CP} = L-1$ is the CP length. Note that this result is valid for all subcarriers, since they are identically distributed in our model.

Besides, due to the convexity of $\log_2(1+\frac{1}{x})$ and using Jensen's inequality as in [1], we obtain the following lower bound on the achievable rate of the k'th user at the ith cell

$$\mathcal{R}^{\mathrm{f}}_{k'i} \geq \widetilde{\mathcal{R}}^{\mathrm{f}}_{k'i} = \xi^{\mathrm{u}}\gamma\left(1-\frac{K}{\mathcal{S}}\right)\log_2\left(1+\left(\frac{1}{\varsigma^{\mathrm{f}}_{k'i}}\right)^{-1}\right), \tag{15}$$

in which the term $\left(1-\frac{K}{\mathcal{S}}\right)$ accounts for the pilot transmission overhead, and ξ^{u} is the fraction of the data transmit interval spent with uplink.

$$\varsigma^{\mathrm{f}}_{k'i} = \frac{M\beta^2_{ik'i}}{M\sum_{\substack{c=1\\c\neq i}}^{C}\beta^2_{ik'c} + \left[\sum_{j=1}^{C}\sum_{k=1}^{K}\beta_{ikj} + \frac{\sigma_n^2}{\gamma\rho_{\mathrm{u}}}\right]\left[\sum_{c=1}^{C}\beta_{ik'c} + \frac{\sigma_n^2}{\rho_{\mathrm{p}}}\right]} \tag{14}$$

$$\varsigma^{\mathrm{t}}_{k'i} = \frac{M\beta^2_{ik'i}}{M\sum_{\substack{c=1\\c\neq i}}^{C}\beta^2_{ik'c} + \left[\sum_{j=1}^{C}\sum_{k=1}^{K}\beta_{ikj} + \frac{\sigma^2_n}{\rho_{\mathrm{u}}}\right]\left[\sum_{c=1}^{C}\beta_{ik'c} + \frac{\sigma^2_n}{\rho_{\mathrm{p}}}\right]} \tag{22}$$

B. TRMRC UNDER SINGLE-CARRIER TRANSMISSION SCHEME

Similarly, given the CIR estimates available at the ith BS (6), and the time-domain received signal in the UL data transmission stage (7), the estimated UL data symbols deploying TRMRC in (8) can be decomposed as

$$\begin{aligned}\widehat{s}^{\mathrm{u}}_{k'i}[t] = A^{\mathrm{t}}_{k'i}s^{\mathrm{u}}_{k'i}[t] + \mathtt{IF}^{\mathrm{t}}_{k'i}[t] + \mathtt{PCI}^{\mathrm{t}}_{k'i}[t] \\ + \mathtt{AI}^{\mathrm{t}}_{k'i}[t] + \mathtt{AN}^{\mathrm{t}}_{k'i}[t],\end{aligned} \tag{16}$$

in which the desired signal term is

$$A^{\mathrm{t}}_{k'i} = \frac{\sqrt{\rho_{\mathrm{u}}}}{M}\mathbb{E}\left[\sum_{l=0}^{L-1}||\mathbf{h}_{ik'il}||^2\right]; \tag{17}$$

the desired signal interference term is

$$\mathtt{IF}^{\mathrm{t}}_{k'i}[t] = \frac{\sqrt{\rho_{\mathrm{u}}}s^{\mathrm{u}}_{k'i}[t]}{M}\left[\sum_{l=0}^{L-1}||\mathbf{h}_{ik'il}||^2 - \mathbb{E}\left[\sum_{l=0}^{L-1}||\mathbf{h}_{ik'il}||^2\right]\right]; \tag{18}$$

the pilot contamination interference term is

$$\mathtt{PCI}^{\mathrm{t}}_{k'i}[t] = \frac{\sqrt{\rho_{\mathrm{u}}}}{M}\sum_{l=0}^{L-1}\sum_{\substack{j=1\\j\neq i}}^{C}||\mathbf{h}_{ik'jl}||^2 s^{\mathrm{u}}_{k'j}[t]; \tag{19}$$

while the additional interference term is

$$\begin{aligned}\mathtt{AI}^{\mathrm{t}}_{k'i}[t] = \frac{\sqrt{\rho_{\mathrm{u}}}}{M}\sum_{c=1}^{C}\sum_{l=0}^{L-1}\mathbf{h}^H_{ik'cl} \\ \times\left[\sum_{j=1}^{C}\sum_{\ell=0}^{L-1}\sum_{k=1}^{K}\mathbf{h}_{ikj\ell}s^{\mathrm{u}}_{kj}[t+l-\ell] - \mathbf{h}_{ik'cl}s^{\mathrm{u}}_{k'c}[t]\right],\end{aligned} \tag{20}$$

and the same differences between pilot contamination and additional interference terms for OFDM hold in this case. Besides, the additive noise term is

$$\begin{aligned}\mathtt{AN}^{\mathrm{t}}_{k'i}[t] = \frac{\sqrt{\rho_{\mathrm{u}}}}{M}\sum_{l=0}^{L-1}\mathbf{v}'^H_{ik'l}\sum_{c=1}^{C}\sum_{\ell=0}^{L-1}\sum_{k=1}^{K}\mathbf{h}_{ikc\ell}s^{\mathrm{u}}_{kc}[t+l-\ell] \\ + \frac{1}{M}\sum_{l=0}^{L-1}\sum_{c=1}^{C}\mathbf{h}^H_{ik'cl}\mathbf{n}'^{\mathrm{u}}_i[t+l] \\ + \frac{1}{M}\sum_{l=0}^{L-1}\mathbf{v}'^H_{ik'l}\mathbf{n}'^{\mathrm{u}}_i[t+l].\end{aligned} \tag{21}$$

Evaluating the power of the terms presented in (16), one can approximate the SINR of the k'th user at the ith cell as $\varsigma^{\mathrm{t}}_{k'i}$ in (22), as shown at the top of this page. Besides, analogously to (15), a lower bound on the achievable rate of the k'th user at the ith cell can be obtained as[2]

$$\mathcal{R}^{\mathrm{t}}_{k'i} \geq \widetilde{\mathcal{R}}^{\mathrm{t}}_{k'i} = \xi^{\mathrm{u}}\left(1 - \frac{K}{\mathcal{S}}\right)\log_2\left(1 + \left(\frac{1}{\varsigma^{\mathrm{t}}_{k'i}}\right)^{-1}\right). \tag{23}$$

Table 1 presents the expected power of the terms in (9) and (16). From (14) and (22), one can see that both schemes attain the same SINR performance, unless the SNR loss of FDMRC due to the CP transmission, expressed by the term γ. Besides, the asymptotic UL performance of both systems converge with infinite number of BS antennas to the same bound of [3]:

$$\lim_{M\to\infty}\varsigma^{\mathrm{f}}_{k'i} = \lim_{M\to\infty}\varsigma^{\mathrm{t}}_{k'i} = \frac{\beta^2_{ik'i}}{\sum_{\substack{c=1\\c\neq i}}^{C}\beta^2_{ik'c}}. \tag{24}$$

IV. NUMERICAL RESULTS

Aiming to validate the tightness of our proposed expressions of Section III, and to compare the investigated schemes, we present in this Section numerical results for the maMIMO system performance under frequency-selective channels. We have adopted the same multicell scenario of [14] with unitary frequency reuse factor, composed of $C = 7$ hexagonal cells of radius $d = 1000$m, where K users are uniformly distributed, except in a circle of 100m radius around the cell centered BS. Besides, only the performance of the users at the central cell were computed, since they experience a more realistic interference. Unless otherwise specified, we have assumed $M = 100$ BS antennas, $K = 4$ users, $N = 256$ subcarriers when OFDM is employed, a time-dispersive channel with $L = 16$, $\xi^{\mathrm{u}} = 0.5$, and an SNR of 0dB for both pilots and UL data transmission. The path loss decay exponent was assumed $\lambda = 3.8$, and the log-normal shadowing standard deviation as 8dB. The presented results were averaged over 100,000 spatial realizations for the users.

A. SYSTEM PERFORMANCE

Figure 2 shows the performance of the investigated schemes, both in terms of simulated results,[3] and as in terms of the proposed analytical expressions. We show the influence of the UL data transmission SNR ($\frac{\rho_{\mathrm{u}}}{\sigma^2_n}$) increase over the SINR performance and over the achievable rates of a given cell. One can see that the maMIMO system is able to operate

[2]Rigorously, referring to Figure 1, the training overhead for SC waveform would be $\left(1 - \frac{KL}{T_c/T_n}\right)$. However, since $\frac{K}{\mathcal{S}} = \frac{KL}{\mathcal{T}N_{\mathrm{sm}}L} = \frac{KL}{\mathcal{T}N} \approx \frac{KL}{T_c/T_s\,T_s/T_n} = \frac{KL}{T_c/T_n}$, we opted to mantain the same form of (15).

[3]Considering independent realizations for the short-term fading, data symbols, and AWGN.

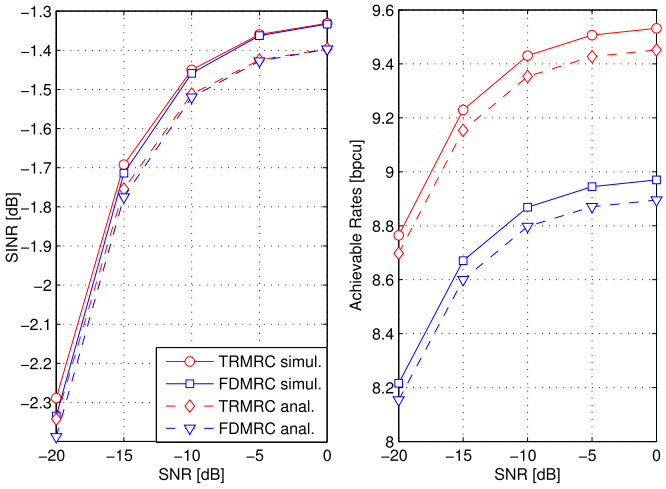

FIGURE 2. **Performance of the investigated schemes with increasing $\frac{\rho_u}{\sigma_n^2}$.**

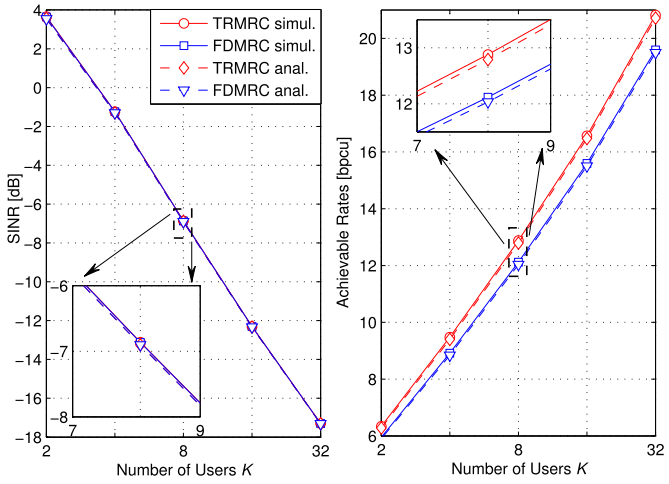

FIGURE 4. **Performance of the investigated schemes with increasing K.**

with low UL SNR's, due to the large number of BS antennas, in such a way that the system performance saturates near 0dB. Besides, both schemes result in very similar SINR performance, but the achievable rates of TRMRC are higher than that of FDMRC due to the inefficiency of the CP transmission, required by the latter. One can also see that our approximate expressions for SINR and the proposed lower bounds for achievable rates are tight. While the error for SINR was about 0.06dB, the error between the simulated rates and the proposed lower bound was about 0.075 bits per channel use (bpcu).

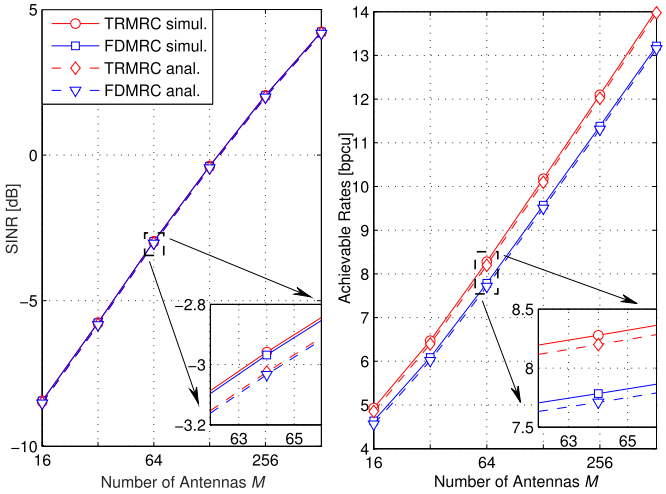

FIGURE 3. **Performance of the investigated schemes with increasing M.**

The performance dependence of the maMIMO system with the increasing number of BS antennas is shown in Figure 3, both in terms of SINR and achievable rates. In the investigated range of M, one can see that it was always beneficial for the system performance to increase the number of BS antennas from the adopted perspectives, since the M in which the convergence to (24) occurs was outside this range. Again, both schemes have resulted in very similar performances, and the approximate SINR expressions as well as the proposed lower bounds for the achievable rates were tight: the same gaps of 0.06dB and 0.075 bpcu were found, respectively.

Figure 4 shows how the maMIMO system performance evolves with the increasing number of users per cell, K. As expected, the average SINR per user decreases, due to the increasing multiuser interference. However, the achievable rates grow with more users, since the sum rate increase of each additional user in the investigated interval compensates the decrease of the individual SINR. Besides, the errors between simulated performances and analytical expressions in terms of individual SINR have decreased for higher values of K, being 0.01dB for $K = 32$. However, the achievable rate errors have increased to 0.09 bpcu for $K = 32$, because the higher number of users makes the accumulated error large.

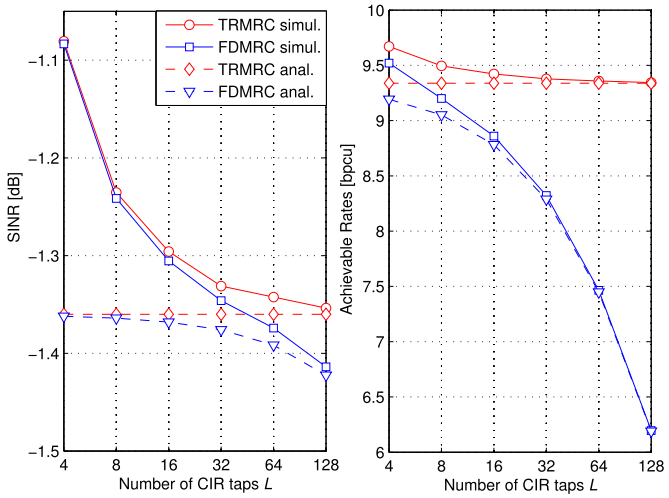

FIGURE 5. **Performance of the investigated schemes with increasing L.**

Finally, Figure 5 depicts the influence that the increasing CIR length L has on the maMIMO system performance. For the FDMRC scheme, it is clear that the system performance degrades with increasing L due to the inefficiency of the

CP transmission ($N_{CP} = L - 1$), that results both in an SINR loss as well as in a capacity loss. On the other hand, for the TRMRC scheme, the system performance is little sensitive to the increase of L. On one hand, a higher value of L results in higher intersymbol interference, but on the other hand it means that the TRMRC receiver has a richer information diversity when extracting the desired data symbols, as shown in (8). It can be seen from the Figure 5 that the error between the simulated performance and the proposed analytical expressions grows for lower values of L, what occurs because the frequency smoothness interval grows as L decreases: $N_{\text{sm}} = N/L$. Thus, the correlation of the channel frequency gains among the different subcarriers increases, making both the approximate SINR as well as the lower bound for the achievable rates less accurate; even though the errors were always lower than 0.3dB and 0.4 bpcu, respectively, in our simulations.

B. COMPLEXITY ANALYSIS

We evaluate the computational complexity of both investigated schemes, in order to establish a performance-complexity trade-off. The computational complexities are evaluated in terms of *floating-point operations (flops)* [15], and the main assumptions we have made are: *i*) A real sum operation has the same complexity than a real multiplication, which are defined as 1 *flop*; *ii*) A complex sum has the complexity of 2 *flops*, while a complex multiplication has the complexity of 6 *flops*; *iii*) An inner product between 2 complex vectors of size M has the complexity of M complex multiplications and $M - 1$ complex additions, resulting in a total complexity of $8M - 2$ *flops*; *iv*) A FFT or IFFT operation of a complex sequence of N samples has the complexity (supposing N power of two and adopting the Cooley Tukey algorithm [15]) of $(N/2)\log_2(N)$ complex multiplications and $N\log_2(N)$ complex additions, and an overall complexity of $5N\log_2(N)$ *flops*; *v*) As a final assumption, we neglect the complexity related with the CSI estimation for all the investigated schemes, since these estimates remain valid for several frame periods, and account in the same way for all the schemes.

For the FDMRC under OFDM, the complexity to detect the N symbols of the OFDM frame is mainly due to: *i*) the N-points IFFT operations of each user transmission ($K[5\,N\log_2(N)]$ *flops*), *ii*) the N-points FFT operations of each BS receive antenna ($M[5\,N\log_2(N)]$ *flops*), and due to *iii*) the N FDMRC data symbols' estimation, as in eq. (4), for each user ($NK[8\,M - 2]$ *flops*). On the other hand, for the TRMRC under single-carrier, the FFT operations are not required and the complexity is only due to N TRMRC data symbols' estimation, as in eq. (8), for each user. Each data symbol estimation is composed of L inner products of M-sized complex vectors, followed by $L - 1$ complex additions, resulting in an overall complexity of $NK[L(8\,M - 2) + 2(L - 1)]$ *flops*.

The computational complexities in terms of *flops* for detecting each frame of N symbols are given in Table 2.

TABLE 2. Number of operations (flops) for each scheme.

Scheme	Number of Operations
FDMRC	$K[5N\log_2(N)] + M[5N\log_2(N)] + NK[8M - 2]$
TRMRC	$NK[L(8M - 2) + 2(L - 1)]$
FC-TRMRC	$K[M(N + L)(10\log_2(2L) + 14) + 2N(M - 1)] + M(N + L)10\log_2(2L)$

Examining such complexity expressions, we identify the most dominant terms as the ones having the product MK. Since this term in the complexity expression of TRMRC is L times greater than this term in the complexity expression of FDMRC, the complexity of the former, for moderate/high number of users and BS antennas, results L times the complexity of the latter, *i.e.*, while the FDMRC complexity results $\mathcal{O}(MK)$ per detected symbol vector, that of TRMRC results $\mathcal{O}(LMK)$. Although the number of the CIR taps L is a fixed system parameter, and $L \ll N$ usually holds, the complexity of TRMRC results somewhat increased in comparison with FDMRC, as can be seen in Figure 6, in which the complexities are plotted with the increase of M and K.

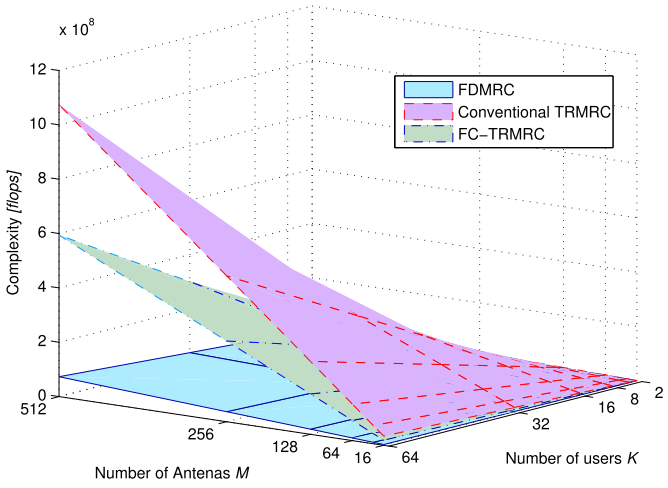

FIGURE 6. Computational complexities of the investigated schemes.

We propose in this paper a low complexity form of performing the TRMRC detection, by employing the fast convolution technique in conjuntion with overlap-and-add method [12]. The TRMRC detection in eq. (8) can be rewritten as

$$\widehat{s}^{\text{u}}_{ki}[t] = \frac{1}{M}\sum_{m=1}^{M}\sum_{l=0}^{L-1}\widehat{h}^{*}_{iklm}r^{\text{u}}_{im}[t + l], \tag{25}$$

which evidences that the TRMRC operation corresponds to the coherent combining of the M outputs of the convolution between the received signal and the reverse CIR. Each convolution can be performed with reduced complexity taking advantage of the convolution theorem and the efficient FFT's algorithms, in the so-called fast convolution algorithms. Such algorithms simply take the FFT of each sequence (in a suitable size), multiply them, and take the IFFT of the result.

Considering the sequences' lengths, the lowest power of 2 size of each FFT operation would often be $2N$. However, as the CIR length is usually much lower than this value, this alternative still may lead to an excessive complexity. A better approach is given by the overlap-and-add method, in which the FFT's are taken with a size of 2 L (supposing L power of 2). Since the sequence $\mathbf{r}_i^{\mathrm{u}}[t]$ is longer than this, it is partitioned into $\mu = (N + L)/L$ segments of length L, which are zero-padded until the length $2L$. The FFT results are multiplied, and the IFFT of the product is taken. The results of each segment are properly overlaped and added, leading to the same result of the conventional convolution with reduced complexity [12].

The complexity of the TRMRC with overlap-and-add method is mainly given by: *i*) μ FFT's of size $2L$ for the received signals of each receive antenna, resulting in a complexity of $M\mu[10\ L\log_2(2L)]$ *flops*; *ii*) For each user and each receive antenna: μ element-wise multiplication of size $2L$ vectors, followed by an IFFT operation of size $2L$, and the addition of the overlaping segments (of size L) $(KM\mu[10\ L\log_2(2L) + 12\ L + 2\ L]$ *flops*); *iii*) For each user, the results of the M fast convolutions are added (only the N elements of interest), with a complexity of $K(2\ N(M-1))$ *flops*. The overall complexity of the TRMRC receiver employing the fast convolution with overlap-and-add method (FC-TRMRC) is also given in Table 2 and plotted in Figure 6.

It can be seen that the complexity of the FC-TRMRC receiver results $\mathcal{O}(\log_2(2L)MK)$ per detected symbol vector, which is a significant complexity reduction in comparison with TRMRC. For example, under a conventional maMIMO setup with $M = 128$, $K = 32$, $N = 256$, and $L = 16$, the computational cost to detect each frame of N symbol vectors is of 10 M*flops* for FDMRC, 134 M*flops* for TRMRC, and 75 M*flops* for FC-TRMRC. Although the complexity of FC-TRMRC is still 7.5 times that of FDMRC, it is about one half of that of TRMRC, with the same result, and the same set of advantages. To name a few: lower PAPR, cheaper and more energy efficient mobile terminals, lower sensitivity to phase noise and carrier frequency offset, CP transmission not required, improving energy and spectral efficiency of the system, and compatibility with previous standards. Besides, the implementation of the FC-TRMRC at the BS hardware can be highly parallelized.

V. OPTIMIZING SYSTEM PARAMETERS

In this Section, we fix the long-term fading coefficients of the users in the derived expressions of Sec. III, for mathematical tractability. Then, based on the simplified expressions for the sum rate of a given cell, some interesting analysis are conducted, as determining the optimal number of users to be served by each cell. Our analysis gives some insights about the dependence of this optimal number with the variation of system parameters, like number of antennas and transmit power. Furthermore, we try to find the best resources' reuse scheme between pilot reuse and frequency reuse to be employed in the investigated maMIMO systems. A total number of $C = 19$ hexagonal cells is adopted in this Section in order to allow the use of resources' reuse policies.

From equations (14) and (22), one can note that the same uplink SINR can be achieved by both TRMRC and FDMRC, except by the uplink transmission power, that is decreased by the factor γ in the OFDM context. Thus, we define the parameter ρ_{u}', which equals $\gamma\rho_{\mathrm{u}}$ for OFDM, and ρ_{u} for SC. We now fix the long-term fading coefficients of the users in the home cell as β_h and of the users in the adjacent cells as β_a, β_b, and β_c, according to the distance between the centers of each user cell and home cell. When fixing these parameters, the idea is to adopt an average case for every coefficient to be fixed. By symmetry, one can note that there are 3 different distances to be considered for the neighboring cells, and a total of $C' = 6$ cells fall in each group. Thus we have adopted: $\beta_h = (d/2)^{-\lambda}$, $\beta_a = (\sqrt{3}d)^{-\lambda}$, $\beta_b = (3\ d)^{-\lambda}$, and $\beta_c = (2\sqrt{3}d)^{-\lambda}$. The distribution of the C hexagonal cells is depicted in Figure 7, as well as the different fixed long-term fading coefficients according to the distance between the home cell and adjacent cells. The grey scale of a given cell in the Figure increases according to its distance to the home cell.

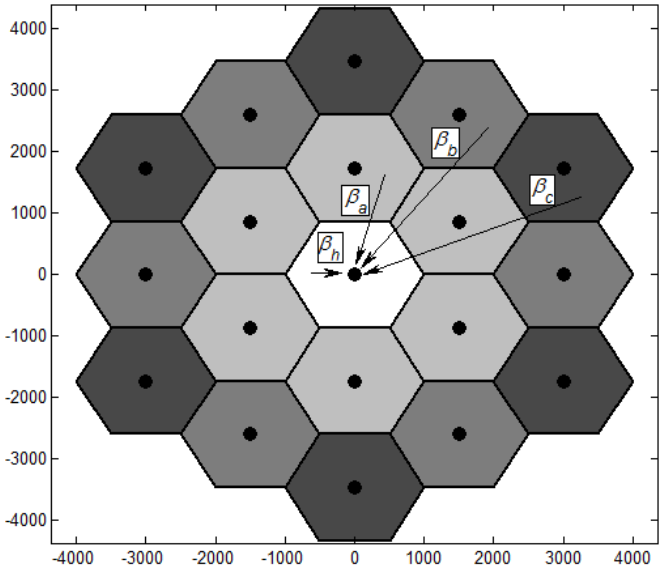

FIGURE 7. Spatial distribution for the $C = 19$ hexagonal cells.

Three major schemes are investigated in this Section: the maMIMO system with universal reuse of frequency and pilots, with pilot reuse factor of 3, and with frequency reuse factor of 3. Thus, the SINR performance of each user and the uplink sum rate of a given cell can be approximated, in an unified way, as

$$\varsigma^{(\mathrm{sc})} = \frac{M\beta_h^2}{MC'\Gamma_1^{(\mathrm{sc})} + \left(K\Gamma_2^{(\mathrm{sc})} + \frac{\sigma_n^2}{\rho_{\mathrm{u}}'}\right)\left(\Gamma_3^{(\mathrm{sc})} + \frac{\sigma_n^2}{\rho_{\mathrm{p}}}\right)}, \quad (26)$$

$$\overline{\mathcal{R}}^{(\mathrm{sc})} = K\xi^{\mathrm{u}}\frac{1}{\zeta^{\mathrm{f}}}\left(1 - \frac{\zeta^{\mathrm{p}}K}{\mathcal{S}}\right)\log_2\left(1 + \varsigma^{(\mathrm{sc})}\right), \quad (27)$$

in which the constants $\Gamma_1^{(\mathrm{sc})}$, $\Gamma_2^{(\mathrm{sc})}$, and $\Gamma_3^{(\mathrm{sc})}$ assume different values according to the investigated scheme, as summarized

TABLE 3. Constants in (26) and (27) for the investigated schemes.

Scheme	Constants
Universal Reuse (ζ^{f}=1, ζ^{p}=1)	$\Gamma_1^{(\mathrm{ur})} = \beta_a^2 + \beta_b^2 + \beta_c^2$
	$\Gamma_2^{(\mathrm{ur})} = \beta_h + C'(\beta_a + \beta_b + \beta_c)$
	$\Gamma_3^{(\mathrm{ur})} = \beta_h + C'(\beta_a + \beta_b + \beta_c)$
Frequency Reuse (ζ^{f}=3, ζ^{p}=1)	$\Gamma_1^{(\mathrm{fr})} = \beta_b^2$
	$\Gamma_2^{(\mathrm{fr})} = \beta_h + C'\beta_b$
	$\Gamma_3^{(\mathrm{fr})} = \beta_h + C'\beta_b$
Pilot Reuse (ζ^{f}=1, ζ^{p}=3)	$\Gamma_1^{(\mathrm{pr})} = \beta_b^2$
	$\Gamma_2^{(\mathrm{pr})} = \beta_h + C'(\beta_a + \beta_b + \beta_c)$
	$\Gamma_3^{(\mathrm{pr})} = \beta_h + C'\beta_b$

in Table 3. Besides, ζ^{f} is the frequency reuse factor, while ζ^{p} is the pilot reuse factor. When employing non-universal pilot reuse, while non-coherent interference reaches the home BS from every user of the system, the pilot contamination interference reaches the cell only from users of cells sharing the same pilots' set, which are distributed according to the maximum relative distance criterion. Thus, we have that $\Gamma_2^{(\mathrm{pr})} \neq \Gamma_3^{(\mathrm{pr})}$, as can be seen in the Table.

Our first objective is to determine the optimal number of users K^* that maximizes (27). For $M \to \infty$, as discussed in [11] for OFDM maMIMO systems, it is not difficult to see that K^* is the closest integer to $\mathcal{S}/(2\zeta^{\mathrm{p}})$. This occurs since the asymptotic uplink SINR $\varsigma^{(\mathrm{sc})} = \frac{\beta_h^2}{C'\Gamma_1^{(\mathrm{sc})}}$ is independent of K, while the concave pre-log factor is maximized by $K = \frac{\mathcal{S}}{2\zeta^{\mathrm{p}}}$. In order to obtain a procedure to find the optimal number of scheduled users for any parameters' set, like number of antennas, transmit SNR, and pilot SNR, we aim to find the maximum of (27). Thus, we take the derivative of $\overline{\mathcal{R}}^{(\mathrm{sc})}$ with respect to K as in (28), as shown at the bottom of this page.

Unfortunately, we do not arrive in a closed form expression for K^* when trying to find the argument that cancels the derivative in (28). Thus, we propose an iterative procedure to find K^* based on the Newton's method. By initializing $K^{(0)} = \frac{\mathcal{S}}{2\zeta^{\mathrm{p}}}$, the iterative procedure is evaluated as

$$K^{(t+1)} = K^{(t)} - \frac{\left.\frac{\partial \overline{\mathcal{R}}^{(\mathrm{sc})}}{\partial K}\right|_{K=K^{(t)}}}{\left.\frac{\partial^2 \overline{\mathcal{R}}^{(\mathrm{sc})}}{\partial K^2}\right|_{K=K^{(t)}}}, \tag{29}$$

in which $\frac{\partial^2 \overline{\mathcal{R}}^{(\mathrm{sc})}}{\partial K^2}$ is given in (30), as shown at the bottom of this page. In our numerical simulations, 4 iterations were sufficient to the algorithm's convergence.

Figure 8 shows the sum rate variation with the increasing number of scheduled users as well as the number of users to be scheduled given by our proposed method (denoted by the markers in the Figure), considering a system with universal reuse, with frequency reuse factor of 3, or with a pilot reuse factor of 3. Several conclusions can be made from the Figure. First, our proposed method indeed finds the number of users that maximizes the sum rate of the cell, for the three investigated system configurations. Besides, the optimal number of scheduled users does not change if the system employs TRMRC or FDMRC, since the difference between such techniques from the SINR performance perspective is just an SNR reduction of γ. For the adopted parameters $N = 256$ and $L = 16$, $\gamma = 0.941$, which represents an SNR

$$\frac{\partial \overline{\mathcal{R}}^{(\mathrm{sc})}}{\partial K} = \xi^{\mathrm{u}} \frac{1}{\zeta^{\mathrm{f}}} \left(\frac{\mathcal{S} - 2\zeta^{\mathrm{p}} K}{\mathcal{S}}\right) \log_2 \left(\frac{MC'\Gamma_1^{(\mathrm{sc})} + \left(K\,\Gamma_2^{(\mathrm{sc})} + \frac{\sigma_n^2}{\rho_{\mathrm{u}}'}\right)\left(\Gamma_3^{(\mathrm{sc})} + \frac{\sigma_n^2}{\rho_{\mathrm{p}}}\right) + M\beta_h^2}{MC'\Gamma_1^{(\mathrm{sc})} + \left(K\,\Gamma_2^{(\mathrm{sc})} + \frac{\sigma_n^2}{\rho_{\mathrm{u}}'}\right)\left(\Gamma_3^{(\mathrm{sc})} + \frac{\sigma_n^2}{\rho_{\mathrm{p}}}\right)}\right) - \xi^{\mathrm{u}} \frac{1}{\zeta^{\mathrm{f}}} \left(\frac{\mathcal{S}K - \zeta^{\mathrm{p}} K^2}{\mathcal{S}}\right)$$
$$\times \frac{M\beta_h^2 \Gamma_2^{(\mathrm{sc})} \left(\Gamma_3^{(\mathrm{sc})} + \frac{\sigma_n^2}{\rho_{\mathrm{p}}}\right)}{\log(2)\left[M\beta_h^2 + MC'\Gamma_1^{(\mathrm{sc})} + \left(K\,\Gamma_2^{(\mathrm{sc})} + \frac{\sigma_n^2}{\rho_{\mathrm{u}}'}\right)\left(\Gamma_3^{(\mathrm{sc})} + \frac{\sigma_n^2}{\rho_{\mathrm{p}}}\right)\right]\left[MC'\Gamma_1^{(\mathrm{sc})} + \left(K\,\Gamma_2^{(\mathrm{sc})} + \frac{\sigma_n^2}{\rho_{\mathrm{u}}'}\right)\left(\Gamma_3^{(\mathrm{sc})} + \frac{\sigma_n^2}{\rho_{\mathrm{p}}}\right)\right]} \tag{28}$$

$$\frac{\partial^2 \overline{\mathcal{R}}^{(\mathrm{sc})}}{\partial K^2} = \xi^{\mathrm{u}} \frac{1}{\zeta^{\mathrm{f}}} \left(\frac{-2\zeta^{\mathrm{p}}}{\mathcal{S}}\right) \log_2 \left(\frac{MC'\Gamma_1^{(\mathrm{sc})} + \left(K\,\Gamma_2^{(\mathrm{sc})} + \frac{\sigma_n^2}{\rho_{\mathrm{u}}'}\right)\left(\Gamma_3^{(\mathrm{sc})} + \frac{\sigma_n^2}{\rho_{\mathrm{p}}}\right) + M\beta_h^2}{MC'\Gamma_1^{(\mathrm{sc})} + \left(K\,\Gamma_2^{(\mathrm{sc})} + \frac{\sigma_n^2}{\rho_{\mathrm{u}}'}\right)\left(\Gamma_3^{(\mathrm{sc})} + \frac{\sigma_n^2}{\rho_{\mathrm{p}}}\right)}\right) - \xi^{\mathrm{u}} \frac{1}{\zeta^{\mathrm{f}}} \left(\frac{\mathcal{S} - 2\zeta^{\mathrm{p}} K}{\mathcal{S}}\right)$$
$$\times \frac{2\,M\beta_h^2 \Gamma_2^{(\mathrm{sc})} \left(\Gamma_3^{(\mathrm{sc})} + \frac{\sigma_n^2}{\rho_{\mathrm{p}}}\right)}{\log(2)\left[M\beta_h^2 + MC'\Gamma_1^{(\mathrm{sc})} + \left(K\,\Gamma_2^{(\mathrm{sc})} + \frac{\sigma_n^2}{\rho_{\mathrm{u}}'}\right)\left(\Gamma_3^{(\mathrm{sc})} + \frac{\sigma_n^2}{\rho_{\mathrm{p}}}\right)\right]\left[MC'\Gamma_1^{(\mathrm{sc})} + \left(K\,\Gamma_2^{(\mathrm{sc})} + \frac{\sigma_n^2}{\rho_{\mathrm{u}}'}\right)\left(\Gamma_3^{(\mathrm{sc})} + \frac{\sigma_n^2}{\rho_{\mathrm{p}}}\right)\right]}$$
$$+ \xi^{\mathrm{u}} \frac{1}{\zeta^{\mathrm{f}}} \left(\frac{\mathcal{S}K - \zeta^{\mathrm{p}} K^2}{\mathcal{S}}\right)$$
$$\times \frac{M\beta_h^2 \left(\Gamma_2^{(\mathrm{sc})}\right)^2 \left(\Gamma_3^{(\mathrm{sc})} + \frac{\sigma_n^2}{\rho_{\mathrm{p}}}\right)^2 \left[M\beta_h^2 + 2MC'\Gamma_1^{(\mathrm{sc})} + 2\left(K\,\Gamma_2^{(\mathrm{sc})} + \frac{\sigma_n^2}{\rho_{\mathrm{u}}'}\right)\left(\Gamma_3^{(\mathrm{sc})} + \frac{\sigma_n^2}{\rho_{\mathrm{p}}}\right)\right]}{\log(2)\left[M\beta_h^2 + MC'\Gamma_1^{(\mathrm{sc})} + \left(K\,\Gamma_2^{(\mathrm{sc})} + \frac{\sigma_n^2}{\rho_{\mathrm{u}}'}\right)\left(\Gamma_3^{(\mathrm{sc})} + \frac{\sigma_n^2}{\rho_{\mathrm{p}}}\right)\right]^2 \left[MC'\Gamma_1^{(\mathrm{sc})} + \left(K\,\Gamma_2^{(\mathrm{sc})} + \frac{\sigma_n^2}{\rho_{\mathrm{u}}'}\right)\left(\Gamma_3^{(\mathrm{sc})} + \frac{\sigma_n^2}{\rho_{\mathrm{p}}}\right)\right]^2} \tag{30}$$

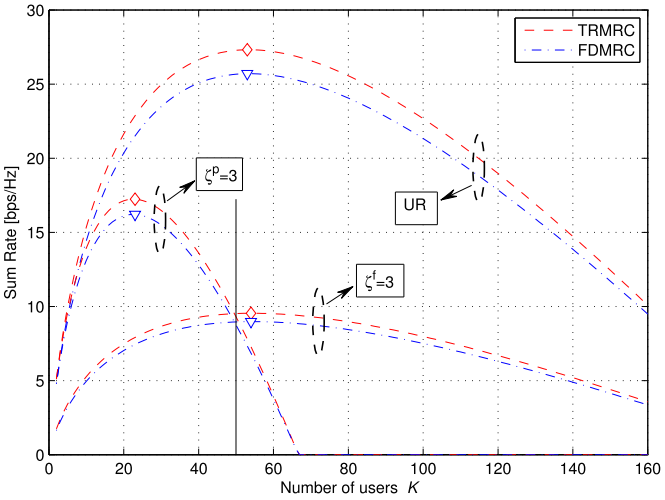

FIGURE 8. Sum Rate with increasing K for $M = 100$ and $\mathcal{S} = 200$.

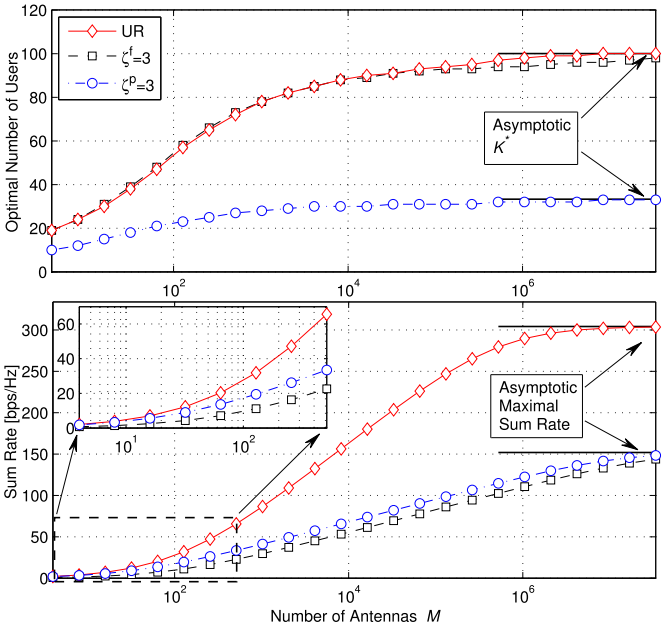

FIGURE 9. K^* and sum rate with increasing M for $\mathcal{S} = 200$.

decrease of 0.263dB when employing OFDM instead of SC. As shown later in this paper (Figure 10), the dependence of K^* with the data SNR variation is much less sensitive than this. The Figure shows that universal reuse is always better than pilot or frequency reuse from the sum rate point of view, irrespective of the number of scheduled users. However, this is not a completely affordable conclusion, since the fixed long-term fading simplification assumption may hide the performance loss due to unfavorable users spatial distribution, which is much more severe for universal reuse than for higher reuse factors. Besides, it is well known from [3], [14] that higher reuse factors are much more advantageous in terms of fairness, which is another fact not represented in the Figure. A more interesting conclusion can be made if one compare the performances achieved by frequency reuse and pilot reuse, since both schemes are able to improve the system fairness. It can be seen that pilot reuse can achieve a higher sum rate than frequency reuse, although the opposite can be seen for specific values of K. We have plotted a vertical line in $K = \mathcal{S}/4$ for reference purposes, that is the point at which the pre-log factors intersect for these schemes. One can see that the performance crossover point is very near this value, in such a way that the SINR gain of frequency reuse in comparison with pilot reuse is negligible, and unable to overcome the penalty of reducing bandwidth. Therefore, when the objective is to improve the network fairness, the best approach is to employ pilot reuse if it is allowed to schedule a number of users lower than $\mathcal{S}/4$. Otherwise, frequency reuse becomes a better alternative.

The dependence of the optimal number of users and the optimal sum rate with the increasing number of antennas is shown in Figure 9. One can note that the optimal number of scheduled users converges with $M \to \infty$ to $\mathcal{S}/(2\zeta^p)$, as discussed in [11]. On the other hand, an interesting conclusion that has not been drawn is that both resources' reuse schemes have the same asymptotic performance. This can be verified by analysing the asymptotic sum rate of a cell in (31), remembering from Table 3 that $\Gamma_1^{(fr)} = \Gamma_1^{(pr)}$. However this equivalence holds only for unpractical values of M, while pilot reuse presents an improved performance in comparison with frequency reuse for a not so large number of antennas.

$$\lim_{M\to\infty} \overline{\mathcal{R}}^{(sc)} = \xi^u \frac{\mathcal{S}}{4\zeta^f\zeta^p} \log_2\left(1 + \frac{\beta_h^2}{C'\Gamma_1^{(sc)}}\right). \quad (31)$$

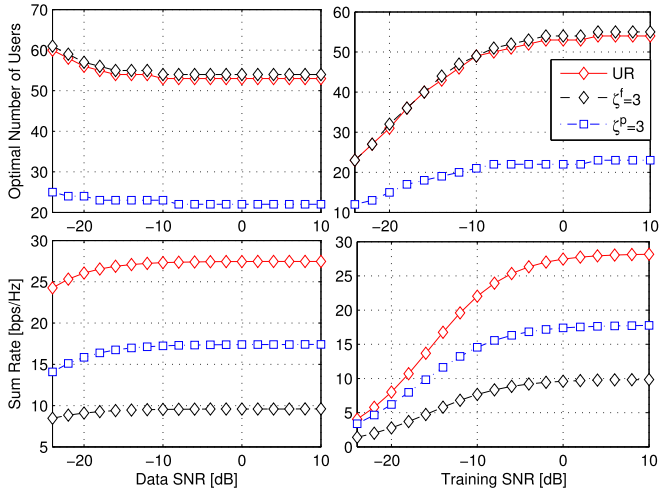

FIGURE 10. K^* and sum rate with increasing data and training SNR for $\mathcal{S} = 200$.

Figure 10 shows how the increasing SNR affects the optimal number of scheduled users and sum rate performance. In the left hand side, it is investigated the increasing data SNR with the training SNR fixed as 0dB, while in the right hand side the increasing training SNR is considered with data SNR fixed as 0 dB. Although any SNR increase has the effect of improving the system sum rate performance,

the optimal number of users in each case have opposite behaviors. While K^* decreases with increasing $\frac{\rho'_u}{\sigma_n^2}$, it increases with increasing $\frac{\rho_p}{\sigma_n^2}$. Besides, the variation of K^* and of sum rate with increasing training SNR is more notorious. This occurs since the increase of $\frac{\rho_p}{\sigma_n^2}$ leads to better CSI estimates, which in turn improves the interference mitigation capacity of the MRC receiver, allowing the scheduling of a higher number of users in order to obtain the optimal sum rate performance. On the other hand, the increasing $\frac{\rho'_u}{\sigma_n^2}$ results in a higher level of multiuser interference, both intra-cell and inter-cell, in such a way that the best sum rate performance is found with a slightly reduced number of users.

VI. CONCLUSION

In this work, we have analysed the performance of maMIMO systems under frequency-selective channels subject to pilot contamination. Two fundamental schemes have been investigated and compared: the conventional FDMRC operating under OFDM transmission, and the TRMRC under single-carrier transmission. We have proposed tight analytical expressions for the SINR performance, as well as lower bounds for the achievable rates, which have been shown by computer simulations to be suitably tight. In general, TRMRC outperforms FDMRC by not requiring CP transmission, which improves spectral and energy efficiencies. Our computational complexity study revealed that TRMRC complexity results $\mathcal{O}(LMK)$, in contrast with the $\mathcal{O}(MK)$ complexity of FDMRC. Thus, we proposed a low complexity implementation of TRMRC by employing the fast convolution with overlap-and-add technique, which was able to achieve the same TRMRC result with a complexity of $\mathcal{O}(\log_2(2L)MK)$. Then, based on slight simplifications on our derived expressions, we developed a method for obtaining the optimal number of users to be served by each cell, in the sense of maximizing sum rate, for any maMIMO configuration and under different frequency or pilot reuse schemes. We have investigated how this optimal number of users is dependent of different system parameters, and several insights were given, as well as a performance comparison between frequency and pilot reuse. Given the several benefits of SC waveform as well as the reduced complexity implementation of TRMRC receiver proposed in this paper, which becomes not so high when compared with FDMRC complexity, the TRMRC under SC constitutes a promising candidate for receiver/waveform of next generation communication systems.

REFERENCES

[1] H. Q. Ngo, E. G. Larsson, and T. L. Marzetta, "Energy and spectral efficiency of very large multiuser MIMO systems," *IEEE Trans. Commun.*, vol. 61, no. 4, pp. 1436–1449, Apr. 2013.
[2] L. Lu, G. Y. Li, A. L. Swindlehurst, A. Ashikhmin, and R. Zhang, "An overview of massive MIMO: Benefits and challenges," *IEEE J. Sel. Topics Signal Process.*, vol. 8, no. 5, pp. 742–758, Oct. 2014.
[3] T. Marzetta, "Noncooperative cellular wireless with unlimited numbers of base station antennas," *IEEE Trans. Wireless Commun.*, vol. 9, no. 11, pp. 3590–3600, Nov. 2010.
[4] T. Marzetta, E. Larsson, H. Yang, and H. Ngo, *Fundamentals Massive MIMO*, 1st ed. New York, NY, USA: Cambridge Univ. Press, 2016.
[5] D. Falconer, S. L. Ariyavisitakul, A. Benyamin-Seeyar, and B. Eidson, "Frequency domain equalization for single-carrier broadband wireless systems," *IEEE Commun. Mag.*, vol. 40, no. 4, pp. 58–66, Apr. 2002.
[6] N. Benvenuto and S. Tomasin, "On the comparison between OFDM and single carrier modulation with a DFE using a frequency-domain feedforward filter," *IEEE Trans. Commun.*, vol. 50, no. 6, pp. 947–955, Jun. 2002.
[7] A. Pitarokoilis, S. K. Mohammed, and E. G. Larsson, "Uplink performance of time-reversal MRC in massive MIMO systems subject to phase noise," *IEEE Trans. Wireless Commun.*, vol. 14, no. 2, pp. 711–723, Feb. 2015.
[8] A. Pitarokoilis, S. K. Mohammed, and E. G. Larsson, "On the optimality of single-carrier transmission in large-scale antenna systems," *IEEE Wireless Commun. Lett.*, vol. 1, no. 4, pp. 276–279, Aug. 2012.
[9] Y. Sheng, Z. Tan, and G. Y. Li, "Single-carrier modulation with ML equalization for large-scale antenna systems over rician fading channels," in *Proc. IEEE Int. Conf. Acoust., Speech Signal Process. (ICASSP)*, May 2014, pp. 5759–5763.
[10] C. Mollén, E. G. Larsson, and T. Eriksson, "Waveforms for the massive MIMO downlink: Amplifier efficiency, distortion, and performance," *IEEE Trans. Commun.*, vol. 64, no. 12, pp. 5050–5063, Dec. 2016.
[11] E. Björnson, E. G. Larsson, and M. Debbah, "Massive MIMO for maximal spectral efficiency: How many users and pilots should be allocated?" *IEEE Trans. Wireless Commun.*, vol. 15, no. 2, pp. 1293–1308, Feb. 2016.
[12] P. Diniz, E. da Silva, and S. Netto, *Digital Signal Processing: System Analysis and Design*, 2nd ed. New York, NY, USA: Cambridge Univ. Press, 2010.
[13] Y. Xin, D. Wang, J. Li, H. Zhu, J. Wang, and X. You, "Area spectral efficiency and area energy efficiency of massive MIMO cellular systems," *IEEE Trans. Veh. Technol.*, vol. 65, no. 5, pp. 3243–3254, May 2016.
[14] J. C. Marinello and T. Abrão, "Pilot distribution optimization in multicellular large scale MIMO systems," *AEU-Int. J. Electron. Commun.*, vol. 70, no. 8, pp. 1094–1103, Aug. 2016.
[15] G. H. Golub and C. F. V. Loan, *Matrix Computations*. Baltimore, MD, USA: The Johns Hopkins Univ. Press, 1996.

JOSÉ CARLOS MARINELLO FILHO received the B.S. (*summa cum laude*) and M.S. (*summa cum laude*) degrees in electrical engineering from Londrina State University, Brazil, in 2012 and 2014, respectively. He is currently pursuing the Ph.D. degree with the Polytechnic School, Sao Paulo University, São Paulo, Brazil. His research interests include signal processing and wireless communications, especially massive multiple-antenna precoding/decoding techniques, acquisition of channel-state information, multicarrier modulation, cross-layer optimization of MIMO/OFDM systems, interference management, and 5G.

CRISTIANO PANAZIO received the engineer's and master's degrees in electrical engineering from the State University of Campinas in 1999 and 2001, respectively, and the Ph.D. degree in telecommunications from the Conservatoire National des Arts et Métiers in 2005. He is currently an Assistant Professor with the Laboratory of Communications and Signals, Escola Politécnica, University of São Paulo. His research interests are adaptive equalization (data aided and blind), synchronization techniques, mobile communications, multicarrier modulation, spread spectrum techniques, and space-time receivers.

TAUFIK ABRÃO (M'97–SM'12) received the B.S., M.Sc., and Ph.D. degrees in electrical engineering from the Polytechnic School, University of São Paulo, São Paulo, Brazil, in 1992, 1996, and 2001, respectively. From 2007 to 2008, he was a Post-Doctoral Researcher with the Department of Signal Theory and Communications, Polytechnic University of Catalonia, Barcelona, Spain. In 2012, he was an Academic Visitor with the Southampton Wireless Research Group, University of Southampton, Southampton, U.K. Since 1997, he has been with the Communications Group, Department of Electrical Engineering, Londrina State University, Paraná, Brazil, where he is currently an Associate Professor in telecommunications and the Head of the Telecommunication and Signal Processing Laboratory. He has participated in several projects funded by government agencies and industrial companies. He has supervised 22 M.Sc. and four Ph.D. students, and two postdocs. He has co-authored nine book chapters on mobile radio communications and over 180 research papers published in specialized/international journals and conferences. His current research interests include communications and signal processing, specially the multi-user detection and estimation, MC-CDMA and MIMO systems, cooperative communication and relaying, resource allocation, and heuristic and convex optimization aspects of 3G and 4G wireless systems. He is a member of SBrT. He is involved in editorial board activities of six journals in the telecommunications area and has served as a TPC Member in several symposiums and conferences. He has been serving as an Editor of the IEEE Communications Surveys and Tutorials since 2013, the IEEE Access since 2016, and the *IET Journal of Engineering* since 2014.

APPENDIX C – Full paper published in the journal "*Emerging Telecommunications Technologies (ETT)*"

Title: Joint uplink and downlink optimization of pilot assignment for massive MIMO with power control.

Authors: José Carlos Marinello Filho, Cristiano Panazio and Taufik Abrão.

Journal: Emerging Telecommunications Technologies (ETT) (ISSN 2161-3915). Volume 28, Issue 12,

Classification (Qualis-CAPES): A2 / IF$= 1.535$ (Engenharias IV).

Publication Date: December 2017.

Received: 28 April 2017 | Revised: 4 August 2017 | Accepted: 22 August 2017

DOI: 10.1002/ett.3250

RESEARCH ARTICLE

WILEY

Joint uplink and downlink optimization of pilot assignment for massive MIMO with power control

José Carlos Marinello Filho[1] | Cristiano Magalhães Panazio[2] | Taufik Abrão[1]

[1]Department of Electrical Engineering, State University of Londrina, Londrina-PR, Brazil

[2]Laboratory of Communications and Signals, Polytechnic School of the University of São Paulo, São Paulo-SP, Brazil

Correspondence
Taufik Abrão, Department of Electrical Engineering, State University of Londrina, Londrina-PR 86057-970, Brazil.
Email: taufik@uel.br

Funding information
National Council for Scientific and Technological Development (CNPq) of Brazil, Grant/Award Number: 304066/2015-0 and 404079/2016-4; Londrina State University, Paraná State Government (UEL)

Abstract

In this paper, we investigate the effects of pilot assignment (PA) in multicell massive multiple-input–multiple-output systems. When deploying linear detection/precoding algorithms and a large number of antennas at base station (BS), it is well-known that system performance in both uplink (UL) and downlink (DL) is mainly restricted by pilot contamination. Such interference is proper of each pilot sequence, and thus, system performance can be improved by suitably assigning the pilots to the users within a given cell, according to a certain desired metric. We show in this paper that UL and DL performances constitute conflicting metrics, since it is not possible to achieve the best performance in UL and DL concomitantly. Thus, we propose an alternative metric, namely, total capacity, aiming to simultaneously achieve a suitable performance in both directions, ie, UL and DL. Since the PA problem is combinatorial, and the search space grows with the number of pilots in a factorial fashion, we also propose a low-complexity suboptimal algorithm that achieves promising capacity performance avoiding the exhaustive search. In addition, to fully benefit from the large excess of BS antennas, we combine our proposed PA schemes with an efficient power control algorithm, unveiling the great potential of the proposed schemes to provide improved performance for more users, even with a not-so-large number of BS antennas. In a limit condition, for example, our numerical results demonstrate that with 64 BS antennas serving 10 users, our proposed method can assure a 95% likely rate of 4.2 Mbps for both DL and UL, and a symmetric 95% likely rate of 1.4 Mbps when serving 32 users. If a higher number of antennas is allowed at BS, the guaranteed rates can be significantly higher.

1 | INTRODUCTION

Pilot contamination is the most salient impairment of massive multiple-input–multiple-output (Ma-MIMO) systems.[1,2] Due to this issue, it can be shown that the interference seen by each user is dependent on the pilot sequence he is using. Thus, one can improve system performance by suitably assigning the pilots to the users in the cell, as discussed in the works of Zhu et al[3] and Marinello and Abrão.[4] The pilot assignment (PA) problem was solved in the work of Zhu et al[3] from the uplink (UL) perspective, and a low-complexity near-optimal solution was proposed. Such simple and very efficient solution was possible due to the simple dependence between performance and the PA seen in UL. Pilot contamination interference in UL is due to the signals transmitted from users in adjacent cells sharing a given pilot sequence that reaches

certain base station (BS). The user that will experience such interference is the one to which this pilot sequence is assigned in the cell. Under a max-min optimization perspective, the solution proposed in the work of Zhu et al[3] simply assigns the worst pilot sequences in a given instant, in terms of pilot contamination arising from adjacent cells, to the best located users, ie, those with the higher long-term fading coefficients. Other techniques have also been proposed to optimize the UL of Ma-MIMO systems, like the graph coloring–based PA in the work of Zhu et al,[5] which consists in drawing a graph with the users as vertexes, and coloring this graph such that no adjacent vertexes are colored with the same color. As each color represents a pilot, some additional constraints must be satisfied like the same color cannot color 2 or more vertexes in a same cell, and a limited number of colors equal to the number of users are available per cell. A similar technique has also been proposed in the work of Xu et al[6] in the context of device to device underlay Ma-MIMO systems. However, as the technique in the work of Zhu et al[3] achieved a better performance with reduced complexity, we adopted it as benchmarking for UL performance.

In the work of Marinello and Abrão,[4] the PA problem was investigated from the downlink (DL) perspective, under several metrics. However, as the dependence of DL signal-to-interference-plus-noise ratio (SINR) with the PA occurs in a more complex way than in UL, the problem was solved only via exhaustive search. Different than UL, pilot contamination interference in DL is due to the signals transmitted from neighboring BS's to the users at their respective cells sharing certain pilot sequence, but that inadvertently reaches the user in the considered cell using this pilot. If this user changes its pilot sequence, part of the pilot contamination reaching him/her remains unchanged, since the distance between the user and adjacent cells and the long-term fading coefficients remain the same. The part of interference that changes is due to the power normalization factors, which retain some dependence with the UL pilot transmission stage, as better clarified in this manuscript, which also proposes low-complexity DL PA schemes.

A greedy PA scheme is proposed for optimizing the DL performance of the cell-free Ma-MIMO systems in the work of Ngo et al.[7] This new concept of Ma-MIMO system comprises a very large number of distributed single-antenna access points simultaneously serving a much smaller number of users. Although having considerably improved performance with respect to conventional collocated Ma-MIMO systems due to the diversity of long-term fading coefficients, the system implementation cost is significantly higher due to the complex backhaul network and the very large number of access points to be installed. In addition, the proposed PA scheme aims to improve just the DL performance. As shown in this paper, UL and DL optimization metrics constitute conflicting objectives, since if one scheme optimizes system DL performance, the UL performance will be close to that attained with random assignment, and vice versa. Thus, our main purpose in this paper is to design a PA methodology able to jointly optimize DL and UL perspectives.

Several PA schemes have been proposed recently based on the location-aware approach.[8,9] Authors have proposed some filtering techniques, which are able to significantly remove pilot contamination from channel estimates if the training signals transmitted from users of different cells sharing a given pilot reach the considered BS with different angle-of-arrivals. For this sake, the location-aware PA technique assigns the pilots for users in the considered cell aiming to ensure that users utilizing the same pilot have distinguishable angle-of-arrivals. However, all these schemes rely on the existence assumption of a line-of-sight component between BS and users, and of small channel angle spread of the multipath components observed at the BS, typically observed in rural and suburban areas, or if the BS is much higher than the surrounded structures with few scatters around.[9] Since this is not always the case, we investigate in this paper, PA schemes to be deployed in less restrictive scenarios.

Power allocation is another efficient way of improving the performance of wireless communication networks. For the multicell massive MIMO scenario, the problem of power allocation was investigated in the work of Zhang et al[10] under the perspective of maximizing the sum rate per cell. It was shown that the proposed method achieves substantial gains over the equal power allocation policy. However, for a practical system, maximizing the sum rate per cell is not the most suitable objective, since the performance of some users (typically those at the edge) may be severely penalized to provide very increased rates for others. On the other hand, in the work of Björnson et al,[11] a power allocation technique able to provide the same performance for all served users in DL and UL is proposed. The UL power allocation policy allocates for each user a power proportional to a desired received signal-to-noise ratio (SNR) at the BS divided by its long-term fading coefficient. Since shadowing has not been assumed in that work, one has just to ensure that the desired SNR level allows the cell boundary user to transmit without exceeding the maximum transmit power of its device. Clearly, in a more realistic scenario, a severely shadowed user near the cell edge may not be able to transmit with such power. A fairer optimization metric is adopted by the power control algorithm proposed in the work of Rasti and Sharafat[12] for a code-division multiple access network, which consists of providing a target performance for the majority of the users in the network. Since such approach is very suitable in the context of Ma-MIMO systems, we have adopted this distributed power control algorithm herein.

In this paper, we address the PA problem from joint UL and DL perspectives. Since the performance bottleneck of Ma-MIMO systems is due to the edge users suffering with severe pilot contamination,[1] we consider the objective of providing a target performance for the majority of the users. For this sake, the pilot allocation metric of maximizing the minimum SINR is the most suitable, and our proposed scheme amalgamates such metric with the power control algorithm in the work of Rasti and Sharafat,[12] by only knowing the power and the long-term fading coefficients of users in adjacent cells. We first propose a low-complexity suboptimal solution of the MaxminSINR DL PA problem in the work of in the work of Marinello and Abrão.[4] Then, we show that the optimization under DL and UL perspectives are conflicting, since the optimal performance in both directions cannot be simultaneously achieved with any pilot configuration. We thus propose an alternative PA procedure from the definition of the overall system capacity, as the sum of DL and UL capacities. Our numerical results demonstrate that, under this metric, significant gains can be achieved in DL and UL concomitantly. In addition, a low-complexity suboptimal approach for solving the joint UL-DL PA problem is discussed. Finally, we adapt the power control algorithm in the work of Rasti and Sharafat[12] to the Ma-MIMO scenario with a finite number of BS antennas and show that much more significant gains can be attained by the PA schemes when combined with an efficient power control algorithm. Different than the work of Zhu et al,[3] which proposed a PA technique that optimizes only the UL, and than the work of Marinello and Abrão,[4] which proposed a PA technique that optimizes only DL, our proposed PA metric is able to provide an improved performance for UL and DL at the same time. This is particularly interesting since the entire communication process occurs in practice with a single pilot distribution, and UL and DL PA metrics are conflicting, as we demonstrate in this paper. In addition, we also propose a low-complexity near-optimal algorithm for avoiding the exhaustive search and combine the PA techniques with the power control algorithm in the work of Rasti and Sharafat[12] adapted to a Ma-MIMO scenario. Our analysis assumes the BS using simpler schemes for detection and precoding: maximum ratio combining (MRC) and maximum ratio transmission (MRT), respectively. Although not optimal in the presence of multiuser interference, these techniques are extensively adopted in massive MIMO literature due to its reduced complexity, simplified implementation, and improved energy efficiency achieved.[13-15]

The rest of this paper is organized as follows. The system model is described in Section 2, whereas the proposed PA optimization schemes are discussed in Section 3. The adopted power control algorithm are described in Section 4. Illustrative numerical results are explored in Section 5. Final remarks and conclusions are offered in Section 6.

2 | SYSTEM MODEL

We consider a similar system model in the works of Zhu et al[3] and Marinello and Abrão,[4] which is composed of L hexagonal cells, each one equipped with N antennas BS serving K single-antenna users. Time-division duplex (TDD) is assumed, thus reciprocity holds, and channel state information (CSI) is acquired by UL training sequences transmission. The $N \times 1$ channel vector between the BS of the ith cell and the k'th user of the jth cell is denoted by $\mathbf{g}_{ik'j} = \sqrt{\beta_{ik'j}}\mathbf{h}_{ik'j}$, in which $\beta_{ik'j}$ denotes the long-term fading coefficient, comprising path loss and log-normal shadowing, $\mathbf{h}_{ik'j} \sim \mathcal{CN}(\mathbf{0}_N, \mathbf{I}_N)$ is the short-term fading channel vector, whereas $\mathbf{0}_N$ is a null column vector of size $N \times 1$, and $\mathbf{I}_N$ is the identity matrix of size N. Under this model, the short-term fading models the random fluctuations of the signal received due to the superposition of several unsolvable wavefronts coming from different paths, but with similar delays. On the other hand, shadow fading models the random variation of the received signal power due to blockage from objects in the signal path that attenuate signal power through absorption, reflection, scattering, and diffraction. Moreover, the deterministic path-loss model should be able to describe and quantify the dissipation of the power radiated by the transmitter toward the receiver and by the effects of the propagation channel.[16] Figure 1 exemplifies our considered scenario considering $L = 7$ cells, and $K = 2$ users.

The pilot sequences' set is $\mathbf{\Psi} = [\boldsymbol{\psi}_1 \ \ \boldsymbol{\psi}_2 \ \ \dots \ \ \boldsymbol{\psi}_K] \in \mathbb{C}^{K \times K}$, and the sequence length is also K. This set of sequences is orthogonal, and thus, $\mathbf{\Psi}^H\mathbf{\Psi} = \mathbf{I}_K$ holds, being $\{\cdot\}^H$ the Hermitian operator. If it is assigned for the k'th user, the sequence $\boldsymbol{\psi}_{k'} = [\psi_{k'1} \ \ \psi_{k'2} \dots \psi_{k'K}]^T$, being $\{\cdot\}^T$ the transpose operator, the received signal at the ith BS during the training stage is

$$\mathbf{Y}_i^{\mathrm{p}} = \sqrt{\rho^{\mathrm{p}}} \sum_{j=1}^{L} \sum_{k=1}^{K} \mathbf{g}_{ikj}\boldsymbol{\psi}_k^H + \mathbf{N}_i^{\mathrm{p}}, \tag{1}$$

in which ρ^{p} is the UL pilot transmit power, and $\mathbf{N}_i^{\mathrm{p}} \in \mathbb{C}^{N \times K}$ is the additive white Gaussian noise (AWGN) matrix with independent and identically distributed elements, following a complex normal distribution with zero mean and variance σ_n^2. Note that we have assumed a uniform power allocation policy in the UL training stage. As discussed in the work of

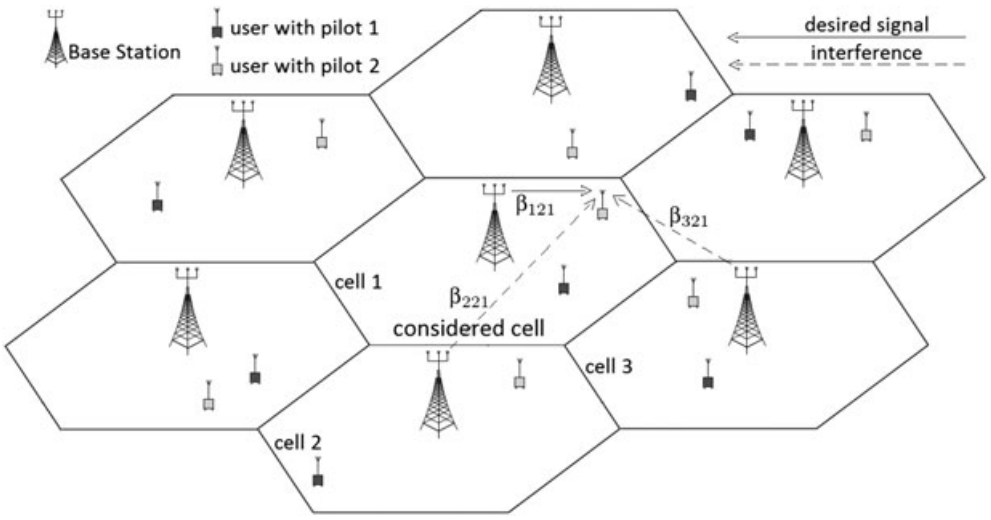

FIGURE 1 Multicell massive multiple-input–multiple-output (Ma-MIMO) scenario adopted, when $L = 7$, and $K = 2$

Fernandes et al,[17] any effect of pilot power allocation can be alternatively achieved through transmit power allocation and constant pilot powers, and thus, no loss is incurred in assigning a constant pilot power ρ^{p} to all users. The ith BS then estimates the k'th user CSI by correlating the received signal $\mathbf{Y}_i^{\mathrm{p}}$ with $\boldsymbol{\psi}_k'$

$$\hat{\mathbf{g}}_{ik'} = \frac{1}{\sqrt{\rho^{\mathrm{p}}}}\mathbf{Y}_i^{\mathrm{p}}\boldsymbol{\psi}_{k'} = \sum_{j=1}^{L}\mathbf{g}_{ik'j} + \mathbf{v}_{ik'}, \tag{2}$$

where $\mathbf{v}_{ik'} = \frac{1}{\sqrt{\rho^{\mathrm{p}}}}\mathbf{N}_i^{\mathrm{p}}\boldsymbol{\psi}_{k'} \sim \mathcal{CN}(\mathbf{0}_N, \frac{\sigma_n^2}{\rho^{\mathrm{p}}}\mathbf{I}_N)$ is an equivalent noise vector. The pilot contamination effect can be clearly seen in the previous expression. By acquiring such CSI estimates, the BS is able to perform linear detection in the UL and linear precoding in the DL, deploying MRC and MRT, respectively. Our choice for these detection/precoding schemes is because of their reduced complexity, simplified implementation, and good performance results when the number of BS antennas increases,[14] tightly approaching the performance of other schemes with higher computational complexity.[13] During UL data transmission, the ith BS receives the signal

$$\mathbf{y}_i^{\mathrm{u}} = \sum_{j=1}^{L}\sum_{k=1}^{K}\sqrt{\rho_{kj}^{\mathrm{u}}}\mathbf{g}_{ikj}x_{kj}^{\mathrm{u}} + \mathbf{n}_i^{\mathrm{u}}, \tag{3}$$

in which ρ_{kj}^{u} and x_{kj}^{u} are the UL data transmit power and the data symbol, respectively, from the kth user of the jth cell, and $\mathbf{n}_i^{\mathrm{u}} \sim \mathcal{CN}(\mathbf{0}_N, \sigma_n^2\mathbf{I}_N)$ is the $N \times 1$ AWGN sample vector. This BS then estimates the transmitted symbol as

$$\hat{x}_{k'i}^{\mathrm{u}} = \hat{\mathbf{g}}_{ik'}^H\mathbf{y}_i^{\mathrm{u}}. \tag{4}$$

Similarly, during a DL data transmission, the k'th user of the jth cell receives the signal

$$y_{k'j}^{\mathrm{d}} = \sum_{i=1}^{L}\sum_{k=1}^{K}\sqrt{\rho_{ik}^{\mathrm{d}}}\mathbf{g}_{ik'j}^T\mathbf{p}_{ik}x_{ik}^{\mathrm{d}} + n_{k'j}^{\mathrm{d}}, \tag{5}$$

where ρ_{ik}^{d} and x_{ik}^{d} is the DL data transmit power and the DL data transmitted from the ith BS to his kth user, and $n_{k'j}^{\mathrm{d}} \sim \mathcal{CN}(0, \sigma_n^2)$ is an AWGN sample. In addition, $\mathbf{p}_{ik}$ is the beamforming vector that the ith BS computes to precode its kth user data. Deploying MRT, this vector is defined as[17]

$$\mathbf{p}_{ik} = \frac{\hat{\mathbf{g}}_{ik}^*}{||\hat{\mathbf{g}}_{ik}||} = \frac{\hat{\mathbf{g}}_{ik}^*}{\alpha_{ik}\sqrt{N}}, \tag{6}$$

in which the scalar $\alpha_{ik} = \frac{||\hat{\mathbf{g}}_{ik}||}{\sqrt{N}}$ is a normalization factor necessary to guarantee that $||\sqrt{\rho_{ik}^{\mathrm{d}}}\mathbf{p}_{ik}x_{ik}^{\mathrm{d}}||^2 = \rho_{ik}^{\mathrm{d}}$.

Following the analysis in the works of Marzetta et al[2] and Filho et al,[14] it can be shown from Equations 4 and 5 that the UL and DL SINR performance of Ma-MIMO systems with MRC and MRT are given, respectively, by

$$\varsigma^{\mathrm{u}}_{k'i} = \frac{\rho^{\mathrm{u}}_{k'i}\beta^2_{ik'i}}{\sum\limits_{\substack{l=1\\ l\neq i}}^{L}\rho^{\mathrm{u}}_{k'l}\beta^2_{ik'l} + \frac{\alpha^2_{ik'}}{N}\left(\sum\limits_{l=1}^{L}\sum\limits_{k=1}^{K}\rho^{\mathrm{u}}_{kl}\beta_{ikl} + \sigma^2_n\right)}, \tag{7}$$

$$\varsigma^{\mathrm{d}}_{k'j} = \frac{\rho^{\mathrm{d}}_{jk'}\beta^2_{jk'j}/\alpha^2_{jk'}}{\sum\limits_{\substack{l=1\\ l\neq j}}^{L}\rho^{\mathrm{d}}_{lk'}\beta^2_{lk'j}/\alpha^2_{lk'} + \frac{1}{N}\left(\sum\limits_{l=1}^{L}\beta_{lk'j}\sum\limits_{k=1}^{K}\rho^{\mathrm{d}}_{lk} + \sigma^2_n\right)}, \tag{8}$$

in which $\alpha^2_{jk} = \sum_{\ell=1}^{L}\beta_{jk\ell} + \frac{\sigma^2_n}{\rho^{\mathrm{p}}}$. It is straightforward to see from Equations 7 and 8 that the asymptotic UL and DL SINR ($N \to \infty$) converge, respectively, to

$$\varsigma^{\mathrm{u}}_{k'i} = \frac{\rho^{\mathrm{u}}_{k'i}\beta^2_{ik'i}}{\sum\limits_{\substack{l=1\\ l\neq i}}^{L}\rho^{\mathrm{u}}_{k'l}\beta^2_{ik'l}}, \qquad \varsigma^{\mathrm{d}}_{k'j} = \frac{\rho^{\mathrm{d}}_{jk'}\beta^2_{jk'j}/\alpha^2_{jk'}}{\sum\limits_{\substack{l=1\\ l\neq j}}^{L}\rho^{\mathrm{d}}_{lk'}\beta^2_{lk'j}/\alpha^2_{lk'}}. \tag{9}$$

Although UL and DL SINR (9) are similar-looking expressions, they have different statistical characteristics, as discussed in the work of Marzetta.[1] While interference in UL is irradiated from users in neighboring cells using the same kth pilot sequence to the ith BS, interference in DL is irradiated from neighboring BS's to the user in the jth cell using the kth pilot sequence. While in UL, the receiver is fixed, and the multiple transmitters are moving, in DL, multiple fixed transmitters communicate with a mobile receiver. In addition, different behaviors will be seen in each direction with respect to PA, as explained in the following.

3 | PA OPTIMIZATION

In this section, the Ma-MIMO system performance is improved by suitably assigning the pilot sequences to the users.[3,4] We assume a decentralized allocation procedure, in which PA is performed sequentially by each cell, regarding its covered users. The convergence of this procedure is discussed in the work of Marinello and Abrão[4] and shown by numerical results in Zhu et al.[3] In addition, in this PA stage, it is assumed that the knowledge of the users' power distribution in the cells, and the focus is at the asymptotic performance expressions in Equation 9 for simplicity. Then, in Section 4, we evaluate the power control algorithm based on the PA obtained here and demonstrate the performance improvements of our proposed schemes for finite number of antennas in Section 5. The SINR expressions in Equation 9 were obtained, assuming that the k'th pilot sequence* is assigned to the k'th user, ie, under a random strategy. However, if we assume that the pth pilot is assigned to the c_pth user in the ith cell, the UL SINR can be rewritten as

$$\varsigma^{\mathrm{u}}_{c_p i} = \frac{\rho^{\mathrm{u}}_{c_p i}\beta^2_{ic_p i}}{\sum\limits_{\substack{j=1\\ j\neq i}}^{L}\rho^{\mathrm{u}}_{pj}\beta^2_{ipj}}, \tag{10}$$

that is the UL SINR of the user in the ith cell using the pth pilot, namely, the c_pth user. The performance bottleneck in Ma-MIMO systems is due to users with severe pilot contamination.[1] Thus, a fair objective is to maximize the minimum UL SINR among the users, as the following optimization problem[3]:

$$\mathcal{PA}_{\mathrm{u}} : \max_{l}\min_{p} \quad \varsigma^{\mathrm{u}}_{c_{lp}i}, \tag{11}$$

in which c_{lp} is the l,pth element of matrix $\mathbf{C} \in \mathbb{N}^{K!\times K}$, which contains every possible PA that a given cell can adopt. c_{lp} means that in the lth PA combination, the pth pilot is assigned to the c_{lp}th user. Obviously, the complexity of solving Equation 11 via an exhaustive search grows with K in a factorial fashion. A viable and heuristic solution is proposed in the work of Zhu et al,[3] where the pilot sequences with the worst interference levels are assigned to the users with the highest long-term fading coefficients. Such *greedy method* achieves a near-optimal solution with reduced complexity.

*With "k'-th pilot sequence", we refer to the pilot of index k' in the set of available pilot sequences.

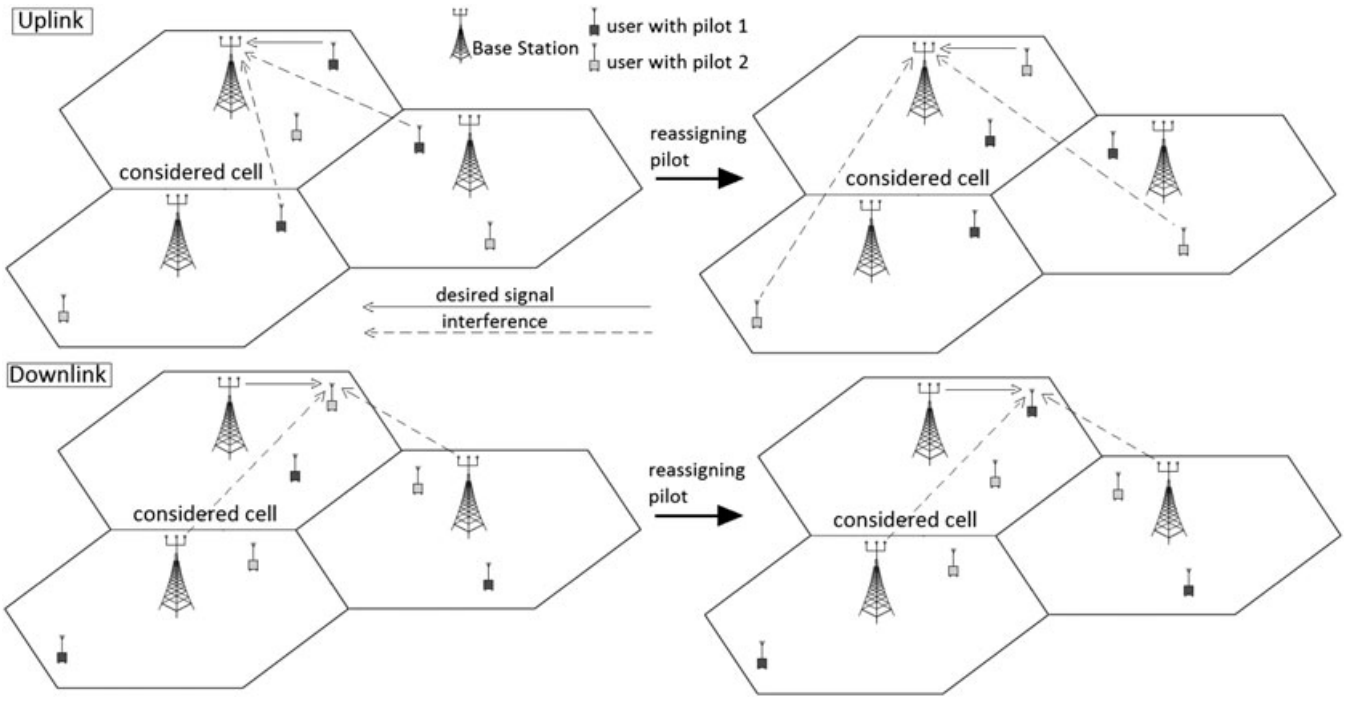

FIGURE 2 Effect of reassigning pilot sequences in the considered cell, in uplink (UL) (up) and downlink (DL) (down). Although it appears from the Figure that reassigning pilots has no effect in DL, the previous UL pilot transmission stage results in some variations on the signals' strength

On the other hand, the DL SINR in Equation 9 can also be improved via PA as in the work of Marinello and Abrão.[4] Assuming that the pth pilot is assigned to the c_pth user in the jth cell, the DL SINR becomes

$$\varsigma^{\mathrm{d}}_{c_p j} = \frac{\rho^{\mathrm{d}}_{jc_p}\beta^2_{jc_p j}}{\beta_{jc_p j} + \vartheta_{jp(j)}} \; \frac{1}{\sum\limits_{\substack{i=1 \\ i\neq j}}^{L} \frac{\rho^{\mathrm{d}}_{ic_p}\beta^2_{ic_p j}}{\beta_{ic_p j}+\vartheta_{ip(j)}}}, \tag{12}$$

where $\vartheta_{ip(j)} = \sum_{\substack{\ell=1 \\ \ell\neq j}}^{L} \beta_{ip\ell} + \frac{\sigma^2_n}{\rho^{\mathrm{p}}}$ does not depend on for what user the pth pilot will be assigned. Thus, an alternative PA optimization procedure for DL is proposed as

$$\mathcal{PA}_{\mathrm{d}} \;:\; \max_{l} \min_{p} \quad \varsigma^{\mathrm{d}}_{c_{lp} j}. \tag{13}$$

One can see that the dependence of the DL SINR with the assignment of pilots to users is not so simple as it is in the UL scenario, and hence, the PA problem of Equation 13 was solved in the work of Marinello and Abrão[4] only via exhaustive search. However, communication systems are usually asymmetric, and the DL data transmission might be predominant in comparison with the UL data transmission. Therefore, solving the optimization problem in Equation 13 in a low-complexity way is also quite appealing in practice. The main difficulty is that the interference in DL for the pth pilot (denominator of the second term in Equation 12) is dependent on what user this sequence is assigned, and thus, a greedy method cannot be applied as in the work of Zhu et al.[3] If a user changes its pilot sequence, the DL interference due to pilot contamination reaching him/her is still mainly dominated by his long-term fading coefficients with respect to neighboring BS's, which do not change, as illustrated in Figure 2. The exception is due to the DL normalization factors, which retain some dependence with the assigned pilot sequence from the UL training channel estimation.

3.1 | Joint UL-DL PA

One can note that the optimization problems of Equations 11 and 13 are conflicting, as numerically demonstrated in the next section. If the UL performance metric is optimized, the DL performance will be close to that attained with a random assignment policy, and vice versa. Thus, we elaborate our analysis aiming to jointly achieve the best possible performance in UL and DL, concurrently. One approach could be adopting multiobjective optimization. In this paper, we prefer a

simpler strategy. We assume in the adopted TDD scheme a channel coherence block of S symbols, of which K are devoted to UL pilot transmission, $\xi^{\mathrm{u}}(\frac{S-K}{S})$ and $\xi^{\mathrm{d}}(\frac{S-K}{S})$ for UL and DL data transmission, respectively, in which the factors ξ^{u} and $\xi^{\mathrm{d}} \in (0,1)$, $\xi^{\mathrm{u}} + \xi^{\mathrm{d}} = 1$, and both $\xi^{\mathrm{u}}(\frac{S-K}{S})$ and $\xi^{\mathrm{d}}(\frac{S-K}{S})$ are integers. Then, for a system bandwidth BW, the total capacity (TC) of the user in the ith cell for which the pth pilot is assigned is defined as

$$C^{\mathrm{T}}_{c_p i} = \mathrm{BW}\left(\frac{S-K}{S}\right)\left[\xi^{\mathrm{u}}\log_2\left(1+\varsigma^{\mathrm{u}}_{c_p i}\right) + \xi^{\mathrm{d}}\log_2\left(1+\varsigma^{\mathrm{d}}_{c_p i}\right)\right]. \tag{14}$$

Hence, an alternative optimization problem can be defined as

$$\mathcal{PA}_{\mathrm{TC}} : \max_{l}\min_{p} \quad C^{\mathrm{T}}_{c_{lp} i}. \tag{15}$$

3.2 | Heuristic PA solutions

For solving the DL assignment problem avoiding the exhaustive search, we first create a cost matrix $\mathbf{\Gamma}^{(i)} \in \mathbb{R}^{K\times K}$, whose j,pth element is the DL SINR achieved by the jth user in the ith cell when the pth pilot sequence is assigned to him/her, ie, $\gamma^{(i)}_{jp} = \varsigma^{\mathrm{d}}_{c_p i}$ when $c_p = j$. Then, *our proposed low-complexity suboptimal solution* consists of finding the pilot, with whom each user achieves its maximal DL SINR. The user with the lowest maximal DL SINR will have such pilot sequence assigned to him/her. This procedure is repeated, excluding the users and the pilots already assigned, until allocating every pilot sequence, as described in Algorithm 1.

In order to obtain a low-complexity form for solving the joint UL-DL PA in Equation 15 while achieving near-optimal performance, this same heuristic procedure can be applied. In this case, we initialize the cost matrix $\mathbf{\Gamma}^{(i)}$ (line 1 in Algorithm 1) in an alternative way, such that $\gamma^{(i)}_{jp} = C^{\mathrm{T}}_{c_p i}$ when $c_p = j$, since the TC as defined in Equation 14 is calculated as a weighted log function of both UL and DL SINRs. Then, we apply our proposed heuristic method in a similar way as in Algorithm 1.

Algorithm 1 Proposed pilot assignment procedure

Input: $\beta_{jkl}, \forall j, l = 1,2,\dots L, k = 1,2,\dots K, \sigma^2_n, \rho_{\mathrm{p}}$.

1: Generate cost matrix $\mathbf{\Gamma}^{(i)}$, of size $K \times K$;
2: **for** $j = 1,2,\dots,K$ **do**
3: **for** $p = 1,2,\dots,K$ **do**
4: Evaluate $\delta_p = \max_{\ell=1,\dots,K} \gamma^{(i)}_{p,\ell}$;
5: Evaluate $\eta_p = \arg\max_{\ell=1,\dots,K} \gamma^{(i)}_{p,\ell}$;
6: **end for**
7: Evaluate $\phi = \arg\min_{p=1,\dots,K} \delta_p$;
8: Evaluate $c^{(i)}_{\eta_\phi} = \phi$;
9: Invalidate the ϕ-th line and η_ϕ-th column of $\mathbf{\Gamma}^{(i)}$;
10: **end for**

Output: $\mathbf{c}^{(i)}$.

4 | POWER CONTROL ALGORITHM

With the purpose of serving the users with a target SINR, the target-SIR-tracking (signal-to-interference ratio) algorithm measures the interference seen by each user and assigns to him/her the exact power to reach the target SINR, unless if this power exceeds the maximum power available. In this case, the maximum power is allocated for this user. It is shown in the work of Rasti and Sharafat[12] that this power allocation procedure is not the most suitable, since assigning the maximum power for the users with poor channel conditions causes an excessive interference for the other users, and waste energy because this user may remain with a low SINR. Being $\hat{\varsigma}^{\mathrm{d}}_{k'\ell}$ the target downlink SINR for the k'th user of the ℓth cell, and $\bar{\rho}^{\mathrm{d}}_{\ell k'}$ the maximum DL transmit power that can be assigned to him/her, the target-SIR-tracking algorithm updates power at the ith iteration according to

$$\rho^{\mathrm{d}}_{\ell k'}(i) = \min\left[\hat{\varsigma}^{\mathrm{d}}_{k'\ell}\mathcal{I}^{\mathrm{d}}_{k'\ell}(i), \bar{\rho}^{\mathrm{d}}_{\ell k'}\right], \tag{16}$$

TABLE 1 Target signal-to-interference-plus-noise ratios (SINRs) of the power control algorithm adopted for each pilot assignment (PA) technique

Number of Users	PA Scheme	DL	UL
$K = 10$	Random	−9 dB	−10 dB
	H-MaxminSINR DL	−2 dB	−9 dB
	H-MaxminSINR UL	−6 dB	−4 dB
	H-MaxminTC	−3 dB	−5 dB
$K = 32$	Random	−11 dB	−14 dB
	H-MaxminSINR DL	−7 dB	−11 dB
	H-MaxminSINR UL	−9 dB	−7 dB
	H-MaxminTC	−7 dB	−8 dB

Abbreviations: DL, downlink; TC, total capacity; UL, uplink.

in which $\mathcal{I}^{\mathrm{d}}_{k'\ell}(i) = \rho^{\mathrm{d}}_{\ell k'}(i-1)/\varsigma^{\mathrm{d}}_{k'\ell}(i-1)$ is the interference plus noise seen by this user (denominator of Equation 8) divided by $\beta^2_{\ell k'\ell}/\alpha^2_{\ell k'}$. By contrast, the power control algorithm proposed in the work of Rasti and Sharafat[12] updates users' powers as

$$\rho^{\mathrm{d}}_{\ell k'}(i) = \begin{cases} \hat{\varsigma}^{\mathrm{d}}_{k'\ell}\mathcal{I}^{\mathrm{d}}_{k'\ell}(i) & \text{if } \mathcal{I}^{\mathrm{d}}_{k'\ell}(i) \leq \frac{\bar{\rho}^{\mathrm{d}}_{\ell k'}}{\hat{\varsigma}^{\mathrm{d}}_{k'\ell}}, \\ \frac{\left(\bar{\rho}^{\mathrm{d}}_{\ell k'}\right)^2}{\hat{\varsigma}^{\mathrm{d}}_{k'\ell}\mathcal{I}^{\mathrm{d}}_{k'\ell}(i)} & \text{otherwise.} \end{cases} \tag{17}$$

One can see that the method in the work of Rasti and Sharafat[12] assigns power to the users in the same way as the target-SIR-tracking algorithm if the target SINR can be achieved for the user at that iteration. Otherwise, instead of allocating him/her the maximum power, it allocates him/her a transmit power inversely proportional to that required to achieve the target. Thus, aside from saving energy relative to users that cannot reach the target SINR, the interference irradiated to other users also decreases. Equivalently, this same procedure can be applied in UL user power allocation as

$$\rho^{\mathrm{u}}_{k'\ell}(i) = \begin{cases} \hat{\varsigma}^{\mathrm{u}}_{k'\ell}\mathcal{I}^{\mathrm{u}}_{k'\ell}(i) & \text{if } \mathcal{I}^{\mathrm{u}}_{k'\ell}(i) \leq \frac{\bar{\rho}^{\mathrm{u}}_{k'\ell}}{\hat{\varsigma}^{\mathrm{u}}_{k'\ell}}, \\ \frac{\left(\bar{\rho}^{\mathrm{u}}_{k'\ell}\right)^2}{\hat{\varsigma}^{\mathrm{u}}_{k'\ell}\mathcal{I}^{\mathrm{u}}_{k'\ell}(i)} & \text{otherwise,} \end{cases} \tag{18}$$

in which $\hat{\varsigma}^{\mathrm{u}}_{k\ell}$ is the target UL SINR of the user, $\bar{\rho}^{\mathrm{u}}_{k\ell}$ its maximum UL transmit power, and

$$\mathcal{I}^{\mathrm{u}}_{k'\ell}(i) = \frac{\sum\limits_{\substack{l=1 \\ l\neq\ell}}^{L} \rho^{\mathrm{u}}_{k'l}(i-1)\beta^2_{\ell k'l} + \frac{\alpha^2_{\ell k'}}{N}\left(\sum\limits_{l}\sum\limits_{k}\rho^{\mathrm{u}}_{kl}(i-1)\beta_{\ell kl} + \sigma^2_n\right)}{\beta^2_{\ell k'\ell}}.$$

When deploying these power control algorithms, the target SINR parameter should be carefully chosen. If a somewhat lower value is adopted, the algorithm saves energy by delivering just the target SINR to the users, taking low advantage of the resources and providing poor performance for the system. If an excessive target SINR is considered, many poor located users will have their powers gradually turned off to provide the desired performance for the other better located users. Hence, in Section 5.2, the target SINR was chosen in each scenario by finding the value that achieves the highest throughput for 95% of the users, by means of numerical simulations. For each investigated PA technique, each number of scheduled users, and for both UL and DL, we have varied the target SINR of the power control algorithm in the range of −15 to 0 dB in steps of 1 dB to find the value that achieved the best 95% likely performance. The adopted values for the target SINRs in the Section 5.2 are indicated in Table 1. Our main objective with this procedure is to show the full potential of the investigated power control algorithm in conjunction with our proposed PA techniques. However, as the obtained values for the target SINR are dependent on the actual conditions of the communication system, like number of users, transmit SNR, and others; in Section 5.3, we explore a more practical and appealing scenario. In this case, the target SINR for the power control algorithm is that required to provide a desired per user rate for both UL and DL. Such rate is chosen in accordance with the number of scheduled users and aiming to provide an appreciable performance for the system as a whole.

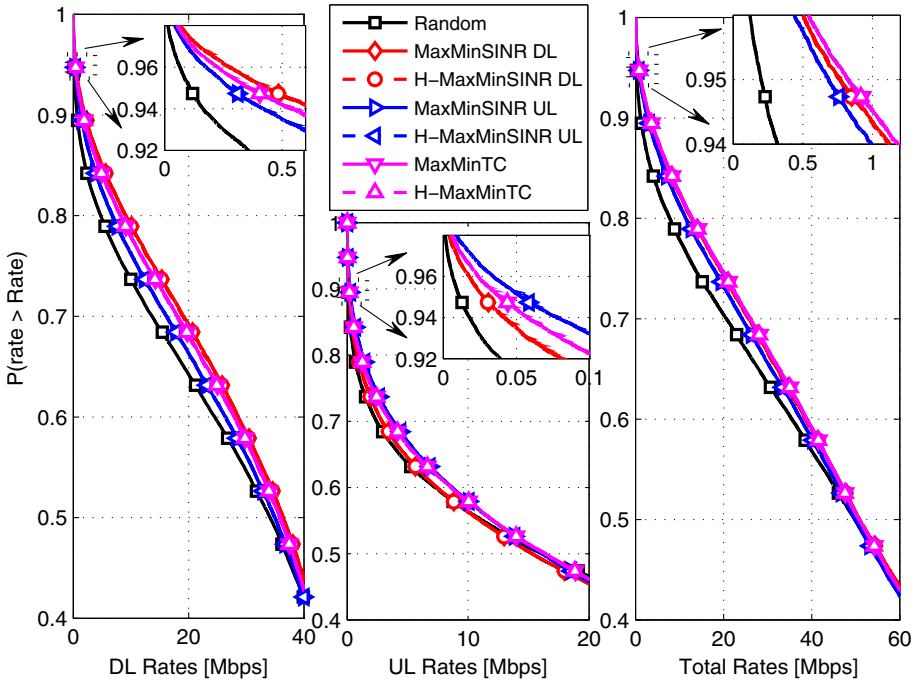

FIGURE 3 Fraction of users above a given rate for $N = 128$ and $K = 4$. A, Downlink (DL); B, Uplink (UL); C, Total

5 | NUMERICAL RESULTS

The Ma-MIMO system performance is numerically evaluated in this Section. We consider $L = 7$ interfering hexagonal cells of 1000-m radius, where K users are uniformly distributed, except in a circle of 100-m radius around the cell centered BS,[4] with universal frequency and pilot reuse. This is equivalent to say that we consider the performance of a given cell with the interference from 6 nearest-neighbor cells, since only the performance metrics of users in central cell are computed. We consider a system bandwidth of 20 MHz, a signal-to-noise ratio of 10 dB for pilot, UL data, and DL data transmission, and a TDD architecture similar to the work of Björnson et al,[11] with $\mathcal{S} = 100$ symbols,[†] of which K are dedicated to UL pilot transmissions, and the remainder are equally divided between UL and DL data transmissions ($\xi^{u} = \xi^{d} = 0.5$). The path-loss decay exponent was adopted as 3.8, and the standard deviation of the log-normal shadowing was assumed to be 8 dB. In addition, since in practice, the number of antennas at the BS is limited by several factors, like physical size constraints, power expenditures, hardware cost, among others, we focus on Ma-MIMO systems with a moderate to high number of antennas, $N \in [64, 512]$.

We refer to the PA that solves Equation 11 as MaxminSINR UL, the one solving Equation 13 as MaxminSINR DL, and the solution of Equation 15 as MaxminTC. In addition, the heuristic approach of each solution is referred by the respective method preceded by "H." Note that MaxminSINR UL and H-MaxminSINR UL were proposed in the work of Zhu et al,[3] whereas MaxminSINR DL was proposed in the work of Marinello and Abrão.[4] The H-MaxminSINR DL consists in applying our proposed heuristic algorithm described in Section 3.2 for solving the PA problem formulation in the work of Marinello and Abrão,[4] avoiding the exhaustive search, whereas MaxminTC and H-MaxminTC consist in the solutions of our proposed PA formulation of Section 3.1 via exhaustive search and via our heuristic algorithm, respectively.

5.1 | Performance of heuristic approach

Our first objective is to show that the *heuristic solutions* of MaxminSINR UL, MaxminSINR DL, and MaxminTC *achieve practically the same performance of that attained with exhaustive search*, but with a feasible complexity. For this sake, Figure 3 depicts the fraction of users above a given rate for 128 BS antennas, in terms of DL, UL, and total rate; and Figure 4 shows the 95% likely rate achieved by each technique with an increasing number of antennas. In both cases,

[†]Which can represent, for instance, a scenario with 1 ms of channel coherence time and 100 KHz of coherence bandwidth as in the work of Björnson et al.[11]

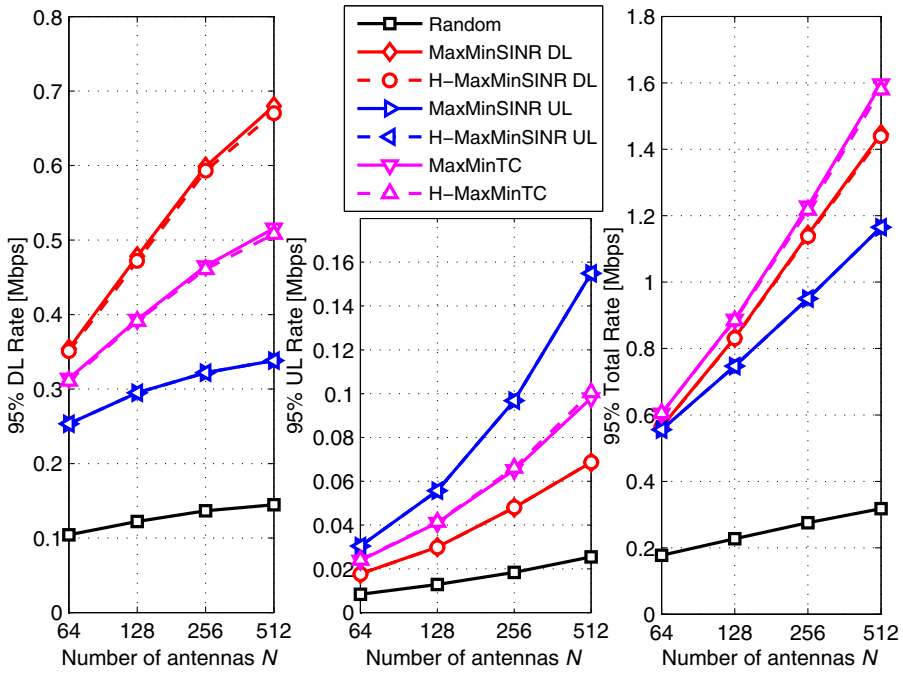

FIGURE 4 Likely rate of 95% for $K = 4$. A, Downlink (DL); B, Uplink (UL); C, Total

a uniform power allocation policy was assumed for simplicity, and $K = 4$ users to allow the evaluation of exhaustive search in a feasible time. It is noteworthy from Figure 3 the very unfair behavior of primitive Ma-MIMO systems (with no pilot and power allocation policies), which provides very high data rates for some portion of the users, while providing low quality of service for others. One can note also that appreciable improvements can be achieved with PA techniques. The conflicting behavior of UL and DL optimization metrics is represented in the Figure 3, since while MaxminSINR DL achieves the best performance in DL, its UL performance is close to that attained by random PA. The opposite occurs with MaxminSINR UL. On the other hand, MaxminTC achieves good performance in both directions, at the same time it achieves the best performance in terms of total rates. In addition, no significant performance loss can be seen for any heuristic PA when compared with its respective exhaustive search solution. Similar findings can be taken from Figure 4, which also reveal that it is always beneficial improving the number of antennas in BS.

5.2 | Performance of PA with power control

Having demonstrated the good performances achieved by the heuristic PA techniques, our goal now is to demonstrate that the power control algorithm achieves a much improved performance when combined with an appropriate PA scheme. In addition, we discard the exhaustive search PA algorithms to enable a higher number of users. For $K = 10$ and using power control, Figure 5 shows the fraction of users above a given rate for $N = 128$, whereas Figure 6 shows the 95% likely rate achieved with an increasing number of antennas. The target SINR's performances of the power control algorithm for each scheme were empirically chosen to provide the higher throughput for 95% of the users, as indicated in Table 1. It can be seen that much more uniform user performances are achieved with power control, and that the assured performance can be considerably improved with a proper choice of the PA used. For example, as can be seen in Figure 6, with random assignment, the 95% likely DL rate increases from 92.5 kbps to 1.528 Mbps with $N = 128$ antennas when using a power control, whereas this DL rate increase is from 388.3 kbps to 5.251 Mbps when the H-MaxminTC is the PA adopted. Similarly, in the UL, the 95% likely UL rate with random assignment increases from 3.4 kbps to 1.235 Mbps when using power control, and from 11.4 kbps to 3.566 Mbps with H-MaxminTC as PA policy and $N = 128$. It can also be seen that H-MaxminTC algorithm with power control procedure has the ability of assuring an appreciable system quality of service improvement by jointly optimizing the DL and UL data rates, contrary to H-MaxminSINR DL and H-MaxminSINR UL that assure good rates only on its preferential direction, ie, either in DL or in UL direction.

Figures 7 and 8 do the same with $K = 32$ users, from which similar findings can be taken. While the 95% likely DL rate for $N = 128$ antennas under random PA increase from 41.3 to 746.2 kbps, this DL rate increase with H-MaxminTC

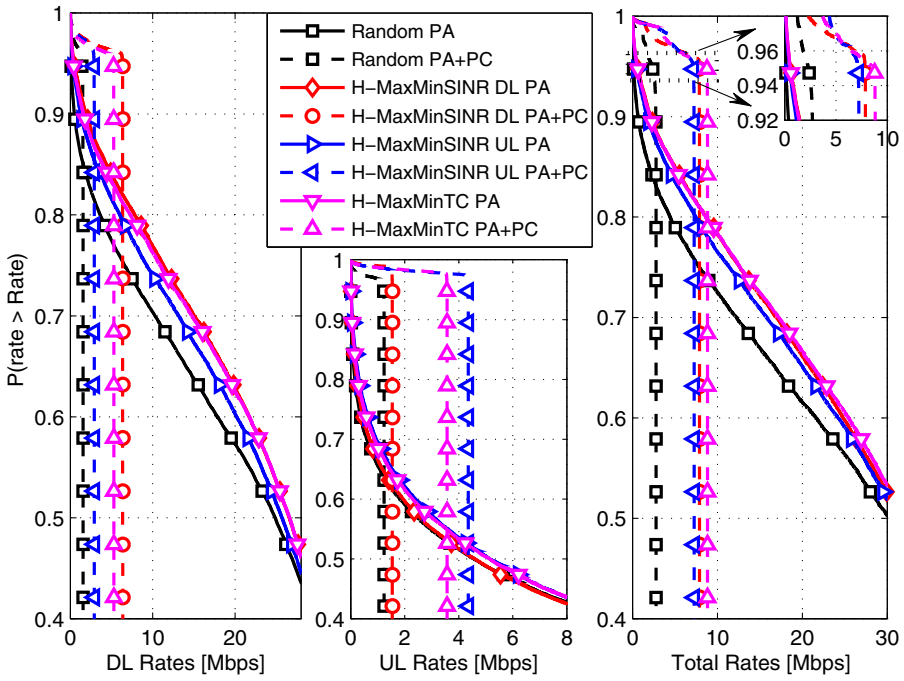

FIGURE 5 Fraction of users above a given rate for $N = 128$ and $K = 10$. A, Downlink (DL); B, Uplink (UL); C, Total. Power control evaluated with target signal-to-interference-plus-noise ratios (SINRs) of Table 1

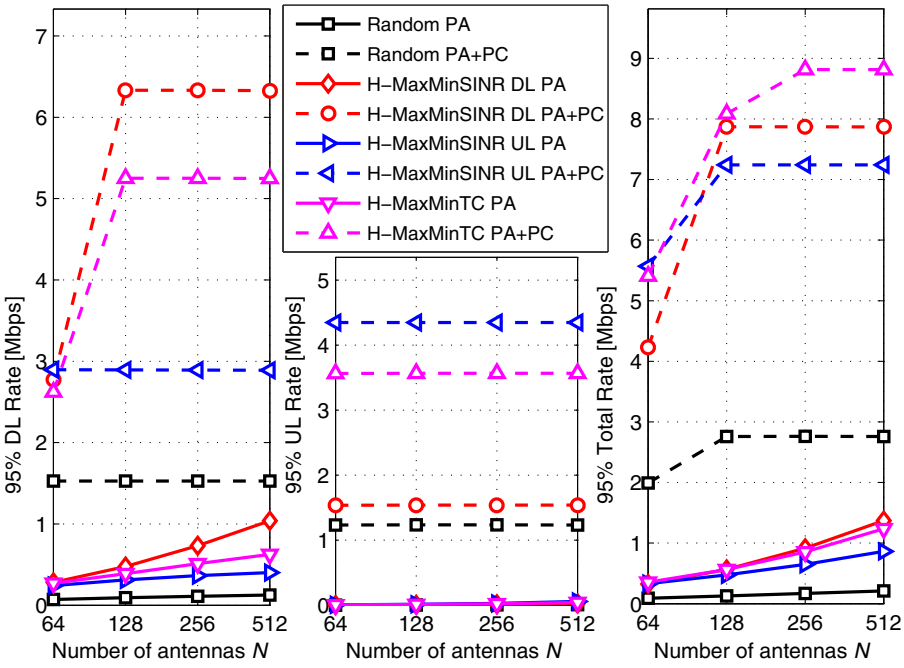

FIGURE 6 Likely rate of 95% for $K = 10$. A, Downlink (DL); B, Uplink (UL); C, Total. Power control evaluated with target signal-to-interference-plus-noise ratios (SINRs) of Table 1

is from 191.6 kbps to 1.782 Mbps. Similarly for the 95% likely UL rate with $N = 128$, this gain under random PA is from 0.5 to 382.5 kbps, and from 2.0 kbps to 1.442 Mbps with H-MaxminTC PA. The decrease in the assured rates with this higher number of users is due not only to the increased multiuser interference but also to the increased pilot overhead necessary to obtain CSI estimates of this increased number of users. On the other hand, it allows the PA schemes to achieve improved gains in comparison with random assignment because of the greater multiuser diversity.

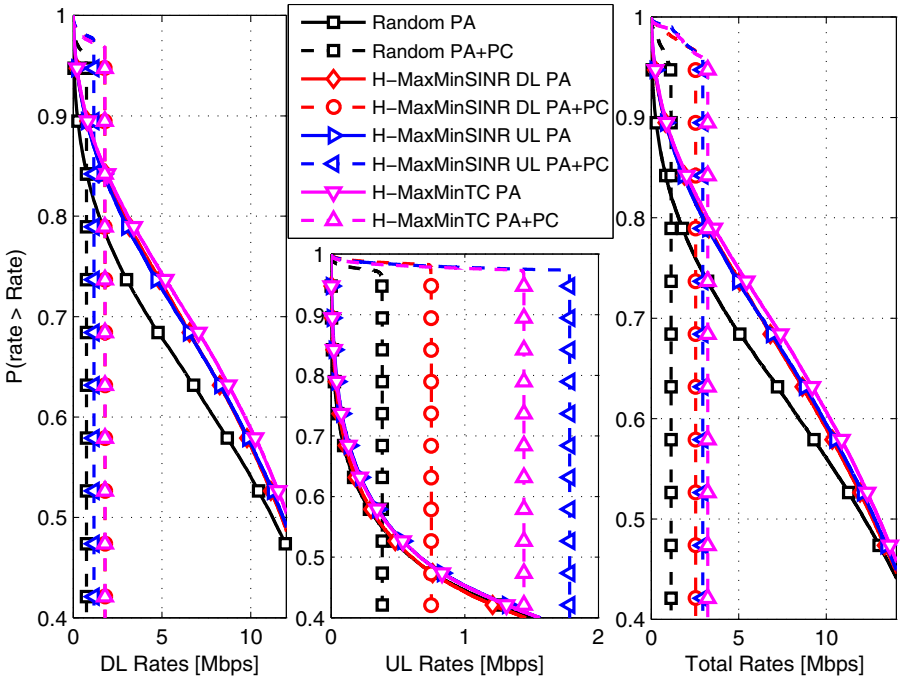

FIGURE 7 Fraction of users above a given rate for $N = 128$ and $K = 32$. A, Downlink (DL); B, Uplink (UL); C, Total. Power control evaluated with target signal-to-interference-plus-noise ratios (SINRs) of Table 1

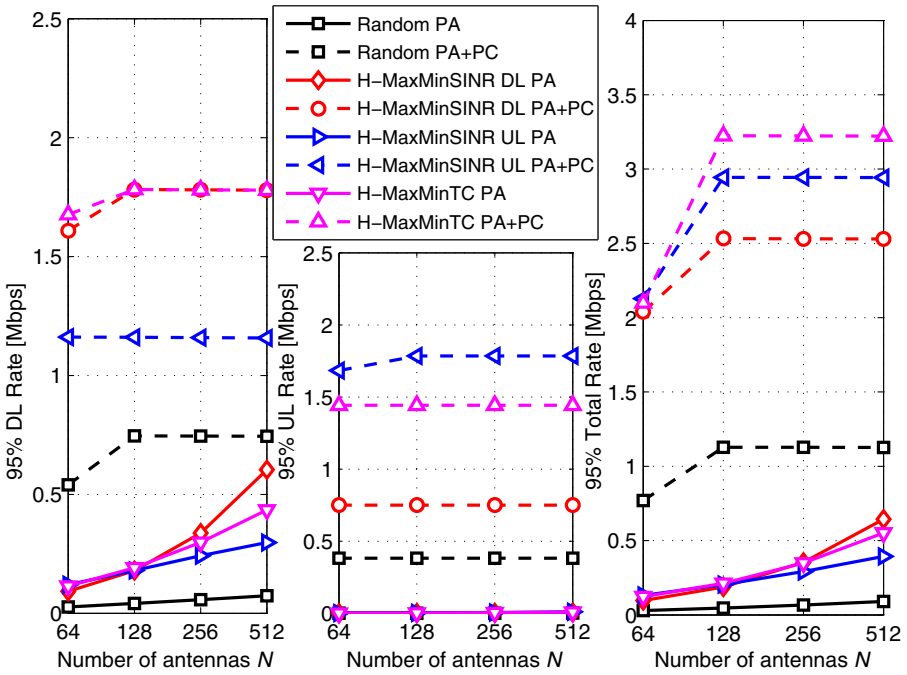

FIGURE 8 Likely rate of 95% for $K = 32$. A, Downlink (DL); B, Uplink (UL); C, Total. Power control evaluated with target signal-to-interference-plus-noise ratios (SINRs) of Table 1

5.3 | Performance with target rates

Performance results with power control as depicted in Figures 5 to 8 were obtained after a careful but nonexhaustive process of finding suitable target SINR performances for each scheme under the considered scenarios, as summarized in Table 1. However, these values of target performances are dependent of the instantaneous conditions of the communications systems, like the number of users served and pilot and data SNRs, which are dynamically changing. Thus, a

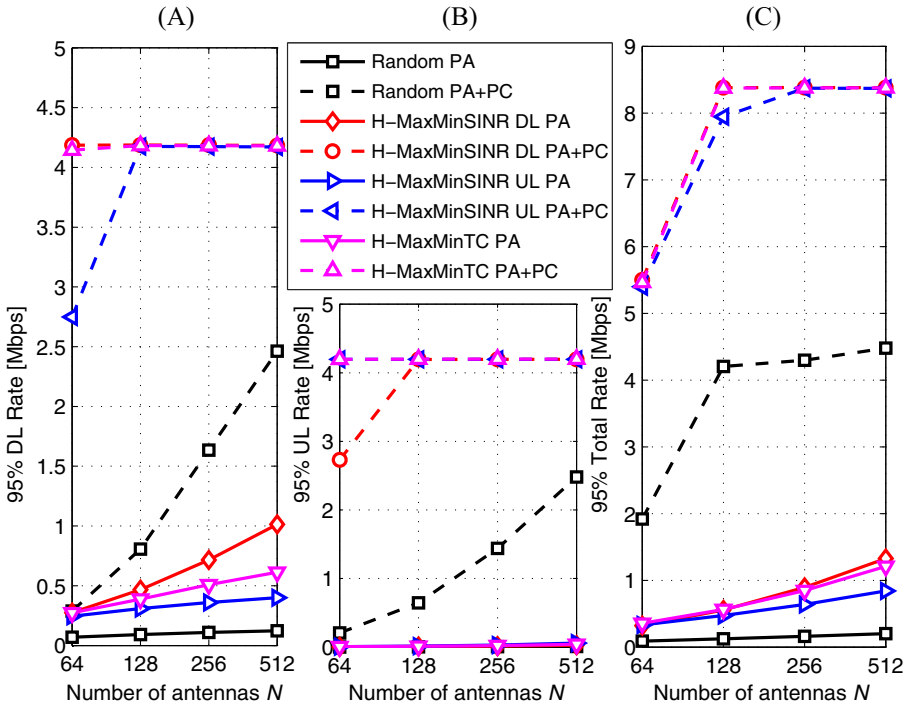

FIGURE 9 Likely rate of 95% for $K = 10$. A, Downlink (DL); B, Uplink (UL); C, Total. Power control evaluated with a target rate of 4.2 Mbps per user, for both UL and DL.

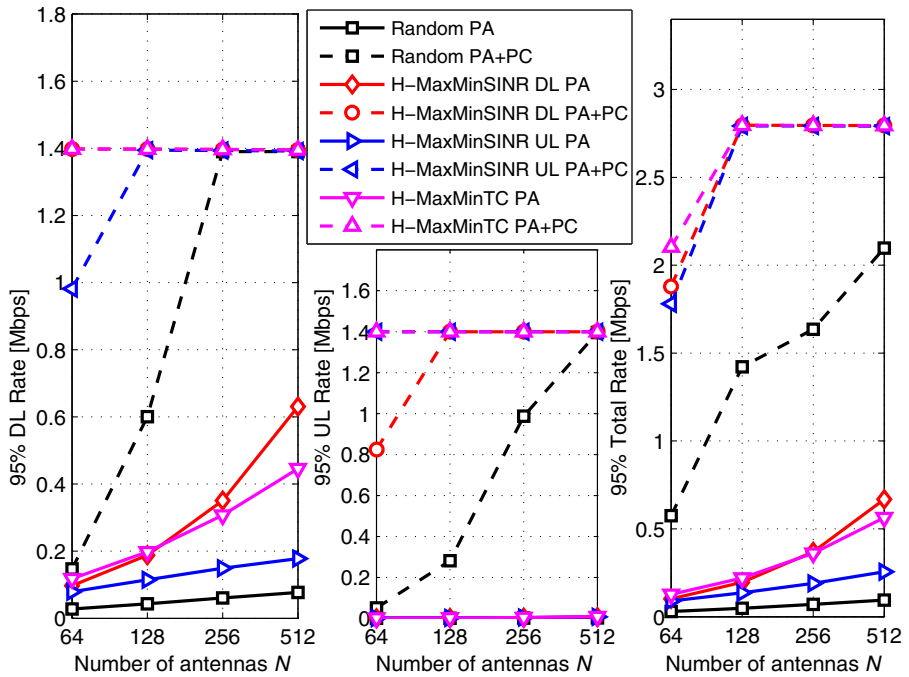

FIGURE 10 Likely rate of 95% for $K = 32$. A, Downlink (DL); B, Uplink (UL); C, Total. Power control evaluated with a target rate of 1.4 Mbps per user, for both UL and DL

more practical scenario consists in fixing a DL and UL target rates, from which the target SINR's input parameters of the power control algorithm are obtained. Under this strategy for the power control algorithm, Figure 9 shows the 95% likely rates obtained when fixing a target per user rate of 4.2 Mbps for both DL and UL when serving $K = 10$ users. Similarly, Figure 10 depicts the same performance metric when fixing a target rate for the power control algorithm of 1.4 Mbps for both DL and UL, considering $K = 32$ users. It can be seen from Figure 9 that H-MaxminTC PA with power control is able

to assure the target rates in both DL and UL even with just $N = 64$ antennas, whereas the H-MaxminSINR DL PA with power control fails in this objective for UL, and the opposite holds for H-MaxminSINR UL. It is important to note that even with the 95% likely DL and UL rate of 4.2 Mbps assured by H-MaxminTC PA with power control, a 95% likely total rate of 8.4 Mbps is not assured, since the set of users that do not achieve the target DL rate is not necessarily the same users that do not achieve the target UL rate. Very similar conclusions can be made from Figure 10, which shows that H-MaxminTC PA with power control is able to assure an appreciable 95% likely DL and UL per user rates of 1.4 Mbps for $K = 32$ users with only $N = 64$ BS antennas. If more BS antennas were allowed, such assured rates could be made higher due to the lower levels of noncoherent interference, as can be inferred from Equations 7 and 8.

6 | CONCLUSIONS

The PA optimization problem was addressed in this paper. Different from previous works, we have investigated the problem from both UL and DL perspectives. Our analysis have shown that, due to the different characteristics of UL and DL SINR expressions in Ma-MIMO, the PA optimization problems in UL and DL are conflicting. If the UL performance is optimized, it incurs in a limited performance in DL, and vice versa. Thus, we have proposed an efficient alternative metric, ie, the TC, which enables the Ma-MIMO system to achieve appreciable performances in both directions simultaneously. In addition, aiming to avoid an exhaustive search of factorial order, a heuristic solution capable of finding a near-optimal solution expending reduced computational resources has been also proposed. Finally, we have adapted the target-SIR-tracking power control algorithm to our scenario of massive MIMO systems with a finite number of BS antennas, and the investigated PA schemes have been combined with it. Our results demonstrated that much more improved gains can be achieved by this power control algorithm if they are applied after a suitable PA procedure, and that such gains can be attained even in more realistic scenarios of a not-so-large number of BS antennas. For example, our proposed H-MaxminTC PA scheme with power control was able to provide a 4.2 Mbps per user rate for both DL and UL directions with 95% probability when serving 10 users with only 64 antennas at BS, while an assured symmetric per user rate of 1.4 Mbps is achieved when serving 32 users with 64 antennas.

ACKNOWLEDGEMENTS

This work was supported in part by the National Council for Scientific and Technological Development (CNPq) of Brazil under Grants 304066/2015-0 and 404079/2016-4, and in part by Londrina State University, Paraná State Government (UEL).

ORCID

José Carlos Marinello Filho http://orcid.org/0000-0002-0980-8220
Cristiano Magalhães Panazio http://orcid.org/0000-0003-3905-6338
Taufik Abrão http://orcid.org/0000-0001-8678-2805

REFERENCES

1. Marzetta T. Noncooperative cellular wireless with unlimited numbers of base station antennas. *IEEE Trans Wirel Commun*. 2010;9(11):3590-3600.
2. Marzetta T, Larsson E, Yang H, Ngo H. *Fundamentals of Massive MIMO*. New York, NY: Cambridge University Press; 2016.
3. Zhu X, Wang Z, Dai L, Qian C. Smart pilot assignment for massive MIMO. *IEEE Commun Lett*. 2015;19(9):1644-1647.
4. Marinello JC, Abrão T. Pilot distribution optimization in multi-cellular large scale MIMO systems. *AEU - Int J Electron Commun*. 2016;70(8):1094-1103.
5. Zhu X, Dai L, Wang Z. Graph coloring based pilot allocation to mitigate pilot contamination for multi-cell massive MIMO systems. *IEEE Commun Lett*. 2015;19(10):1842-1845.
6. Xu H, Huang N, Yang Z, Shi J, Wu B, Chen M. Pilot allocation and power control in D2D underlay massive MIMO systems. *IEEE Commun Lett*. 2017;21(1):112-115.
7. Ngo HQ, Ashikhmin A, Yang H, Larsson EG, Marzetta TL. Cell-free massive MIMO versus small cells. *IEEE Trans Wirel Commun*. 2017;16(3):1834-1850.
8. Zhao P, Wang Z, Qian C, Dai L, Chen S. Location-aware pilot assignment for massive MIMO systems in heterogeneous networks. *IEEE Trans Veh Technol*. 2016;65(8):6815-6821.

9. Wang Z, Zhao P, Qian C, Chen S. Location-aware channel estimation enhanced TDD based massive MIMO. *IEEE Access*. 2016;4:7828-7840.
10. Zhang Q, Jin S, McKay M, Morales-Jimenez D, Zhu H. Power allocation schemes for multicell massive MIMO systems. *IEEE Trans Wirel Commun*. 2015;14(11):5941-5955.
11. Björnson E, Larsson EG, Debbah M. Massive MIMO for maximal spectral efficiency: how many users and pilots should be allocated? *IEEE Trans Wirel Commun*. 2016;15(2):1293-1308.
12. Rasti M, Sharafat A-R. Distributed uplink power control with soft removal for wireless networks. *IEEE Trans Commun*. 2011;59(3):833-843.
13. Marzetta TL. Massive MIMO: an introduction. *Bell Labs Tech J*. 2015;20:11-22.
14. Filho JCM, Panazio C, Abrão T. Uplink performance of single-carrier receiver in massive MIMO with pilot contamination. *IEEE Access*. 2017;5:8669-8681.
15. Prasad KNRSV, Hossain E, Bhargava VK. Energy efficiency in massive MIMO-based 5G networks: opportunities and challenges. *IEEE Wirel Commun*. 2017;24(3):86-94.
16. Goldsmith A. *Wireless Communications*. New York, NY: Cambridge University Press; 2005.
17. Fernandes F, Ashikhmin A, Marzetta T. Inter-cell interference in noncooperative TDD large scale antenna systems. *IEEE J Sel Areas Commun*. 2013;31(2):192-201.

How to cite this article: Marinello Filho JC, Panazio CM, Abrão T. Joint uplink and downlink optimization of pilot assignment for massive MIMO with power control. *Trans Emerging Tel Tech*. 2017;e3250. https://doi.org/10.1002/ett.3250

APPENDIX D – Full paper published in the journal "*Telecommunication Systems*"

Title: Massive MIMO pilot assignment optimization based on total capacity.

Authors: José Carlos Marinello Filho, Cristiano Panazio and Taufik Abrão.

Journal: Telecommunication Systems (ISSN 1018-4864).

Classification (Qualis-CAPES): A2 / IF$= 0.822$ (Engenharias IV).

Publication Date: April 2018.

Telecommunication Systems
https://doi.org/10.1007/s11235-018-0452-2

Massive MIMO pilot assignment optimization based on total capacity

José Carlos Marinello[1,2] · Cristiano Magalhães Panazio[2] · Taufik Abrão[1]

Abstract
We investigate the effects of pilot assignment in multi-cell massive multiple-input multiple-output systems. When deploying a large number of antennas at base station (BS), and linear detection/precoding algorithms, the system performance in both uplink (UL) and downlink (DL) is mainly limited by pilot contamination. This interference is proper of each pilot, and thus system performance can be improved by suitably assigning the pilot sequences to the users within the cell, according to the desired metric. We show in this paper that UL and DL performances constitute conflicting metrics, in such a way that one cannot achieve the best performance in UL and DL with a single pilot assignment configuration. Thus, we propose an alternative metric, namely total capacity, aiming to simultaneously achieve a suitable performance in both links. Since the PA problem is combinatorial, and the search space grows with the number of pilots in a factorial fashion, we also propose a low complexity suboptimal algorithm that achieves promising capacity performance avoiding the exhaustive search. Besides, the combination of our proposed PA schemes with an efficient power control algorithm unveils the great potential of the proposed techniques in providing improved performance for a higher number of users. Our numerical results demonstrate that with 64 BS antennas serving 10 users, our proposed method can assure a 95%-likely rate of 4.2 Mbps for both DL and UL, and a symmetric 95%-likely rate of 1.4 Mbps when serving 32 users.

Keywords Massive MIMO · Pilot contamination · Pilot assignment · Joint uplink-downlink optimization · Heuristic · Power control

1 Introduction

Pilot contamination is the most salient impairment of massive multiple-input multiple-output (Ma-MIMO) systems [1,2]. Due to this issue, it can be shown that interference seen by each user is dependent on the pilot sequence he is employing. Thus, one can improve system performance by suitably assigning the pilots to the users in the cell, as discussed in [3] and [4]. The pilot assignment (PA) problem was solved in [3] from the uplink (UL) perspective, and a low-complexity near-optimal solution was proposed. Such simple and very efficient solution was possible due to the simple dependence between performance and pilot assignment seen in UL. Pilot contamination interference in UL is due to the signals transmitted from users in adjacent cells sharing a given pilot sequence that reaches certain base station (BS). The user that will experience such interference is the one to which this pilot sequence is assigned in the cell. Under a max-min optimization perspective, the solution proposed in [3] simply assigns the worst pilot sequences in a given instant, in terms of pilot contamination arising from adjacent cells, to the best located users, i.e., those with the higher long-term fading coefficients.

In [4], the PA problem was investigated from the downlink (DL) perspective, under several metrics. However, as the dependence of DL signal-to-interference-plus-noise ratio (SINR) with the pilot assignment occurs in a more complex way than in UL, the problem was solved only via exhaustive search. Different than UL, pilot contamination interference in DL is due to the signals transmitted from neighbouring BS's to the users at their respective cells sharing certain pilot sequence, but that inadvertently reaches the user in the considered cell employing this pilot. If this user changes its

✉ Taufik Abrão
taufik@uel.br

José Carlos Marinello
zecarlos.ee@gmail.com

Cristiano Magalhães Panazio
cpanazio@lcs.poli.usp.br

1 Department of Electrical Engineering, State University of Londrina, Londrina, PR, Brazil

2 Laboratory of Communications and Signals, Polytechnic School of the University of São Paulo, São Paulo, SP, Brazil

Published online: 12 April 2018

pilot sequence, part of the pilot contamination reaching him remains unchanged, since the distance between the user and adjacent cells as well as the long-term fading coefficients remain the same. The part of interference that changes is due to the power normalization factors, that retain some dependence with the UL pilot transmission stage, as better clarified in this manuscript, which also proposes low-complexity DL pilot assignment schemes.

A greedy PA scheme is proposed for optimizing the DL performance of cell-free Ma-MIMO systems in [5]. This new concept of Ma-MIMO system comprises a very large number of distributed single-antenna access points simultaneously serving a much smaller number of users. Although having considerably improved performance with respect to conventional collocated Ma-MIMO systems due to the diversity of long-term fading coefficients, the system implementation cost is significantly higher due to the complex backhaul network and the very large number of access points to be installed. Besides, the proposed PA scheme aims to improve just the DL performance. As shown in this paper, UL and DL optimization metrics constitute conflicting objectives, since if one scheme optimizes system DL performance, the UL performance will be close to that attained with random assignment, and vice-versa. Thus, our main purpose in this paper is to design a PA methodology able to jointly optimize DL and UL perspectives.

Another promising PA technique is proposed in [6] to improve UL performance, in which a weighted graph-coloring-based pilot decontamination scheme is developed. The solution consists in constructing an edge-weighted interference graph aiming to depict the potential pilot contamination between users, whereby two users in different cells are connected by a weighted edge, indicating the interference strength when they reuse the same pilot. Then, inspired by classical graph coloring algorithms, the proposed solution denotes each color as a pilot and each vertex as a user in the interference graph, which is able to improve performance by assigning different pilots to connected users with a large weight in a greedy way. On the other hand, an efficient PA technique for improving DL performance of wideband massive MIMO systems is proposed in [7] by exploiting channel sparsity. Authors employ Karhunen-Loéve Transform and Discrete Fourier Transform to capture the hidden sparsity of the channel, and find that the subspaces of the desired and interference channels are approximately orthogonal when the channels are represented with the aid of DFT basis. Then, a pilot assignment policy is designed to help identify the subspace of the desired channel, and a desired channel subspace aware least square channel estimator is derived to remove pilot contamination.

Several pilot assignment schemes have been proposed recently based on the location-aware approach [8,9]. Authors have proposed some filtering techniques which are able to significantly remove pilot contamination from channel estimates if the training signals transmitted from users of different cells sharing a given pilot reach the considered BS with different angle-of-arrivals (AOAs). For this sake, the location-aware PA technique assigns the pilots for users in the considered cell aiming to ensure that users utilizing the same pilot have distinguishable AOAs. However, all these schemes rely on the existence assumption of a line-of-sight component between BS and users, and of small channel angle spread of the multi-path components observed at the BS, typically observed in rural and sub-urban areas, or if the BS is much higher than the surrounded structures with few scatters around [9]. Since this is not always the case, we investigate in this paper PA schemes to be deployed in a less restrictive scenarios.

Power allocation is another efficient way of improving the performance of wireless communication networks. For the multicell massive MIMO scenario, the problem of power allocation was investigated in [10] under the perspective of maximizing the sum rate per cell. It was shown that the proposed method achieves substantial gains over the equal power allocation policy. However, for a practical system, maximizing the sum rate per cell is not the most suitable objective, since the performance of some users (tipically those at the edge) may be severely penalized in order to provide very increased rates for another ones. In [11], a max-min power allocation policy is proposed in conjunction with a multicell-aware regularized zero-forcing precoding to improve fairness in the massive MIMO DL. The proposed technique achieves substantially higher network-wide minimum rates than conventional techniques, but is applicable only for DL. On the other hand, in [12], a power allocation technique able to provide the same performance for all served users in DL and UL is proposed. The UL power allocation policy allocates for each user a power proportional to a desired received signal-to-noise ratio (SNR) at the BS divided by its long-term fading coefficient. Since shadowing have not been assumed in that work, one has just to ensure that this desired SNR level allows the cell boundary user to transmit without exceeding the maximum transmit power of its device. Clearly, in a more realistic scenario, a severely shadowed user near the cell edge may not be able to transmit with such power. A fairer optimization metric is adopted by the power control algorithm proposed in [13] for a code division multiple access network, which consists of providing a target performance for the majority of the users in the network. Since such approach is very suitable in the context of Ma-MIMO systems, we have adopted this distributed power control algorithm herein.

In this paper, we address the PA problem from jointly UL and DL perspectives. Since the performance bottleneck of Ma-MIMO systems is due to the edge users suffering with severe pilot contamination [1], we consider the objective of providing a target performance for the majority of

the users. For this sake, the pilot allocation metric of maximizing the minimum SINR is the most suitable, and our proposed scheme amalgamates such metric with the power control algorithm of [13], by only knowing the power and the long-term fading coefficients of users in adjacent cells. We first propose a low-complexity suboptimal solution of the MaxminSINR DL PA problem of [4]. Then, we show that the optimization under DL and UL perspectives are conflicting, since the optimal performance in both directions cannot be simultaneously achieved with any pilot configuration. We thus propose an alternative PA procedure from the definition of the overall system capacity, as the sum of DL and UL capacities. Our numerical results demonstrate that, under this metric, significant gains can be achieved in DL and UL concomitantly. Besides, a low complexity suboptimal approach for solving the joint UL-DL PA problem is discussed. Finally, we adapt the power control algorithm of [13] to the Ma-MIMO scenario with finite number of BS antennas, and show that much more significant gains can be attained by the PA schemes when combined with an efficient power control algorithm.

Our main contributions can be summarized as follows: i) different than [4] that solved the DL PA problem only via exhaustive search, we propose a near optimal low-complexity method for solving it; ii) different than [3–7], we investigate the PA optimization problem from both UL and DL perspectives, showing that a single pilot assignment configuration cannot lead to the optimal performance in both links at the same time; iii) we then formulate a novel PA optimization metric, namely the total capacity, which is able to achieve good performances in both links concomitantly; iv) a near optimal low-complexity solution for the total capacity PA problem is also proposed; v) we then combine the investigated PA techniques with an efficient power control algorithm, showing that even more impressive performances can be achieved.

The rest of this paper is organized as follows. The system model is described in Sect. 2, while the proposed pilot assignment optimization schemes are discussed in Sect. 3. The adopted power control algorithm are described in Sect. 4. Illustrative numerical results are explored in Sect. 5. Final remarks and conclusions are offered in Sect. 6.

2 System model

We consider a similar system model of [3,4], which is composed of L hexagonal cells, each one equipped with a N antennas BS serving K single-antenna users. Time division duplex (TDD) is assumed, thus reciprocity holds, and channel state information (CSI) is acquired by UL training sequences transmission. The $N \times 1$ channel vector between the BS of i-th cell and the k'-th user of j-th cell is denoted by $\mathbf{g}_{ik'j} = \sqrt{\beta_{ik'j}}\mathbf{h}_{ik'j}$, in which $\beta_{ik'j}$ denotes the long-term fading coefficient, comprising path loss and log-normal shadowing, $\mathbf{h}_{ik'j} \sim \mathcal{CN}(\mathbf{0}_N, \mathbf{I}_N)$ is the short-term fading channel vector, while $\mathbf{0}_N$ is a null column vector of size $N \times 1$, and $\mathbf{I}_N$ is the identity matrix of size N.

The pilot sequences' set is $\boldsymbol{\Psi} = [\boldsymbol{\psi}_1\ \boldsymbol{\psi}_2 \ldots \boldsymbol{\psi}_K] \in \mathbb{C}^{K\times K}$, and the sequence length is also K. This set of sequences is orthogonal, and thus $\boldsymbol{\Psi}^H\boldsymbol{\Psi} = \mathbf{I}_K$ holds, being $\{\cdot\}^H$ the Hermitian operator. If for the k'-th user is assigned the sequence $\boldsymbol{\psi}'_k = [\psi_{k'1}\ \psi_{k'2} \ldots \psi_{k'K}]^T$, being $\{\cdot\}^T$ the transpose operator, the received signal at the i-th BS during the training stage is

$$\mathbf{Y}_i^{\mathrm{p}} = \sqrt{\rho^{\mathrm{p}}}\sum_{j=1}^{L}\sum_{k=1}^{K}\mathbf{g}_{ikj}\boldsymbol{\psi}_k^H + \mathbf{N}_i^{\mathrm{p}}, \tag{1}$$

in which ρ^{p} is the UL pilot transmit power, $\mathbf{N}_i^{\mathrm{p}} \in \mathbb{C}^{N\times K}$ is the additive white Gaussian noise (AWGN) matrix with i.i.d. elements following a complex normal distribution with zero mean and variance σ_n^2. Note that we have assumed an uniform power allocation policy in the UL training stage. As discussed in [14], any effect of pilot power allocation can be alternatively achieved through transmit power allocation and constant pilot powers, and thus no loss is incurred in assigning a constant pilot power ρ^{p} to all users. The i-th BS then estimates the k'-th user CSI by correlating the received signal $\mathbf{Y}_i^{\mathrm{p}}$ with $\boldsymbol{\psi}'_k$

$$\widehat{\mathbf{g}}_{ik'} = \frac{1}{\sqrt{\rho^{\mathrm{p}}}}\mathbf{Y}_i^{\mathrm{p}}\boldsymbol{\psi}_{k'} = \sum_{j=1}^{L}\mathbf{g}_{ik'j} + \mathbf{v}_{ik'}, \tag{2}$$

where $\mathbf{v}_{ik'} = \frac{1}{\sqrt{\rho^{\mathrm{p}}}}\mathbf{N}_i^{\mathrm{p}}\boldsymbol{\psi}_{k'} \sim \mathcal{CN}(\mathbf{0}_N, \frac{\sigma_n^2}{\rho^{\mathrm{p}}}\mathbf{I}_N)$ is an equivalent noise vector. The pilot contamination effect can be clearly seen in the previous expression. By acquiring such CSI estimates, the BS is able to perform linear detection in the UL and linear precoding in the DL, deploying maximum ratio combining (MRC) and maximum ratio transmission (MRT), respectively. It is important to note that only BS has CSI estimates, obtained directly from UL pilot transmissions in (2), and thus no feedback channel is required. During UL data transmission, the i-th BS receives the signal

$$\mathbf{y}_i^{\mathrm{u}} = \sum_{j=1}^{L}\sum_{k=1}^{K}\sqrt{\rho_{kj}^{\mathrm{u}}}\mathbf{g}_{ikj}x_{kj}^{\mathrm{u}} + \mathbf{n}_i^{\mathrm{u}}, \tag{3}$$

in which ρ_{kj}^{u} and x_{kj}^{u} are the UL data transmit power and the data symbol, respectively, from the k-th user of the j-th cell, and $\mathbf{n}_i^{\mathrm{u}} \sim \mathcal{CN}(\mathbf{0}_N, \sigma_n^2\mathbf{I}_N)$ is the $N \times 1$ AWGN sample vector. This BS then estimates the transmitted symbol as

$$\widehat{x}_{k'i}^{\mathrm{u}} = \widehat{\mathbf{g}}_{ik'}^H\mathbf{y}_i^{\mathrm{u}}. \tag{4}$$

Similarly, during a DL data transmission, the k'-th user of the j-th cell receives the signal

$$y^{\mathrm{d}}_{k'j} = \sum_{i=1}^{L}\sum_{k=1}^{K}\sqrt{\rho^{\mathrm{d}}_{ik}}\mathbf{g}^{T}_{ik'j}\mathbf{p}_{ik}x^{\mathrm{d}}_{ik} + n^{\mathrm{d}}_{k'j}, \tag{5}$$

where ρ^{d}_{ik} and x^{d}_{ik} is the DL data transmit power and the DL data transmitted from the i-th BS to his k-th user, and $n^{\mathrm{d}}_{k'j} \sim \mathcal{CN}(0, \sigma^2_n)$ is an AWGN sample. Besides, $\mathbf{p}_{ik}$ is the beamforming vector that the i-th BS computes to precode its k-th user data. Deploying MRT, this vector is defined as [14]:

$$\mathbf{p}_{ik} = \frac{\widehat{\mathbf{g}}^{*}_{ik}}{||\widehat{\mathbf{g}}_{ik}||} = \frac{\widehat{\mathbf{g}}^{*}_{ik}}{\alpha_{ik}\sqrt{N}}, \tag{6}$$

in which the scalar $\alpha_{ik} = \frac{||\widehat{\mathbf{g}}_{ik}||}{\sqrt{N}}$ is a normalization factor necessary to guarantee that $||\sqrt{\rho^{\mathrm{d}}_{ik}}\mathbf{p}_{ik}x^{\mathrm{d}}_{ik}||^2 = \rho^{\mathrm{d}}_{ik}$.

Following the analysis in [2], it can be shown from (4) and (5) that the UL and DL SINR performance of Ma-MIMO systems with MRC and MRT are given, respectively, by

$$\varsigma^{\mathrm{u}}_{k'i} = \frac{\rho^{\mathrm{u}}_{k'i}\beta^2_{ik'i}}{\sum_{\substack{l=1\\ l\neq i}}^{L}\rho^{\mathrm{u}}_{k'l}\beta^2_{ik'l} + \frac{\alpha^2_{ik'}}{N}\left(\sum_{l=1}^{L}\sum_{k=1}^{K}\rho^{\mathrm{u}}_{kl}\beta_{ikl} + \sigma^2_n\right)}, \tag{7}$$

$$\varsigma^{\mathrm{d}}_{k'j} = \frac{\rho^{\mathrm{d}}_{jk'}\beta^2_{jk'j}/\alpha^2_{jk'}}{\sum_{\substack{l=1\\ l\neq j}}^{L}\rho^{\mathrm{d}}_{lk'}\beta^2_{lk'j}/\alpha^2_{lk'} + \frac{1}{N}\left(\sum_{l=1}^{L}\beta_{lk'j}\sum_{k=1}^{K}\rho^{\mathrm{d}}_{lk} + \sigma^2_n\right)}, \tag{8}$$

in which $\alpha^2_{jk} = \sum_{\ell=1}^{L}\beta_{jk\ell} + \frac{\sigma^2_n}{\rho^{\mathrm{p}}}$. It is straightforward to see from (7) and (8) that the asymptotic UL and DL SINR ($N \to \infty$) converge, respectively, to

$$\varsigma^{\mathrm{u}\infty}_{k'i} = \frac{\rho^{\mathrm{u}}_{k'i}\beta^2_{ik'i}}{\sum_{\substack{l=1\\ l\neq i}}^{L}\rho^{\mathrm{u}}_{k'l}\beta^2_{ik'l}}, \qquad \varsigma^{\mathrm{d}\infty}_{k'j} = \frac{\rho^{\mathrm{d}}_{jk'}\beta^2_{jk'j}/\alpha^2_{jk'}}{\sum_{\substack{l=1\\ l\neq j}}^{L}\rho^{\mathrm{d}}_{lk'}\beta^2_{lk'j}/\alpha^2_{lk'}}. \tag{9}$$

Although UL and DL SINR (9) are similar-looking expressions, they have different statistical characteristics as discussed in [1]. While interference in UL is irradiated from users in neighboring cells using the same k-th pilot sequence to the i-th BS, interference in DL is irradiated from neighboring BS's to the user in j-th cell employing the k-th pilot sequence. While in UL the receiver is fixed and the multiple transmitters are moving, in DL multiple fixed transmitters communicate with a mobile receiver. Besides, different behaviors will be seen in each direction with respect to pilot assignment, as explained in the following.

The performance of the Ma-MIMO system can be improved both via pilot assignment and by power control. The optimal performance is achieved solving a joint optimization problem of increased complexity due to the mixed variables' types: the pilot assignment is of discrete nature, while power control is of continuous nature. In this paper, we adopt a decoupled approach, in which the pilot assignment is performed assuming uniform power allocation, followed by a power control algorithm evaluated from the optimized pilot distribution.

3 Pilot assignment optimization

In this section, the Ma-MIMO system performance is improved by suitably assigning the pilot sequences to the users [3,4]. We assume a decentralized allocation procedure, in which PA is performed sequentially by each cell, regarding its covered users. The convergence of this procedure after few PA optimization rounds is discussed in [4], and shown by numerical results in [3].[1] Besides, in this pilot assignment stage, it is assumed the knowledge of users' power distribution in the cells, and the focus is at the asymptotic performance expressions in (9) for simplicity. Then, in Sect. 4, we evaluate the power control algorithm based on the pilot assignment obtained here, and demonstrate the performance improvements of our proposed schemes for finite number of antennas in Sect. 5. SINR expressions in (9) were obtained assuming that the k'-th pilot sequence[2] is assigned to the k'-th user, i.e., under a random strategy. However, if we assume that the p-th pilot is assigned to the c_p-th user in the i-th cell, the UL SINR can be rewritten as

$$\varsigma^{\mathrm{u}\infty}_{c_pi} = \frac{\rho^{\mathrm{u}}_{c_pi}\beta^2_{ic_pi}}{\sum_{\substack{j=1\\ j\neq i}}^{L}\rho^{\mathrm{u}}_{pj}\beta^2_{ipj}}, \tag{10}$$

that is the UL SINR of the user in the i-th cell employing the p-th pilot, namely the c_p-th user. The fixed uplink power distribution ρ^{u}_{pj}, for $p = 1, \ldots K$ and $j = 1, \ldots L$, is known for the i-th cell. The performance bottleneck in Ma-MIMO systems is due to users with severe pilot contamination [1]. Thus, a fair objective is to maximize the minimum UL SINR among the users, as the following optimization problem

[1] With the aid of game theory in [4][Sec. 4.1], it is shown that the PA problem can be seen as a restricted potential game, in which each cell is a player that chooses its strategy following a selfish best response dynamics. Therefore, the convergence of the game to a Nash equilibrium is guaranteed. Moreover, in [3][Fig. 3(c)], it is noted that the number of optimization rounds to PA convergence among cells decreases as long as the number of antennas at BS increases. For instance, three rounds are sufficient for convergence under 128 BS antennas.

[2] With "k'-th pilot sequence", we refer to the pilot of index k' in the set of available pilot sequences.

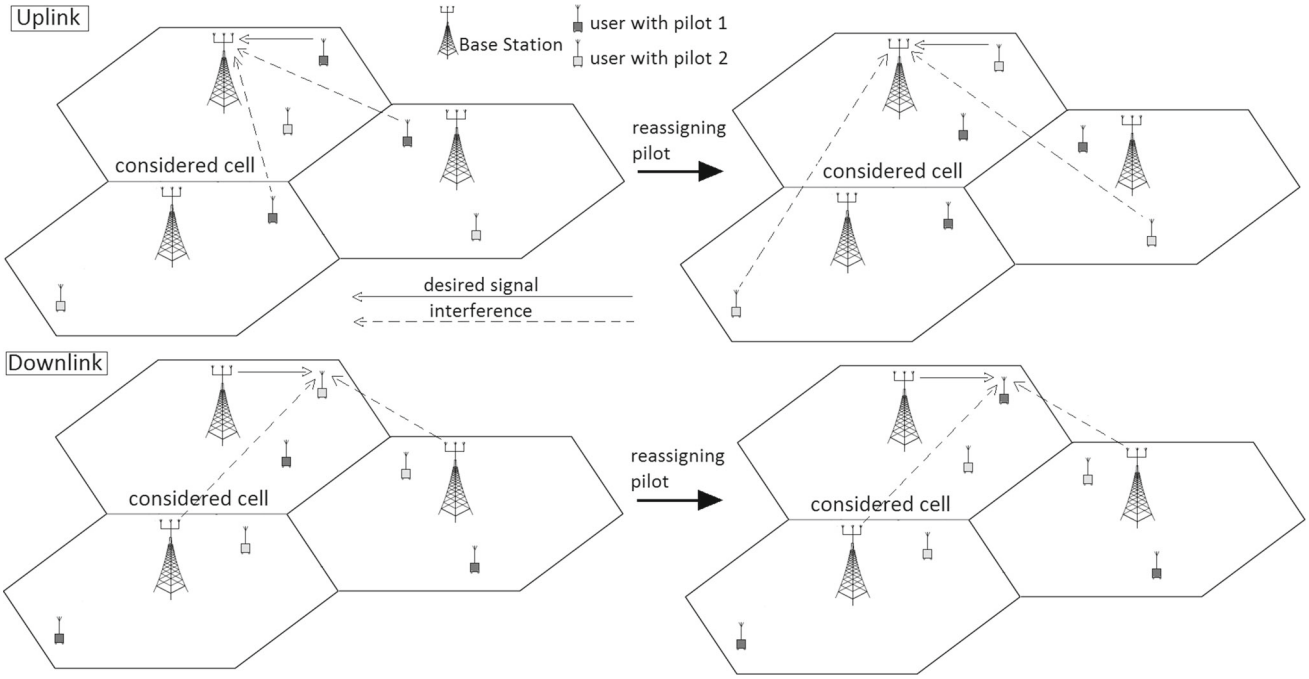

Fig. 1 Effect of reassigning pilot sequences in the consired cell, in UL (up) and DL (down). Although it appears from the Figure that reassigning pilots has no effect in DL, the previous UL pilot transmission stage results in some variations on the signals' strength

$$\mathcal{PA}_{\mathrm{u}} : \max_{l} \min_{p} \quad \varsigma^{\mathrm{u}\infty}_{c_{lp} i}, \tag{11}$$

in which c_{lp} is the l, p-th element of matrix $\mathbf{C} \in \mathbb{N}^{K! \times K}$, which contains every possible pilot assignment that a given cell can adopt. c_{lp} means that in the l-th PA combination, the p-th pilot is assigned to the c_{lp}-th user. According to (11), the obtained solution is the pilot assignment configuration in which the UL SINR of the user in the worst conditions is the highest possible. In terms of fairness and when aiming to provide a good and homogeneous performance to the users, this approach is much more effective than simply improving the average performance, as will be shown in Sect. 5.1. Obviously, the complexity of solving (11) via an exhaustive search grows with K in a factorial fashion. A viable and heuristic solution is proposed in [3], where the pilot sequences with the worst interference levels are assigned to the users with the highest long-term fading coefficients. Such *greedy method* achieves a near-optimal solution with reduced complexity.

On the other hand, the DL SINR in (9) can also be improved via pilot assignment. Assuming that the p-th pilot is assigned to the c_p-th user in the j-th cell, and that the downlink power distribution is known for the j-th cell, the DL SINR becomes

$$\varsigma^{\mathrm{d}\infty}_{c_p j} = \frac{\rho^{\mathrm{d}}_{j c_p} \beta^2_{j c_p j}}{\beta_{j c_p j} + \vartheta_{jp(j)}} \frac{1}{\sum_{\substack{i=1 \\ i \neq j}}^{L} \frac{\rho^{\mathrm{d}}_{i c_p} \beta^2_{i c_p j}}{\beta_{i c_p j} + \vartheta_{ip(j)}}}, \tag{12}$$

where $\vartheta_{ip(j)} = \sum_{\substack{\ell=1 \\ \ell \neq j}}^{L} \beta_{ip\ell} + \frac{\sigma_n^2}{\rho^{\mathrm{p}}}$ does not depend on for what user the p-th pilot will be assigned. Thus, an alternative PA optimization procedure for DL is proposed as:

$$\mathcal{PA}_{\mathrm{d}} : \max_{l} \min_{p} \quad \varsigma^{\mathrm{d}\infty}_{c_{lp} j}, \tag{13}$$

whose solution, similarly as (11), is the pilot assignment configuration in which the DL SINR of the user in the worst conditions is the highest possible.

One can see that the dependence of the DL SINR with the assignment of pilots to users is not so simple as it is in the UL scenario. However, communication systems are usually asymmetric, and DL data transmission might be predominant in comparison with UL data transmission. Therefore, solving the optimization problem in (13) in a low-complexity way is also quite appealing in practice. The main difficulty is that the interference in DL for the p-th pilot (denominator of the second term in (12)) is dependent on what user this sequence is assigned, and thus a greedy method cannot be applied as in [3]. If a user changes its pilot sequence, the DL interference due to pilot contamination reaching him is still mainly dominated by his long-term fading coefficients with respect to neighboring BS's, which do not change, as illustrated in Fig. 1. The exception is due to the DL normalization factors, that retain some dependence with the assigned pilot sequence from the uplink training channel estimation.

3.1 Joint UL-DL pilot assignment

One can note that the optimization problems of (11) and (13) are conflicting, as numerically demonstrated in the next Section. If the UL performance metric is optimized, the DL performance will be close to that attained with random assignment policy, and vice-versa. Thus, we elaborate our analysis aiming to jointly achieve the best possible performance in UL and DL, concurrently. One approach could be adopting multiobjective optimization. In this paper, we prefer a simpler strategy. We assume in the adopted TDD scheme a channel coherence block of $\mathcal{S}$ symbols, of which K are devoted to UL pilot transmission, $\xi^{\mathrm{u}}\left(\frac{\mathcal{S}-K}{\mathcal{S}}\right)$ and $\xi^{\mathrm{d}}\left(\frac{\mathcal{S}-K}{\mathcal{S}}\right)$ for UL and DL data transmission, respectively, in which the factors ξ^{u} and $\xi^{\mathrm{d}} \in (0, 1)$, $\xi^{\mathrm{u}}+\xi^{\mathrm{d}} = 1$, and both $\xi^{\mathrm{u}}(\mathcal{S}-K)$ and $\xi^{\mathrm{d}}(\mathcal{S}-K)$ are integers. Note that the factor $\left(\frac{\mathcal{S}-K}{\mathcal{S}}\right)$ represents the pilot overhead, since for each coherence block of $\mathcal{S}$ symbols, K are spent sending uplink pilots. Then, for a system bandwidth BW, the total capacity (TC) of the user in the i-th cell for which the p-th pilot is assigned is defined as

$$\mathcal{C}^{\mathrm{T}}_{c_p i} = \mathrm{BW}\left(\frac{\mathcal{S}-K}{\mathcal{S}}\right)\left[\xi^{\mathrm{u}}\log_2\left(1+\varsigma^{\mathrm{u}}_{c_p i}\right) + \xi^{\mathrm{d}}\log_2\left(1+\varsigma^{\mathrm{d}}_{c_p i}\right)\right] \tag{14}$$

Hence, an alternative optimization problem can be defined as

$$\mathcal{PA}_{\mathrm{TC}} : \max_{l}\min_{p} \quad \mathcal{C}^{\mathrm{T}\infty}_{c_{lp} i}, \tag{15}$$

in which $\mathcal{C}^{\mathrm{T}\infty}_{c_{lp} i}$ is obtained evaluating (14) from $\varsigma^{\mathrm{u}\infty}_{c_p i}$ and $\varsigma^{\mathrm{d}\infty}_{c_p i}$. In this case, the solution of (15) is the PA configuration in which the total capacity of the user in the worst conditions is the highest possible.

3.2 Heuristic pilot assignment solutions

For solving the DL assignment problem avoiding the exhaustive search, we first create a cost matrix $\mathbf{\Gamma}^{(i)} \in \mathbb{R}^{K\times K}$, whose j, p-th element is the DL SINR achieved by the j-th user in the i-th cell when the p-th pilot sequence is assigned to him, i.e., $\gamma^{(i)}_{jp} = \varsigma^{\mathrm{d}}_{c_p i}$ when $c_p = j$. Then, *our proposed low-complexity suboptimal solution* consists of finding the pilot with which each user achieves its maximal DL SINR. The user with the lowest maximal DL SINR will have such pilot sequence assigned to him. This procedure is repeated, excluding the users and the pilots already assigned, until allocating every pilot sequence, as described in Algorithm 1.

In order to obtain a low-complexity form for solving the joint UL-DL PA in (15) while achieving near-optimal performance, this same heuristic procedure can be applied. In this case, we initialize the cost matrix $\mathbf{\Gamma}^{(i)}$ (line 1 in Algorithm 1) in an alternative way, such that $\gamma^{(i)}_{jp} = \mathcal{C}^{\mathrm{T}}_{c_p i}$ when $c_p = j$, since the total capacity as defined in (14) is calculated as a weighted log function of both UL and DL SINR's. Then, we apply our proposed heuristic method in a similar way as in Algorithm 1.

Algorithm 1 Proposed Pilot Assignment Procedure

Input: $\beta_{jkl}, \forall j, l = 1, 2, \ldots L, k = 1, 2, \ldots K, \sigma^2_n, \rho_{\mathrm{p}}$.

1: Generate cost matrix $\mathbf{\Gamma}^{(i)}$, of size $K \times K$;
2: **for** $j = 1, 2, \ldots, K$ **do**
3: **for** $p = 1, 2, \ldots, K$ **do**
4: Evaluate $\delta_p = \max_{\ell=1,\ldots,K} \gamma^{(i)}_{p,\ell}$;
5: Evaluate $\eta_p = \arg\max_{\ell=1,\ldots,K} \gamma^{(i)}_{p,\ell}$;
6: **end for**
7: Evaluate $\phi = \arg\min_{p=1,\ldots,K} \delta_p$;
8: Evaluate $c^{(i)}_{\eta_\phi} = \phi$;
9: Invalidate the ϕ-th line and η_ϕ-th column of $\mathbf{0}^{(i)}$;
10: **end for**

Output: $\mathbf{c}^{(i)}$.

4 Power control algorithm

We assume a decentralized power allocation procedure, similarly to pilot assignment. With the purpose of serving the users with a target SINR, the target-SIR-tracking algorithm measures the interference seen by each user, and assigns to him the exact power to reach the target SINR, unless if this power exceeds the maximum power available. In this case, the maximum power is allocated for this user. It is shown in [13] that this power allocation procedure is not the most suitable, since assigning the maximum power for the users with poor channel conditions causes an excessive interference for the other users, and waste energy because this user may remain with a low SINR. Being $\hat{\varsigma}^{\mathrm{d}}_{k'\ell}$ the target downlink SINR for the k'-th user of the ℓ-th cell, and $\overline{\rho}^{\mathrm{d}}_{\ell k'}$ the maximum DL transmit power that can be assigned to him, the target-SIR-tracking algorithm updates power at the i-th iteration according to

$$\rho^{\mathrm{d}}_{\ell k'}(i) = \min\left[\hat{\varsigma}^{\mathrm{d}}_{k'\ell}\mathcal{I}^{\mathrm{d}}_{k'\ell}(i), \overline{\rho}^{\mathrm{d}}_{\ell k'}\right], \tag{16}$$

in which $\mathcal{I}^{\mathrm{d}}_{k'\ell}(i) = \rho^{\mathrm{d}}_{\ell k'}(i-1)/\varsigma^{\mathrm{d}}_{k'\ell}(i-1)$ is the interference plus noise seen by this user (denominator of (8)) divided by $\beta^2_{\ell k'\ell}/\alpha^2_{\ell k'}$. By contrast, the power control algorithm proposed in [13] updates users' powers as

$$\rho^{\mathrm{d}}_{\ell k'}(i) = \begin{cases} \hat{\varsigma}^{\mathrm{d}}_{k'\ell}\mathcal{I}^{\mathrm{d}}_{k'\ell}(i) \text{ if } \quad \mathcal{I}^{\mathrm{d}}_{k'\ell}(i) \le \frac{\overline{\rho}^{\mathrm{d}}_{\ell k'}}{\hat{\varsigma}^{\mathrm{d}}_{k'\ell}}, \\ \frac{\left(\overline{\rho}^{\mathrm{d}}_{\ell k'}\right)^2}{\hat{\varsigma}^{\mathrm{d}}_{k'\ell}\mathcal{I}^{\mathrm{d}}_{k'\ell}(i)} \quad \text{otherwise.} \end{cases} \tag{17}$$

One can see that the method of [13] assigns power to the users in the same way as the target-SIR-tracking algorithm if the target SINR can be achieved for the user at that iteration. Otherwise, instead of allocating him the maximum power, *it allocates him a transmit power inversely proportional to that required to achieve the target*. Thus, besides of saving energy relative to users that cannot reach the target SINR, the interference irradiated to other users also decreases. This procedure is repeated for a predefined number of iterations N_{it}, and the power coefficients for each user can be initialized with half of the maximum transmit power for him, as described in Algorithm 2. The convergence of such algorithm is proved in [13], and in our simulations we have noted that 10 iterations were sufficient for achieving convergence. Equivalently, this same procedure can be applied in UL user power allocation as

$$\rho^{\mathrm{u}}_{k'\ell}(i) = \begin{cases} \hat{\varsigma}^{\mathrm{u}}_{k'\ell}\mathcal{I}^{\mathrm{u}}_{k'\ell}(i) \text{ if } \mathcal{I}^{\mathrm{u}}_{k'\ell}(i) \leq \frac{\overline{\rho}^{\mathrm{u}}_{k'\ell}}{\hat{\varsigma}^{\mathrm{u}}_{k'\ell}}, \\ \frac{\left(\overline{\rho}^{\mathrm{u}}_{k'\ell}\right)^2}{\hat{\varsigma}^{\mathrm{u}}_{k'\ell}\mathcal{I}^{\mathrm{u}}_{k'\ell}(i)} \quad \text{otherwise,} \end{cases} \tag{18}$$

in which $\hat{\varsigma}^{\mathrm{u}}_{k\ell}$ is the target UL SINR of the user, $\overline{\rho}^{\mathrm{u}}_{k\ell}$ its maximum UL transmit power, and

$$\mathcal{I}^{\mathrm{u}}_{k'\ell}(i) = \frac{\sum_{\substack{l=1 \\ l\neq\ell}}^{L} \rho^{\mathrm{u}}_{k'l}(i-1)\beta^2_{\ell k'l} + \frac{\alpha^2_{\ell k'}}{N}\left(\sum_l \sum_k \rho^{\mathrm{u}}_{kl}(i-1)\beta_{\ell kl} + \sigma^2_n\right)}{\beta^2_{\ell k'\ell}}.$$

When deploying these power control algorithms, the target SINR parameter should be carefully chosen. If a somewhat lower value is adopted, the algorithm saves energy by delivering just the target SINR to the users, taking low advantage of the resources and providing poor performance for the system. If an excessive target SINR is considered, many poor located users will have their powers gradually turned off in order to provide the desired performance for the other users. Hence, in this paper, the target SINR was chosen in each scenario by finding the value that achieves the higher throughput for 95% of the users, by means of numerical simulations, as indicated in Table 3.

5 Numerical results

The Ma-MIMO system performance is numerically evaluated in this Section. We consider $L = 7$ interfering hexagonal cells of radius 1000 m, where K users are uniformly distributed, except in a circle of 100 m radius around the cell centered BS [4], with universal frequency and pilot reuse. This is equivalent to say that we consider the performance of a given cell with the interference from 6 nearest-neighbor cells, since only the performance metrics of users in central cell are computed. We consider a system bandwidth of

Algorithm 2 Power Control Algorithm

Input: β_{jkl} and $\overline{\rho}^{\mathrm{d}}_{lk}, \forall j, l = 1, 2, \ldots L, k = 1, 2, \ldots K, \sigma^2_n, \rho_{\mathrm{p}}$.

Initialize $\rho^{\mathrm{d}}_{jk'}(0) = 0.5\ \overline{\rho}^{\mathrm{d}}_{jk'}$;
for $i = 1, 2, \ldots, N_{it}$ **do**
  for $k' = 1, 2, \ldots, K$ **do**
    Evaluate $\mathcal{I}^{\mathrm{d}}_{k'j}(i) = \rho^{\mathrm{d}}_{jk'}(i-1)/\varsigma^{\mathrm{d}}_{k'j}(i-1)$;
    if $\mathcal{I}^{\mathrm{d}}_{k'j}(i) \leq \frac{\overline{\rho}^{\mathrm{d}}_{jk'}}{\hat{\varsigma}^{\mathrm{d}}_{k'j}}$ **then**
      Evaluate $\rho^{\mathrm{d}}_{jk'}(i) = \hat{\varsigma}^{\mathrm{d}}_{k'j}\mathcal{I}^{\mathrm{d}}_{k'j}(i)$;
    else
      Evaluate $\rho^{\mathrm{d}}_{jk'}(i) = \frac{\left(\overline{\rho}^{\mathrm{d}}_{jk'}\right)^2}{\hat{\varsigma}^{\mathrm{d}}_{k'j}\mathcal{I}^{\mathrm{d}}_{k'j}(i)}$;
    end if
  end for
end for
Output: $\rho^{\mathrm{d}}_{jk'}$.

20 MHz, a signal-to-noise ratio of 10 dB for pilot, UL data, and DL data transmission, and a TDD architecture similar to [12], with $\mathcal{S} = 100$[3] symbols, of which K are dedicated to UL pilot transmissions, and the remainder are equally divided between UL and DL data transmissions ($\xi^{\mathrm{u}} = \xi^{\mathrm{d}} = 0.5$). The path loss decay exponent was adopted as 3.8, and the standard deviation of the log-normal shadowing was assumed to be 8 dB. Besides, Table 1 describes the notation adopted when referring to the different techniques investigated in this Section.

5.1 Performance comparison between max-min and average PA optimization approaches

Our first objective in this Section is to justify the max-min approach choice when solving the PA optimization problem. For this purpose, we compare the performance of max-min approach with the conventional average approach, i.e., a PA strategy that finds the highest average SINR performance via exhaustive search. As described in Table 1, we refer to the PA method that obtains the highest mean DL SINR as MaxSINR DL, the one that obtains the highest mean UL SINR as MaxSINR UL, and the one that obtains the highest mean total capacity as MaxTC. Besides, we refer to the PA that solves (11) as MaxminSINR UL, the one solving (13) as MaxminSINR DL, and the solution of (15) as MaxminTC. Considering $N = 128$ antennas and $K = 4$ users, Table 2 shows the performance achieved by the different PA schemes in terms of mean achievable rates. As expected, MaxSINR DL, MaxSINR UL and MaxTC obtain the best mean performance on their respective metric (shown in bold in the Table). On the other hand, MaxminSINR DL, MaxminSINR UL, and MaxminTC presented a small decrease in mean

[3] Which can represent, for instance, a scenario with 1 ms of channel coherence time and 100 KHz of coherence bandwidth.

Table 1 Acronyms for the investigated schemes

Acronym	Technique
MaxSINR DL	The PA method that obtains the highest mean DL SINR via exhaustive search
MaxMinSINR DL	The PA method that solves (13) via exhaustive search
H-MaxMinSINR DL	Our proposed PA method that solves (13) applying Algorithm 1
H-MaxMinSINR DL PA+PC	H-MaxMinSINR DL combined with the power control of Algorithm 2
MaxSINR UL	The PA method that obtains the highest mean UL SINR via exhaustive search
MaxMinSINR UL	The PA method that solves (11) via exhaustive search
H-MaxMinSINR UL	The PA method that solves (11) proposed in [3]
H-MaxMinSINR UL PA+PC	H-MaxMinSINR UL combined with the power control of Algorithm 2
MaxTC	The PA method that obtains the highest mean Total Capacity via exhaustive search
MaxMinTC	The PA method that solves (15) via exhaustive search
H-MaxMinTC	Our proposed PA method that solves (15) applying Algorithm 1
H-MaxMinTC PA+PC	H-MaxMinTC combined with the power control of Algorithm 2

Table 2 Mean achievable rates for $N = 128$ and $K = 4$

PA Technique	DL (Mbps)	UL (Mbps)	TC (Mbps)
Random	28.46	24.79	53.25
MaxMinSINR DL	30.24	24.35	54.59
MaxSINR DL	**30.36**	24.45	54.8
MaxMinSINR UL	29.13	24.22	53.35
MaxSINR UL	28.07	**25.48**	53.55
MaxMinTC	29.79	24.41	54.21
MaxTC	29.92	25.32	**55.53**

achievable rates when compared to that obtained by MaxSINR DL, MaxSINR UL and MaxTC.

The main advantage of adopting the max-min approach instead of the average approach when solving the PA problem can be shown in Fig. 2, which compares the 95%-likely rate achieved by each PA technique with the increasing number of antennas. The 95%-likely rate corresponds to the rate assured to the users with probability of 95%, and thus can be used to compare how fair is the performance of a given technique. As one can note from Fig. 2, a significant gain can be seen when comparing a max-min based PA technique with its average based counterpart in terms of its respective performance metric. For example with 128 BS antennas, there is a 0.12 Mbps improvement in the 95%-likely DL rate of MaxminSINR DL in comparison with MaxSINR DL. Similarly, there is 0.05 Mbps improvement in the 95%-likely UL rate of MaxminSINR UL in comparison with MaxSINR UL, and a 1.01 Mbps improvement in the 95%-likely total capacity of MaxminTC in comparison with MaxTC. The reason why a higher 95%-likely performance is achieved at the same time that a lower average performance when adopting the max-min approach instead of the average one is depicted in Fig. 3 for the case of total capacity metric. A higher average performance is obtained by MaxTC PA providing higher rates for the users in the best channel conditions, while providing poor rates to the users in the worst channel conditions. On the other hand, MaxminTC PA aims to provide the best possible performance to the users in the worst channel conditions, while the users with higher channel coefficients still present good performances. This behavior is characterized by the PA performance curves crossing each other in Fig. 3, which means that the portion of users with very poor performances is higher in MaxTC than in MaxminTC, while the portion of users with very high performances is lower in MaxminTC than in MaxTC.

5.2 Performance of heuristic approach

We analyze in this subsection the performance obtained by the near optimal low-complexity PA solution of equations (11), (13) and (15). Besides, we discard the average based PA techniques like MaxSINR DL, MaxSINR UL, and MaxTC, since our main objective is to improve the performance guaranteed for the majority of users. The heuristic approach of each solution is referred by the respective method preceded by "H". Our objective herein is to demonstrate that the *heuristic solutions* of MaxminSINR UL, MaxminSINR DL, and MaxminTC *achieve practically the same performance of that attained with exhaustive search*, but with a feasible complexity. For this sake, Fig. 4 depicts the fraction of users above a given rate for 128 BS antennas, in terms of DL, UL, and total rate, and Fig. 5 shows the 95%-likely rate achieved by

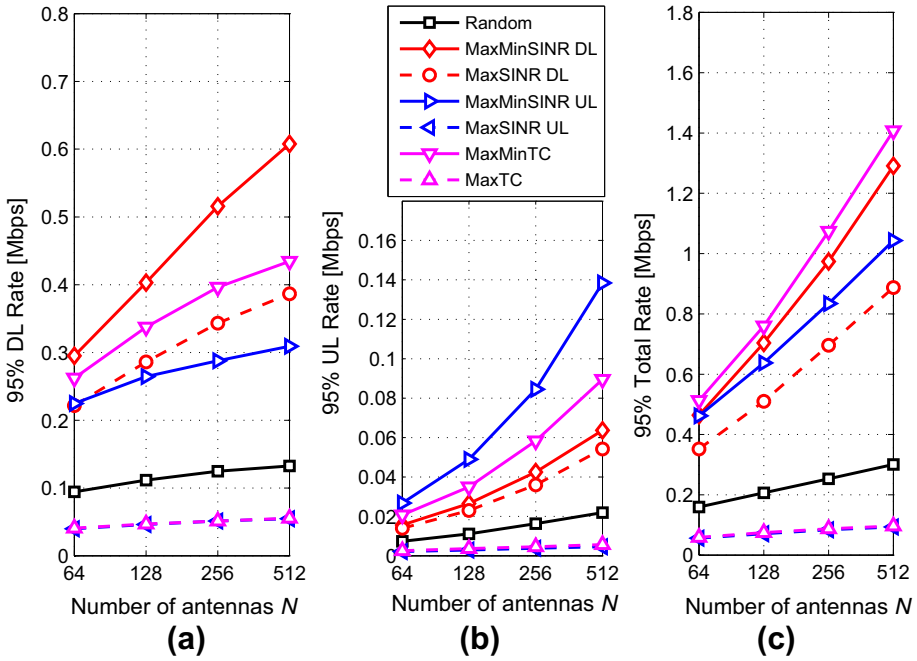

Fig. 2 95%-likely rate for $K = 4$: **a** DL; **b** UL; **c** Total

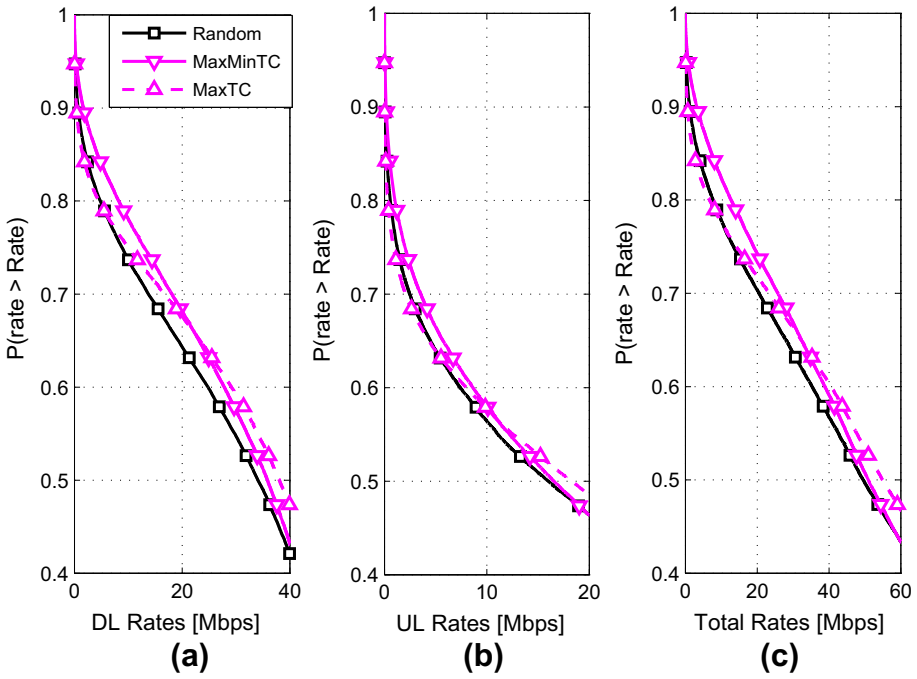

Fig. 3 Fraction of users above a given Rate for $N = 128$ and $K = 4$: **a** DL; **b** UL; **c** Total

each technique with increasing number of antennas. In both cases, an uniform power allocation policy was assumed for simplicity, and $K = 4$ users in order to allow the evaluation of exhaustive search in a feasible time. It is noteworthy from Fig. 4 the very unfair behavior of primitive Ma-MIMO systems (with no pilot and power allocation policies), which provides very high data rates for some portion of the users, while providing low quality of service for others. One can note also that appreciable improvements can be achieved with PA techniques, represented in Fig. 4 by a slight horizontal shift of the PA curves in the region of high probability. The conflicting behavior of UL and DL optimization metrics is also represented in the Figure, since while MaxminSINR DL achieves the best performance in DL, its UL performance is close to that attained by random PA. The opposite occurs with MaxminSINR UL. On the other hand, MaxminTC achieves good performance in both directions, at the same time that it achieves the best performance in terms of total rates. Besides, no significant performance loss can be seen for any heuristic PA when compared with its respective exhaus-

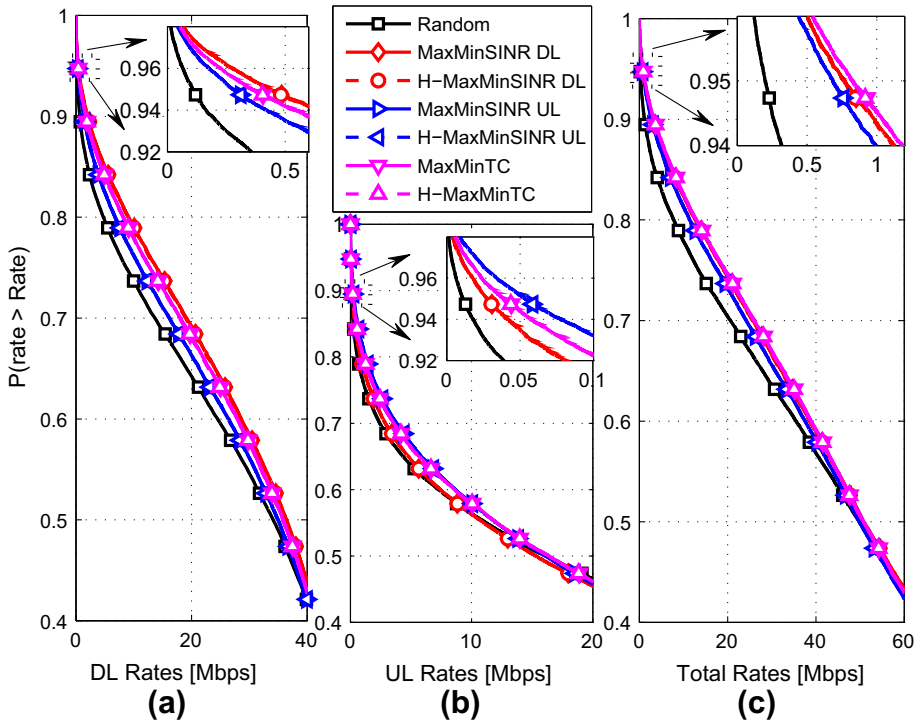

Fig. 4 Fraction of users above a given Rate for $N = 128$ and $K = 4$: **a** DL; **b** UL; **c** Total

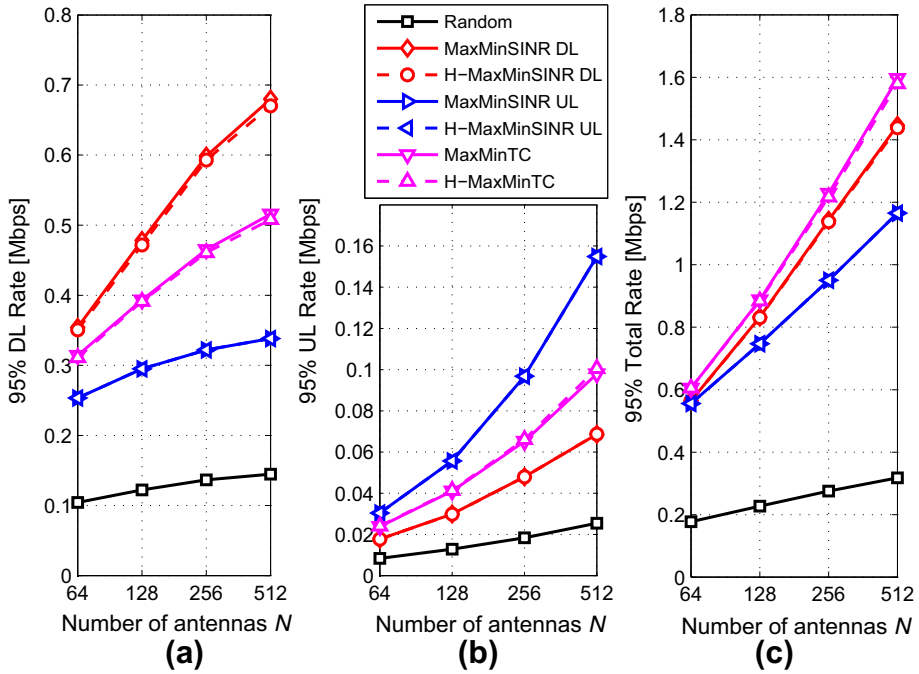

Fig. 5 95%-likely rate for $K = 4$: **a** DL; **b** UL; **c** Total

tive search solution. Similar findings can be taken from Fig. 5, that also reveals that is always beneficial improving the number of antennas in BS. One can note from Fig. 5 that MaxminSINR DL achieves the best 95%-likely DL rate, while MaxminSINR UL achieves the best 95%-likely UL rate and MaxminTC achieves the best 95%-likely total capacity. Besides, its heuristic counterparts produce almost the same 95%-likely performance of them.

5.3 Performance of pilot assignment with power control

Having demonstrated the good performances achieved by the heuristic PA techniques, our goal now is to demonstrate that the power control algorithm achieves a much improved performance when combined with an appropriate PA scheme. Besides, we discard the exhaustive search PA algorithms in

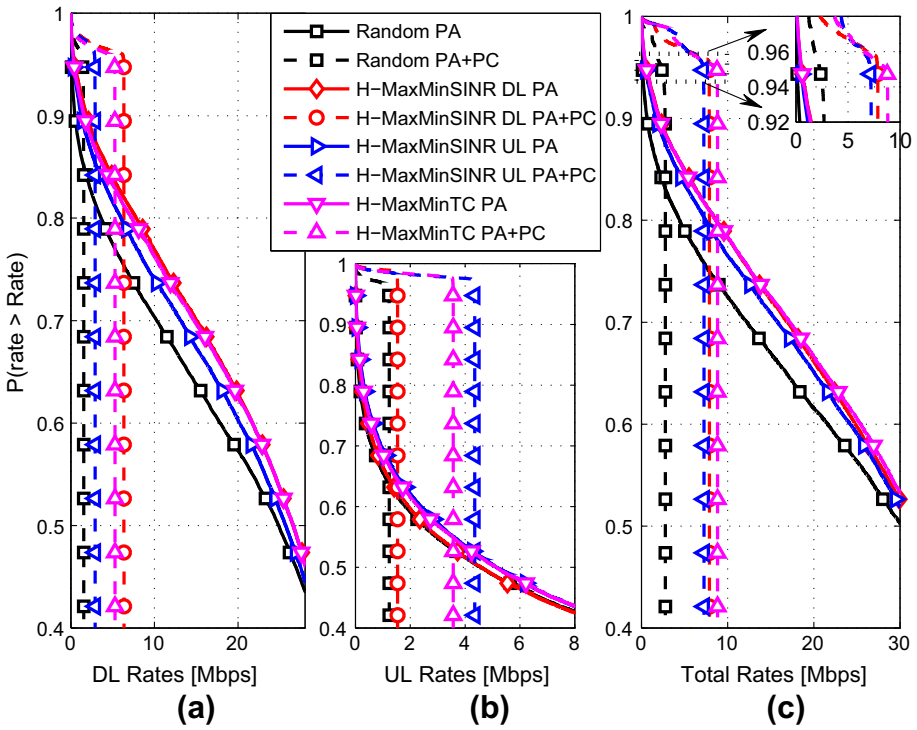

Fig. 6 Fraction of users above a given Rate for $N = 128$ and $K = 10$: **a** DL; **b** UL; **c** total. Power control evaluated with target SINR's of Table 3

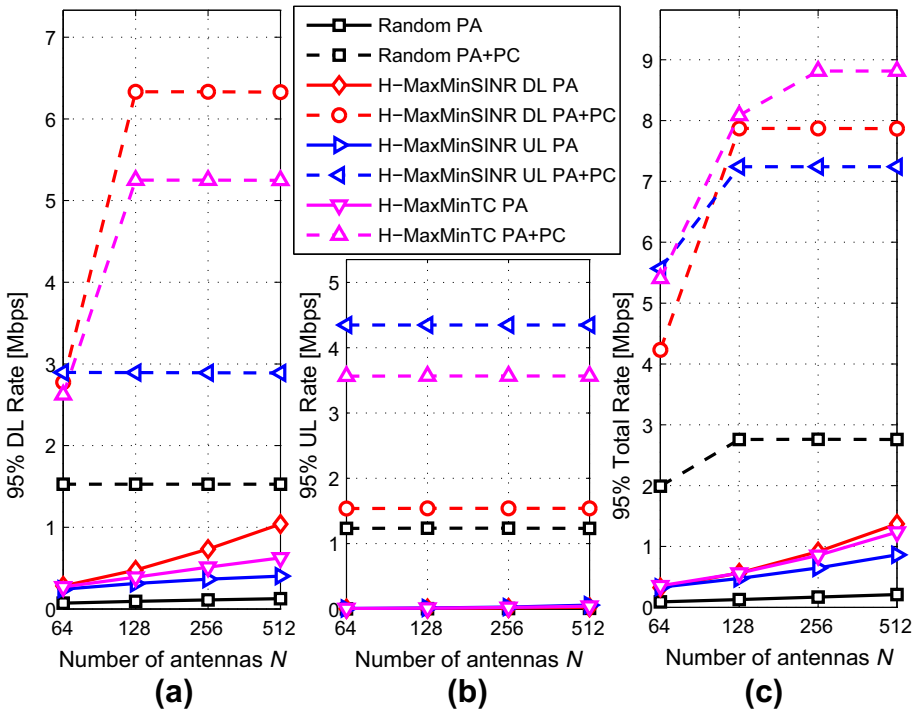

Fig. 7 95%-likely rate for $K = 10$: **a** DL; **b** UL; **c** total. Power control evaluated with target SINR's of Table 3

order to enable a higher number of users. For $K = 10$ and employing power control, Fig. 6 shows the fraction of users above a given rate for $N = 128$, while Fig. 7 shows the 95%-likely rate achieved with increasing number of antennas. The target SINR's performances of power control algorithm for each scheme were empiricaly chosen in order to provide the higher throughput for 95% of the users, as indicated in Table 3. It can be seen that much more uniform user performances are achieved with the power control scheme of Algorithm 2, and that the assured performance can be considerably improved with a proper choice of the PA employed. For example, as can be seen in Fig. 7, with random assignment the 95%-likely DL rate increases from 92.5 to 1.528 Mbps with $N = 128$ antennas when employing power control, while

Table 3 Target SINR's of power control algorithm adopted for each PA technique

Number of users	PA scheme	DL (dB)	UL (dB)
$K = 10$	Random	− 9	− 10
	H-MaxminSINR DL	− 2	− 9
	H-MaxminSINR UL	− 6	− 4
	H-MaxminTC	− 3	− 5
$K = 32$	Random	− 11	− 14
	H-MaxminSINR DL	− 7	− 11
	H-MaxminSINR UL	− 9	− 7
	H-MaxminTC	− 7	− 8

this DL rate increase is from 388.3 to 5.251 Mbps when the H-MaxminTC is the PA adopted. Similarly, in the UL, the 95%-likely UL rate with random assignment increases from 3.4 to 1.235 Mbps when employing power control, and from 11.4 to 3.566 Mbps with H-MaxminTC as PA policy and $N = 128$. It can also be seen that H-MaxminTC with power control has the ability of jointly assure an appreciable quality of service in both DL and UL, contrary to H-MaxminSINR DL and H-MaxminSINR UL that assure good rates only on its preferential direction. These results demonstrate that much more significant performance improvements can be obtained from the power control algorithm with a proper choice of the PA method.

Figures 8 and 9 do the same with $K = 32$ users, from which similar findings can be taken. While the 95%-likely DL rate for $N = 128$ antennas under random pilot assignment increase from 41.3 to 746.2 kbps, this DL rate increase with H-MaxminTC is from 191.6 to 1.782 Mbps. Similarly for the 95%-likely UL rate with $N = 128$, this gain under random PA is from 0.5 to 382.5 kbps, and from 2.0 kbps to 1.442 Mbps with H-MaxminTC PA. The decrease in the assured rates with this higher number of users is due not only to the increased multiuser interference, but also to the increased pilot overhead, necessary to obtain CSI estimates of this increased number of users. On the other hand, it allows the PA schemes to achieve improved gains in comparison with random assignment because of the greater multiuser diversity.

5.4 Performance with target rates

Performance results with power control as depicted in Figs. 6, 7, 8 and 9 were obtained after a careful but non-exhaustive process of finding suitable target SINR performances for each scheme under the considered scenarios, as summarized in Table reftab:SINRspstgt. However, this values of target performances are dependent of the instantaneous conditions of the communications systems, like the number of users served and pilot and data SNR's, which are dynamically changing. Thus, a more practical scenario consists in fixing a DL and UL target rates, from which the target SINR's input parameters of the power control algorithm are obtained. Under this strategy, Fig. 10 shows the 95%-likely rates obtained when fixing a target per user rate of 4.2 Mbps for both DL and

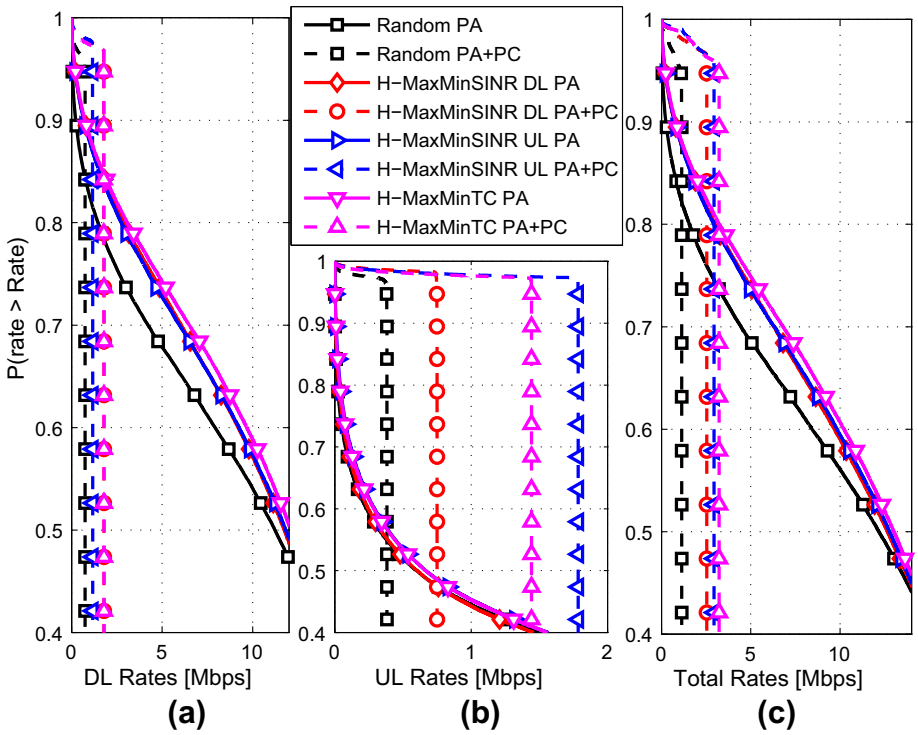

Fig. 8 Fraction of users above a given rate for $N = 128$ and $K = 32$: **a** DL; **b** UL; **c** total. Power control evaluated with target SINR's of Table 3

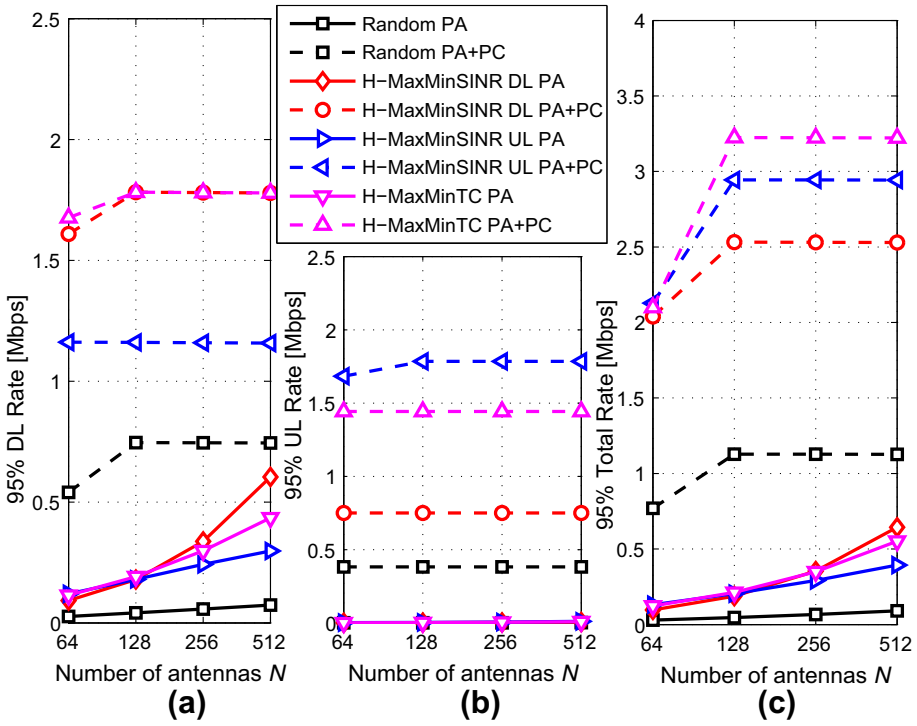

Fig. 9 95%-likely rate for $K = 32$: **a** DL; **b** UL; **c** total. Power control evaluated with target SINR's of Table 3

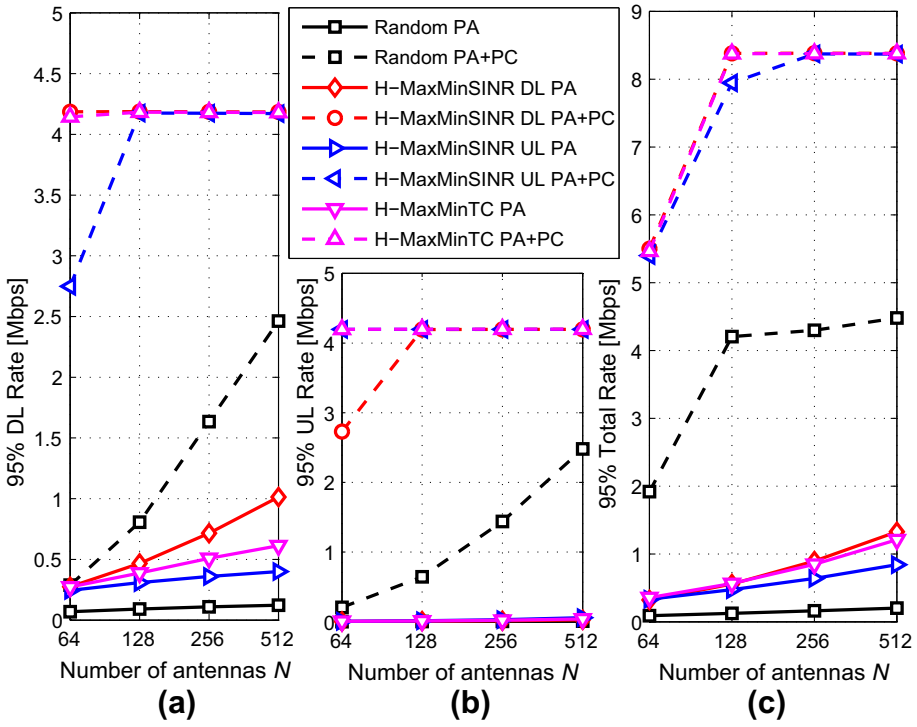

Fig. 10 95%-likely rate for $K = 10$: **a** DL; **b** UL; **c** total. Power control evaluated with a target rate of 4.2 Mbps per user, for both UL and DL

UL when serving $K = 10$ users, while Fig. 11 does the same with 1.4 Mbps of target rates for both DL and UL when serving $K = 32$ users. It can be seen from Fig. 10 that H-MaxminTC PA with power control is able to assure the target rates in both DL and UL even with just $N = 64$ antennas, in a situation where the multiuser interference is only partially supressed by the moderate number of BS antennas. On the other hand, H-MaxminSINR DL PA with power control fails in this objective in UL for $N = 64$, while H-MaxminSINR UL could not achieve this target performance in DL with this same number of antennas. It is important to note that even with the 95%-likely DL and UL rate of 4.2,Mbps assured

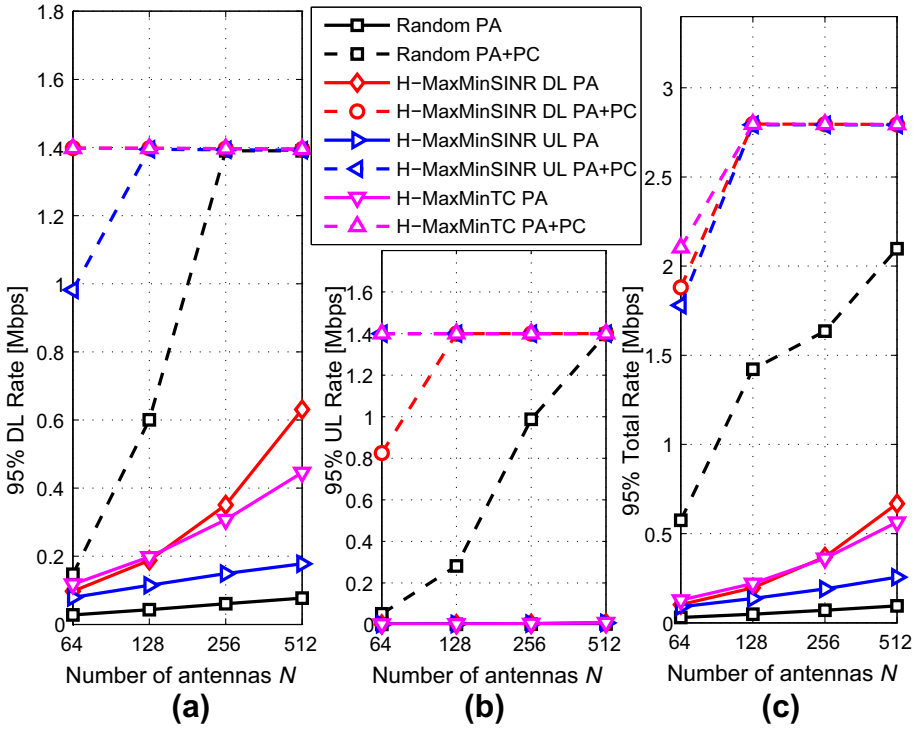

Fig. 11 95%-likely rate for $K = 32$: **a** DL; **b** UL; **c** total. Power control evaluated with a target rate of 1.4 Mbps per user, for both UL and DL

by H-MaxminTC PA with power control, it is not assured a 95%-likely total rate of 8.4 Mbps, since the set of users that do not achieve the target DL rate is not necessarily the same that do not achieve the target UL rate. Very similar conclusions can be made from Fig. 11, which shows that H-MaxminTC PA with power control is able to assure an appreciable 95%-likely DL and UL per user rates of 1.4 Mbps for $K = 32$ users with only $N = 64$ BS antennas. Again, these results demonstrate the great potential of PA techniques in conjunction with power control algorithms in providing improved and homogeneous performance for a larger number of users in both DL and UL.

6 Discussion and final remarks

The PA optimization problem was addressed in this paper. Different from previous works, we have investigated the problem from both UL and DL perspectives. We demonstrate that the max-min approach when solving the PA problem is much more effective than the average approach when aiming to provide a good performance for the majority of the users. Our analysis have also shown that, due to the different characteristics of UL and DL SINR expressions in Ma-MIMO, the PA optimization problems in UL and DL are conflicting. If the UL performance is optimized, it incurs in a limited performance in DL, and vice-versa. Thus defining a simple alternative metric, i.e., the total capacity, one can find a PA strategy for Ma-MIMO that achieves promising performance in both directions simultaneously. To avoid exhaustive search of factorial order, a heuristic solution capable of finding a near-optimal solution expending reduced computational complexity has been also proposed. Finally, we have adapted the target-SIR-tracking power control algorithm to our scenario of massive MIMO systems with finite number of BS antennas, and the investigated PA schemes have been combined with it. Our results demonstrated that much more improved gains can be achieved by this power control algorithm if applied after a suitable pilot assignment procedure. For example, our proposed H-MaxminTC PA scheme with power control was able to provide a 4.2 Mbps per user rate for both DL and UL with 95% probability when serving 10 users with only 64 antennas at BS, while an assured symmetric per user rate of 1.4 Mbps is achieved when serving 32 users with 64 antennas.

Acknowledgements This work was supported in part by the National Council for Scientific and Technological Development (CNPq) of Brazil under Grant 304066/2015-0 and in part by Londrina State University - Paraná State Government (UEL).

References

1. Marzetta, T. (2010). Noncooperative cellular wireless with unlimited numbers of base station antennas. *IEEE Transactions on Wireless Communications*, *9*(11), 3590–3600.
2. Marzetta, T., Larsson, E., Yang, H., & Ngo, H. (2016). *Fundamentals of Massive MIMO*. New York, NY: Cambridge University Press.

3. Zhu, X., Wang, Z., Dai, L., & Qian, C. (2015). Smart pilot assignment for massive MIMO. *IEEE Communications Letters*, *19*(9), 1644–1647.
4. Marinello, J. C., & Abrão, T. (2016). Pilot distribution optimization in multi-cellular large scale MIMO systems. *AEU - International Journal of Electronics and Communications*, *70*(8), 1094–1103.
5. Ngo, H. Q., Ashikhmin, A., Yang, H., Larsson, E. G., & Marzetta, T. L. (2017). Cell-free massive MIMO versus small cells. *IEEE Transactions on Wireless Communications*, *16*(3), 1834–1850.
6. Zhu, X., Dai, L., Wang, Z., & Wang, X. (2017). Weighted-graph-coloring-based pilot decontamination for multicell massive MIMO systems. *IEEE Transactions on Vehicular Technology*, *66*(3), 2829–2834.
7. Chen, Z., & Yang, C. (2016). Pilot decontamination in wideband massive MIMO systems by exploiting channel sparsity. *IEEE Transactions on Wireless Communications*, *15*(7), 5087–5100.
8. Zhao, P., Wang, Z., Qian, C., Dai, L., & Chen, S. (2016). Location-aware pilot assignment for massive MIMO systems in heterogeneous networks. *IEEE Transactions on Vehicular Technology*, *65*(8), 6815–6821.
9. Wang, Z., Zhao, P., Qian, C., & Chen, S. (2016). Location-aware channel estimation enhanced TDD based massive MIMO. *IEEE Access*, *4*, 7828–7840.
10. Zhang, Q., Jin, S., McKay, M., Morales-Jimenez, D., & Zhu, H. (2015). Power allocation schemes for multicell massive MIMO systems. *IEEE Transactions on Wireless Communications*, *14*(11), 5941–5955.
11. Zarei, S., Aulin, J., Gerstacker, W., & Schober, R. (2017). Max-min multicell-aware precoding and power allocation for downlink massive MIMO systems. *IEEE Signal Processing Letters*, *24*(10), 1433–1437.
12. Björnson, E., Larsson, E. G., & Debbah, M. (2016). Massive MIMO for maximal spectral efficiency: How many users and pilots should be allocated? *IEEE Transactions on Wireless Communications*, *15*(2), 1293–1308.
13. Rasti, M., & Sharafat, A.-R. (2011). Distributed uplink power control with soft removal for wireless networks. *IEEE Transactions on Communications*, *59*(3), 833–843.
14. Fernandes, F., Ashikhmin, A., & Marzetta, T. (2013). Inter-cell interference in noncooperative TDD large scale antenna systems. *IEEE Journal on Selected Areas in Communications*, *31*(2), 192–201.

José Carlos Marinello received his B.S. and M.S. degree in Electrical Engineering (the first with Summa Cum Laude) from Londrina State University, PR, Brazil, in December 2012 and Sept 2014, respectively. He is currently working towards his Ph.D. at Polytechnic School of Sao Paulo University, São Paulo, Brazil. His research interests include signal processing and wireless communications, especially massive multiple-antenna precoding/decoding techniques, acquisition of channel-state information, multicarrier modulation, cross-layer optimization of MIMO/OFDM systems, interference management and 5G.

Cristiano Panazio received Engineer's and Master's degrees in Electrical Engineering in 1999 and 2001, respectively, from State University of Campinas and a PhD degree in Telecommunications in 2005 from the Conservatoire National des Arts et Métiers. Currently, he is assistant professor at the Laboratory of Communications and Signals of the Escola Politécnica of the University of São Paulo. He is a member of the Brazilian Telecommunications Society (SBrT) and has served as an Associate Editor of the IEEE TRANSACTIONS ON CIRCUITS AND SYSTEMS – I from 2015 to 2017. His research interests are adaptive equalization (data aided and blind), synchronization techniques, mobile communications, multicarrier modulation and space-time transceivers.

Taufik Abrão (M'97–SM'12) received the B.S., M.Sc., and Ph.D. degrees in electrical engineering from the Polytechnic School, University of São Paulo, São Paulo, Brazil, in 1992, 1996, and 2001, respectively. Since 1997, he has been with the Communications Group, Department of Electrical Engineering, Londrina State University, Paraná, Brazil, where he is currently an Associate Professor of Telecommunications and the Head of the Telecomm and Signal Processing Laboratory. From 2007 to 2008, he was a Post-Doctoral Researcher with the Department of Signal Theory and Communications, Polytechnic University of Catalonia, Barcelona, Spain. In 2012, he was an Academic Visitor with the Southampton Wireless Research Group, University of Southampton, Southampton, U.K. He has participated in several projects funded by government agencies and industrial companies. He is involved in editorial board activities of six journals in the telecommunications area and has served as a TPC Member in several symposiums and conferences. He has supervised 23 M.Sc. and three Ph.D. students, and three post-doctoral students, co-authored ten book chapters on mobile radio communications and more than 230 research papers published in specialized/international journals and conferences. His current research interests include communications and signal processing, especially massive MIMO, multiuser detection and estimation, Filter bank, OFDM, CDMA systems, cooperative communication, resource allocation, heuristic and convex optimization aspects for 5G wireless systems. He is a senior member of the IEEE and SBrT. He has served as an associate Editor of the *IEEE Communications Surveys and Tutorials* since 2013, the *IET Journal of Engineering* since 2014, the *IEEE Access* since 2016, and as an executive Editor of the *Transactions on Emerging Telecommunication Technologies Wiley* since 2018.

APPENDIX E – Full paper submitted to the journal "*IEEE Systems Journal*"

Title: Total Energy Efficiency of TD- and FD-MRC Receivers for Massive MIMO Uplink.

Authors: José Carlos Marinello Filho, Cristiano Panazio, Taufik Abrão and Stefano Tomasin.

Journal: IEEE Systems Journal (ISSN 1932-8184).

Classification (Qualis-CAPES): A1 / IF$= 3.882$ (Engenharias IV).

Submission Date: February 2018.

Total Energy Efficiency of TD- and FD-MRC Receivers for Massive MIMO Uplink

José Carlos Marinello, Cristiano Panazio, Taufik Abrão, Stefano Tomasin

***Abstract*—This paper proposes a detailed investigation on the uplink (UL) performance of massive multiple-input-multiple-output (maMIMO) systems employing maximum-ratio combining at the receiver. While most papers in maMIMO literature assume orthogonal frequency-division multiplexing (OFDM), current standards like LTE employ single-carrier (SC) waveform in the UL due to several benefits. We thus perform a systemic comparison between two fundamental schemes: the time-reversal MRC (TRMRC) operating under SC, and the frequency-domain MRC (FDMRC) employed with OFDM. It was recently shown that TRMRC outperforms FDMRC in terms of achievable rates, since SC systems do not require the cyclic prefix (CP) of OFDM. On the other hand, the computational complexity of TRMRC algorithm is higher than that of FDMRC, even when efficient solutions are employed (e.g., fast convolution with the overlap-and-add method). Hence, the best scheme for the UL maMIMO systems still remains an open question. The main contribution of this paper is the comparison of the total energy efficiency of both TRMRC and FDMRC when used in the UL of maMIMO systems. Our results show that, for current typical system parameters, FDMRC/OFDM achieves a higher total energy efficiency than TRMRC/SC. However, if the cell radius is below 300m and/or the computational efficiency increases by 30% regarding the current processors, the TRMRC under SC waveform becomes more attractive for the UL of maMIMO systems.**

***Index Terms*—Large Scale MIMO; Energy Efficiency; TDD; single-carrier, multi-carrier; optimization.**

I. Introduction

Massive multiple-input-multiple-output (maMIMO) technology is one of the most promising candidates for the physical layer of the upcoming fifth generation of mobile communications systems (5G) [1]. It is widely known that maMIMO systems achieve very appreciable spectral and energy efficiencies [2], and thus they have been the focus of several research papers recently. As long as the number of base station (BS) antennas of a time-division duplex (TDD) multicellular system grows without bound, coherent interference is the only limiting effect under independent and identically distributed (i.i.d.) Rayleigh fading channels [1]. This kind of interference results from pilot contamination, which in turn results from the unavoidable reuse of reverse-link pilot sequences between users of different cells due to the limited channel coherence block. On the other hand, every type of non-coherent interference, *i.e.*, thermal noise, intracell interference, and intercell interference from users with different pilots, vanishes in this scenario [1]. As a positive consequence, the simplest schemes for detection in uplink (UL) and for precoding in downlink (DL) become optimal [3], like maximum ratio combining (MRC) and maximum ratio transmission (MRT), respectively.

Most papers in the area of maMIMO assumes orthogonal frequency-division multiplexing (OFDM) as a way of dealing with inter-symbol interference. In the seminal maMIMO paper [3], the author has highlighted several aspects of the proposed technology in conjunction with OFDM waveform. In [2], a first detailed investigation about maMIMO energy and spectral efficiencies have been conducted, assuming OFDM waveform. In [4], the authors have found the conditions in which the maximal spectral efficiency of maMIMO systems employing OFDM waveform can be achieved in different scenarios. A detailed study about power allocation schemes applied to OFDM based maMIMO systems has been conducted in [5].

On the other hand, single-carrier (SC) waveform has been widely used in the UL of current standards, such as LTE. Several advantages of employing SC in the UL instead of OFDM can be highlighted [6], [7], such as: **i**) the transmit signal lower peak-to-average power ratio (PAPR), which results in cheaper and more energy efficient mobile terminals (MTs). Besides, this incurs in a reduced distortion level imposed by the transmit amplifier, and consequently in a lower out-of-band radiation, simplifying spectrum shaping and increasing spectral efficiency due to a lower guard band required. **ii**) Lower sensitivity to phase noise and carrier frequency offset (CFO). **iii**) Reduced complexity of the MT since the inverse fast Fourier transform (IFFT) operation is not required. **iv**) Under the maMIMO condition, it is shown in [7] that cyclic prefix (CP) transmission is not required employing TRMRC in conjunction with SC, while improving spectral and energy efficiencies. Due to the above mentioned benefits, in conjunction with the compatibility with the current standards, this waveform has been seen as a promising candidate for implementation in standards, such as 5G [8].

SC receivers normally require complex equalization techniques in either time or frequency domain, such as decision-feedback equalizer (DFE) [9]. The computational complexity of frequency domain equalization is often lower than that of its time-domain version [10], but usually requiring CP transmission and one fast Fourier transform (FFT) module per receive antenna similarly to OFDM. On the other hand, time-domain equalization provide a good performance at the expense of higher complexity, not requiring CP and FFT operations. However, when combined with maMIMO, a different time-domain receiver can be employed, which alleviates the equalization complexity by taking advantage of the large excess of BS

J. C. Marinello and T. Abrão are with the Electrical Engineering Department, State University of Londrina, PR, Brazil. E-mail: zecarlos.ee@gmail.com; taufik@uel.br

C. Panazio is with the Laboratory of Communications and Signals, Polytechnic School of the University of São Paulo, SP, Brazil. E-mail: cpanazio@lcs.poli.usp.br

S. Tomasin is with the Department of Information Engineering, University of Padova, Via Gradenigo 6/B, 35131, Padova, Italy. E-mail: tomasin@dei.unipd.it

antennas, namely the time-reversal MRC (TRMRC) receiver [11]. The TRMRC receiver coherently combines the received symbols arising from different paths with the appropriate channel impulse response (CIR) vector. The robustness of this scheme was investigated in [11] against the phase noise effect, and a DL version of the scheme was proposed in [12], but under a scenario with no pilot contamination in both cases.

In [13], an improved TRMRC receiver is proposed which performs the CFO estimation/compensation together with the equalization procedure. Authors have shown that the proposed scheme performance approaches the ideal/zero CFO performance with the increasing frequency selectivity of the channel. Another DL SC solution for massive MIMO [14] proposes a SC frequency domain precoding scheme. The main difference of this scheme with respect to that of [12] is the frequency domain processing, which significantly reduces the computational complexity. Besides, several other papers regarding SC combine this waveform with spatial modulation (SM) [15], [16], a promising multiple antenna modulation scheme which activates only a subset of the available antennas, and the indices of the activated antennas convey information. Schemes combining SM and SC have attracted much research attention recently aiming at combining the advantages of both schemes, for example lower number of required radio-frequency chains of SM, and lower PAPR of SC.

An interesting comparison of receiver/waveforms for the UL of maMIMO systems has been conducted in [7] and [17]. In [17], the UL performance of SC and OFDM receivers are compared for single cell maMIMO systems employing one-bit analog-to-digital converters (ADCs), which significantly reduce the power consumption of BSs. Both schemes have a very similar performance and one-bit ADCs work well with maMIMO systems in the investigated scenario without pilot contamination. On the other hand, under pilot contamination, the TRMRC scheme operating with SC waveform has been compared with the conventional FDMRC in conjunction with OFDM in [7]. The authors have found very similar expressions for the performance of both schemes in terms of signal-to-interference-plus-noise ratio (SINR). However, higher achievable rates can be attained by TRMRC under SC, since this scheme does not require CP transmission, in contrast with FDMRC and OFDM. However, it was shown that the computational complexity demanded by the former is somewhat higher. Even if employing a reduced complexity algorithm with the aid of fast convolution techniques with overlap-and-add, similarly as the overlap-and-save method applied for single-input-single-output (SISO) SC systems in [10], the complexity of the TRMRC algorithm is $\mathcal{O}(\log_2(2L)MK)$, in contrast with the ($\mathcal{O}(MK)$) of FDMRC [7]. At this point, the question of what scheme consists in a better candidate for the UL of upcoming maMIMO systems remains without a complete answer, since each scheme has advantages from different perspectives.

In [18] and [19], the authors have assessed the total energy efficiency of maMIMO systems operating with OFDM waveform. In [18], authors found that the optimal energy efficiency is attained with a maMIMO setup wherein hundreds of antennas are deployed to serve a relatively large number of users if using zero forcing processing. The total energy efficiency metric computes how many bits are transmitted per Joule of energy, but taking into account every energy expenditure of the communication system. Accurate power consumption models are presented in [18] for the several stages of a practical communication system, like the power consumed by the transceiver chains, the channel estimation process, the coding and decoding units, the backhaul, the linear processing algorithms, and also by the radiated signal power.

In this paper, our main objective is to *answer which waveform between SC and OFDM is the most suitable for implementation in the maMIMO UL considering MRC receiver*. Our choice for these two waveforms is because they are the most consolidated technologies, and therefore the most prominent for implementation in future standards, contrary to, for example, filter bank multicarrier which is still in development stage. Besides, MRC does not require matrix inversion, being highly parallelizable, and asymptotically optimal in i.i.d. Rayleigh fading channels [1]. For this purpose, we evaluate the total energy efficiency of maMIMO systems employing the TRMRC technique under SC waveform in the UL, and compare the obtained results with the total energy efficiency achieved by FDMRC with OFDM. The comparison results allow us to indicate *which scheme (receiver/waveform) is more advantageous for implementation in the UL of maMIMO systems* since the *total energy efficiency metric can weight in a unified systemic analysis the better attainable rates of TRMRC against the lower complexity burden of FDMRC*.

Our main contributions are fourfold: **i**) Differently than [18], which have assessed the total energy efficiency of maMIMO systems employing OFDM waveform, we have also evaluated the overall energy efficiency of maMIMO systems using SC waveform in the UL, besides of extending the total energy efficiency concept to a more generic scenario; **ii**) Differently than our previous work [7], in which the performance of maMIMO systems employing TRMRC under SC in UL is obtained only under the spectral efficiency perspective, we have evaluated the performance of such systems under the comprehensive view of total energy efficiency metric, which is also quite appealing currently aiming to reduce power consumption; **iii**) Our total energy efficiency analysis and comparison allowed us to indicate the best scheme to be implemented in the maMIMO UL, since it weights both achievable rates as well as computational complexities; **iv**) We have also extended the total energy efficiency comparison to scenarios with decreasing cell radius, and with increasing computational efficiency, in order to indicate the best scheme even in these different scenarios.

Besides this introductory section, the system model is described in Section II. We define the total energy efficiency of massive MIMO systems in Section III, as well as describing our adopted realistic circuit power consumption models. Representative numerical results comparing the uplink SC against OFDM maMIMO total energy efficiency and spectral efficiency performance are presented in Section IV. Section V concludes the paper.

Notations: Boldface lower and upper case symbols represent vectors and matrices, respectively. $\mathbf{I}_N$ denotes the identity

matrix of size N, while $\mathbf{1}_K$ and $\mathbf{0}_K$ are the unitary vector and null vector of length K, respectively. $\{\cdot\}^T$ and $\{\cdot\}^H$ denotes the transpose and the Hermitian transpose operator, respectively. Besides, we use $\mathcal{CN}(\mathbf{m}, \mathbf{V})$ when referring to a circular symmetric complex Gaussian distribution with mean vector $\mathbf{m}$ and covariance matrix $\mathbf{V}$.

II. System Model

We consider a MIMO system composed by C BSs, each equipped with M transmit antennas, and communicating with K single-antenna users, similarly as [7]. Reciprocity holds due to the TDD assumption, and thus uplink training signals transmission provides channel state information (CSI) to the BSs. We divide our system model description for OFDM and SC waveforms.

A. OFDM waveform

The available time-frequency resources are divided into channel coherence blocks of $\mathcal{S} = T_c W_c$ symbols [4], where T_c is the channel coherence time in seconds, and W_c is the channel coherence bandwidth in Hz[1]. Each coherence time interval comprises $\mathcal{T}$ OFDM symbols ($T_c = \mathcal{T} T_s$, with T_s representing the OFDM symbol period), distributed as uplink pilot transmissions, downlink and uplink data transmissions [3]. The number of available orthogonal pilot sequences is equal to its length, τ. In the same way as [3] and [7], CSI is estimated in the frequency domain. With the system employing N subcarriers, and the CIR being represented by L i.i.d. taps, the frequency smoothness interval is composed of $N_{\text{sm}} = N/L$ subcarriers. Therefore, it is not required to each user to send pilots in all the N subcarriers, but only in $N/N_{\text{sm}} = L$ equally spaced subcarriers, since a interpolation procedure can provide the frequency domain CSI (FDCSI) for the intermediate ones. In the training stage, up to τ users can send pilots in the same subcarriers, while a maximum total number of $K_{\max} = \tau N_{\text{sm}}$ users can be covered by each cell. The set of subcarriers in which the kth user sends pilots is defined as $\boldsymbol{\mathcal{I}}_k = \{\mathcal{I}_k(0), \mathcal{I}_k(1), \ldots, \mathcal{I}_k(L-1)\}$, while $\mathcal{I}_k(0) \in [0, N_{\text{sm}} - 1]$ and $\mathcal{I}_k(i) - \mathcal{I}_k(i-1) = N_{\text{sm}}, \forall i = 0, 1, \ldots, L-1$. Fig. 1 outlines how training and data transmission stages are divided in time and frequency domains for a given user, being T_n the Nyquist sampling interval.

The $M \times 1$ vector $\mathbf{g}_{ikjn}$ denotes the FD actual channel between the ith BS and the kth user at the jth cell in the nth subcarrier. It holds that $\mathbf{g}_{ikjn} = \sqrt{\beta_{ikj}}\underline{\mathbf{g}}_{ikjn}$, in which β_{ikj} is the long-term fading power coefficient, comprising path loss and log-normal shadowing, and $\underline{\mathbf{g}}_{ikjn}$ is the short-term fading channel vector, following $\underline{\mathbf{g}}_{ikjn} \sim \mathcal{CN}(\mathbf{0}_M, \mathbf{I}_M)$. The orthogonal pilot sequences' set is $\boldsymbol{\Psi} = [\boldsymbol{\psi}_1\ \boldsymbol{\psi}_2\ \ldots\ \boldsymbol{\psi}_\tau] \in \mathbb{C}^{\tau \times \tau}$, and $\boldsymbol{\Psi}^H \boldsymbol{\Psi} = \mathbf{I}_\tau$ holds. With the sequence $\boldsymbol{\psi}_k = [\psi_{k1}\ \psi_{k2} \ldots \psi_{k\tau}]^T$ assigned to the kth user, the received signal at the ith BS for the nth subcarrier ($n \in \boldsymbol{\mathcal{I}}_k$) during the training stage is

$$\mathbf{Y}_{in}^{\text{p}} = \sqrt{\rho_{\text{p}}} \sum_{j=1}^{C} \sum_{k=1}^{\tau} \mathbf{g}_{ikjn} \boldsymbol{\psi}_k^H + \mathbf{N}_{in}^{\text{p}}, \tag{1}$$

[1] $W_c = \frac{1}{T_d}$ holds, being T_d the largest possible delay spread.

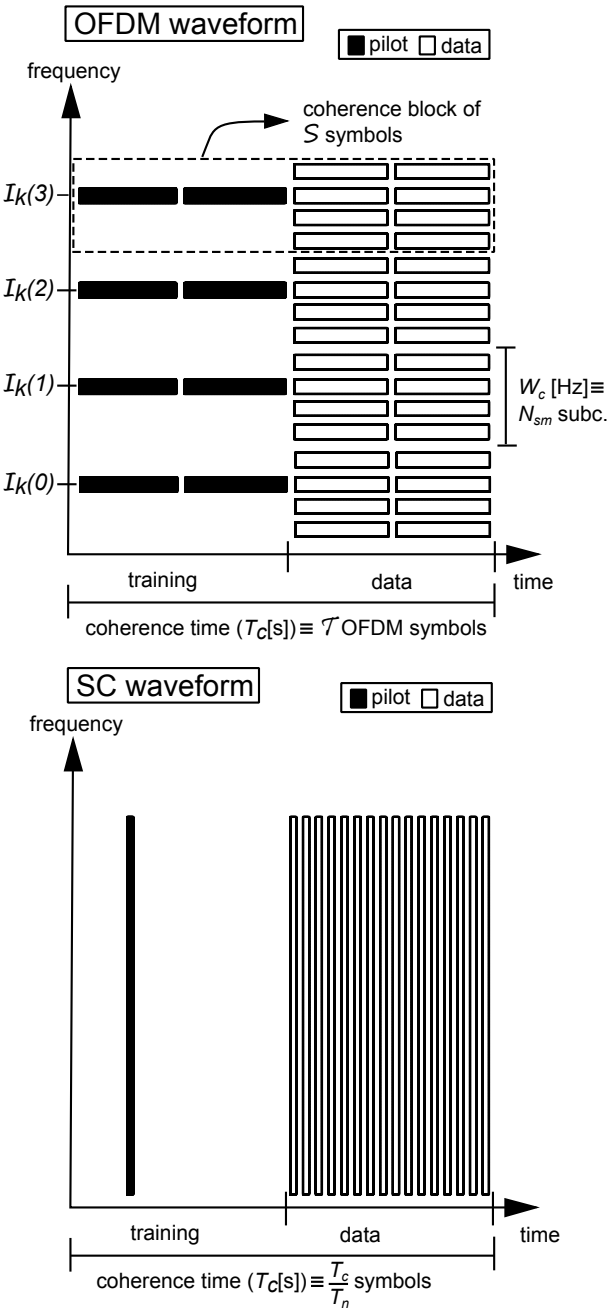

Fig. 1. Time-frequency diagram illustrating the division of training and data transmission stages for the kth user, for OFDM and SC waveforms: $N = 16$, $L = 4$, $N_{\text{sm}} = 4$, $\mathcal{T} = 4$, $\mathcal{S} = 16$ for OFDM; $T_c/T_n = 32$ for SC. Besides, $K_{\max} = 8$ for both schemes.

with ρ_{p} representing the UL pilot transmit power, and $\mathbf{N}_{in}^{\text{p}} \in \mathbb{C}^{M \times \tau}$ the additive white Gaussian noise (AWGN) matrix with i.i.d. elements following a complex normal distribution with zero mean and variance σ_n^2. By correlating the received signal $\mathbf{Y}_{in}^{\text{p}}$ with $\boldsymbol{\psi}_k$, the ith BS then estimates the kth user nth subcarrier FDCSI as

$$\widehat{\mathbf{g}}_{ikn} = \frac{1}{\sqrt{\rho_{\text{p}}}} \mathbf{Y}_{in}^{\text{p}} \boldsymbol{\psi}_k = \sum_{j=1}^{C} \mathbf{g}_{ikjn} + \mathbf{v}_{ikn}, \tag{2}$$

where $\mathbf{v}_{ikn} = \frac{1}{\sqrt{\rho_{\text{p}}}} \mathbf{N}_{in}^{\text{p}} \boldsymbol{\psi}_k \sim \mathcal{CN}(\mathbf{0}_M, \frac{\sigma_n^2}{\rho_{\text{p}}} \mathbf{I}_M)$ is an equivalent noise vector. The previous expression clearly demonstrates the

pilot contamination effect [3]. The other $N-L$ subcarriers FDCSI estimates are obtained by interpolation. The BS is now able to perform linear detection in the UL deploying the FDMRC scheme. During UL data transmission, the ith BS receives in the nth subcarrier the signal

$$\mathbf{y}_{in}^{\mathrm{u}} = \sqrt{\rho_{\mathrm{u}}} \sum_{j=1}^{C} \sum_{k=1}^{K} \mathbf{g}_{ikjn} x_{kjn}^{\mathrm{u}} + \mathbf{n}_{in}^{\mathrm{u}}, \tag{3}$$

where ρ_{u} represents the UL data transmit power, x_{kjn}^{u} is the data symbol from the kth user of the jth cell in the nth subcarrier, and $\mathbf{n}_{in}^{\mathrm{u}} \sim \mathcal{CN}(\mathbf{0}_M, \sigma_n^2 \mathbf{I}_M)$ is the $M \times 1$ AWGN sample vector. This BS then deploys FDMRC to obtain the estimated transmitted symbol as

$$\widehat{x}_{kin}^{\mathrm{u}} = \frac{1}{M} \widehat{\mathbf{g}}_{ikn}^{H} \mathbf{y}_{in}^{\mathrm{u}}. \tag{4}$$

B. SC waveform

The tth CIR vector tap between the ith BS and the kth user of the jth cell and its FD actual channel vector are related by

$$\mathbf{h}_{ikjt} = \frac{1}{L} \sum_{l=0}^{L-1} \mathbf{g}_{ikj\mathcal{I}_k(l)} e^{\mathrm{j}2\pi lt/L}. \tag{5}$$

We assume in this work a normalized uniform power delay profile (PDP) for all users, such that $\mathbf{h}_{ikjt} \sim \mathcal{CN}(\mathbf{0}_M, \frac{1}{L}\mathbf{I}_M)$ for $t = 0, 1, \ldots L-1$, since this is the most generic scenario. When employing single-carrier waveform, a training scheme for estimating the CIR of the users served by the cell is discussed in [7] and [11], which is alternative to conventional frequency domain training. In this alternative scheme, the users transmit uplink training signals sequentially in time, in such a way that at most one user per cell is transmitting at any given time. The kth user sends an impulse of amplitude $\sqrt{L\rho_{\mathrm{p}}}$ (in order to spend the same average power as in FD training (1)) at the $(k-1)L$th channel use and is idle for the remaining portion of the training phase. Besides, the next user waits $L-1$ channel uses to send its training signal. It is worth noting that the same maximal number of users $K_{\max}$ is supported in this scheme. This can be proved by noting that the total interval spent with training signals is $K_{\max} L T_n = \tau N_{\mathrm{sm}} L T_n = \tau N T_n \approx \tau T_s$ is nearly the same as in FD training, as illustrated in Fig. 1. This scheme provides the channel estimation in time domain, avoiding the transmission of FD pilots and the use of FFT at the receiver, not otherwise required in SC transmission [11].

This procedure provides to the ith BS the following CIR estimates for its k-th user

$$\widehat{\mathbf{h}}_{ikt} = \sum_{j=1}^{C} \mathbf{h}_{ikjt} + \mathbf{v}'_{ikt}, \tag{6}$$

in which $\mathbf{v}'_{ikt} \sim \mathcal{CN}(\mathbf{0}_M, \frac{\sigma_n^2}{L\rho_{\mathrm{p}}}\mathbf{I}_M)$ is an equivalent AWGN vector. Note that pilot contamination also takes place in (6), since the CIR estimates are also corrupted by the signals of users in adjacent cells transmitting at the same time.

Considering SC waveform, the time-domain received signal at the ith BS in time t during UL data transmission is

$$\mathbf{r}_i^{\mathrm{u}}[t] = \sqrt{\rho_{\mathrm{u}}} \sum_{j=1}^{C} \sum_{k=1}^{K} \sum_{l=0}^{L-1} \mathbf{h}_{ikjl} s_{kj}^{\mathrm{u}}[t-l] + \mathbf{n}'^{\mathrm{u}}_i[t], \tag{7}$$

in which $s_{kj}^{\mathrm{u}}[t-l]$ is the time-domain UL data transmitted by the kth user of the jth cell at time $t-l$, and $\mathbf{n}'^{\mathrm{u}}_i[t] \sim \mathcal{CN}(\mathbf{0}_M, \sigma_n^2 \mathbf{I}_M)$ is an AWGN vector. Note that the time aligned received signals in (7) are resultant from a perfect timing advance assumed at the users, as in [7], [17]. The BS can then estimate the information symbols deploying TRMRC as

$$\widehat{s}_{ki}^{\mathrm{u}}[t] = \frac{1}{M} \sum_{l=0}^{L-1} \widehat{\mathbf{h}}_{ikl}^{H} \mathbf{r}_i^{\mathrm{u}}[t+l]. \tag{8}$$

For causality purpose, (8) demonstrates that $L-1$ shift registers are necessary per BS receive antenna when employing TRMRC, while this number for FDMRC is $N-1$, since the entire frame has to be received to perform FFT operation. This implies not only hardware simplification, but also latency reduction. Besides, TRMRC does not require CP as seen from (8), since given a sufficiently large M, the BS extracts the desired information symbol vector from $\mathbf{r}_i^{\mathrm{u}}[t+l]$, even if the asynchronous interference belongs to the previous frame of symbols [7]. This is in fact one of the main advantages of TRMRC in comparison with FDMRC, which comes, however, at the cost of increased computational complexity of the time domain processing, as discussed in Section II-D.

C. System Performance

The analytical SINR performance of the k'th user at the ith cell achieved by FDMRC and TRMRC schemes have been found in [7] as

$$\varsigma_{k'i}^{\mathrm{F}} = \frac{M\beta_{ik'i}^2}{M\sum_{\substack{c=1 \\ c\neq i}}^{C} \beta_{ik'c}^2 + \alpha_{ik'}^2 \left[\sum_{j=1}^{C}\sum_{k=1}^{K} \beta_{ikj} + \frac{\sigma_n^2}{\gamma\rho_{\mathrm{u}}}\right]} \tag{9}$$

and

$$\varsigma_{k'i}^{\mathrm{T}} = \frac{M\beta_{ik'i}^2}{M\sum_{\substack{c=1 \\ c\neq i}}^{C} \beta_{ik'c}^2 + \alpha_{ik'}^2 \left[\sum_{j=1}^{C}\sum_{k=1}^{K} \beta_{ikj} + \frac{\sigma_n^2}{\rho_{\mathrm{u}}}\right]}, \tag{10}$$

in which $\alpha_{ik'}^2 = \sum_{c=1}^{C} \beta_{ik'c} + \frac{\sigma_n^2}{\rho_{\mathrm{p}}}$. The parameter $\gamma = \frac{N}{N+N_{CP}}$ accounts for the transmit power loss due to CP, since we have assumed for a fair comparison that both schemes spend the same energy with data transmission, and $N_{CP} = L-1$ is the CP length. Note that this result is valid for all subcarriers, since they are identically distributed in this model.

Remark 1: One can note from (9) and (10) that the same SINR performance can be achieved by both TRMRC/SC and FDMRC/OFDM schemes, except by the decrease in the transmit power of the latter due to the CP transmission. Besides, analysing both expressions, we note that the desired signal power is mainly dependent on the large-scale fading coefficient of the user, and scales with M. The first interference term is due to the users in adjacent cells sharing the same pilot sequence, and is also called as coherent interference, since the receiver processing is not able to mitigate this term which

also scales with M. The second term in the denominator involves interference from users with different pilots and noise, and is so-called non-coherent interference, since the receiver processing is able to mitigate this term, for example with more BS antennas.

Besides, due to the convexity of $\log_2(1+\frac{1}{x})$ and using Jensen's inequality as in [2], we obtain for FDMRC the following lower bound on the achievable rate of the k'th user at the ith cell

$$\mathcal{R}^{\mathrm{F}}_{k'i} \geq \widetilde{\mathcal{R}}^{\mathrm{F}}_{k'i} = \xi^{\mathrm{u}}\gamma\left(1-\frac{K}{\mathcal{S}}\right)\log_2\left(1+\left(\frac{1}{\varsigma^{\mathrm{F}}_{k'i}}\right)^{-1}\right), \quad (11)$$

in which the term $\left(1-\frac{K}{\mathcal{S}}\right)$ accounts for the pilot transmission overhead, and ξ^{u} is the fraction of the data transmit interval spent with uplink.

For TRMRC we have similarly:

$$\mathcal{R}^{\mathrm{T}}_{k'i} \geq \widetilde{\mathcal{R}}^{\mathrm{T}}_{k'i} = \xi^{\mathrm{u}}\left(1-\frac{K}{\mathcal{S}}\right)\log_2\left(1+\left(\frac{1}{\varsigma^{\mathrm{T}}_{k'i}}\right)^{-1}\right). \quad (12)$$

Furthermore, the asymptotic UL performance of both systems converge with infinite number of BS antennas to the same bound of [3]:

$$\lim_{M\to\infty}\varsigma^{\mathrm{F}}_{k'i} = \lim_{M\to\infty}\varsigma^{\mathrm{T}}_{k'i} = \frac{\beta^2_{ik'i}}{\sum_{\substack{c=1\\c\neq i}}^{C}\beta^2_{ik'c}}. \quad (13)$$

D. Complexity Analysis

The computational complexity of both investigated schemes is evaluated in [7], in terms of *floating-point operations (flops)* [20]. The main assumptions that have been made are: *i*) A real sum operation has the same complexity than a real multiplication, which are defined as 1 *flop*[2]; *ii*) A complex sum has the complexity of 2 *flops*, while a complex multiplication has the complexity of 6 *flops*; *iii*) An inner product between 2 complex vectors of size M has the complexity of M complex multiplications and $M-1$ complex additions, resulting in a total complexity of $8M-2$ *flops*; *iv*) A FFT or IFFT operation of a complex sequence of N samples has the complexity (supposing N power of two and adopting the Cooley Tukey algorithm [20]) of $(N/2)\log_2(N)$ complex multiplications and $N\log_2(N)$ complex additions, and an overall complexity of $5N\log_2(N)$ *flops*. *v*) Finally, the complexity related with the CSI estimation has been neglected for all the investigated schemes, since these estimates remain valid for several frame periods, and account in the same way for all the schemes.

For the FDMRC under OFDM, the complexity to detect the N symbols of the OFDM frame is mainly due to: *i*) the N-points IFFT operations of each user transmission ($K[5N\log_2(N)]$ *flops*), *ii*) the N-points FFT operations of each BS receive antenna ($M[5N\log_2(N)]$ *flops*), and due to *iii*) the N FDMRC data symbols' estimation, as in (4), for each user ($NK[8M-2]$ *flops*). On the other hand, the complexity of the TRMRC with overlap-and-add method is mainly given by: *i*) $\mu = (N+L)/L$ FFT's of size $2L$ for the received signals of each receive antenna, resulting in a complexity of $M\mu[10L\log_2(2L)]$ *flops*; *ii*) For each user and each receive antenna: μ element-wise multiplication of size $2L$ vectors, followed by an IFFT operation of size $2L$, and the addition of the overlaping segments (of size L) ($KM\mu[10L\log_2(2L)+12L+2L]$ *flops*); *iii*) For each user, the results of the M fast convolutions are added (only the N elements of interest), with a complexity of $K(2N(M-1))$ *flops*. The overall complexity of the TRMRC receiver employing the fast convolution with overlap-and-add method is also given in Table I.

TABLE I
NUMBER OF OPERATIONS (FLOPS) FOR EACH SCHEME.

Scheme	Number of Operations
FDMRC	$K[5N\log_2(N)]+M[5N\log_2(N)]$ $+NK[8M-2]$
TRMRC	$K[M(N+L)(10\log_2(2L)+14)+2N(M-1)]$ $+M(N+L)10\log_2(2L)$

III. TOTAL ENERGY EFFICIENCY

We define in this subsection the *total energy efficiency* of a maMIMO system employing either FDMRC or TRMRC in the UL. Our main objective with this analysis is to identify the best scheme to be implemented in the upcoming maMIMO systems based on a comprehensive analysis. The choice of the total energy efficiency metric is due to its ability of incorporating different aspects of each investigated topology, making the analysis more comprehensive and fair. The higher achievable rates of TRMRC, the reduced complexity of FDMRC, and also the consequent better power efficiency of the power amplifier in a SC scheme due to the lower PAPR levels are examples of different features that are incorporated on this analysis.

The total energy efficiency metric is defined as

$$\mathrm{EE} = \frac{\sum_{k=1}^{K}\left(\mathcal{R}^{\mathrm{UL}\star}_{ki}+\mathcal{R}^{\mathrm{DL}}_{ki}\right)}{P^{\mathrm{UL}\star}_{\mathrm{TX}}+P^{\mathrm{DL}}_{\mathrm{TX}}+P^{\mathrm{tr}\star}_{\mathrm{TX}}+P^{\star}_{\mathrm{CP}}}. \quad (14)$$

The superscript $\{\cdot\}^\star$ is used in order to indicate that a given parameter depends on which waveform/detector has been employed in UL. In (14), $\mathcal{R}^{\mathrm{UL}\star}_{ki}$ constitutes the UL rate of the kth user of the ith cell, and can be found by (11) or (12), *i.e.*, $\mathcal{R}^{\mathrm{UL}\star}_{ki}=\mathcal{R}^{\mathrm{F}}_{ki}$ or $\mathcal{R}^{\mathrm{UL}\star}_{ki}=\mathcal{R}^{\mathrm{T}}_{ki}$. Besides, $\mathcal{R}^{\mathrm{DL}}_{ki}$ is the DL rate of this user. We assume that a MRT precoding has been employed in downlink under OFDM waveform, since the practical appeal for SC usage in DL is not so strong as it is in UL, and thus $\mathcal{R}^{\mathrm{DL}}_{ki}$ can be found similarly to (11) as:

$$\mathcal{R}^{\mathrm{DL}}_{k'i} \geq \widetilde{\mathcal{R}}^{\mathrm{DL}}_{k'i} = \xi^{\mathrm{d}}\gamma\left(1-\frac{K}{\mathcal{S}}\right)\log_2\left(1+\left(\frac{1}{\varsigma^{\mathrm{DL}}_{k'i}}\right)^{-1}\right), \quad (15)$$

[2]It is important to note that the exact factor between the complexities of sum and multiplication operations does not play a significant role in our results, since in a complexity analysis, the most significant operations dominate the final complexity expressions; our analysis is comparative, and thus changing this relative factor would impact on the complexities of both schemes in a similar manner; in the total energy efficiency analysis the computational processing energy accounts for only part of the total energy expenditures. Although some works [21] [22] have shown that the energy of the multiplication operation between two double precision floating point numbers is about four times the energy of the addition operation, the memory access energy may be dominant and similar for both operations.

in which ξ^{d} is the fraction of the data transmit interval spent with downlink, and

$$\varsigma_{k'i}^{\mathrm{DL}} = \frac{\beta_{ik'i}^2/\alpha_{ik'}^2}{\sum_{\substack{l=1\\ l\neq i}}^{C} \beta_{lk'i}^2/\alpha_{lk'}^2 + \frac{1}{M}\left(K\sum_{l=1}^{C}\beta_{lk'i} + \frac{\sigma_n^2}{\rho^{\mathrm{d}}}\right)} \tag{16}$$

is the DL SINR of the k'th user of the ith cell, while ρ^{d} is the uniform DL transmit power.

Furthermore, $P_{\mathrm{TX}}^{\mathrm{UL}\star}$, $P_{\mathrm{TX}}^{\mathrm{DL}}$, and $P_{\mathrm{TX}}^{\mathrm{tr}\star}$ in (14) represent the power consumed by the power amplifiers (PA) in UL, DL, and UL pilot transmission, respectively. In our scenario of uniform power allocation we have

$$P_{\mathrm{TX}}^{\mathrm{UL}\star} = \frac{K\xi^{\mathrm{u}}\left(1-\frac{K}{\mathcal{S}}\right)\rho^{\mathrm{u}}}{\eta^{\mathrm{u}\star}}, \tag{17}$$

$$P_{\mathrm{TX}}^{\mathrm{DL}} = \frac{K\xi^{\mathrm{d}}\left(1-\frac{K}{\mathcal{S}}\right)\rho^{\mathrm{d}}}{\eta^{\mathrm{d}}}, \tag{18}$$

$$P_{\mathrm{TX}}^{\mathrm{tr}\star} = \frac{K\left(\frac{K}{\mathcal{S}}\right)\rho^{\mathrm{p}}}{\eta^{\mathrm{u}\star}}, \tag{19}$$

in which $\eta^{\mathrm{u}\star}$ and η^{d} represent the PA efficiency at the MT's and at the BS's, respectively. The parameter $\eta^{\mathrm{u}\star}$ is specific for each topology chosen as waveform/detector, since a PA with better eficiency can be employed in the MT's if SC is adopted instead of OFDM.

Finally, $P_{\mathrm{CP}}^{\star}$ accounts for the circuit power consumption, which is discussed in detail in the following.

A. Realistic Circuit Power Consumption Model

We discuss in this subsection realistic models for the circuit power consumption of the different stages in a practical MIMO communication system. The adopted approach is similar to that of [18]. Adopting a realistic circuit power consumption model, the parameter $P_{\mathrm{CP}}^{\star}$ is not fixed, but dependent on several factors, like number of antennas, number of users, waveform employed, adopted precoding and detector schemes, data throughput, among others. Following [18], a refined circuit power consumption model for multi-user MIMO systems can be stated as

$$P_{\mathrm{CP}}^{\star} = P_{\mathrm{FIX}} + P_{\mathrm{TC}} + P_{\mathrm{CE}} + P_{\mathrm{C/D}}^{\star} + P_{\mathrm{BH}}^{\star} + P_{\mathrm{LP}}^{\star}, \tag{20}$$

in which P_{FIX} is a constant quantity accounting for the fixed power consumption required for site-cooling, control signaling, and load-independent power of backhaul infrastructure and baseband processors [18]. The other terms in (20) are defined in the following subsections.

1) Transceiver Chains: In (20), P_{TC} accounts for the power consumption of the transceiver chains. As described in [18], [23], one can quantify the power consumption of a set of transmitters and receivers as

$$P_{\mathrm{TC}} = P_{\mathrm{SYN}} + MP_{\mathrm{BS}} + KP_{\mathrm{MT}}, \tag{21}$$

in which P_{SYN} is the power consumed by the local oscillator, P_{BS} is the power necessary to the circuit components of each BS antenna operate, like converters, mixers, and filters, while P_{MT} accounts for the power required by the circuit components of each single-antenna MT operate, including amplifiers, mixer, oscillator and filters.

2) Channel Estimation: P_{CE} accounts for the power consumption of channel estimation in (20). We assume only UL training by UL pilot transmissions. Thus, all processing is carried out at the BS, which has a *computational efficiency* of $\mathcal{L}_{\mathrm{BS}}\left[\frac{\mathrm{flops}}{\mathrm{Watt}}\right]$. The pilot-based CSI estimation is performed once per coherence block, and there are $B/\mathcal{S}$ coherence blocks per second, being $B = 1/T_n$ the total bandwidth. The CSI estimation procedure as described in (2) consists of simply multiplying the $M \times \tau$ matrix $\mathbf{Y}_{in}^{\mathrm{p}}$ with the $\tau \times 1$ pilot sequence $\boldsymbol{\psi}_k$ of each user, demanding thus $MK(8\tau-2)$ *flops*. Therefore, the power consumption spent with the channel estimation procedure is [18]

$$P_{\mathrm{CE}} = \frac{B}{\mathcal{S}}\frac{MK(8\tau-2)}{\mathcal{L}_{\mathrm{BS}}}. \tag{22}$$

3) Coding and Decoding: In (20), $P_{\mathrm{C/D}}^{\star}$ accounts for the power consumption of the channel coding and decoding units. The BS performs channel coding and modulation to K sequences of information symbols in the DL, while each MT performs some suboptimal fixed-complexity algorithm for decoding its own sequence [18]. The opposite is performed in the UL. The consumed power on these procedures will thus depend on the actual rates, being expressed as

$$P_{\mathrm{C/D}}^{\star} = \sum_{k=1}^{K}\left(\mathcal{R}_{ki}^{\mathrm{UL}\star} + \mathcal{R}_{ki}^{\mathrm{DL}}\right)\left(\mathcal{P}_{\mathrm{COD}} + \mathcal{P}_{\mathrm{DEC}}\right). \tag{23}$$

where $\mathcal{P}_{\mathrm{COD}}$ and $\mathcal{P}_{\mathrm{DEC}}$ are the coding and decoding *power densities*, respectively, in $\left[\frac{\mathrm{Watt}}{\mathrm{bit/s}}\right]$. In the same way as [18], it was assumed for simplicity that the power densities $\mathcal{P}_{\mathrm{COD}}$ and $\mathcal{P}_{\mathrm{DEC}}$ are the same in UL and DL.

4) Backhaul: $P_{\mathrm{BH}}^{\star}$ accounts for the power consumption of the load-dependent backhaul in (20), which is necessary to transfer UL/DL data between the BS and the core network. The backhaul consumption power is usually modeled with two components [18], one load-independent and one load-dependent. For convenience, the first one can be included in P_{FIX}, while the second one is proportional to the average sum rate. Therefore, the load-dependent backhaul consumption power can be computed as

$$P_{\mathrm{BH}}^{\star} = \sum_{k=1}^{K}\left(\mathcal{R}_{ki}^{\mathrm{UL}\star} + \mathcal{R}_{ki}^{\mathrm{DL}}\right)\mathcal{P}_{\mathrm{BT}}, \tag{24}$$

in which $\mathcal{P}_{\mathrm{BT}}$ is the *backhaul traffic power density* in $\left[\frac{\mathrm{Watt}}{\mathrm{bit/s}}\right]$.

5) Linear Processing: In (20), $P_{\mathrm{LP}}^{\star}$ accounts for the power consumption of the linear processing at the BS. This power component can be divided for UL and DL. The power spent with the DL linear processing, which is a common factor for both investigated schemes, is represented as the sum of two terms: the first one is that required by making one matrix-vector multiplication per DL data symbol, and the second one is that required to obtain the precoding matrix. Each multiplication between a $M \times K$ precoding matrix and a $K \times 1$ symbol vector demands the complexity of $M(8K-2)$

flops. Besides, in order to obtain the MRT precoders, it is just necessary to normalize the CSI estimate vectors aiming to obtain the precoding vector of each user, demanding thus $K(14M-2)$ *flops*. Therefore, the power consumption of the DL linear processing at the BS can be quantified as

$$P_{\text{LP}}^{\text{DL}} = B\left(1-\frac{\tau}{\mathcal{S}}\right)\xi^{\text{d}}\frac{M(8K-2)}{\mathcal{L}_{\text{BS}}} + \frac{B}{\mathcal{S}}\frac{K(14M-2)}{\mathcal{L}_{\text{BS}}}. \quad (25)$$

The computational complexity of UL linear processing when employing FDMRC scheme under OFDM waveform is presented in Table I. As the first term refers to a processing evaluated at the MT's, while the others refer to BS processing, this power can be quantified as

$$P_{\text{LP}}^{\text{UL-F}} = B\left(1-\tfrac{\tau}{\mathcal{S}}\right)\xi^{\text{u}}\left[K\tfrac{5N\log_2(N)}{\mathcal{L}_{\text{MT}}} + M\tfrac{5N\log_2(N)}{\mathcal{L}_{\text{BS}}} + N\tfrac{K(8M-2)}{\mathcal{L}_{\text{BS}}}\right], \quad (26)$$

in which $\mathcal{L}_{\text{MT}}$ is the computational efficiency of MT's in $\left[\frac{\text{flops}}{\text{Watt}}\right]$. Note that, different than [18], we included the power required to the MT's perform OFDM modulation, and the power required to the BS's perform OFDM demodulation. The computational complexity of UL linear processing when employing TRMRC scheme under SC waveform is also presented in Table I. As this processing is entirely evaluated at the BS, the power can be quantified as

$$P_{\text{LP}}^{\text{UL-T}} = B\left(1-\tfrac{\tau}{\mathcal{S}}\right)\tfrac{\xi^{\text{u}}}{\mathcal{L}_{\text{BS}}}\{K[M(N+L)(10\log_2(2L)+14) + 2N(M-1)] + M(N+L)10\log_2(2L)\} \quad (27)$$

Finally, the total power required by linear processing is given by

$$P_{\text{LP}}^{\star} = P_{\text{LP}}^{\text{DL}} + P_{\text{LP}}^{\text{UL}\star}, \quad (28)$$

in which $P_{\text{LP}}^{\text{UL}\star} = P_{\text{LP}}^{\text{UL-F}}$ or $P_{\text{LP}}^{\text{UL}\star} = P_{\text{LP}}^{\text{UL-T}}$.

B. Other Issues Affecting Total Energy Efficiency

We discuss in this subsection the influence of other factors which can impact on the total energy efficiency of the investigated systems. The PAPR is an impairment which affects much more a multicarrier system like OFDM than SC systems. Increasing the number of subcarriers, N, has the positive effect of diminishing the inefficiency of the CP transmission, since $\gamma = \frac{N}{N+N_{CP}}$. However, it also increases the PAPR, which either requires a power amplifier with a larger linear operation range and thus lower energy efficiency, or increases the distortion levels if the PAPR is controlled by clipping the signal peaks. Note that any alternative results in a total energy efficiency loss for the OFDM waveform: the first by decreasing η^{d} and η^{uF}, which increases P_{TX} in (14), and the second by decreasing the achievable rates $\mathcal{R}^{\text{UL}}$ and $\mathcal{R}^{\text{DL}}$ due to the increased distortion levels imposed by clipping. This is one of the strongest motivations for using SC waveform. Further details about how the distortion levels imposed by clipping affects OFDM performance can be found in [24].

The CFO impact in maMIMO system performance has been discussed in [11] and [13]. As presented in [25], the CFO is another example of adverse effect much more severe for multicarrier systems, due to the longer duration of the OFDM symbol and the intercarrier interference due to the orthogonality loss. The impact of CFO in the total energy efficiency works as a performance-complexity trade-off: if a simple estimator is employed, the distortion imposed by carrier offset and/or phase noise decreases the achievable rates, while if a better estimator is used, the gains in achievable rates come at the price of either increased complexity or increased length of pilots. Note that both alternatives decrease the total energy efficiency. However, this trade-off is much more noticeable for OFDM than for SC, which constitutes another motivation for employing SC. Besides, an efficient method for improving CFO compensation is proposed in [13] for the TRMRC receiver operating in the maMIMO scenario, while also showing that the performance degradation due to imperfect CFO estimation diminishes with the increasing frequency selectivity of the channel, measured by the number of channel taps L.

The CP size also has a primary influence on the total energy efficiency of OFDM systems, but not in SC systems employing TRMRC which does not require CP. The minimum CP length is $N_{CP} = L-1$. While more extended CPs decrease the achievable rates of OFDM. Besides, for a given required CP length, one way of mitigating the impact of CP transmission on the achievable rates is increasing the number of subcarriers N. However, this strategy has an adverse effect on the PAPR, as discussed above. For the SC case, no CP is needed, as discussed in Section II-B, in such a way that only the number of channel taps L impacts on the SC maMIMO system. While L does not affect the achievable rates of TRMRC/SC, as can be seen in (10) and (12), the computational complexity of such scheme depends on this parameter (see Table I), and therefore the total energy efficiency also decreases with L.

IV. Numerical Results

Aiming at comparing the investigated schemes, we present in this Section numerical results for the maMIMO system performance under frequency-selective channels. We have adopted the same multicell scenario and parameters of [7] with unitary frequency reuse factor, composed of $C = 7$ hexagonal cells of radius $r_{\text{cell}} = 500$m, where K users are uniformly distributed, except for a circle of 50m radius around the BS. The adopted multicell parameters are similar to that adopted in [1], [18]. Besides, only the performance of the users at the central cell were computed, since they experience a more realistic interference. Unless otherwise specified, we have assumed $M = 100$ BS antennas, $K = 4$ users, $N = 256$ subcarriers when OFDM is employed, a time-dispersive channel with $L = 16$, $\xi^{\text{d}} = 0.6$, $\xi^{\text{u}} = 0.4$, and an SNR of 0dB for both pilots and UL data transmission. The path loss decay exponent was assumed $\lambda = 3.8$, and the log-normal shadowing standard deviation as 8dB. The presented results were averaged over 100,000 spatial realizations for the users.

In [7] it has been shown that the maMIMO system is able to operate with low UL SNR's, due to the large number of BS antennas, in such a way that the system performance

TABLE II
SIMULATION PARAMETERS.

Parameter	**Value**
Cell radius: r_{cell}	500 m
Minimum distance: $d_{\min}$	50 m
Transmission bandwidth: B	20 MHz
Channel coherence bandwidth: B_C	100 kHz
Channel coherence time: T_C	2 ms
Total noise power: σ_n^2	-96 dBm
UL transmit power: ρ_{u}	200 mW
UL pilot transmit power: ρ_{p}	200 mW
DL radiated transmit power: $P_{\text{TX}}^{\text{DL}} \cdot \eta^{\text{d}}$	2 W
Coherence block: $\mathcal{S}$	200 symbols
Computational efficiency at BSs: $\mathcal{L}_{\text{BS}}$	12.8 $\left[\frac{\text{Gflops}}{\text{W}}\right]$
Computational efficiency at MTs: $\mathcal{L}_{\text{MT}}$	5.0 $\left[\frac{\text{Gflops}}{\text{W}}\right]$
Fraction of DL transmission: ξ^{d}	0.60
Fraction of UL transmission: ξ^{u}	0.40
PA efficiency at the BSs: η^{d}	0.39
PA efficiency at the MTs under OFDM: η^{uF}	0.30
PA efficiency at the MTs under SC: η^{uT}	0.50
Fixed power consumption: P_{FIX}	18 W
Power consumed by local oscillators at BSs: P_{SYN}	2 W
Power required to run the circuit components at BSs: P_{BS}	1 W
Power required to run the circuit components at MTs: P_{MT}	0.10 W
Power density required for coding of data signals: $\mathcal{P}_{\text{COD}}$	0.10 $\left[\frac{\text{W}}{\text{Gbits}}\right]$
Power density required for decoding of data signals: $\mathcal{P}_{\text{DEC}}$	0.80 $\left[\frac{\text{W}}{\text{Gbits}}\right]$
Power density required for backhaul traffic: $\mathcal{P}_{\text{BT}}$	0.25 $\left[\frac{\text{W}}{\text{Gbits}}\right]$

saturates near 0dB. Moreover, both schemes have very similar SINR performance, but the achievable rates of TRMRC are slightly higher than that of FDMRC due to the inefficiency of the CP transmission, required by the latter in UL. Fig. 2 compares the UL and DL spectral efficiencies achieved by the TRMRC/SC *vs* FDMRC/OFDM schemes with increasing M and K. Indeed, one can see that both have very close performances. This happens since both employ OFDM in DL, thus achieving the same spectral efficiency, while in UL the spectral efficiency of TRMRC/SC is slightly higher by not transmitting the CP. It has also been shown in [7] that the approximate expressions for SINR and the lower bounds for achievable rates are tight. While the error with respect to Monte-Carlo simulations of SINR was about 0.06 dB, the error between the simulated rates and the lower bound was about 0.075 bpcu.

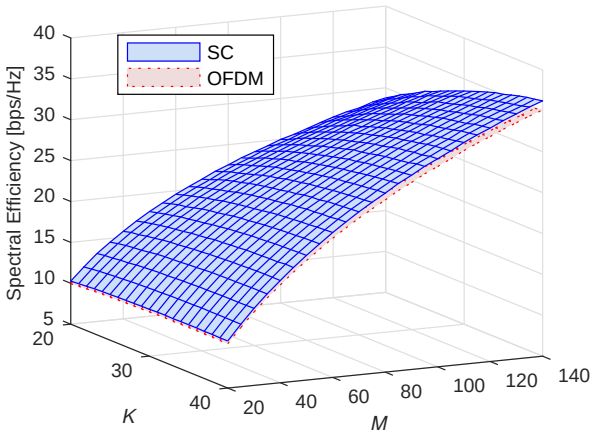

Fig. 2. Spectral efficiency *vs* M and K for both investigated schemes.

A. Total Energy Efficiency Evaluation

We evaluate in this subsection the total energy efficiencies of maMIMO systems employing either OFDM/FDMRC or SC/TRMRC as waveform/detector in the UL. The main parameters adopted in our simulations summarized in Table II are similar to those adopted in [18], [19]. Fig. 3 depicts the total energy efficiencies of the investigated systems, with the variation of both number of BS antennas M and number of users K. As can be seen, the maMIMO system employing FDMRC detector under OFDM waveform has a higher total energy efficiency than TRMRC under SC. The only exception occurs with low number of BS antennas ($M < 35$), in which TRMRC/SC outperforms FDMRC/OFDM. However, in the massive MIMO scenario (typically with $M > 80$), the total energy efficiency of FDMRC/OFDM is higher. Fig. 4 corrobo-

rates this result, showing the total energy efficiency percentage gain of FDMRC/OFDM in comparison with TRMRC/SC. As one can note from the figure, the total energy efficiency gain can achieve almost 20% in the range of our investigation, and can be even higher for increased values of M and K.

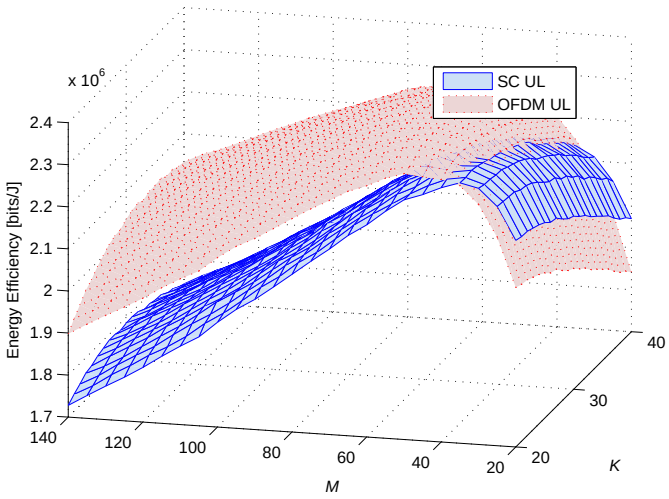

Fig. 3. Total energy efficiency *vs* M and K for both investigated schemes.

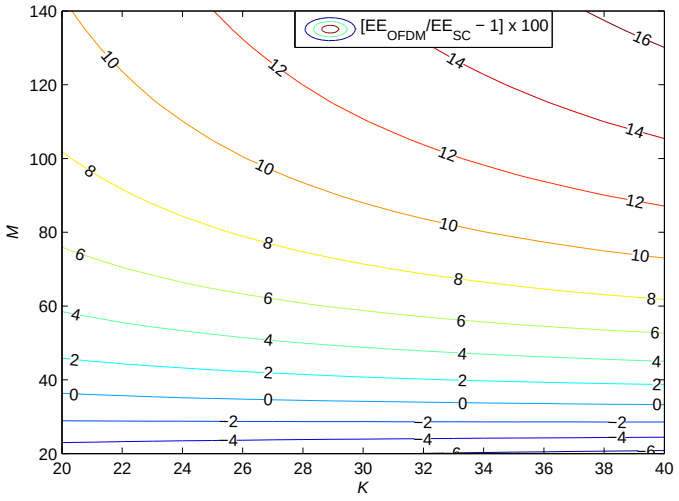

Fig. 4. Contour plot showing the total energy efficiency gain (%) of OFDM/FDMRC in comparison with SC/TRMRC.

Then, aiming to compare the best total energy efficiencies achieved by each scheme, we restrict the range of K and M in a shorter interval centered on their maxima. Fig. 5 shows that the optimal total energy efficiency achieved by TRMRC/SC is of 2.315 Mbits/J, which is attained with $M = 35$ antennas serving $K = 22$ users. On the other hand, the optimal operation point for FDMRC/OFDM is attained with $M = 50$ antennas serving $K = 22$ users, in which a total energy efficiency of 2.359 Mbits/J can be achieved. Therefore, FDMRC/OFDM is able to provide a total energy efficiency improvement of 0.044 Mbits/J with respect to TRMRC/SC, considering both schemes in their respective optimal total energy efficiency operation points.

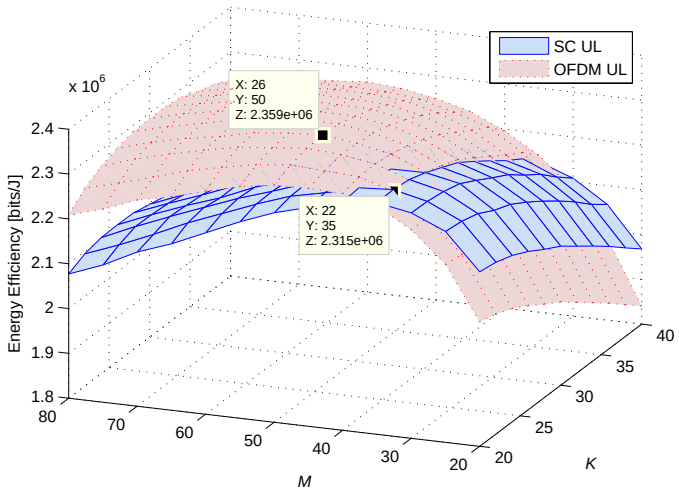

Fig. 5. Total energy efficiency as a function of M and K (zoom of Fig. 3).

Finally, Fig. 6 shows the total energy efficiency and spectral efficiency trade-off for both investigated schemes. Each curve shows the total energy efficiency against spectral efficiency achieved for each scheme with the increasing number of BS antennas. For each number of BS antennas, the number of active users is set as the one leading to the maximum total energy efficiency for a given detector/waveform, as can be seen in Figure 3. As one can infer, TRMRC/SC is a good alternative only for low number of BS antennas ($M < 35$). Indeed, for higher values of M, FDMRC/OFDM provides a higher total energy efficiency under the same spectral efficiency, or alternatively a higher spectral efficiency under a target total energy efficiency.

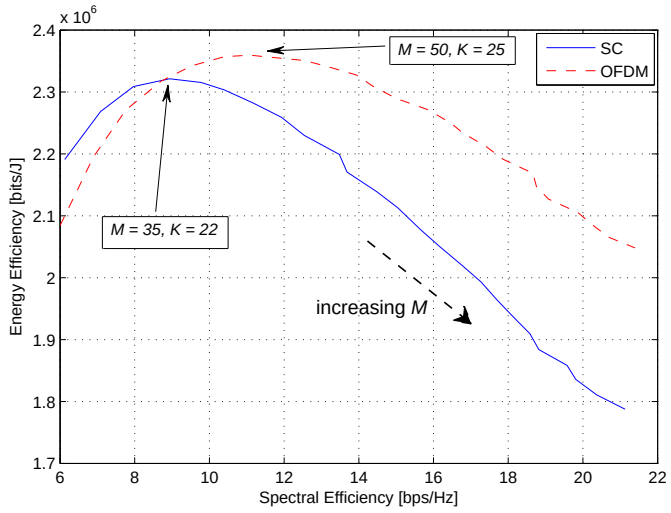

Fig. 6. Total energy efficiency and sum spectral efficiency trade-off with increasing M.

B. Analysis with Decreasing Cell Radius and CP Length

We analyse in this subsection the total energy efficiency of the investigated schemes with a decreasing cell radius. As long as the cell size diminishes, the CIR length L also

decreases, in such a way that a smaller CP can be employed. We start from $L = 16$, $r_{\text{cell}} = 500$m, and $d_{\min} = 50$m, and gradually decrease r_{cell} and $d_{\min}$ in linear steps of 100 and 10, respectively, while L is decreased by half in each step. Table III shows the obtained results for the maximum total energy efficiency $\text{EE}_{\max}$, showing also the number of antennas, number of users and sum spectral efficiency ($\text{SE} = \sum_{k=1}^{K} (\mathcal{R}_k^{\text{UL}\star} + \mathcal{R}_k^{\text{DL}})$) for which the maximum energy efficiency is obtained in each scenario. As one can see, TRMRC/SC achieves a higher total energy efficiency than FDMRC/OFDM when the cell radius decreases under 300m. This happens due to the lower value of L, which decreases the computational burden of TRMRC processing in Eq. (8), while not changing the computational complexity of FDMRC. The table also shows that the maximum total energy efficiency operation point always occurs under a higher sum spectral efficiency for FDMRC/OFDM than for TRMRC/SC, due to the higher number of employed BS antennas and served users.

TABLE III
MAXIMUM TOTAL ENERGY EFFICIENCY WITH DECREASING CELL RADIUS FOR EACH SCHEME.

Scheme	r_{cell} [m]	$d_{\min}$ [m]	L	$\text{EE}_{\max}$ [Mbits/J]	SE [bps/Hz]	M	K
SC	500	50	16	2.319	9.005	35	22
	400	40	8	2.803	10.925	37	22
	300	30	4	**3.351**	13.753	40	25
	200	20	2	**3.884**	15.606	40	25
	100	10	1	**4.218**	17.060	41	27
OFDM	500	50	16	**2.361**	**11.085**	50	25
	400	40	8	**2.831**	**13.396**	50	26
	300	30	4	3.332	**15.473**	49	25
	200	20	2	3.786	**17.722**	49	26
	100	10	1	4.016	**18.628**	47	28

C. Analysis with Increasing Computational Efficiency

Our previous results demonstrated that TRMRC/SC achieves a higher sum rate than FDMRC/OFDM, while spending less power with the irradiated signal and power amplifier. However, the higher computational complexity of TRMRC processing makes its total energy efficiency lower than that of FDMRC/OFDM. In this subsection we conjecture that such situation may change in few years, since the evolution of computers and processors tends to improve the computational efficiency parameters, $\mathcal{L}_{\text{BS}}$ and $\mathcal{L}_{\text{MT}}$. Therefore, the power required to run the TRMRC processing would decrease, increasing its total energy efficiency. Fig. 7 shows the maximum total energy efficiency achieved by both schemes with increasing computational efficiencies, *i.e.*, the $\mathcal{L}_{\text{BS}}$ and $\mathcal{L}_{\text{MT}}$ in Table II were scaled by the factor represented in the horizontal axis. As depicted in the figure, a 30% improvement in computational efficiencies is sufficient to make the total energy efficiency of TRMRC/SC higher than that of FDMRC/OFDM. Therefore, employing TRMRC under SC waveform in the UL of maMIMO systems may become a promising alternative in a near future aiming to implement very energy efficient communication systems.

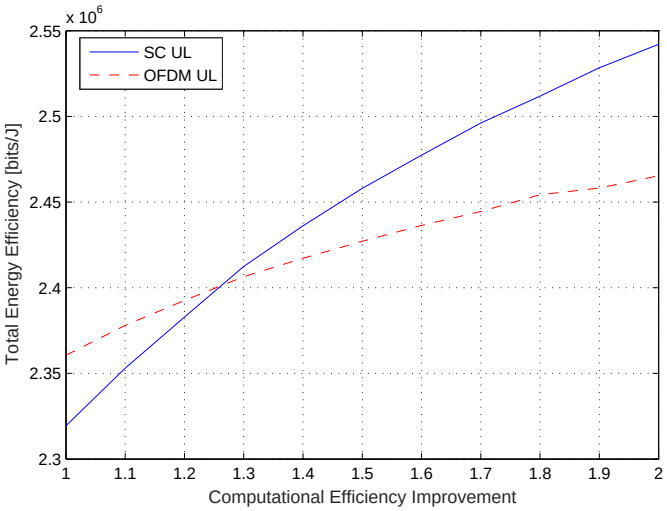

Fig. 7. Total energy efficiency with increasing computational efficiency (both $\mathcal{L}_{\text{BS}}$ and $\mathcal{L}_{\text{MT}}$), for L=16 and $r_{\text{ext}} = 500$.

V. CONCLUSION

In this work, we have evaluated the total energy efficiency of maMIMO systems under frequency-selective fading channels in the presence of pilot contamination. We have compared the conventional FDMRC receiver operating with OFDM versus the TRMRC receiver operating under SC waveform. Our choice for the total energy efficiency metric is due to its comprehensiveness, and ability of incorporating several different aspects in a unified analysis. Our results demonstrated the superiority of FDMRC receiver under OFDM waveform in terms of total energy efficiency. Despite of the higher sum rates achieved by TRMRC/SC, and the lower power expenditures related to the transmitted signal and power amplifier, the higher computational complexity required to run the TRMRC processing makes the total energy efficiency of this scheme lower than that achieved by FDMRC under OFDM. However, this complexity is highly dependent on the CIR length L, in such a way that if a shorter cell size is considered, TRMRC/SC becomes a better alternative in terms of total energy efficiency. Besides, the power required to run the detection algorithms decreases if the computational efficiency of the available equipments increase. Our analysis have indicated that a 30% increase on the computational efficiency makes the TRMRC/SC scheme more efficient than FDMRC/OFDM. Therefore, the latter topology could be a promising alternative for implementation in the UL of maMIMO systems in the next few years.

ACKNOWLEDGEMENTS

This work was supported in part by the National Council for Scientific and Technological Development (CNPq) of Brazil under Grants 304066/2015-0 and 404079/2016-4; in part by Londrina State University, Paraná State Government (UEL); and in part by Escola Politécnica of the University of São Paulo (EPUSP).

REFERENCES

[1] T. Marzetta, E. Larsson, H. Yang, and H. Ngo, *Fundamentals of Massive MIMO*. New York, NY, USA: Cambridge University Press, 2016.

[2] H. Q. Ngo, E. Larsson, and T. Marzetta, "Energy and spectral efficiency of very large multiuser MIMO systems," *IEEE Transactions on Communications*, vol. 61, no. 4, pp. 1436–1449, April 2013.

[3] T. Marzetta, "Noncooperative cellular wireless with unlimited numbers of base station antennas," *IEEE Transactions on Wireless Communications*, vol. 9, no. 11, pp. 3590–3600, 2010.

[4] E. Björnson, E. G. Larsson, and M. Debbah, "Massive MIMO for maximal spectral efficiency: How many users and pilots should be allocated?" *IEEE Transactions on Wireless Communications*, vol. 15, no. 2, pp. 1293–1308, Feb 2016.

[5] Q. Zhang, S. Jin, M. McKay, D. Morales-Jimenez, and H. Zhu, "Power Allocation Schemes for Multicell Massive MIMO Systems," *IEEE Transactions on Wireless Communications*, vol. 14, no. 11, pp. 5941–5955, Nov 2015.

[6] D. Falconer, S. L. Ariyavisitakul, A. Benyamin-Seeyar, and B. Eidson, "Frequency domain equalization for single-carrier broadband wireless systems," *IEEE Communications Magazine*, vol. 40, no. 4, pp. 58–66, Apr 2002.

[7] J. C. M. Filho, C. Panazio, and T. Abrão, "Uplink performance of single-carrier receiver in massive MIMO with pilot contamination," *IEEE Access*, vol. 5, pp. 8669–8681, 2017.

[8] L. Lu, G. Y. Li, A. L. Swindlehurst, A. Ashikhmin, and R. Zhang, "An overview of massive MIMO: Benefits and challenges," *IEEE Journal of Selected Topics in Signal Processing*, vol. 8, no. 5, pp. 742–758, Oct 2014.

[9] N. Benvenuto and S. Tomasin, "On the comparison between OFDM and single carrier modulation with a DFE using a frequency-domain feedforward filter," *IEEE Transactions on Communications*, vol. 50, no. 6, pp. 947–955, Jun 2002.

[10] S. Tomasin, "Overlap and save frequency domain DFE for throughput efficient single carrier transmission," in *2005 IEEE 16th International Symposium on Personal, Indoor and Mobile Radio Communications*, vol. 2, Sept 2005, pp. 1199–1203 Vol. 2.

[11] A. Pitarokoilis, S. K. Mohammed, and E. G. Larsson, "Uplink performance of time-reversal MRC in massive MIMO systems subject to phase noise," *IEEE Transactions on Wireless Communications*, vol. 14, no. 2, pp. 711–723, Feb 2015.

[12] ——, "On the optimality of single-carrier transmission in large-scale antenna systems," *IEEE Wireless Communications Letters*, vol. 1, no. 4, pp. 276–279, August 2012.

[13] S. Mukherjee and S. K. Mohammed, "Impact of Frequency Selectivity on the Information Rate Performance of CFO Impaired Single-Carrier Massive MU-MIMO Uplink," *IEEE Wireless Communications Letters*, vol. 5, no. 6, pp. 648–651, Dec 2016.

[14] Z. Mokhtari, M. Sabbaghian, and R. Dinis, "Massive MIMO Downlink Based on Single Carrier Frequency Domain Processing," *IEEE Transactions on Communications*, vol. 66, no. 3, pp. 1164–1175, March 2018.

[15] Y. Sun, J. Wang, L. He, and J. Song, "Uplink Spectral Efficiency Analysis and Optimization for Massive SC-SM MIMO With Frequency Domain Detection," *IEEE Transactions on Vehicular Technology*, vol. 67, no. 5, pp. 3937–3949, May 2018.

[16] Y. Sun, J. Wang, and L. He, "Spectral Efficiency Enhancement With Power Allocation for Massive SC-SM MIMO Uplink," *IEEE Communications Letters*, vol. 22, no. 1, pp. 101–104, Jan 2018.

[17] C. Mollén, J. Choi, E. G. Larsson, and R. W. Heath, "Uplink Performance of Wideband Massive MIMO With One-Bit ADCs," *IEEE Transactions on Wireless Communications*, vol. 16, no. 1, pp. 87–100, Jan 2017.

[18] E. Björnson, L. Sanguinetti, J. Hoydis, and M. Debbah, "Optimal design of energy-efficient multi-user MIMO systems: Is massive MIMO the answer?" *IEEE Transactions on Wireless Communications*, vol. 14, no. 6, pp. 3059–3075, June 2015.

[19] H. Yang and T. L. Marzetta, "Total energy efficiency of cellular large scale antenna system multiple access mobile networks," in *2013 IEEE Online Conference on Green Communications (OnlineGreenComm)*, Oct 2013, pp. 27–32.

[20] G. H. Golub and C. F. V. Loan, *Matrix Computations*. Maryland, USA: Johns Hopkins University Press, 1996.

[21] A. Pedram, S. Richardson, M. Horowitz, S. Galal, and S. Kvatinsky, "Dark Memory and Accelerator-Rich System Optimization in the Dark Silicon Era," *IEEE Design Test*, vol. 34, no. 2, pp. 39–50, April 2017.

[22] M. Horowitz, "1.1 computing's energy problem (and what we can do about it)," in *2014 IEEE International Solid-State Circuits Conference Digest of Technical Papers (ISSCC)*, Feb 2014, pp. 10–14.

[23] S. Cui, A. J. Goldsmith, and A. Bahai, "Energy-efficiency of MIMO and cooperative MIMO techniques in sensor networks," *IEEE Journal on Selected Areas in Communications*, vol. 22, no. 6, pp. 1089–1098, Aug 2004.

[24] C. H. A. Tavares, J. C. M. Filho, C. M. Panazio, and T. Abrão, "Input Back-Off Optimization in OFDM Systems Under Ideal Pre-Distorters," *IEEE Wireless Communications Letters*, vol. 5, no. 5, pp. 464–467, Oct 2016.

[25] T. Pollet, M. V. Bladel, and M. Moeneclaey, "BER sensitivity of OFDM systems to carrier frequency offset and Wiener phase noise," *IEEE Transactions on Communications*, vol. 43, no. 2/3/4, pp. 191–193, Feb 1995.

José Carlos Marinello Filho received his B.S. and M.S. degree in Electrical Engineering (the first with Summa Cum Laude) from Londrina State University, PR, Brazil, in December 2012 and Sept 2014, respectively. He is currently working towards his Ph.D. at Polytechnic School of Sao Paulo University, São Paulo, Brazil. His research interests include signal processing and wireless communications, especially massive multiple-antenna precoding/decoding techniques, acquisition of channel-state information, multicarrier modulation, cross-layer optimization of MIMO/OFDM systems, interference management and 5G.

Cristiano Panazio received Engineer's and Master's degrees in Electrical Engineering in 1999 and 2001, respectively, from State University of Campinas and a PhD degree in Telecommunications in 2005 from the Conservatoire National des Arts et Métiers. Currently, he is assistant professor at the Laboratory of Communications and Signals of the Escola Politécnica of the University of São Paulo. His research interests are adaptive equalization (data aided and blind), synchronization techniques, mobile communications, multicarrier modulation, spread spectrum techniques and space-time receivers.

Taufik Abrão (M'97-SM'12) (http://www.uel.br/pessoal/taufik) received the B.S., M.Sc., and Ph.D. degrees in electrical engineering from the Polytechnic School of the University of São Paulo, São Paulo, Brazil, in 1992, 1996, and 2001, respectively. Since March 1997, he has been with the Communications Group, Department of Electrical Engineering, Londrina State University, Paraná, Brazil, where he is currently an Associate Professor in Telecommunications and the Head of the Telecomm. & Signal Processing Lab. In 2012, he was an Academic Visitor with the Southampton Wireless Research Group, University of Southampton, Southampton, U.K. From 2007 to 2008, he was a Post-doctoral Researcher with the Department of Signal Theory and Communications, Polytechnic University of Catalonia (TSC/UPC), Barcelona, Spain. He has participated in several projects funded by government agencies and industrial companies. He is involved in editorial board activities of six journals in the telecommunications area and has served as TPC member in several symposiums and conferences. He has also served as an Editor for the IEEE Comm. Surveys & Tutorials since 2013, the IEEE Access since 2016, and the IET-JoE since 2014 and ETT-Wiley since 2018. He is a member of SBrT and a senior member of IEEE. His current research interests include communications and signal processing, specially the detection and estimation, multicarrier and massive MIMO systems, resource allocation, as well as heuristic and convex optimization aspects of 4G and 5G wireless systems. He has supervised 24 M.Sc. and 4 Ph.D. students, as well as 2 postdocs, co-authored 11 book chapters on mobile radio communications and +180 research papers published in international journals and conferences.

Stefano Tomasin (M'99-SM'11) (http://www.dei.unipd.it/~tomasin/ received the Laurea degree and the Ph.D. degree in Telecommunications Engineering from the University of Padova, Italy, in 1999 and 2003, respectively. In the Academic year 1999-2000 he was on leave at the IBM Research Laboratory, Zurich, Switzerland, doing research on signal processing for magnetic recording systems. In the Academic year 2001-2002 he was on leave at Philips Research, Eindhoven, the Netherlands, studying multicarrier transmission for mobile applications. He joined University of Padova first as contractor researcher for a national research project (2002), then as Assistant Professor (2005) and since 2016 he is Associate Professor. In the second half of 2004 he was visiting faculty at Qualcomm, San Diego (CA) doing research on interference cancelation for mobile cellular systems. In 2007 he has been visiting Polytechnic University in Brooklyn, NY, working with prof. Elza Erkip on cooperative networks. From December 2014 to December 2015, he has been on a sabbatical leave as Principal Engineer at the Mathematical and Algorithmic Sciences Laboratory, France Research Center of Huawei Technologies, in Boulogne-Billancourt, France. His current research interests include physical layer security, signal processing for wireless communications, optimization techniques for smart grids, synchronization, scheduling of communication resources. He is senior member of IEEE since 2011 and member of IEEE since 1999. Since 2011 he is Editor of both IEEE Transactions of Vehicular Technologies and EURASIP Journal of Wireless Communications and Networking. Since 2016 he is Editor of IEEE Transactions on Signal Processing. He was co-recipient of a best paper student award in 2009. Stefano Tomasin has participated in various industrial and academic research projects, receiving grants from the Italian Ministry for Education (FIRB project), collaborating with the Italian broadcasting company RAI and with companies in both Europe and Asia.

APPENDIX F – Letter submitted to the journal "*IEEE Transactions on Vehicular Technology*"

Title: Collision Resolution Protocol via Soft Decision Retransmission Criterium.

Authors: José Carlos Marinello Filho and Taufik Abrão.

Journal: IEEE Transactions on Vehicular Technology (ISSN 0018-9545).

Classification (Qualis-CAPES): A1 / IF$= 4.066$ (Engenharias IV).

Submission Date: June 2018.

Collision Resolution Protocol via Soft Decision Retransmission Criterium

José Carlos Marinello, Taufik Abrão

***Abstract*—The strongest-user collision resolution (SUCRe) protocol [1] resolves the majority of pilot collisions in crowded machine-type massive MIMO scenarios. We show in this letter that the random access (RA) performance of SUCRe can be improved by replacing the hard decision retransmission rule by a soft decision one, so that each user decides to retransmit or not its pilot sequence with a suitable probability. First, we propose to obtain this probability by mapping the ratio between the signal gain of each UE and the sum of the contenders' signal gains with the aid of a sigmoid function. Then, we propose to determine the retransmission probability of each UE according to the probability of this UE being the strongest contender, while proposing also an approximated probability expression for this event. Our results demonstrate an improvement in terms of a** *lower number of access attempts* **and a** *lower fraction of failed access attempts* **compared to the SUCRe protocol, while maintaining its features of being decentralized and uncoordinated.**

***Index Terms*—Large-scale MIMO; Crowded massive MIMO; random access; collision resolution; machine-type communication; pilot contamination; decentralized decision.**

I. Introduction

It has been shown recently that the random access (RA) in crowded networks can be substantially benefited if combined with massive multiple-input multiple-output (MIMO) technology, due to the massive MIMO properties of favorable propagation and channel hardening [2], [3]. Several works have been then disseminated aiming to improve RA performance in a decentralized fashion by exploiting massive MIMO properties [1], [4], [5], [6]. The strongest-user collision resolution (SUCRe) protocol [1] is a very efficient solution to improve RA functionality in crowded massive MIMO networks, which is able to resolve around 90% of all collisions. Furthermore, the SUCRe protocol exploits the massive MIMO properties of channel hardening and favorable propagation in order to enable distributed collision detection and resolution at the UEs, as described in the following, being thus highly scalable with respect to the number of UEs in the cell.

Some variants of the SUCRe protocol are proposed in [4] and [5]. In the proposed SUCRe combined idle pilots access (SUCR-IPA) of [4], the base station (BS) detects the idle pilots after the UEs' pilot transmission in the first stage, and broadcasts the indices of these pilots as well as an access class barring (ACB) factor to the UEs in the second stage. Then, the UEs who did not judge theirselves as the strongest ones in the third stage will select a new pilot based on the indices of idle pilots and the ACB factor. As shown in [4], a slight RA performance improvement can be achieved by this scheme, however at the cost of an increased overhead due to the higher control information exchange, which penalizes the entire system. Similarly, in the SUCRe combined graph-based pilots access (SUCR-GBPA) of [5], the BS also broadcasts the indices of idle pilots in the second stage, but no ACB factor. Then, all failed user equipments (UEs) randomly select a pilot from the pilots that are not selected by any UE in the initial step. By exploiting the characteristic that the channel responses between UEs and the base station are invariant within the coherence time, a bipartite graph is established where active UEs and selected pilots are considered variable nodes and factor nodes, respectively. Based on this bipartite graph, a successive interference cancellation algorithm is employed to estimate the channel response of each UE.

J.C. Marinello and T. Abrão are with Electrical Engineering Dept., State University of Londrina; taufik@uel.br

Another approach regarding the problem of random access in crowded massive MIMO networks does not focus in avoiding pilot collisions, but in developing improved coding schemes in order to enable the communication even in the presence of pilot collisions. In the protocol proposed in [6], the transmission is organized into transmission frames consisting of multiple transmission slots. When a device has a data codeword to transmit, it divides the codeword into multiple parts and, within a transmission frame, transmits the codeword parts in multiple transmission slots. The channels are estimated from uplink (UL) pilots every time the device transmits. In each time slot, each active device selects pseudo-randomly a pilot from a predetermined pilot codebook and, during the rest of the slot, it sends a part of the data codeword. Hence, a device performs pilot-hopping over multiple slots and the hopping pattern can be used to identify the device and appropriately merge and decode the parts of its codeword at the BS.

In this paper, we investigate the RA functionality in crowded machine-type massive MIMO networks. Our interest is to improve RA performance, decreasing the average number of access attempts and the probability of failed access attempts even in very crowded scenarios, in a decentralized and uncoordinated manner, avoiding periodically exchange of control information. The SUCRe protocol appears as one of the most promising solutions; however, one of the main shortcomings of SUCRe protocol is that it requires a noticeable disparity between large-scale fading coefficients of contending users to successfully resolve a pilot collision through its hard decision retransmission rule. Since this requirement is satisfied more rarely as long as the number of UEs becomes very large, it can be seen as a cause of the RA performance degradation in very crowded networks. Aiming to improve this situation, the main contribution of this paper is *to propose a soft decision retransmission rule for the SUCRe protocol, by introducing the idea of retransmission probability*. Two approaches are proposed: the first one in which the retransmission probability is simply computed with the aid of a sigmoid function, and the second in which the retransmission probability for a given UE is associated with the probability of it being the strongest contender. Based on the information available at the UE side, we propose an approximated expression for computing this probability, while numerical results corroborate its effectiveness in improving RA performance in over-crowded machine-type scenarios.

II. System Model

We consider cellular networks where each BS is equipped with M antennas, and the system operates in time-division

duplexing (TDD) mode with the time-frequency resources being divided into coherence blocks of T channel uses [1]. Let $\mathcal{U}_i$ denotes the set of UEs in cell i, while $\mathcal{A}_i \subset \mathcal{U}_i$ is the subset of users in this cell that are active at any given time. Tipically, in crowded machine-type network scenarios the UE set is very large, such that $|\mathcal{U}_i| \gg T$, but the active UEs satisfy $|\mathcal{A}_i| < T$, and the BS can temporarily assign orthogonal pilots to these UEs and reclaim them when they finish their transmissions. We focus on an arbitrary cell, referred as cell 0 without loss of generality, and consider how interference from other cells impacts on the considered cell. Let $\mathcal{K}_0 = \mathcal{U}_0 \backslash \mathcal{A}_0$ denote the set of inactive UEs in cell 0, and one can say that there are $K_0 = |\mathcal{K}_0|$ inactive UEs in this cell. These K_0 users are assumed to share τ_p mutually orthogonal RA pilot sequences $\boldsymbol{\psi}_1 \dots \boldsymbol{\psi}_{\tau_p} \in \mathbb{C}^{\tau_p}$ which span τ_p UL channel uses and satisfy $||\boldsymbol{\psi}_t||^2 = \tau_p$.

The UEs in $\mathcal{K}_0$ randomly select one of the τ_p pilots in each RA block: UE k selects pilot $c(k) \in \{1, 2, \dots, \tau_p\}$. Besides, the probability of each UE would like to become active is $P_a \leq 1$. The UE k makes an access attempt by transmitting the pilot $\boldsymbol{\psi}_{c(k)}$ with a non-zero power $\rho_k > 0$. The set $\mathcal{S}_t = \{k : c(k) = t, \rho_k > 0\}$ contains the indices of the UEs that transmit pilot t. Therefore, $|\mathcal{S}_t|$ which is the number of UEs transmitting $\boldsymbol{\psi}_t$ presents a binomial distribution [1]:

$$|\mathcal{S}_t| \sim \mathfrak{B}\left(K_0, \frac{P_a}{\tau_p}\right). \tag{1}$$

We denote the channel vector between UE k and its BS by $\mathbf{h}_k \in \mathbb{C}^M$. Since the number of BS antennas is large, the massive MIMO properties of channel hardening and asymptotic favorable propagation hold [3]. The channel vector also satisfies $\mathbf{h}_k = \sqrt{\beta_k}\underline{\mathbf{h}}_k$, in which β_k is the large-scale fading coefficient between kth user and its cell, comprising path loss and shadowing, and each coefficient of the small-scale fading vector $\underline{\mathbf{h}}_k$ is distributed as $\mathcal{CN}(0,1)$. We assume that β_k is known to UE k since it was estimated in step 0 of SUCRe protocol [1].

In step 1 of the SUCRe protocol the BS receives the signal $\mathbf{Y} \in \mathbb{C}^{M \times \tau_p}$ from the pilot transmission:

$$\mathbf{Y} = \sum_{k \in \mathcal{K}_0} \sqrt{\rho_k}\mathbf{h}_k \boldsymbol{\psi}_{c(k)}^T + \mathbf{W} + \mathbf{N}, \tag{2}$$

where $\mathbf{N} \in \mathbb{C}^{M \times \tau_p}$ is the matrix of noise coefficients at the BS with each element following $\mathcal{CN}(0, \sigma^2)$, and the matrix $\mathbf{W} \in \mathbb{C}^{M \times \tau_p}$ representing the interference from adjacent cells. The BS then correlates $\mathbf{Y}$ with $\boldsymbol{\psi}_t$ to obtain

$$\begin{aligned} \mathbf{y}_t &= \mathbf{Y}\frac{\boldsymbol{\psi}_t^*}{||\boldsymbol{\psi}_t||} = \sum_{i \in \mathcal{S}_t} \sqrt{\rho_i}||\boldsymbol{\psi}_t||\mathbf{h}_i + \mathbf{W}\frac{\boldsymbol{\psi}_t^*}{||\boldsymbol{\psi}_t||} + \mathbf{n}_t \\ &= \sum_{i \in \mathcal{S}_t} \sqrt{\rho_i \tau_p}\mathbf{h}_i + \mathbf{W}\frac{\boldsymbol{\psi}_t^*}{||\boldsymbol{\psi}_t||} + \mathbf{n}_t, \end{aligned} \tag{3}$$

in which $\mathbf{n}_t = \mathbf{N}\frac{\boldsymbol{\psi}_t^*}{||\boldsymbol{\psi}_t||} \sim \mathcal{CN}(\mathbf{0}, \sigma^2\mathbf{I}_M)$ is the effective receiver noise. The inter-cell interference can be modeled as

$$\mathbf{W} = \sum_l \mathbf{w}_l \mathbf{d}_l^T + \sum_{t=1}^{\tau_p} \sum_{k \in \mathcal{S}_t^{\text{interf}}} \sqrt{\rho_{t,k}}\mathbf{g}_{t,k}\boldsymbol{\psi}_t^T. \tag{4}$$

The first term in (4) refers to the interfering data transmissions from neighboring cells that use a different resource block (in time-frequency domain) as RA block than cell 0 [1][Fig.2]. $\mathbf{w}_l \in \mathbb{C}^M$ is the channel vector of the lth interferer to the BS in cell 0 and $\mathbf{d}_l \in \mathbb{C}^{\tau_p}$ is the random data the interfering user transmits. The second term in (4) refers to the interfers in neighboring cells using the same resource block as RA block as cell 0, which are also performing RA. Such users are gathered in the set $\mathcal{S}_t^{\text{interf}}$, and the member $k \in \mathcal{S}_t^{\text{interf}}$ uses the transmit power $\rho_{t,k}$ and has the channel $\mathbf{g}_{t,k}$ to the BS in cell 0. It can be shown that

$$\frac{\left|\mathbf{W}\frac{\boldsymbol{\psi}_t^*}{||\boldsymbol{\psi}_t||}\right|}{M} \to \underbrace{\sum_l \beta_{w,l}\frac{|\mathbf{d}_l^T\boldsymbol{\psi}_t^*|^2}{||\boldsymbol{\psi}_t||^2} + \sum_{k \in \mathcal{S}_t^{\text{interf}}} \rho_{t,k}\tau_p\beta_{t,k}}_{\omega_t} \tag{5}$$

as $M \to \infty$, in which $\beta_{w,l}$ is the large-scale fading coefficients related to $\mathbf{w}_l$ ($\frac{||\mathbf{w}_l||^2}{M} \to \beta_{w,l}$), and $\beta_{t,k}$ is the ones related to $\mathbf{g}_{t,k}$ ($\frac{||\mathbf{g}_{t,k}||^2}{M} \to \beta_{t,k}$). Interference in ω_t come from both data transmission and RA pilots in other cells, but the first is often dominant since the closest neighboring cells transmit data. On the other hand, the other cells performing RA in the same resource block as cell 0 are farther [1].

In the second step of SUCRe protocol, the BS responds to the RA pilots by sending orthogonal precoded downlink (DL) pilot signal $\mathbf{V} \in \mathbb{C}^{M \times \tau_p}$ with respect to each pilot sequence:

$$\mathbf{V} = \sqrt{q}\sum_{t=1}^{\tau_p} \frac{\mathbf{y}_t^*}{||\mathbf{y}_t||}\boldsymbol{\psi}_t^T, \tag{6}$$

where q is the DL transmit power. The received signal $\mathbf{z}_k \in \mathbb{C}^{\tau_p}$ at UE $k \in \mathcal{S}_t$ is

$$\mathbf{z}_k^T = \mathbf{h}_k^T\mathbf{V} + \boldsymbol{\nu}_k^T + \boldsymbol{\eta}_k^T, \tag{7}$$

in which $\boldsymbol{\nu}_k \in \mathbb{C}^{\tau_p}$ is the inter-cell interference, and $\boldsymbol{\eta}_k \sim \mathcal{CN}(\mathbf{0}, \sigma^2\mathbf{I}_{\tau_p})$ is the receiver noise. Then, by correlating $\mathbf{z}_k$ with its respective pilot sequence $\boldsymbol{\psi}_t$, the UE obtains

$$z_k = \mathbf{z}_k^T\frac{\boldsymbol{\psi}_t^*}{||\boldsymbol{\psi}_t||} = \sqrt{q\tau_p}\mathbf{h}_k^T\frac{\mathbf{y}_t^*}{||\mathbf{y}_t||} + \boldsymbol{\nu}_k^T\frac{\boldsymbol{\psi}_t^*}{||\boldsymbol{\psi}_t||} + \eta_k, \tag{8}$$

in which $\eta_k \sim \mathcal{CN}(0, \sigma^2)$ is the effective receiver noise.

Defining the sum of the signal and interference gains received at the BS during the UL transmission of pilot $\boldsymbol{\psi}_t$:

$$\alpha_t = \sum_{i \in \mathcal{S}_t} \rho_i\beta_i\tau_p + \omega_t, \tag{9}$$

an asymptotically error free estimator for α_t in [1] is:

$$\hat{\alpha}_{t,k} = \max\left(\left[\frac{\Gamma(M + \frac{1}{2})}{\Gamma(M)}\right]^2 \frac{q\rho_k\beta_k^2\tau_p^2}{[\Re(z_k)]^2} - \sigma^2,\ \rho_k\beta_k\tau_p\right), \tag{10}$$

in which $\Re(\cdot)$ gives the real part of its argument.

The main goal of the SUCRe protocol is to resolve pilot collisions in a decentralized and uncoordinated manner in the third step, so that each pilot is retransmitted by only one UE (collision resolved). Each UE $k \in \mathcal{S}_t$ knows its own average signal gain $\rho_k\beta_k\tau_p$ and has an estimate $\hat{\alpha}_{t,k}$ of the sum of the signal gains of the contender UEs and inter-cell interference.

Therefore, they apply the following distributed *decision rule*:

$$\mathcal{R}_k: \quad \text{if} \quad \rho_k\beta_k\tau_p > \frac{\hat{\alpha}_{t,k}}{2} + \epsilon_k \qquad \text{(repeat)} \tag{11}$$

$$\mathcal{I}_k: \quad \text{if} \quad \rho_k\beta_k\tau_p \leq \frac{\hat{\alpha}_{t,k}}{2} + \epsilon_k \qquad \text{(inactive)}. \tag{12}$$

The bias parameter $\epsilon_k \in \mathbb{R}$ can be used to tune the system behavior to the final performance criterion, and is empirically adjusted in [1] to $\epsilon_k = \frac{-\beta_k}{\sqrt{M}} - \frac{\overline{\omega}}{2}$, where the *average UL interference* is given by $\overline{\omega} = \frac{1}{M} \cdot \mathbb{E}\left\{ \left\| \mathbf{W} \frac{\boldsymbol{\psi}_t^*}{||\boldsymbol{\psi}_t||} \right\|^2 \right\}$, in which the expectation is taken over user locations and shadow fading realizations.

III. Retransmission Probability Criterium with Soft Decision Rule

The SUCRe protocol is able to resolve great part of the pilot collisions in crowded machine-type massive-MIMO scenarios while continues to admit UEs efficiently in overloaded networks [1]. However, one of the main limitations of the SUCRe protocol is because it requires a noticeable disparity between the large-scale fading coefficients of the contending UEs, so that the decision rule of (11) is true for only one contending UE. With a not so large number of UEs, this condition is usually satisfied in the few cases when a collision occurs. On the other hand, as long as the number of UEs within the cell increases, the collisions occur more often and sometimes with more than two contenders, so that the probability of the strongest user signal gain be higher than half of the sum of contending's signal gains decreases, with no UE retransmitting the pilot in the third step.

This fact has motivated we propose in this letter a different decision rule for the UEs retransmit their pilots. From (11), one can note that the SUCRe protocol in [1] implements a hard decision rule, since if the condition is true the UE retransmit its pilot, but if it is false the UE remains inactive. We show in the sequel that the protocol performance can be improved by making the decision rule soft, in such a way that the UE retransmits its pilot with a probability as high as its signal gain compared with the estimated sum of signal gains. Our first approach is to obtain this probability with the aid of a sigmoid function (Sec. III-A). Then, we propose to determine the probability of retransmission for a given UE according to the probability of this UE being the strongest contender (Sec. III-B), taking advantage of knowing $\rho_k\beta_k\tau_p$ and $\hat{\alpha}_{t,k}$ quantities.

A. First Approach: Soft Sigmoid Function

A given kth user decides to retransmit its chosen pilot sequence in step 3 if the following distributed decision rule is satisfied

$$\rho_k\beta_k\tau_p > \widehat{\alpha}_{t,k}/2 + \epsilon_k = 0.5\,(\widehat{\alpha}_{t,k} + 2\epsilon_k) \tag{13}$$

Defining $\gamma_{t,k} = \widehat{\alpha}_{t,k} + 2\epsilon_k$, eq.(13) can be rewritten as:

$$\frac{\rho_k\beta_k\tau_p}{|\gamma_{t,k}|} > \text{sign}(\gamma_{t,k})\ 0.5, \tag{14}$$

in which $\text{sign}(\cdot)$ is the signal operator, and $\gamma_{t,k}$ can assume positive or negative values.

The SUCRe decentralized decision rule is characterized by a hard decision: if $\frac{\rho_k\beta_k\tau_p}{|\gamma_{t,k}|}$ is higher than $\text{sign}(\gamma_{t,k})\ 0.5$, the user retransmits its sequence. This hard decision criterium may lead to contradictory situations in which if $\frac{\rho_k\beta_k\tau_p}{|\gamma_{t,k}|}$ for a given user is approaching $\text{sign}(\gamma_{t,k})\ 0.5$ by the left, this user remains inactive in step 3, but if it is approaching it by the right, this user decides to retransmit its pilot. Besides, in situations in which there are a higher number of users contending for the same pilot resource, and the difference in their large-scale coefficients is not so apparent, it becomes quite difficult to the decision rule in (14) be satisfied for any contending user, in such a way that there are no chance of retransmission for these users. Hence, herein we investigate a soft decision rule for the SUCRe protocol, in which the value of $\frac{\rho_k\beta_k\tau_p}{|\gamma_{t,k}|}$ can be mapped into a probability of retransmission for each user, without losing the decentralized and uncoordinated features.

Our first approach consists in smoothing the hard decision in (14) with the aid of a sigmoid function[1], as depicted in Figure 1. It was assumed in the Figure the case of positive $\gamma_{t,k}$. If $\gamma_{t,k}$ is negative, the soft decision curve is horizontally shifted in order to be centered in -0.5. Besides, the λ parameter sets the smoothness of the sigmoid curve: the curve becomes sharper with the increase of λ values.

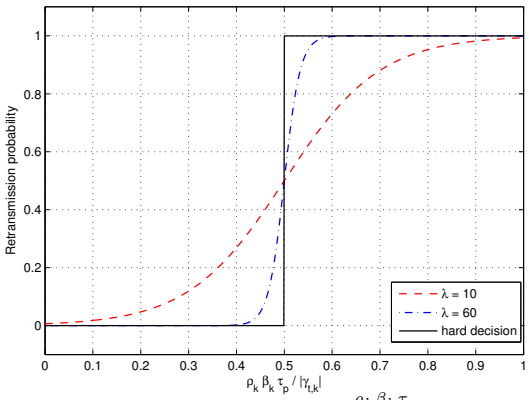

Fig. 1. Probability of retransmission according $\frac{\rho_k\beta_k\tau_p}{|\gamma_{t,k}|}$, for the conventional SUCRe decision rule (hard decision) and the proposed soft decision rule

B. Second Approach: Strongest Contender Probability

Our second approach is to associate the retransmission probability for a given UE with the probability of this UE being the strongest contender. For this sake, we obtain in this subsection an approximated expression for this probability. We denote by $\mathbf{x}_k \in \mathbb{R}^2$ the physical location of UE k with respect to the BS (assumed to be located in the origin), and assume a uniform distribution for the UEs' positions in a circular cell with radius d_{max} and minimum distance d_{min} (in order to consider only non-line-of-sight propagation) [7]. This user distribution is described by the following density function

$$f(\mathbf{x}_k) = \begin{cases} \frac{1}{\pi(d_{\text{max}}^2 - d_{\text{min}}^2)} & , \quad d_{\text{min}} \leq ||\mathbf{x}_k|| \leq d_{\text{max}}, \\ 0 & , \quad \text{otherwise.} \end{cases} \tag{15}$$

[1]A sigmoid function refers to the special case of the logistic function, and defined by $f(x) = \frac{1}{1+e^{-\lambda x}}$, $\forall x \in \mathbb{R}$.

Let the large-scale fading be dominated by path-loss [7]. This is often modeled as

$$\beta_k = \frac{\overline{d}}{||\mathbf{x}_k||^{\kappa}} \quad \text{for} \quad ||\mathbf{x}_k|| \geq d_{\text{min}}, \tag{16}$$

where $\kappa \geq 2$ is the path-loss exponent and the constant $\overline{d} > 0$ regulates the channel attenuation at distance d_{min} [8]. The uniform user location distribution in (15) results in the following distribution for $||\mathbf{x}_k||$

$$f(||\mathbf{x}_k||) = \begin{cases} \frac{2\,||\mathbf{x}_k||}{(d_{\text{max}}^2 - d_{\text{min}}^2)} & , \quad d_{\text{min}} \leq ||\mathbf{x}_k|| \leq d_{\text{max}}, \\ 0 & , \quad \text{otherwise.} \end{cases} \tag{17}$$

This distribution can be directly mapped with the aid of (16) to obtain the distribution of the β_k coefficients as

$$f(\beta_k) = \begin{cases} \frac{2\,\overline{d}^{\frac{2}{\kappa}}}{\kappa(d_{\text{max}}^2 - d_{\text{min}}^2)}\,\beta_k^{-\frac{\kappa+2}{\kappa}} & , \quad \beta_{\text{min}} \leq \beta_k \leq \beta_{\text{max}}, \\ 0 & , \quad \text{otherwise,} \end{cases} \tag{18}$$

in which $\beta_{\text{min}} = \frac{\overline{d}}{(d_{\text{max}})^{\kappa}}$ and $\beta_{\text{max}} = \frac{\overline{d}}{(d_{\text{min}})^{\kappa}}$.

The kth UE has knowledge of β_k and $\hat{\alpha}_{t,k}$, which is an estimate of $\sum_{i \in \mathcal{S}_t} \rho_i \beta_i \tau_p + \omega_t$. Therefore, if another contender $k' \in \mathcal{S}_t$ is the strongest, its large scale fading coefficient is within the interval $\beta_k < \beta_{k'} \leq \overline{\beta}_{t,k}$, in which $\overline{\beta}_{t,k} = \frac{\hat{\alpha}_{t,k} - \overline{\omega}}{\rho\,\tau_p}$ is an estimated upper bound for the large scale fading coefficient of any contending of pilot $\boldsymbol{\psi}_t$ that UE k can adopt. The probability of this event can be readily obtained from (18), resulting in (19).

The kth UE will not be the strongest contender if another contender (any of them) has a higher large-scale fading coefficient. Since the average number of contenders is $K_0\,P_a$, we can approximate the probability of the UE k be the strongest $P_{\text{strong}}(k) = P\left(\beta_k > \beta_{k'}, \forall k' \in \mathcal{S}_t, k' \neq k\right)$, for $K_0 > 1/P_a$, as

$$P_{\text{strong}}(k) = 1 - \min\left[(K_0\,P_a - 1)\,P(\beta_{k'} > \beta_k), 1\right]. \tag{20}$$

Therefore, in our second proposed approach, each UE compute $P_{\text{strong}}(k)$ in (20), and then use this value as its probability of retransmission in step 3, under a decentralized and uncoordinated manner.

IV. Numerical Results and Discussion

The average number of access attempts and the probability of failed access attempts (when the number of attempts exceeds 10) are evaluated in this Section for the SUCRe protocol of [1], and the SUCRe using the soft decision rule approaches for the retransmission probability proposed in this letter. The probability of activation for each device is $P_a = 0.1\%$, the length of training sequences is $\tau_p = 10$, and the number of inactive devices K_0 is varied. The adopted parameters are summarized in Table I.

Figure 2 depicts the performance of the proposed SUCRe with the soft decision rule with $\lambda = 10$ for the sigmoid function. As one can see, a worse performance is achieved when the number of UEs is lower than $\tau_p/P_a = 10000$, but a better performance is obtained above this threshold. This can be justified since the motivation of employing a soft decision rule in SUCRe is to resolve collisions with high number of contentions and/or a low disparity between their large-scale fading coefficients, which occurs more often when $K_0 > \tau_p/P_a$. Under this threshold the soft decision rule is not so efficient, since it introduces a probability of the strongest user remain inactive and a probability of weaker users retransmit pilots.

TABLE I
System Parameters

Parameter	Value
Soft decision rule	Sigmoid function (Sec. III-A)
	$P_{\text{strong}}(k)$ (Sec. III-B)
Sigmoid smoothness	$\lambda \in [5;\ 90]$
Device activation probability	$P_a = 0.1\%$
Length of training sequences	$\tau_p = 10$
# Inactive devices	$K_0 \in [1;\ 16000]$
d_{max}	250m
d_{min}	25m
$\overline{d}$	$10^{-3.53}$
κ	3.8
Shadowing standard deviation	8 dB

A. Tuning λ with increasing Inactive Devices K_0

Aiming to investigate the best value for the λ parameter with increasing inactive machine-type devices K_0, we let the sigmoid smoothness parameter vary in the range $\lambda \in [5, 90]$, and find for each value of K_0 the best performance obtained by the SUCRe with soft sigmoid decision rule. Figure 3 shows the best performance achieved following this methodology. As one can see from the Figure, an appreciable performance improvement can be obtained when adopting the soft decision rule in the SUCRe protocol in the very crowded scenario ($K_0 > \tau_p/P_a$). Table II shows the reduction in the average number of access attempts of the proposed SUCRe protocol with soft decision rule via sigmoid function (denoted as sSUCRe1 in the Table) in comparison with conventional SUCRe, with and without intercell interference. One can see for example that 0.497 less RA attempts are required on average for 11000 UEs without interference, while 0.336 less RA attempts for 12000 UEs with interference. Besides, one can see from the Figure that the probability of failed access attempts can reduce from 16.39% to 15.12% for 16000 UEs with interference. It means that adopting the soft decision rule can provide successful access to $0.0127 \times 16000 \times P_a = 0.2032$ additional devices on average if compared to the conventional SUCRe, *i.e.*, in about one out of 5 frame periods, the SUCRe protocol with soft decision rule will have one additional active UE in comparison with the conventional SUCRe. Table III shows the average number of additional active devices of our proposed RA protocol in comparison with SUCRe.

Analysing the best values of the λ parameter, we have noted that it have randomly oscillated near values around 60 in the range of $K_0 < \frac{0.9\tau_p}{P_a}$, indicating that any high λ value, which is able to approach the hard decision, will be suitable in this moderately crowded scenario, but it have converged to 10 for $K_0 \approx \tau_p/P_a$ and slightly decreased to 9 for $K_0 \approx 1.4\tau_p/P_a$. Therefore, a suitable solution in practice is to switch between the conventional SUCRe in the scenario with $K_0 < \tau_p/P_a$ to

$$P(\beta_{k'} > \beta_k) = \begin{cases} 0 & , \quad \text{if} \quad \beta_k \geq \overline{\beta}_{t,k}, \\ \int_{\beta_k}^{\overline{\beta}_{t,k}} f(\beta)d\beta = \frac{\overline{d}^{\frac{2}{\kappa}}}{\kappa(d_{\max}^2 - d_{\min}^2)} \left(\beta_k^{-\frac{2}{\kappa}} - (\overline{\beta}_{t,k})^{-\frac{2}{\kappa}}\right) & , \quad \text{if} \quad \beta_k < \overline{\beta}_{t,k} < \beta_{\max}, \\ \int_{\beta_k}^{\beta_{\max}} f(\beta)d\beta = \frac{\overline{d}^{\frac{2}{\kappa}}}{\kappa(d_{\max}^2 - d_{\min}^2)} \left(\beta_k^{-\frac{2}{\kappa}} - (\beta_{\max})^{-\frac{2}{\kappa}}\right) & , \quad \text{if} \quad \beta_k < \beta_{\max} < \overline{\beta}_{t,k}. \end{cases} \tag{19}$$

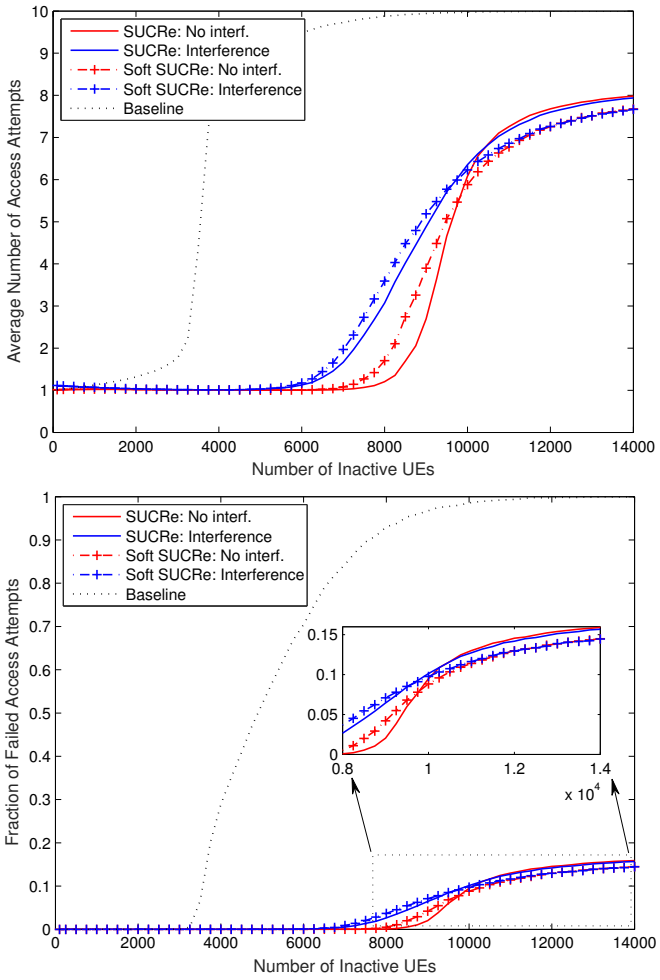

a) Average number of RA attempts b) Probability of failed RA attempt

Fig. 2. RA performance in a crowded machine-type network as a function of the number of devices in a cell. $\lambda = 10$ for the soft SUCRe.

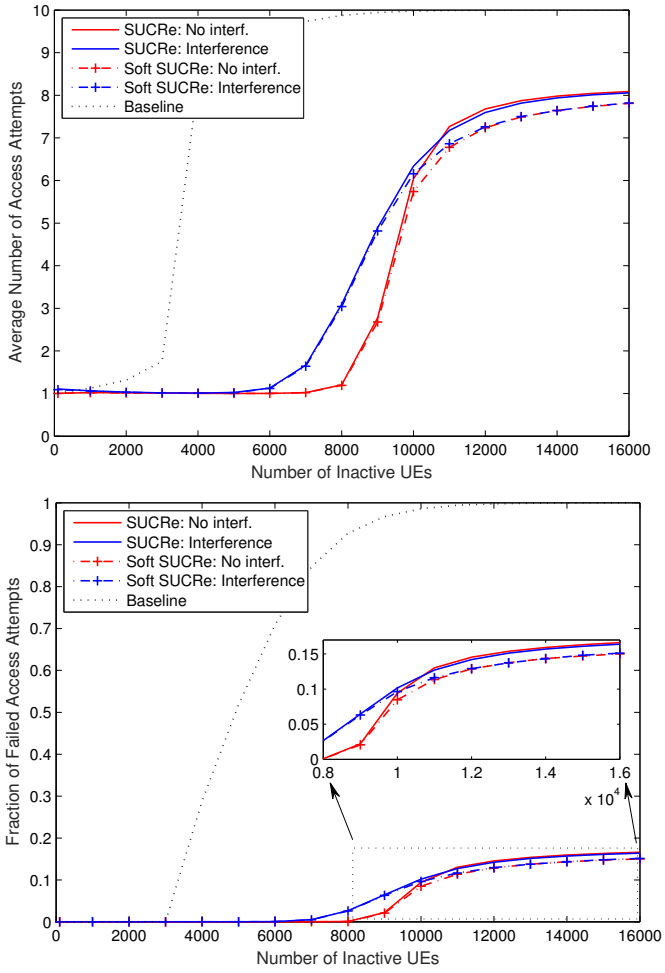

a) Average number of RA attempts b) Probability of failed RA attempt

Fig. 3. RA performance in a crowded machine-type network as a function of the number of devices in a cell. Best $\lambda \in [5, 90]$ for the soft SUCRe.

the SUCRe with soft decision rule with $\lambda = 10$ when $K_0 > \tau_p/P_a$ (over-crowded scenarios).

B. Computing the Probability of being the Strongest User

We present in this subsection the numerical results adopting a soft decision rule, in which the probability of retransmission for each UE is computed as in eq. (20) and (19). Figure 4 depicts the average number of access attempts and the probability of failed RA attempt, while Tables II and III shows the reduction on the average number of access attempts and the average number of active UEs increase in comparison with conventional SUCRe, respectively. The SUCRe with soft decision rule discussed in this subsection is denoted as sSUCRe2 in both Tables. In terms of the average number of access attempts, the soft decision can achieve a reduction on this number of 2.336 in the scenario without intercell interference with $K_0 = \tau_p/P_a = 10000$ UEs, and of 1.392 in the presence of intercell interference for the same number of UEs. Moreover, in terms of the probability of failed access attempts, the soft decision approach is able to reduce this number from 11.61% to 5.59% in the scenario without interference with $K_0 = \tau_p/P_a = 10000$ UEs, providing access to 0.6327 additional UEs in comparison with conventional SUCRe. In the scenario with intercell interference, 0.4446 additional active UEs can be supported for 11000 UEs. This shows that computing the retransmission probability of SUCRe employing our proposed expression for the probability of the UE being the strongest contender can be a promising

solution for RA in crowded massive MIMO networks, while still benefiting of the decentralized and uncoordinated features of SUCRe protocol.

TABLE II
AVERAGE NUMBER OF ACCESS ATTEMPTS REDUCTION IN COMPARISON WITH CONVENTIONAL SUCRE.

Interf.	Scheme	K_0					
		8000	9000	10000	11000	12000	16000
without	sSUCRe1	0.014	0.098	0.306	**0.497**	0.441	0.276
	sSUCRe2	-0.196	1.414	**2.336**	1.592	1.049	0.372
with	sSUCRe1	0.053	0.078	0.181	0.313	**0.336**	0.240
	sSUCRe2	-0.100	0.955	**1.392**	1.239	0.973	0.384

TABLE III
AVERAGE NUMBER OF ACTIVE UES INCREASE IN COMPARISON WITH CONVENTIONAL SUCRE.

Interf.	Scheme	K_0					
		8000	9000	10000	11000	12000	16000
without	sSUCRe1	0.0015	0.0120	0.0936	0.1837	0.2004	**0.2560**
	sSUCRe2	-0.0073	0.2892	**0.6327**	0.5569	0.4728	0.3504
with	sSUCRe1	0.0054	0.0121	0.0518	0.1188	0.1548	**0.2032**
	sSUCRe2	-0.0104	0.2198	0.4033	**0.4446**	0.4224	0.3408

V. CONCLUSION

The RA problem of crowded massive MIMO networks has been addressed in this letter. The recently proposed SUCRe protocol constitutes a very efficient solution for this problem. We have shown in this letter that its performance can be improved by implementing a soft decision rule as retransmission criterium instead of its original hard decision rule. We first proposed a soft decision rule with the aid of a sigmoid function, which shown itself as a very simple solution that achieves marginal improvements compared to the conventional SUCRe. Then we have proposed a second soft approach relating the probability of retransmission for each UE with our approximated probability expression for this user being the strongest contender. This latter strategy have presented even more significant improvements in the crowded and over-crowded scenarios, being able for example to provide access to 0.6327 additional UEs on average if compared to the conventional SUCRe with 10000 UEs in the cell with $\tau_p = 10$, without losing the desirable features of being a decentralized and uncoordinated procedure. Besides of providing access for a higher number of UEs, implementing our proposed soft decision approach can also decrease the delay to establish connection, while saving energy and improving the autonomy of the device batteries due to the lower number of access attempts required.

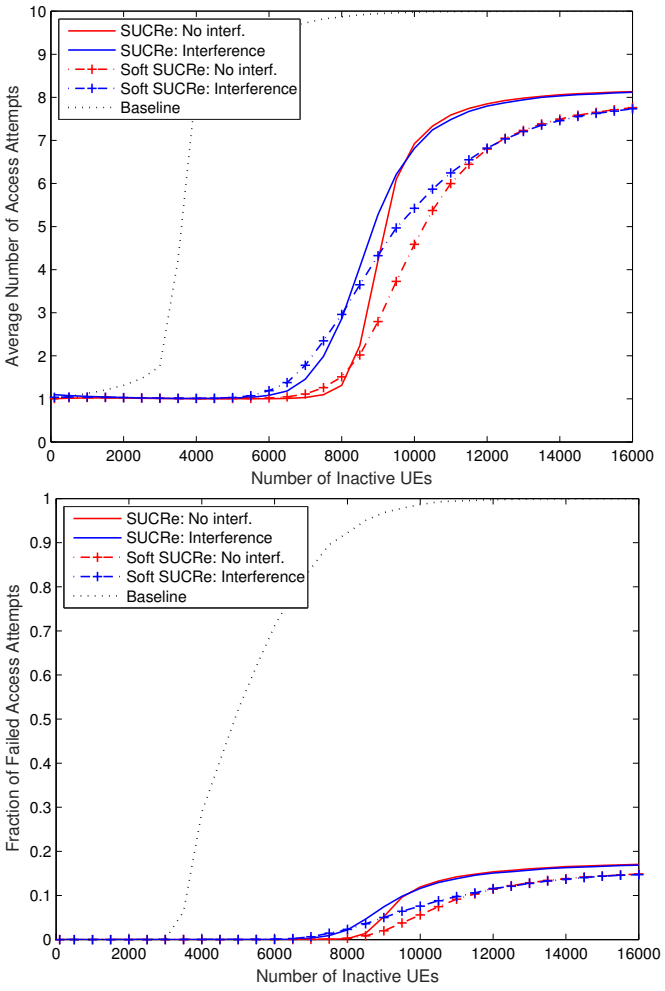

a) Average number of RA attempts b) Probability of failed RA attempt

Fig. 4. RA performance in a crowded machine-type network as a function of the number of devices in a cell. Soft SUCRe (**second**) approach computing the probability of being the strongest user.

REFERENCES

[1] E. Björnson, E. de Carvalho, J. H. Sørensen, E. G. Larsson, and P. Popovski, "A Random Access Protocol for Pilot Allocation in Crowded Massive MIMO Systems," *IEEE Transactions on Wireless Communications*, vol. 16, no. 4, pp. 2220–2234, April 2017.

[2] T. Marzetta, "Noncooperative Cellular Wireless with Unlimited Numbers of Base Station Antennas," *IEEE Transactions on Wireless Communications*, vol. 9, no. 11, pp. 3590–3600, 2010.

[3] T. Marzetta, E. Larsson, H. Yang, and H. Ngo, *Fundamentals of Massive MIMO*. New York, NY, USA: Cambridge University Press, 2016.

[4] H. Han, X. Guo, and Y. Li, "A High Throughput Pilot Allocation for M2M Communication in Crowded Massive MIMO Systems," *IEEE Transactions on Vehicular Technology*, vol. 66, no. 10, pp. 9572–9576, Oct 2017.

[5] H. Han, Y. Li, and X. Guo, "A Graph-Based Random Access Protocol for Crowded Massive MIMO Systems," *IEEE Transactions on Wireless Communications*, vol. 16, no. 11, pp. 7348–7361, Nov 2017.

[6] E. de Carvalho, E. Björnson, J. H. Sørensen, E. G. Larsson, and P. Popovski, "Random Pilot and Data Access in Massive MIMO for Machine-Type Communications," *IEEE Transactions on Wireless Communications*, vol. 16, no. 12, pp. 7703–7717, Dec 2017.

[7] E. Björnson, L. Sanguinetti, J. Hoydis, and M. Debbah, "Optimal Design of Energy-Efficient Multi-User MIMO Systems: Is Massive MIMO the Answer?" *IEEE Transactions on Wireless Communications*, vol. 14, no. 6, pp. 3059–3075, June 2015.

[8] *Further Advancements for E-UTRA Physical Layer Aspects (Release 9)*. 3GPP TS 36.814, March 2010.